



Decellularised Human Pancreata and Livers
for the Study of
Pancreatic Ductal Adenocarcinoma:
Development, Metastasis
and Chemoresistance

Walid Al-Akkad Abu-Zeina

A thesis presented for the degree of

Doctor of Philosophy

Supervised by:

Prof. Krista Rombouts

Prof. Massimo Pinzani

University College London

Division of Medicine

December 2019

This thesis is dedicated to my cousin Lama Alkurdy.

17th July 1971 – 28th September 2018.

DECLARATION

I, Walid Al-Akkad Abu-Zeina, confirm that the work presented in this thesis is my own. Where information has been derived from other sources, I confirm that this has been indicated in the thesis.

ACKNOWLEDGMENTS

• In the name of God, the Most Gracious, the Most Merciful •

It is a privilege to express my gratitude to my supervisors Prof. Krista Rombouts and Prof. Massimo Pinzani for their constant and constructive help, care and guidance throughout my time at UCL and up to the final moment. I would also like to thank Giuseppe Mazza for his guidance and direction. His contribution to my development on both a professional and personal manner is highly appreciated.

I would like to extend my thanks to Luca Frenguelli for being a great lab partner and friend; his input in and out of the lab was invaluable. I would like to thank Maria-Giovanna Vilia, for our great friendship and for her key contributions to several experiments within this thesis.

A big thank you goes to my friends and lab partners, Martina Marrali, Domenico Bagordo, Eric Felli, Simone Canastrari, Marco Curti, Elisabetta Caon, Stefano Granieri, Paolo Giuffrida, David Martos Ruiz, Lisa Longato, Marco Castelli, Oliver Wallace, Katrin Schelzel, all members of Prof Pinzani/Krista Rombouts' lab and everyone in the carrel room. Last but not least, I would like to show my gratitude to Korsaa Khan for being a great operational manager and friend.

I would like to acknowledge Andrew Hall for all his assistance and help in obtaining immunohistochemical analysis of decellularised scaffolds and for being a good friend since I arrived at UCL. I would also like to express my thanks to Pilar Acedo Nunez, who has been an amazing lab partner and whom I alongside performed most of the chemoresistance experiments.

I would like to additionally thank all the surgeons who contributed to the surgical work within this thesis, starting with my amazing friends Alex Ney and Domenico Tamburrino, as well as Gabrielle Spoletini and Peter Labib (who I also enjoyed sharing a desk with for 3 years). Last but not least, I would like to thank Prof. Kito Fusai for his surgical input and guidance, as well as his contribution in funding part of my PhD through the Fiorina Fund (part of the Royal Free Charity).

I would also like to show my appreciation to Prof. Steve Pereira and his team, for their contribution to this project and the immunohistochemistry analysis of the recellularised scaffolds, to Prof Ludovic Vallier and the Sanger Institute members who contributed to this project and the RNAseq, and to Dr Amir Gander and the TAPB team for their contribution to this project and the organ retrievals.

Last but not least, to my family. I would like to send my deepest of appreciation to my beloved parents, father Khaled Al-Akkad and mother Isam Abu-Zeina. Thank you for instilling me with a strong passion for learning and doing anything and everything to put me on a path towards success. Each thing you did and continue to do for me is a stair I climb to reach the platform where I now stand; you are the source of my life, and you are also my life itself.

I would also like to thank my Uncle, Ma'amoun Abu-Zeina, I am ever so grateful for the numerous ways you have supported me through my life and academic experience. Thank you does not seem enough, but nothing else is fitting. You have been mindful of me in everyway and I cherish all your guidance, advice and love and I am honoured and blessed to have you.

My deepest appreciation goes to my wife Eda Xhelaj who has been passionately supportive of me throughout this entire process and has made countless sacrifices to help me get to this point. Without your love, never ending support and encouragement I never would have made here. I would also like to show my gratitude to all my family in-law, Lulzim Xhelaj, Marieta Gega, Ira Xhelaj and Arbi Baho, who have been constantly loving, caring and encouraging.

To my sister Haya Al-Akkad and brothers Tariq Al-Akkad and Badre Al-Kurdy, thank you for being there for me at every moment. You have pushed me to continue to strive to be the best version of myself. You are my greatest blessing. Finally, a special thank you goes to my best friend Fayez Shihabbudin, who has never stopped believing in me.

ABSTRACT

Background and Aims: Over 80% of patients with pancreatic ductal adenocarcinoma (PDAC) are diagnosed with concurrent metastases. Over the last 50 years, conventional treatment approaches have had little impact on the course of this disease. Therefore, the development of new treatment strategies to control PDAC is needed. We propose the use of 3D extracellular matrix (ECM) scaffolds that could redefine *in vitro* models of PDAC and preclinical testing of novel therapies.

Methods: Decellularised human pancreata and livers were characterised for the elimination of cellular material and preservation of ECM proteins and micro-architecture using histology, immunohistochemistry (IHC) and quantification kits. Both primary (PANC-1 and MIA PaCa-2) and metastatic pancreatic tumour cells (PK-1) were seeded onto 5 mm³ scaffolds, as well as 2D cultures. Histological analyses were used to confirm cell attachment and migration/invasion. Further, changes in protein expression (IHC) and gene expression (qPCR and RNAseq) were evaluated at day 14 post reseeding. Treatments with doxorubicin and Gemcitabine were performed; viability (AlamarBlue), protein expression (IHC) and gene expression (RNAseq) analyses were performed to test therapy-resistance in the 3D systems.

Results: All primary PDAC cell lines were able to migrate and invade the pancreas scaffolds whereas several of these cells were only able to attach superficially onto the liver scaffolds. PK1 cells were able to exclusively migrate and invade the liver scaffolds and only attached superficially onto the pancreatic scaffolds. These differences were supported by significant deregulations in gene and protein expression (i.e. MMP9, WNT1, β -CATENIN) between pancreas scaffolds, liver scaffolds and 2D culture. Interestingly, both primary and metastatic cells were found significantly more resistant to all chemotherapy treatments in the 3D models when compared to 2D cultures, even though confocal microscopy confirmed the uptake of drugs into the cells.

Conclusion: Our results suggest that primary and metastatic pancreatic cancer cells manifest a conserved invasive behaviour depending on the 3D ECM structure of origin. Moreover, there is an evident alteration in cell response to different cancer-therapies in the presence of a natural ECM niche. These observations provide a proof of concept for the development of an effective bio-engineered model for drug discovery, therapy screening and biomarker discovery.

IMPACT STATEMENT

Pancreatic ductal adenocarcinoma (PDAC) accounts for over 90% of all pancreatic cancers and affects over 350,000 new cases per year globally. PDAC is currently considered the fourth leading cause of cancer death and is projected to become the second biggest cancer killer by 2030. The striking similarity between incidence and fatalities highlights the dismal prognosis of this disease. The median survival is less than 6 months, and the 5-year survival rate is between 3-5%. This low survival rate is multifactorial, mainly attributed to its aggressive biology, its capacity to rapidly disseminate to the lymphatic system and distant organs and its resistance to conventional therapies. This is further complicated by PDAC's relatively asymptomatic clinical course. Indeed, this disease is almost incurable, with patients commonly diagnosed at a metastatic or locally advanced stage

Therapeutic options are limited and until recently, there was no standard second-line chemotherapy option. Despite intensive research, the median survival time of patients with PDAC has remained nearly constant during the last four decades. Currently, surgery followed by adjuvant therapy remains the standard of care for patients with resectable and non-metastatic PDAC. Unfortunately, tumour recurrence rates are high after resections, reaching up to 70%. There is a clear lack of translation between initial clinical response and overall survival. Several studies have attempted to understand the underlying reasons for such therapeutic failure. The two most common theories involve biological chemoresistance and physiological chemoresistance. However, investigating these theories is not straightforward. Whatcott and colleagues highlight this issue, stating, "...studies of its [physiological chemoresistance] clinical relevance are made difficult by the lack of good models to study their effects."

With this in mind, my thesis introduced the use of 3D extracellular matrix (ECM) scaffolds that could redefine *in vitro* models of PDAC and preclinical testing of novel therapies. Decellularised human pancreata and livers were seeded with both primary and metastatic PDAC cells. The resultant models demonstrated a conserved tissue-specific cell behaviour depending on the 3D ECM of origin. Moreover, there was an evident alteration in cell response to different cancer-therapies in the presence of a

natural ECM niche. These observations provide validated and effective bio-engineered *in vitro* models for therapy screening, development and biomarker discovery.

Indeed, the models presented in this thesis have been utilised by other academic research groups to study (i) patient derived xenograft cells, (ii) photodynamic therapies, (iii) pancreatic neuroendocrine tumours and (iv) NK cell immunotherapy. All the work carried out as part of these collaborations is currently being prepared into manuscripts for publication. Additionally, the models, techniques and datasets presented here have been licensed to a UCL spin-out biotechnology company, Engitix Therapeutics, to identify novel drug targets and effective therapeutics for PDAC. Finally, the decellularised pancreata described here can further be utilised to produce tissue-specific ECM hydrogels for high throughput screening for drug discovery.

TABLE OF CONTENTS

DECLARATION	2
ACKNOWLEDGMENTS.....	3
ABSTRACT.....	5
IMPACT STATEMENT.....	6
TABLE OF CONTENTS.....	8
TABLE OF FIGURES	11
TABLE OF TABLES	14
LIST OF ABBREVIATIONS	15
1. INTRODUCTION.....	19
1.1 Background and Vision.....	19
1.1.1 Three Dimensional Scaffolds.....	19
1.1.2 2D versus 3D cultures.....	23
1.1.3 Animal Models <i>versus</i> 3D Decellularised Scaffolds.....	25
1.1.4 Importance of 3D Cultures for Pharmaceuticals.....	25
1.2 Tissue Decellularisation.....	26
1.2.1 Physical Forces	27
1.2.2 Hypotonic and Hypertonic Solutions	29
1.2.3 Chemical Agents.....	30
1.2.4 Enzymatic Reagents	33
1.3 Pancreas Anatomy, Function and Diseases	35
1.3.1 Macro and Microanatomy of the Pancreas	35
1.3.2 Pancreas Cells and their Microscopic Organization	37
1.4 Pancreatic Ductal Adenocarcinoma.....	39
1.4.1 Concept, Epidemiology and Pathophysiology.....	39
1.4.2 Diagnosis and Staging.....	40
1.4.3 Precursor Lesions	42
1.4.4 Therapies.....	44
1.4.5 Molecular Genetics	48
1.4.6 The Tumour Stroma in Pancreatic Cancer	49
1.4.7 Chemoresistance.....	53
2. AIM and OBJECTIVES.....	63
2.1 Human Pancreas Decellularisation	63
2.1.1 Aim	63

2.1.2	Objectives.....	63
2.2	Developing primary and metastatic <i>in vitro</i> PDAC models.....	63
2.2.1	Aim	63
2.2.2	Objectives.....	63
2.3	Chemoresistance in PDAC.....	64
2.3.1	Aim	64
2.3.2	Objectives.....	64
3.	METHODS & MATERIALS	66
3.1	Tissue Retrieval and Preparation.....	66
3.2	Pancreas and Liver Cubes Decellularisation	67
3.3	Pancreas Decellularisation by Perfusion	67
3.4	DNA Quantification.....	73
3.5	Maintenance of Pancreatic Cells in Culture	73
3.6	Scaffold Sterilisation and Preparation for Bioengineering.....	74
3.7	3D Cell Cultures in Decellularised Scaffolds.....	74
3.8	Histology and Immunohistochemistry	75
3.8.1	Histology.....	75
3.8.2	Immunohistochemistry	76
3.9	RNA extraction and gene expression analysis	78
3.9.1	RNA Extraction	78
3.9.2	Reverse-Transcription	78
3.9.3	Real-Time qPCR	79
3.10	Chemotherapy	81
3.10.1	Determining Suitable Dosage of Chemotherapeutic Drugs on 2D Cultures.....	81
3.10.2	Treatment of 3D Bioengineered Scaffolds with Chemotherapeutics	82
3.11	Cell Viability Assay.....	82
3.11.1	Cells on 2D Cultures.....	82
3.12.2	Cells on 3D Cultures.....	82
3.12	Confirmation of Doxorubicin Uptake	83
3.13	Analysis of Cell Size	83
3.14	RNAseq.....	84
3.15	RNAseq Data Analysis	84
3.15.1	Pathway Analysis.....	85
3.15.2	Gene Ontology Analysis	87
3.15.3	Predicted Upstream Regulator Analysis.....	88
3.6	Statistics and Data Analysis	91

4. RESULTS.....	93
4.1 Decellularisation of Human Pancreata.....	93
4.1.1 Decellularisation of Pancreas Cubes by Agitation.....	93
4.1.2 Decellularisation of Whole Human Pancreas by Perfusion.....	95
4.2 PDAC Cell Cultures.....	105
4.2.1 Histological Characterisation	105
4.2.2 Genetic Profiling of PDAC Cell Lines in their Natural Tissue	115
4.2.3 qRT-PCR Analysis of the effect of Tissue-Specificity and 2D Plastic on PDAC.....	123
4.2.4 Next Generation Sequencing Evaluation of the Effect of Tissue-Specificity on PDAC.....	124
4.3 Tissue-Specific PDAC Models to Evaluate Chemotherapeutics	146
4.3.1 Evaluation of PDAC Response to Different Chemotherapy Drug Dose on 2D Plastic.....	146
4.3.2 Analysis of Cell Response to Chemotherapy in Tissue-Specific PDAC models.....	148
5. DISCUSSION.....	191
5.1 Pancreas Decellularisation	192
5.1.1 Elimination of Cellular Debris and Preservation of the ECM	192
5.1.2 Reseeding with PDAC cells.....	195
5.2 Retention of Tissue-Specificity within the 3D PDAC Models	197
5.2.1 Importance of Tissue-specificity for the Accurate Study of PDAC Biology	197
5.2.2 Role of Tissue-specific ECM in Tumour Progression	199
5.3 Tissue-specific PDAC models for the study of Chemoresistance.....	205
5.3.1 Increase in Chemoresistance of PDAC cells in Tissue-specific ECM models	206
5.3.2 Role of the ECM in Gemcitabine Resistance of PDAC cells	208
6. CONCLUSION.....	215
REFERENCES.....	217
SUPPLEMENTARY TABLES	252

TABLE OF FIGURES

FIGURE 1. SCHEMATIC COMPARISON OF DIFFERENT 3D SCAFFOLDS.	20
FIGURE 2. SCHEMATIC COMPARING EFFECT OF 2D AND 3D CULTURES ON CELLS.	24
FIGURE 3. GROSS ANATOMY OF THE PANCREAS AND ITS ANATOMICAL RELATIONSHIPS.	36
FIGURE 4. THE VASCULATURE OF THE PANCREAS.	37
FIGURE 5. MICROANATOMY OF THE PANCREAS.	38
FIGURE 6. PROGRESSION OF THREE DISTINCT PRECURSOR LESIONS PRECEDING PDAC.	42
FIGURE 7. THE PANIN PRECURSOR LESION MODEL.	43
FIGURE 8. SCHEMATIC REPRESENTATION OF PDAC STROMA.	50
FIGURE 9. BIOREACTOR COMPONENTS AND SETUP FOR DECELLULARISATION.	69
FIGURE 10. SCHEMATIC PRESENTING THE TIMELINE FOR 3D CELL CULTURE.	75
FIGURE 11. HYPERGEOMETRIC DISTRIBUTION.	85
FIGURE 12. SUM OF PROBABILITIES.	86
FIGURE 13. OVER-REPRESENTATION P-VALUE.	86
FIGURE 14. PERTURBATION FACTOR OF AN INDIVIDUAL GENE.	86
FIGURE 15. ACCUMULATION OF GENES.	87
FIGURE 16. TARGET GENES CONSISTENT WITH THE HYPOTHESIS CONSIDERED.	89
FIGURE 17. THE SET OF ALL GENES INCLUDES THE SET OF MEASURED GENES THAT ARE ALSO TARGETS IN THE NETWORK, OR MEASURED TARGETS (MT).	89
FIGURE 18. UPSTREAM REGULATORS Z-SCORE.	90
FIGURE 19. HISTOLOGICAL IMAGES OF FRESH AND DECELLULARISED PANCREAS USING AGITATION.	94
FIGURE 20. MACROSCOPIC VIEW OF PANCREATA DECELLULARISED USING DIFFERENT PERFUSION PROTOCOLS.	96
FIGURE 21. HISTOLOGICAL IMAGES OF PANCREAS HP1 DECELLULARISED BY PERFUSION.	98
FIGURE 22. HISTOLOGICAL IMAGES OF PANCREAS HP2 DECELLULARISED BY PERFUSION USING A BIOREACTOR.	101
FIGURE 23. HISTOLOGICAL IMAGES OF PANCREAS HP3 DECELLULARISED BY PERFUSION USING A BIOREACTOR.	102
FIGURE 24. DNA QUANTIFICATION OF FRESH AND DECELLULARISED PANCREAS.	103
FIGURE 25. IMMUNOHISTOCHEMISTRY IMAGES OF FRESH AND DECELLULARISED PANCREAS.	104
FIGURE 26. PANC-1 CELLS CULTURED ON PANCREAS AND LIVER SCAFFOLDS.	106
FIGURE 27. MIA PACA-2 CELLS CULTURED ON PANCREAS AND LIVER SCAFFOLDS.	107
FIGURE 28. PK-1 CELLS CULTURED ON PANCREAS AND LIVER SCAFFOLDS.	108
FIGURE 29. IMMUNOHISTOCHEMISTRY ANALYSIS OF PANC-1 CELLS CULTURED ON PANCREAS SCAFFOLDS.	111
FIGURE 30. IMMUNOHISTOCHEMISTRY ANALYSIS OF PANC-1 CELLS CULTURED ON LIVER SCAFFOLDS.	112
FIGURE 31. IMMUNOHISTOCHEMISTRY ANALYSIS OF PK-1 CELLS CULTURED ON PANCREAS SCAFFOLDS.	113
FIGURE 32. IMMUNOHISTOCHEMISTRY ANALYSIS OF PK-1 CELLS CULTURED ON LIVER SCAFFOLDS.	114
FIGURE 33. QUANTITATIVE COMPARISON OF GENES RELATED TO “TISSUE REMODELLING AND ANGIOGENESIS”.	118
FIGURE 34. QUANTITATIVE COMPARISON OF GENES RELATED TO “CYTOKINES/GROWTH FACTORS AND RECEPTORS”.	119
FIGURE 35. QUANTITATIVE COMPARISON OF GENES RELATED TO “ONCOGENES AND TUMOUR SUPPRESSORS”.	119
FIGURE 36. QUANTITATIVE COMPARISON OF GENES RELATED TO “CELL CYCLE REGULATORS”.	120
FIGURE 37. QUANTITATIVE COMPARISON OF GENES RELATED TO “AKT/PKB SIGNALLING PATHWAYS”.	120
FIGURE 38. QUANTITATIVE COMPARISON OF GENES RELATED TO “TGF/SMAD SIGNALLING PATHWAYS”.	121
FIGURE 39. QUANTITATIVE COMPARISON OF GENES RELATED TO “JAK/STAT SIGNALLING PATHWAYS”.	121
FIGURE 40. QUANTITATIVE COMPARISON OF GENES RELATED TO “RAS/MAPK SIGNALLING PATHWAYS”.	122
FIGURE 41. QUANTITATIVE COMPARISON OF “OTHER PDAC RELATED TO GENES”.	122

<u>FIGURE 42. QUANTITATIVE GENE EXPRESSION COMPARISON OF PANC-1 CELLS ON DIFFERENT MATERIALS.</u>	125
<u>FIGURE 43. QUANTITATIVE GENE EXPRESSION COMPARISON OF PK-1 CELLS.</u>	126
<u>FIGURE 44. PATHWAY MAP FOR ECM-RECEPTOR INTERACTION REPRESENTING THE SIGNIFICANTLY DIFFERENTIALLY EXPRESSED GENES FROM RNASEQ OF PANC-1 CELLS CULTURED ON PANCREAS VS LIVER SCAFFOLDS.</u>	134
<u>FIGURE 45. PREDICTED ACTIVATED UPSTREAM REGULATORS OF RNASEQ DATA OF PANC-1 CELLS ON PANCREAS VS LIVER SCAFFOLDS.</u>	135
<u>FIGURE 46. PREDICTED INHIBITED UPSTREAM REGULATORS OF RNASEQ DATA OF PANC-1 CELLS ON PANCREAS VS LIVER SCAFFOLDS.</u>	136
<u>FIGURE 47. PATHWAY MAP FOR CELL CYCLE REPRESENTING THE SIGNIFICANTLY DIFFERENTIALLY EXPRESSED GENES FROM RNASEQ OF PANC-1 CELLS CULTURED ON PANCREAS VS LIVER SCAFFOLDS.</u>	143
<u>FIGURE 48. PREDICTED ACTIVATED UPSTREAM REGULATORS OF RNASEQ DATA OF PK-1 CELLS ON PANCREAS VS LIVER SCAFFOLDS.</u>	144
<u>FIGURE 49. PREDICTED INHIBITED UPSTREAM REGULATORS OF RNASEQ DATA OF PK-1 CELLS ON PANCREAS VS LIVER SCAFFOLDS.</u>	145
<u>FIGURE 50. 2D CULTURED PDAC CELL TREATED WITH CHEMOTHERAPEUTICS.</u>	147
<u>FIGURE 51. CHEMOTHERAPEUTICS TREATMENT OF PANC-1 CELL CULTURED ON PANCREAS SCAFFOLDS.</u>	150
<u>FIGURE 52. CHEMOTHERAPEUTICS TREATMENT OF PANC-1 CELL CULTURED ON LIVER SCAFFOLDS.</u>	151
<u>FIGURE 53. CHEMOTHERAPEUTICS TREATMENT OF MIA PACA-2 CELL CULTURED ON PANCREAS SCAFFOLDS.</u>	153
<u>FIGURE 54. CHEMOTHERAPEUTICS TREATMENT OF MIA PACA-2 CELL CULTURED ON LIVER SCAFFOLDS.</u>	154
<u>FIGURE 55. CHEMOTHERAPEUTICS TREATMENT OF PK-1 CELL CULTURED ON PANCREAS SCAFFOLDS.</u>	155
<u>FIGURE 56. CHEMOTHERAPEUTICS TREATMENT OF PK-1 CELL CULTURED ON LIVER SCAFFOLDS.</u>	156
<u>FIGURE 57. INTER-EXPERIMENT COMPARISON OF GEMCITABINE TREATED PANC-1 CELL CULTURED ON 3D SCAFFOLDS.</u>	158
<u>FIGURE 58. INTER-EXPERIMENT COMPARISON OF GEMCITABINE TREATED MIA PACA-2 CELL CULTURED ON 3D SCAFFOLDS.</u>	159
<u>FIGURE 59. INTER-EXPERIMENT COMPARISON OF GEMCITABINE TREATED PK-1 CELL CULTURED ON 3D SCAFFOLDS.</u>	160
<u>FIGURE 60. COMPARISON OF PDAC CELLS' RESPONSE TO CHEMOTHERAPEUTIC TREATMENTS IN 3D SCAFFOLDS VS 2D PLASTIC.</u>	162
<u>FIGURE 61. VALIDATION OF DOXORUBICIN UPTAKE BY PDAC CELLS.</u>	164
<u>FIGURE 62. IMMUNOHISTOCHEMISTRY ANALYSIS OF CHEMOTHERAPY TREATED PANC-1 CELLS CULTURED ON 3D SCAFFOLDS.</u>	167
<u>FIGURE 63. IMMUNOHISTOCHEMISTRY ANALYSIS OF CHEMOTHERAPY TREATED MIA PACA-2 CELLS CULTURED ON 3D SCAFFOLDS.</u>	168
<u>FIGURE 64. IMMUNOHISTOCHEMISTRY ANALYSIS OF CHEMOTHERAPY TREATED PK-1 CELLS CULTURED ON 3D SCAFFOLDS.</u>	169
<u>FIGURE 65. COMPUTATIONAL QUANTIFICATION OF TREATED AND UNTREATED PDAC CELL SIZE IN 3D SCAFFOLDS.</u>	170
<u>FIGURE 66. PATHWAY MAP FOR CYTOKINE-CYTOKINE RECEPTOR INTERACTIONS REPRESENTING THE SIGNIFICANTLY DIFFERENTIALLY EXPRESSED GENES FROM RNASEQ OF UNTREATED VS GEMCITABINE TREATED PANC-1 CELLS CULTURED ON PANCREAS SCAFFOLDS.</u>	177
<u>FIGURE 67. PREDICTED ACTIVATED UPSTREAM REGULATORS OF RNASEQ DATA OF UNTREATED VS GEMCITABINE TREATED PANC-1 CELLS CULTURED ON PANCREAS SCAFFOLDS.</u>	178
<u>FIGURE 68. PREDICTED INHIBITED UPSTREAM REGULATORS OF RNASEQ DATA OF UNTREATED VS GEMCITABINE TREATED PANC-1 CELLS CULTURED ON PANCREAS SCAFFOLDS.</u>	179
<u>FIGURE 69. PATHWAY MAP FOR DNA REPLICATION REPRESENTING THE SIGNIFICANTLY DIFFERENTIALLY EXPRESSED GENES FROM RNASEQ OF UNTREATED VS GEMCITABINE TREATED PK-1 CELLS CULTURED ON LIVER SCAFFOLDS.</u>	187
<u>FIGURE 70. PREDICTED ACTIVATED UPSTREAM REGULATORS OF RNASEQ DATA OF UNTREATED VS GEMCITABINE TREATED PK-1 CELLS CULTURED ON PANCREAS SCAFFOLDS.</u>	188

FIGURE 71. PREDICTED INHIBITED UPSTREAM REGULATORS OF RNASEQ DATA OF UNTREATED VS GEMCITABINE TREATED PK-1 CELLS CULTURED ON PANCREAS SCAFFOLDS. 189

FIGURE 72. MMP9 GENE EXPRESSION OF PK-1 AND PANC-1 CELLS CULTURED ON LIVER AND PANCREAS SCAFFOLDS...... 203

FIGURE 73. GEMCITABINE: TRANSPORT, INTRACELLULAR ACTIVATION/DEACTIVATION AND MECHANISM OF ACTION. 210

TABLE OF TABLES

<u>TABLE 1. DECELLULARISATION METHODS; MODE OF ACTION AND EFFECT ON THE ECM.....</u>	35
<u>TABLE 2. STAGES OF PANCREATIC CANCER AS DEFINED BY AJCC.....</u>	41
<u>TABLE 3. RELATIVE PANCREATIC CANCER 5-YEAR SURVIVAL BY STAGE.</u>	45
<u>TABLE 4. MULTI-DRUG REGIMENS FOR TREATMENT OF LOCALLY ADVANCED AND METASTATIC PDAC.</u>	46
<u>TABLE 5. SELECTED TARGETED THERAPIES AND IMMUNOTHERAPIES FOR PDAC.</u>	52
<u>TABLE 6. GEMCITABINE-BASED COMBINATION THERAPIES.</u>	57
<u>TABLE 7. KEY FACTORS INFLUENCING INCREASED SENSITIVITY TO GEMCITABINE.....</u>	60
<u>TABLE 8. KEY FACTORS INFLUENCING INCREASED RESISTANCE TO GEMCITABINE.</u>	61
<u>TABLE 9. PROTOCOL FOR THE DECELLULARISATION OF HUMAN LIVER CUBES BY AGITATION.....</u>	67
<u>TABLE 10. PROTOCOLS FOR THE DECELLULARISATION OF HUMAN PANCREAS CUBES BY AGITATION.</u>	69
<u>TABLE 11. PROTOCOL FOR THE DECELLULARISATION OF WHOLE HUMAN PANCREAS HP1 BY PERFUSION.....</u>	70
<u>TABLE 12. PROTOCOL FOR THE DECELLULARISATION OF WHOLE HUMAN PANCREAS HP2 BY PERFUSION USING BIOREACTOR.</u>	71
<u>TABLE 13. PROTOCOL FOR THE DECELLULARISATION OF WHOLE HUMAN PANCREAS HP3 BY PERFUSION USING BIOREACTOR.</u>	72
<u>TABLE 14. PREPARATION OF 2X REVERSE TRANSCRIPTION MASTER MIX.</u>	79
<u>TABLE 15. PROGRAM OF THE THERMAL CYCLER.</u>	79
<u>TABLE 16. LIST OF TAQMAN GENE IN THE ARRAY PLATE AND THEIR CORRESPONDING ID'S.</u>	80
<u>TABLE 17. LIST OF INDIVIDUALLY TESTED TAQMAN GENES AND THEIR CORRESPONDING ID'S.</u>	80
<u>TABLE 18. GENE ONTOLOGY TERMS OF RNASEQ DATA OF PANC-1 CELLS ON PANCREAS VS LIVER SCAFFOLDS.</u>	130
<u>TABLE 19. SIGNIFICANTLY IMPACTED PATHWAYS FROM RNASEQ DATA OF PANC-1 CELLS ON PANCREAS VS LIVER SCAFFOLDS.</u>	132
<u>TABLE 20. GENE ONTOLOGY TERMS OF RNASEQ DATA OF PK-1 CELLS ON PANCREAS VS LIVER SCAFFOLDS.</u>	140
<u>TABLE 21. SIGNIFICANTLY IMPACTED PATHWAYS FROM RNASEQ DATA OF PK-1 CELLS ON PANCREAS VS LIVER SCAFFOLDS. PATHWAYS ARE ORDERED BY SIGNIFICANCE (LOWEST P-VALE TO HIGHEST).....</u>	142
<u>TABLE 22. GENE ONTOLOGY TERMS OF RNASEQ DATA OF GEMCITABINE TREATED VS UNTREATED PANC-1 CELLS ON PANCREAS SCAFFOLDS.....</u>	175
<u>TABLE 23. SIGNIFICANTLY IMPACTED PATHWAYS FROM RNASEQ DATA OF GEMCITABINE TREATED VS UNTREATED PANC-1 CELLS ON PANCREAS SCAFFOLDS.</u>	176
<u>TABLE 24. GENE ONTOLOGY TERMS OF RNASEQ DATA OF GEMCITABINE TREATED VS UNTREATED PK-1 CELLS ON LIVER SCAFFOLDS.</u>	184
<u>TABLE 25. SIGNIFICANTLY IMPACTED PATHWAYS FROM RNASEQ DATA OF GEMCITABINE TREATED VS UNTREATED PK-1 CELLS ON LIVER SCAFFOLDS.....</u>	186

LIST OF ABBREVIATIONS

5-FU	Fluorouracil
ABC	ATP-Binding Cassette Protein
ABCB1	ATP-Dependent Translocase ABCB1
ABCG2	Broad Substrate Specificity ATP-Binding Cassette Transporter ABCG2
AJCC	American Joint Committee On Cancer
ATP	Adenosine Triphosphate
BD	Branch Duct
CAFs	Cancer-Associated Fibroblasts
CD133	Cluster Of Differentiation 133
CEA	Carcinoembryonic Antigen
CHAPS	3-[(3-Cholamidopropyl)Dimethylammonio]-1-Propanesulfonate
CTLA-4	Cytotoxic T-Lymphocyte-Associated Protein 4
dCK	Deoxycytidine Kinase
DFS	Disease-Free Survival
DNA	Deoxyribonucleic Acid
dsDNA	Double Stranded Deoxyribonucleic Acid
ECM	Extracellular Matrix
EDTA	Ethylenediaminetetraacetic Acid
EGF	Epithelial Growth Factor
EGFR	Epithelial Growth Factor Receptor
EMT	Epithelial-To-Mesenchymal Transition
ERK	Extracellular Regulated Kinases
FDA	U.S. Food And Drug Administration
FL	Follicular Lymphoma
GAGs	Glycosaminoglycans
Gem	Gemcitabine
H ₂ O	Water
HA	Hyaluronic Acid
hENT1	Human Equilibrative Nucleoside Transporter 1
HER2	Human Epidermal Growth Factor Receptor 2
HGF	Hepatocyte Growth Factor
IGF	Insulin-Like Growth Factor Receptor
IGFR	Insulin-Like Growth Factor Receptor
IL	Interleukin
IPMNs	Intraductal Papillary Mucinous Neoplasms
JAK	Janus Kinase
KRAS	Kirsten Rat Sarcoma Viral Proto-Oncogene
MAPK	Mitogen-Activated Protein Kinase
MCN	Mucinous Cystic Neoplasm
MD	Main Duct
MEK	Mitogen-Activated Protein Kinase Kinase
MET	Mesenchymal -To- Epithelial Transition
mOS	Mean Overall Survival

MRPs	Multidrug Resistance Proteins
mTOR	Mammalian Target of Rapamycin
NF-κB	Nuclear Factor Kappa-Light-Chain-Enhancer of Activated B Cells
NICE	National Institute for Health And Care Excellence
NIH	National Institutes of Health
OS	Overall Survival
PanIN	Pancreatic Intraepithelial Neoplasia
PBS	Phosphate Buffered Saline
PBT	Polybutylene Terephthalate
PCU	Polycarbonate-Urethane
PDAC	Pancreatic Ductal Adenocarcinoma
PDGF	Platelet-Derived Growth Factor
PDLA	Poly(D-Lactic Acid)
PDLLA	Poly(DL-Lactic Acid)
PEFG	Cisplatin, Epirubicin, 5-Fluorouracil, Gemcitabine
PEG	Polyethylene Glycol
PFS	Progression-Free Survival
PGA	Polyglycolide
PI3K	Phosphoinositide 3-Kinase
PLA	Poly(Lactic) Acid
PLGA	Poly(Lactic-Co-Glycolic Acid)
PLLA	Poly(L-Lactic Acid)
POSS	Polyoligosilsesquioxanes
PS	Performance Status
PSCs	Pancreatic Stellate Cells
PTEN	Phosphatase and Tensin Homolog
RNA	Ribonucleic Acid
ROS	Reactive Oxygen Species
RR	Response Rate
RRM1	Ribonucleotide Reductase Catalytic Subunit M1
RRM2	Ribonucleotide Reductase Catalytic Subunit M2
RUNX3	Runt-Related Transcription Factor 3
SA	Single Arm
SDC	Sodium Dodecyl Sulfate
SDS	Sodium Deoxycholate
SEER	National Cancer Institute, Surveillance, Epidemiology, And End Results
SHH	Sonic Hedgehog
SMV	Superior Mesenteric Vein
STAT3	Signal Transducer and Activator of Transcription 3
T2R10	Taste 2 Receptor Member 10
T2R38	Taste 2 Receptor Member 38
TAMs	Tumor-Associated Macrophages
TGF	Transforming Growth Factor
TK	Thymidine Kinase
TNF	Tumor Necrosis Factor
TNM	Timour-Nodes-Metastasis

TRIS	Trisaminomethane
U87-MG	Uppsala 87 Malignant Glioma
UCL	University College London
UK	United Kingdom
USA	United States of America
VEGF	Vascular Endothelial Growth Factor
VEGFR	Vascular Endothelial Growth Factor Receptor
vs	Versus

• CHAPTER 1 •

“I think there are two keys to being creatively productive. One is not being daunted by one's fear of failure. The second is sheer perseverance.”

- *Mary-Claire King*

1. INTRODUCTION

1.1 Background and Vision

Over 50% of patients with pancreatic cancer are diagnosed at the metastatic stage and die due to the debilitating metabolic effects of their unrestrained growth (1). Despite efforts in the past 50 years, conventional treatment approaches have had little impact on the course of this aggressive neoplasm. Therefore, the development of new treatment strategies to control cancer growth and metastasis is of immediate urgency. Fulfilment of this challenging task relies on our knowledge of the cellular and molecular biology of both primary and metastatic pancreatic cancer and the use of suitable 3D extracellular matrix (ECM) models will undoubtedly help defining individual and collective aspects of this complicated process.

1.1.1 Three Dimensional Scaffolds

Tissue engineering has recently emerged as an exciting field for both regenerative medicine and *in vitro* 3D cell cultures (Figure 1). The focal point of tissue engineering since its emergence has been biomaterials, as it is the most understudied and challenging component amongst the three pillars of tissue engineering, i.e. scaffolds, cells, and growth factors. All biomaterials have one role, and that is to mimic the ECM, which is composed of multiple protein components depending on the tissue source. Although some tissue contain the same components such as collagen, glycosaminoglycans, fibronectin and different growth factors, it is according to Martinez-Hernandez and Amenta, “the different concentrations, ratios, and associations of these components that result in an ECM tailored to the needs and functions of specific organs” (2). Therefore, the ECM components define cellular processes required for sufficient function of tissues and organs (3, 4).

1.1.1.1 Biological Scaffolds: Decellularised Tissue

Decellularised tissue scaffolds are derived by stripping tissues or organs of their native cellular material while attempting to retain as much of the ECM components, microarchitecture and microscale biomechanical properties and functions as possible, in the form of the ECM. There are many strategies available to achieve this, and the best combination depends on the composition of individual tissues (further described in section 1.2).

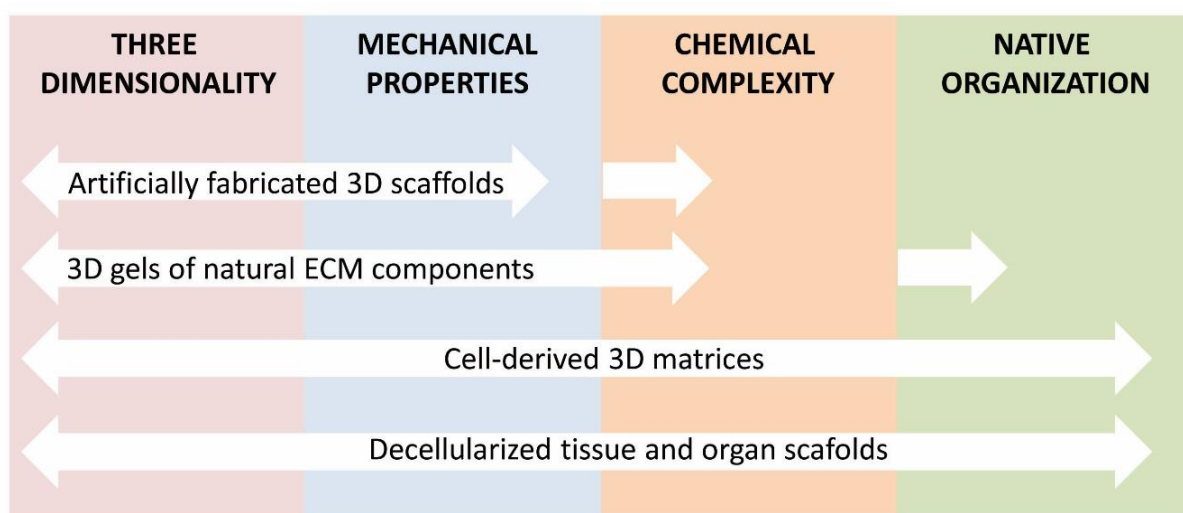


Figure 1. Schematic comparison of different 3D scaffolds. Decellularised tissue and cell-derived matrices comprise all four characteristics of 3D scaffolds; three dimensionality, mechanical properties, chemical complexity and native organisation. Artificially fabricated and gel scaffolds are less complex and only possess some of these features. Image from Evangelatov et al (5)

1.1.1.2 Biological Scaffolds: Natural Polymers

Natural polymers are those derived from “natural sources” such as animal/human tissue or plants. These include polymers derived from the ECM such as; collagen, laminin, elastin, fibronectin and GAGs. Collagen, a family of at least 29 members (6), is the most abundant protein in all mammals (7). They serve different functions but are all defined by a triple helix of proline rich tripeptide Gly-X-Y (8). Collagen scaffolds have been investigated concerning heart valves (9), lung cancer (10), pancreas

cultures (11), renal regeneration (12) among others. An advantage of collagen scaffolds includes the abundance of the protein, which could also represent one of its disadvantages; where collagen 1, 3 and 4 can be produced with relative ease but the remaining collagens are rarer and much harder to isolate. Additionally, another evident disadvantage is the cross-linkers used to maintain the 3D architecture which usually involves cytotoxic substances e.g. glutaraldehyde (13).

Chitosan is an example of a natural polymers found on the exoskeleton of crustaceans and insects or the cell wall of fungi (14). It is produced from chitin to form a linear polysaccharide of de-acetylated and acetylated glucosamine (15) which can be cross-linked to produce scaffolds (16). Chitosan based scaffolds, usually in combination with other polymers, have been studied for several tissue engineering applications that include skin (17-19), bone (20, 21), cartilage (22-24), liver (25, 26) and pancreas (27-29) among others. Chitosan scaffolds are commonly fabricated into two forms; hydrogel or sponges, which have similar advantages but different disadvantages. Advantages of chitosan include biodegradability (30, 31), bio- and cyto-compatibility (32) and modifiable mechanical properties (33-35). However, chitosan is very hard to solubilise (36) and chitosan hydrogel was found to produce uncontrollable dissolutions (37) along with undesirable cross-linking (38). On the other hand, chitosan sponges were found to shrivel and have low porosity (39).

Agarose is another natural polymer extensively used in the field of tissue engineering. It is extracted from Agar which is found in the algae Rhodophyta and is also a linear polysaccharide of repetitive agarobiose (40). Agarose scaffolds are most commonly produced either as layers of fibres or as hydrogels. Examples of agarose fiber scaffolds that have been used for tissue engineering include application in wound healing (41, 42) and neural tissue repair (43). Agarose hydrogels make them more suitable for a larger amount of scaffold applications which include that for cartilage (44, 45), vascularisation (46), spinal cord (47), pancreas (48) and liver (49). Agarose is an appropriate material in the field of tissue engineering as it's easily accessible, highly soluble, biodegradable and biocompatible (50). A few notable disadvantages of using agarose include difficulties in pre-encapsulating cells within the scaffold due to a high

gelling temperature, even though successful efforts into reducing the gelling point, but with a higher cost, have been established.

1.1.1.3 Synthetic Scaffolds

These scaffolds are composed of synthetic polymers produced through a chemical process. The major classes of degradable polymers used in the field of tissue engineering are polyesters, polyether esters and polyurethanes because of their ability to be easily tailored to suite desirable mechanical properties, pore sizes and degradation kinetics. Examples of polyesters include polyglycolic acid (PGA), polylactic acid (PLA) and their copolymers. PGA is used extensively as a mesh, due to its rapid degradation *in vivo* (51). Whereas, PLA is less prone to degradation owing to its higher degree of hydrophobicity (52). PLA can be produced in different forms that include L or D enantiomers (PLLA and PDLA) and a combination of both (PDLLA) (53). These forms have shown to be highly successful for cell attachment and proliferation (54). Further, copolymerisation of PGA and PLA (PLGA) has been fabricated and used extensively in tissue engineering as it combines the advantageous properties of both polymers. Indeed, it is one of the most used synthetic polymer in tissue engineering (55) and has been utilised for liver (56), skin (57), skeletomuscular (58-60) and nerve studies (61). As a result of extensive studies on polyesters, their limitations are very well recognised and include acidic by-products (62), non-specific signalling to cells (63) and an inflammatory response (64) and graft necrosis (65) when implanted.

Polyether esters are most commonly found in the field of tissue engineering as polyethylene glycol (PEG) and polybutylene terephthalate (PBT). Indeed, the combination of PEG and PBT as scaffolds has attracted much research due to their elasticity and stiffness, respectively (66). This research has focused mainly on bone regeneration, as has been demonstrated by several groups, which presented an excellent capability of PEG/PBT to adhere bone marrow stromal cells and enhance bone bonding (67). PEG and PBT have also been explored for other tissue, mainly for microencapsulation of cells, including hepatocytes (68) and islet cells (69). Studies

have shown that unmodified polyether esters, when transplanted, cause ROS induction and injury to endogenous tissue (70), while coated/modified polyether esters resulted in a reduction of protein absorption within the scaffolds (71).

Polyurethanes have been regarded unworthy in the field of tissue engineering for many years due to its toxic by-product 2,4-diaminotoluene (72). This has recently changed when research on the conjugated form of polycarbonate urethanes (PCU), a polyurethane, with polyhedral oligomeric silsesquioxane (POSS) was found to eliminate the degradation of 2,4-diaminotoluene and form a strong and highly viscoelastic nanocomposite (73). POSS-PCU has been used extensively for vascular tissue engineering due to its ability to increase the viability of endothelial cells (74). Additionally, POSS-PCU has been explored for cardiovascular bypass grafts (75), lacrimal ducts (76), and tracheas (77). Overall, not enough studies have been performed on POSS-PCU for limitations to be determined, however transplanted POSS-PCU tracheas proved to be controversial with all patients being deceased shortly after the procedure (78). Additionally, comparisons of different trachea grafts after transplantation in animals showed that POSS-PCU had worst morbidity and mortality compared to Herberhold and decellularised grafts (79).

1.1.2 2D versus 3D cultures

2D cultures have represented the primary approach used in molecular and cell biology research. Much of the 21st century's scientific breakthroughs have taken place on 2D cell cultures. However, 2D cell cultures have also demonstrated various limitations depending on the cell type used. A significant limitation associated with 2D cultures is irregular cell growth, which was represented by Hess et al. using a human glioblastoma cell line U87-MG (80). Such limitations include the unnatural, stiff and flat (monolayered) polystyrene dishes, which results in denatured and distorted cells (80). Additionally, the area of the cell attached to the plastic is not suitable for cellular uptake, and this makes cell survival a more significant challenge (81). Therefore, 2D cultures significantly alter cell morphology, which is highly regulated by cell-matrix and cell-cell attachment.

To overcome these limitations, 3D cultures were introduced. Naderi et al. observed that in 3D cultures, the growth environment mimics the natural conditions of organs and tissues (82). This nature of 3D cultures promotes physical cell-cell attachments and helps to generate cells with natural structures and compositions (83, 84). Also, 3D bioscaffolds allow cells to have more gap junctions than 2D cultures (85). Gap junctions' advance cell-cell communication through the exchange of molecules, electrical currents, and ions (Figure 2). This property of 3D bioscaffold cultures, and more specifically decellularised scaffolds, encourages gene expression in cells and thus overcomes the unnatural signal transduction experienced with 2D cultures (86).

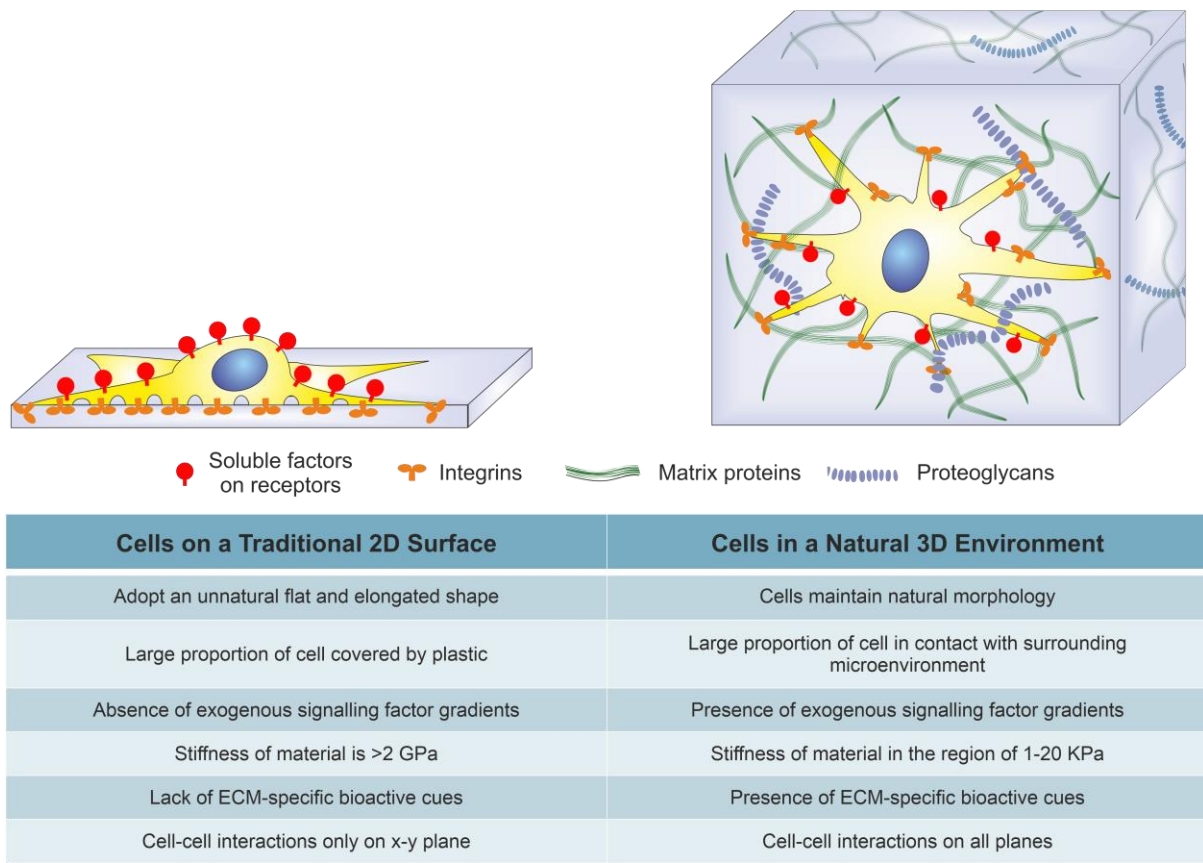


Figure 2. Schematic comparing effect of 2D and 3D cultures on cells. 3D culture microenvironments maintain essential cellular cues. Image adapted from Baker and Chen (87)

1.1.3 Animal Models *versus* 3D Decellularised Scaffolds

Animal models are critical in experimental testing as they can be used to investigate disease progression and to study the impact of drugs *in vivo*. According to Hartung, like all models, animal models too have their limitations (88). One of the critical barriers associated with animal models in experimental testing is the insufficient correlation between animal/rodent experiments and humans. Moreover, where same experimental procedures were performed on distinct animal species, the correlation was found to be only 70% (88). In this regard, animal model experiments have critical inaccuracies. The second major limitation considers variation in the pharmacology of drugs between humans and animals. There are usually significant differences regarding drugs pharmacokinetics between humans and animals. This makes it difficult to directly relate results obtained from animal model experiments to human conditions (89).

With the introduction of decellularised scaffold as 3D *in vitro* cultures, many of the limitations connected with animal models can be eliminated. To begin, Robinson states that 3D bioscaffold cultures can overcome inaccuracies experienced while using animal models, by helping researchers detect potential changes that will take place in humans (90). This is because bioscaffold cultures use preserved human matrices (91). Using decellularised scaffolds, human cells and tissues that resemble the natural human organs can be produced. This makes it possible to predict the real toxicological impacts that a drug may have on humans (90). An additional benefit of 3D bioscaffold cultures is that the ethical issues encountered with animal models could be eliminated (92).

1.1.4 Importance of 3D Cultures for Pharmaceuticals

Pharmaceutical companies are becoming increasingly wary of the expenses incurred in exploring and developing new drugs. In 2010, Eli Lilly and Company conducted a study to estimate the costs incurred in drug discovery and development (93). Using data from 2008 and of thirteen major pharmaceuticals, the study found that \$1.8 billion

was the entire cost incurred while producing a single drug (93). Despite the staggering amounts spent on drug discovery and development, drug failures are witnessed in many companies, and these failures are typically detected during human clinical trials (93). At the heart of drug failures lie inadequate and unreliable drug screening processes that primarily depend on 2D *in vitro* cell cultures (Figure 2), or on animal models (94).

3D bioscaffold cultures can be introduced to help pharmaceuticals overcome this challenge, by closing the gap between 2D cultures and animal models as well as animal model and human trials. Growing cells in decellularised scaffolds enables drugs to be tested on native *in vitro* human tissue and cells (95, 96). Thus, the potential toxic effects and ineffective components of drugs can be established and investigated adequately before the clinical trials (97). 3D bioscaffold cultures also deliver exhaustive culture information, which is predictive of the *in vivo* drugs responses and representative of tissue morphology (98). In summary, the features that 3D bioscaffolds can offer will significantly advance drug screening processes, which would help pharmaceuticals reduce costs connected with failed drugs and animal experiments (99).

1.2 Tissue Decellularisation

Several factors need to be taken into consideration when attempting to develop an effective decellularisation protocol. This is due to the distinct composition of the different types of tissue. A good example of this high ECM variability between different tissues/organs would be healthy pancreas tissue compared to healthy tendon tissue; i) the pancreas is composed of more than 8 cell types (100), whereas tendons are composed of only two (101, 102). ii) The pancreas has a hydroxyproline density of 20,000-34,000 ug/g of dry tissue (103) compared to the tendon's 12,000-20,000 ug/g of dry tissue (104). iii) The pancreas is packed as layers of ECM interconnected by supporting connective tissue (105), whereas tendons have a fibril and fascicle packing

ECM structure (106). These factors are only 3 out of many variables that can affect the decellularisation profile of the tissue in hand and therefore, for optimal results, the reagents and protocols employed should not only be generalised to the specific tissue type, but also to specific characteristics of the tissue, e.g. disease or healthy. This section will review the mechanisms and reagents used in literature for tissue decellularisation (Table 1), while focusing on those that can be most useful for healthy pancreas tissue.

1.2.1 Physical Forces

Regardless of the reagents used, there should always be some sort of mechanical or physical aspect to the protocol. Tissue placed in reagents in a static state would certainly not cause it to decellularise. The two main reasons for this is that 1) the reagents need to be flushed through the tissue to be able to reach into its core and 2) a mechanical and physical stress to the cells would lead to a much more efficient cell lysis. It is the mechanical and physical forces that lead to faster and more efficient decellularisation protocols/systems.

1.2.1.1 Temperature

Researchers have extensively used freeze-thaw cycles for tissue decellularisation. The rationale behind such cycles is to cause cell lysis by the ice crystals forming during freezing. The protocol normally includes freezing the tissue to around -75 °C and then rapidly thawing it back to around 37 °C. This method has proved to be extremely effective at breaking cells apart in several tissue types, including adipose tissue (107), lung (108), tendons (102, 109), ligaments (110) and nerve (111). The freeze-thaw protocol needs to be carefully controlled as the ice-crystals can also disrupt the ECM ultrastructure. This has been demonstrated by both Prasertsung *et al.* while decellularising porcine skin, and Hopkinson *et al.* while decellularising amniotic membrane (112, 113). While freeze-thaw cycles have been used for low ECM density,

e.g. lung decellularisation, the effort needed to keep all condition exceptionally controlled could eclipse the advantages of using such a method (114). It is clearly noticeable that using freeze-thaw cycles for decellularisation is more useful and less destructive to tissues with denser ECM. Such limitations explain the lack of publications that use freeze-thaw cycles for liver decellularisation.

1.2.1.2 Agitation

Agitation is the mechanical abrasion of cells within the tissue. Several techniques/systems have been used to cause this effect. These can be summed up into two categories, direct and indirect mechanical agitation. Sonication is a form of indirect mechanical agitation, in which sound waves (>20 kHz) are used to agitate particles within the cells, which in turn causes cell lysis. Sonication is not a common technique, but has been used by several labs for tissue decellularisation, including heart and small intestine tissue (115-118). The reason for this is that, similar to freeze-thaw cycles, sonication cannot be used during the whole protocol, and is mainly used as an additional step within a protocol. Therefore, sonication is usually followed by another agitating process during chemical and enzymatic treatments for it to be effective (118, 119). Olivier *et al.* tested several decellularisation techniques, which included sonication, and found that sonication on its own is ineffective for complete tissue decellularisation. The only exception to this is a novel system developed by Azhim *et al.*, which allows for continuous sonication, at 170 kHz frequencies, while aortic tissue is being treated with chemical reagents. Azhim and collaborators managed to slightly reduce the overall time needed for complete decellularisation (120, 121).

Another system used for agitation is a shaker, which involves a flat board moving in horizontal rotational oscillations. The first use of such agitation for the purpose of decellularisation was performed by Brendel *et al.* in 1989 (122). Since then, many labs have picked up on this, and it has become the most commonly used technique for direct mechanical agitation during decellularisation (122-128). Unfortunately, none of the papers that mention the use of a shaker reveal the speed of the oscillation used,

and only one patent does (124). Yet again, the patent by Bishopric *et al.* describes the speed in rpm (110 rpm precisely), not in G-force, which does not indicate anything without diametric measurements of the shaker's plate (124, 129). This could explain why no one else describes the speed, as it is difficult to calculate the diameter of movement of a shaker.

Direct and indirect mechanical agitations have similar effect on the tissue. If all other variables are null (e.g. time, chemical and enzymatic reagents), then both direct and indirect agitation results in a well preserved ECM. Thus, the challenge lies in the exploitation of these agitations, and to what extent they can be used to compromise between time and ECM preservation.

1.2.2 Hypotonic and Hypertonic Solutions

Hypotonic and hypertonic solutions are primarily used to cause an osmotic shock to the cells, leading to the burst of the cells. Hypotonic solutions lead to the flow of water from the solution into the cells in an attempt to equilibrate the water concentration inside and outside the cell. The opposite is true for hypertonic solutions. It is assumed that a hypertonic solution has a greater effect on the nucleus in comparison to the actual cell membrane. Regardless, almost all decellularisation techniques include some sort of hypotonic or hypertonic solution (125, 130, 131). A hypotonic solution usually consists of distilled water, although in some cases TRIS buffer has been added to the distilled water to make it more hypotonic (124).

1.2.3 Chemical Agents

1.2.3.1 *Acids and Bases*

Acids and bases are known for their catabolic effect on proteins. Acids tend to oxidize proteins and cellular debris whereas bases usually reduce them. This causes the denaturation of proteins by disrupting the quaternary, tertiary and secondary structure of proteins. Furthermore, acids and bases disrupt nucleic acids thereby, breaking down RNA and DNA. De Filippo *et al.* showed that using ammonium hydroxide as part of the decellularisation protocol resulted in the removal of cellular remnants (132). Peracetic acid, best known for sterilisation, is also used during decellularisation. It is alleged that peracetic acid is useful for DNA and RNA removal, as it is effective at breaking down the phosphate backbone and therefore, making the removal of nucleic acids from tissue much more efficient (133). Other acids including; hydrochloric acid (84), acetic acid (134) and sulphuric acid (135) have also been recognised as positive additives to decellularisation protocols. Although the aforementioned is desirable for decellularisation, acids also affect the ECM equally. Many acids including those mentioned above have displayed undesirable effects; mainly by lysing essential molecules such as glycosaminoglycans (GAGs) from collagenous tissue (136). Bases on the other hand are usually avoided as decellularisation reagents. Bases are known for their aggressive mode of action. In this case, they have a catastrophic effect on growth factors within the ECM. They also decrease the mechanical properties of the tissue in hand. This is due to the cleavage of collagen fibrils (137).

1.2.3.2 *Ionic and Non-ionic Detergent*

All publications involving tissue decellularisation use at least one ionic or non-ionic detergent within their decellularisation protocol. There is no perfect detergent and each detergent has both its advantages and disadvantages. As mentioned earlier, the efficiency of decellularisation greatly depends on the time of exposure of the tissue to the reagents, which in turn varies significantly according to; (i) the type of tissue, (ii) the species of which the tissue has been obtained from, (iii) age of the donor and (iv) the state of the tissue (i.e. diseased *versus* healthy).

Non-ionic detergents function by cleaving lipid-lipid and lipid-protein interactions. On the other hand, they cannot process protein-protein interactions, meaning that ECM proteins should be preserved following non-ionic treatment (138). One non-ionic reagent that has stood out from the rest is Triton X-100. Searching for the topic “triton” and “decellul*” results in 227 publications on webofknowledge.com, which is only bettered by “SDS” (see ionic reagents) resulting in 269 publications. As expected, Triton X-100 differed greatly in its efficiency to remove cells between tissues. A study by Dahl *et al.* demonstrated that using Triton X-100 was not effective enough at eliminating cellular or nuclear debris from vessels (125). Whereas another study by Grauss *et al.*, found that using Triton X-100 on aortic valves was efficient at removing nuclear material, but ineffective at removing cellular debris (139). In another study on mice livers, Triton X-100 managed to completely decellularise the tissue (140). Regardless of the decellularisation efficacy, in all three mentioned studies, Triton X-100 managed to preserve collagen’s integrity, but left almost no GAGs attached. It is obvious that Triton X-100 can be beneficial for tissue decellularisation, but again, all factors mentioned earlier should be considered, including other chemical/enzymatic reagents that could be used in conjunction with Triton X-100.

On the other hand, ionic detergents, whose mode of action is almost the opposite to that of non-ionic detergents, are effective in disrupting protein-protein interactions, meaning they are successful at destroying cellular debris, but also at destroying key components of the ECM. Two widely used ionic detergents are Sodium dodecyl sulfate (SDS) and Sodium deoxycholate (SDC). Starting with SDS, it appears that it is the most effective detergent if all variables are considered. Most publications, regardless of the tissue used, seem to agree that SDS removes most of the cellular components and manages to break down the nuclear membrane, leaving behind a small fraction of nuclear waste (91, 130, 141-145). Unfortunately, all papers also agree that SDS alters the ECM, disrupting the integrity of collagen (91, 130, 141-145). It also removes GAGs from the ECM, although not to the extent of Triton X-100 (146). Another limitation of SDS is the fact that it is very hard to wash out of the tissue, some researchers have solved this issue by following SDS with Triton X-100, but as mentioned earlier, this would be catastrophic to anyone wishing to preserve GAGs (147).

SDC is very similar to SDS, with the exception that SDC removes more of the cellular components and breaks down the nuclear membrane (91, 130, 141-145). It is argued in several publications that SDC causes greater damage to the ECM than SDS, but it is hard to prove such claims, as SDC is ineffective on its own, and therefore it is hard to prove that SDC is solely responsible for the damage. SDC is usually also followed by some sort of DNA/RNA extracting agent (e.g. nucleases) (148).

1.2.3.3 Other reagents

Other reagents are also used for decellularisation, including zwitterions and chelating agents. These reagents are commonly combined to ionic or non-ionic detergents. Zwitterions are special because they contain both ionic and non-ionic properties. An example of a zwitterion used in decellularisation is 3-[(3-cholamidopropyl)dimethylammonio]-1-propanesulfonate (CHAPS). CHAPS and zwitterions, in general, are harsher on ECM proteins, as they are a stronger protein inhibitor. Petersen *et al.* attempted to decellularise lung tissues with a high concentration of CHAPS, and no ionic or non-ionic reagents (149). The authors managed to demonstrate that collagen was fully retained, but there was a significant decrease in the amount of elastin and GAGs available after decellularisation (149).

Chelating reagents are ions that form a specific ring shape and bind to metal ions (150). This makes chelating reagents useful in detaching cells from the ECM. This is accomplished by breaking the calcium and magnesium ions needed for cell attachment (151). EDTA, the most used chelating agent and similar to CHAPS, is hardly ever used on its own. Other reagents, e.g. SDS, SDC or Triton X-100 need to be used prior to EDTA to lyse cells into debris, which would then allow EDTA to work more efficiently at flushing cell debris out the ECM (123, 152, 153).

1.2.4 Enzymatic Reagents

Enzymatic reagents can be categorised into: (i) enzymes that aim to detach cells from the ECM, e.g. trypsin and (ii) those that aim to break down and remove nuclear material, e.g. nucleases. Trypsin is widely used in 2D cultures to detach adherent cells, and therefore, in conjunction with EDTA, was used much more frequently during the late 1990s and early 2000s for the decellularisation process. With time, investigators realised that trypsin has drastic effects on the ECM and almost completely removed elastin, fibronectin, laminin and GAGs (123, 152, 153). Nucleases on the other hand, have little or no effect on the ECM, but are not without an adverse effect on the overall outcome of tissue. Nucleases are used when other reagents e.g. SDS, SDC or Triton X-100, do not manage to remove enough nuclear material, under what is accepted (“<50 ng dsDNA per mg ECM dry weight”) (154). The amount of DNA removed has been demonstrated to have a direct correlation to agitation speed. In other words, faster agitation speed would result in a better flow of reagents through the tissue, which in turn would result in a more efficient flush of nuclear material out of the tissue (154). Nevertheless, increasing speed of agitation could result in a higher ECM damage. Therefore, as most protocols use mild agitation, nucleases are often used (126, 130, 149, 155); though, nucleases are hard to remove from the tissue, and therefore there have been arguments regarding the immunogenic response that can be caused by the nucleases themselves.

Method	Mode of action	Effects on ECM	Ref.
Physical forces			
<i>Snap freezing</i>	Intracellular ice crystals disrupt cell membrane	ECM can be disrupted or fractured during rapid freezing	(102, 107-114)
<i>Direct mechanical agitation</i>	Can cause cell lysis, but more commonly used to facilitate chemical exposure and cellular material removal	Aggressive agitation can disrupt ECM as the cellular material is removed	(122-129)
<i>Sonication</i>	Can cause cell lysis by disrupting cell membrane	Aggressive sanitation can disrupt ECM as the cellular material is removed	(115-121)
Chemical Agents			
<i>Acids and Bases</i>	Solubilises cytoplasmic components of cells, disrupts nucleic acids, tend to denature proteins	May damage collagen, GAG, and growth factors	(84, 132-134) (135-137)
<i>Hypotonic and Hypertonic solutions</i>	Cell lysis by osmotic shock, disrupt DNA-protein interactions	Effectively lyses cells, but does not effectively remove cellular residues	(124, 125, 130, 131)
Non-Ionic detergents			
<i>Triton X-100</i>	Disrupts lipid–lipid and lipid–protein interactions, while leaving protein–protein interactions intact	Mixed results; efficiency dependent on tissue, removes GAGs	(125, 138-140)
Ionic detergent			
<i>Sodium dodecyl sulphate (SDS)</i>	Solubilises cytoplasmic cells and nuclear cellular membrane tends to denature proteins	Removes nuclear remnants and cytoplasmic proteins; tends to disrupt native tissue structure, remove GAGs and damage collagen	(91, 130, 141-145)
<i>Sodium deoxycholate (SDC)</i>	Very similar mechanism to SDS	Mixed results with efficacy dependent on tissue thickness, some disruption of ultrastructure and removal of GAG	(91, 130, 141-145, 148, 150)
Zwitterionic detergents			
<i>CHAPS</i>	Exhibit properties of non-ionic and ionic detergents	Efficient cell removal with ECM disruption similar to that of Triton X-100	(149)

<i>EDTA</i>	Chelating agents that bind divalent metallic ions, thereby disrupting cell adhesion to ECM	No isolated exposure, typically used with enzymatic methods (e.g., trypsin)	(123, 150-153)
Enzymes			
<i>Nucleases</i>	Catalyze the hydrolysis of ribonucleotide and deoxyribonucleotide chains	Difficult to remove from the tissue, could invoke an immune response	(126, 130, 149, 154, 155)
<i>Trypsin</i>	Difficult to remove from the tissue, could invoke an immune response	Prolonged exposure can disrupt ECM ultrastructure, removes ECM constituents such as collagen, laminin, fibronectin, elastin, and GAG, slower removal of GAG compared to detergents	(123, 152, 153)

Table 1. Decellularisation methods; mode of action and effect on the ECM. Adapted from Crapo et al. 2011 and Gilbert et al. 2006 (150, 154).

1.3 Pancreas Anatomy, Function and Diseases

1.3.1 Macro and Microanatomy of the Pancreas

In a retroperitoneal manner, the pancreas is situated at the level of the first lumbar vertebrae (L1) and the third lumbar vertebrae (L3) (156). On average, the pancreas is 15 cm in length, 3 cm in breadth, 1.5 cm in thickness and weighs about 100 grams (157, 158). The head of the pancreas is the most extensive section, while the tail is the thinnest. Superior to the pancreas lays the lesser sac, the transverse mesocolon is situated on its anterior, and the greater sac is to its inferior (Figure 3) (158).

The head of the pancreas is located within the concavity of the duodenum on the right side of the human body and is elongated inferiorly and medially to cover the region posterior to the superior mesenteric vessels (SMV) (Figure 3) (159). The inferior half

of the head extends towards the left side of the human body forming the uncinata process that is located between SMV and aorta. Its neck is the constricted portion of the gland lying anteriorly to the SMV while the body is a horizontal portion that lies behind the stomach and the lesser sac. The splenic vein is situated dorsally to the body whereas the neck is located between the celiac trunk and the SMV and has an average length of 1.5 cm. The tail is located near the hilum of the kidney touching the anterior side of the spleen while the body and the tail run obliquely upward towards the left at the anterior part of the aorta and the left kidney ducts carry bile away from hepatocytes into larger ducts and the gallbladder (Figure 3) (160, 161).

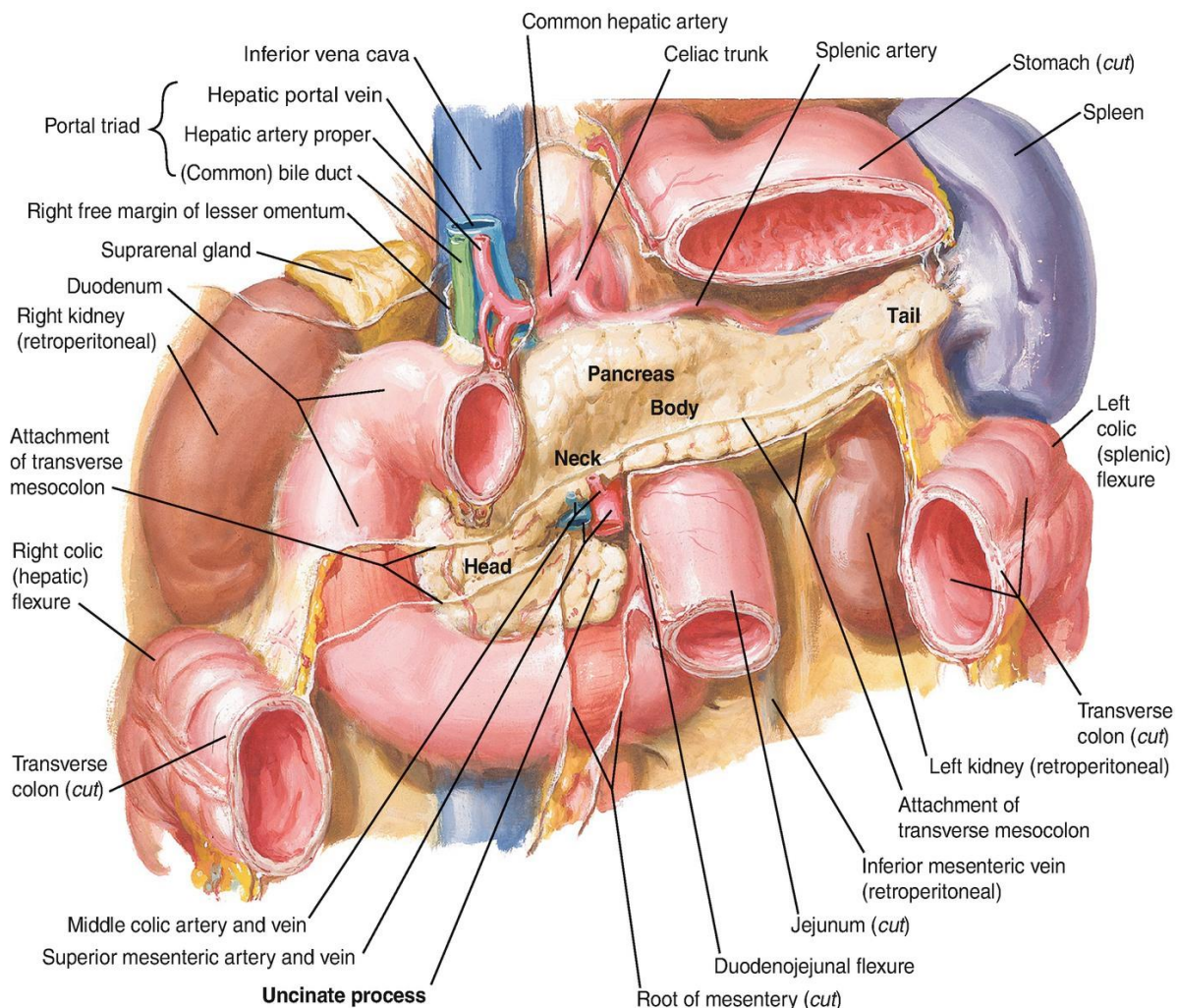


Figure 3. Gross anatomy of the pancreas and its anatomical relationships. Image obtained from Zambirinis and Allen (162).

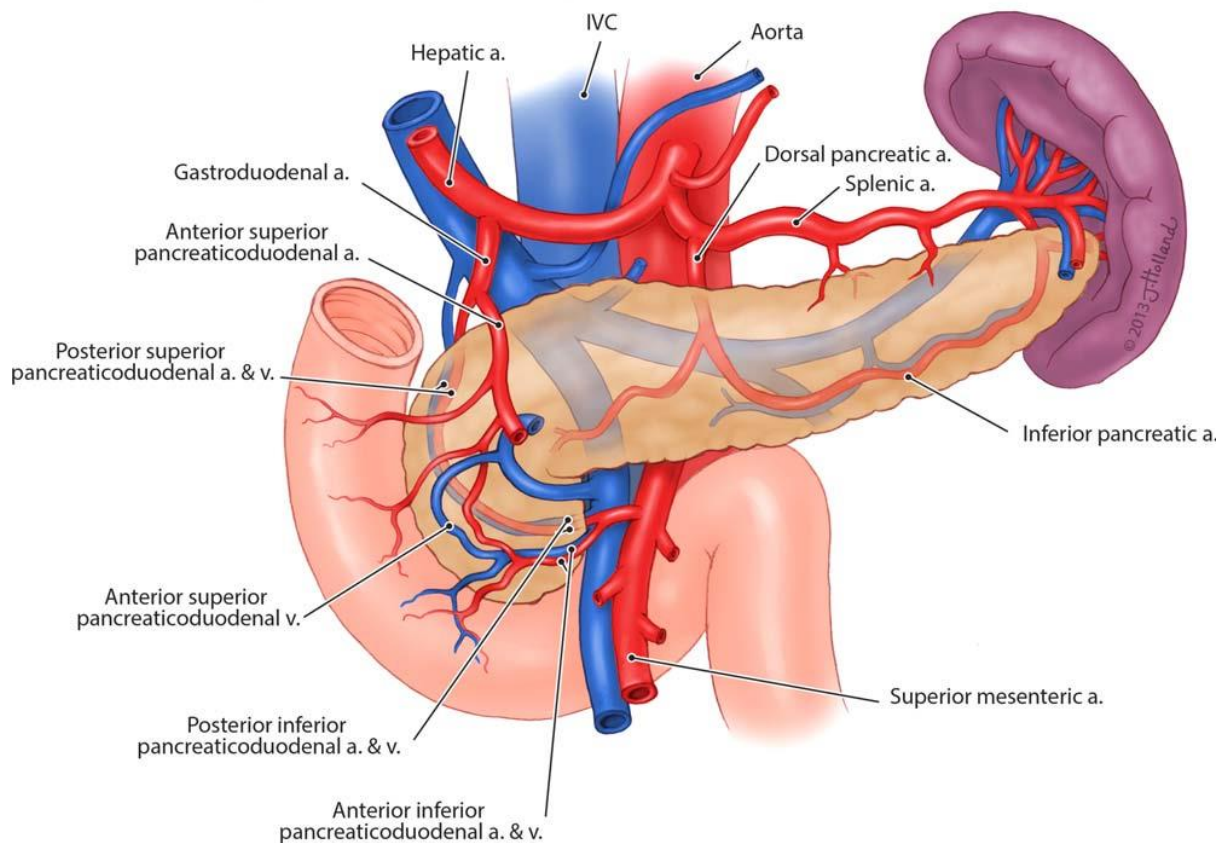


Figure 4. The vasculature of the pancreas. The arterial supply is derived from branches from both the superior mesenteric artery and the celiac trunk. The splenic artery, a branch from the celiac trunk, provides the dorsal pancreatic, inferior pancreatic and various other branches along the neck, body, and tail of the pancreas. The gastroduodenal artery, a branch from the hepatic artery of the celiac trunk, provides arterial supply to the head of the pancreas via the anterior and posterior pancreaticoduodenal arteries, whereas the inferior pancreaticoduodenal branches from the superior mesenteric artery, provide for the uncinete process. The venous drainage of the pancreas follows a similar pattern as the corresponding arterial supply, with the head of the pancreas being drained by the pancreaticoduodenal veins into the portal vein or the superior mesenteric vein (SMV), whereas the neck, body, and tail of the pancreas drain into the splenic vein prior to its merger with SMV to form the portal vein. Image obtained from Cesmebas et al. (163)

1.3.2 Pancreas Cells and their Microscopic Organization

The pancreas is made up of majorly three groups of cells: acinar cells, ductal cells, and pancreatic islet cells (Figure 5). The secretory unit of the pancreas is known as the acini and comprises ~85 % of pancreatic cells (164). Acini are composed of clusters of acinar cells that form lobules engulfed by connective tissue septa. The acinus is made up of one layer of pyramid-shaped broad-based cells that are attached to a basal lamina. The acinus' secretion is emptied into its lumen and enters the duct system through the ductules. The acinus lumen is lined with both acinar and

centroacinar cells. The centroacinar cells present in the acinus form the ductules, which deliver acinar secretions into intercalated ducts, which then convey these secretions to intralobular ducts that join interlobular ducts with the main duct (165).

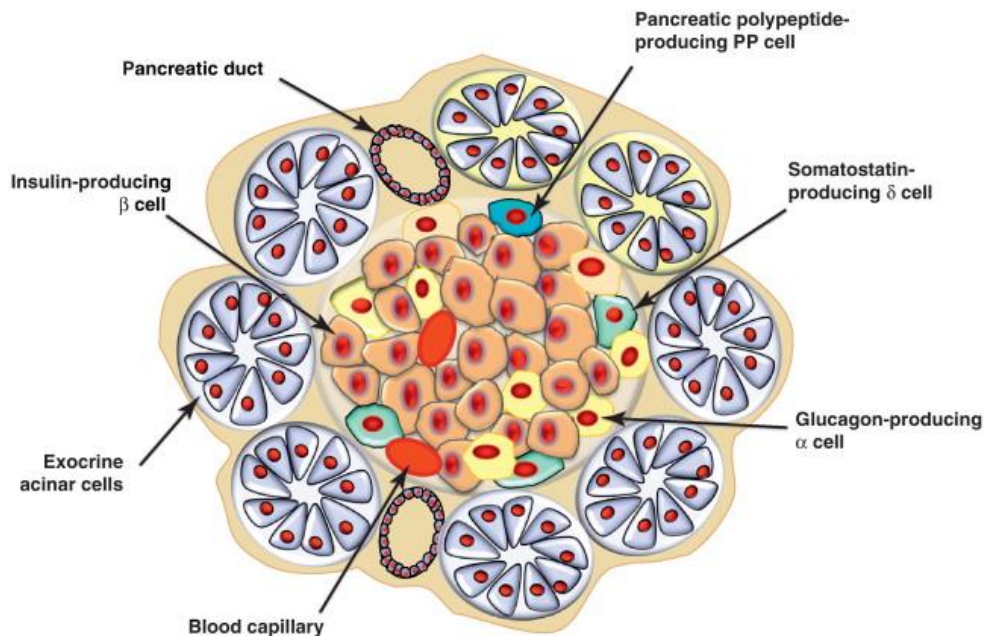


Figure 5. Microanatomy of the pancreas. An Islet of Langerhans within several acini and ducts. Image from Efrat and Russ (100).

Ductal cells, which make up 10 % of all the pancreatic cells, line the epithelium of ducts that convey enzymes secreted by acinar cells into the duodenum (166). Additionally, ductal cells are involved in the secretion of bicarbonates needed to neutralize the acidity of chyme. These cells are characterised by unspecialized cytoplasm, which contains mucin granules, microvilli, cilium, and extensively interlinked plasma membrane (167).

Finally, the pancreas is made up of cell clusters known as the islet of Langerhans which are ovoid in shape (168). Islets of Langerhans make up ~4.5% of the total pancreatic cells, are mostly endocrine and are enclosed by the acini (169). The islets of Langerhans' are in the range of 75 and 175 micrometres in dimension and can reach about 1.5 million cells per normal pancreas (170).

In between the islet cells, numerous blood capillaries are present, which are partially delimited by reticular fibrils and Schwann cell sheath derived from autonomic nerve fibres entering these cells (171, 172). Even though the Schwann cells cover most parts of the islet surface, the axons are found along with the capillaries (171, 172). On average, 75 % of the islets cells are β -cells, 20 % α -cells, and 5 % δ -cells. The β -cells are primarily situated in the centre of the islet, whereas the α -cells and δ -cells are located at the periphery (173). C-cells are rarely found in humans while E-cells do not occur in humans (173). The islets of Langerhans can be categorized into two types: juxtaduodenal islets whose function is to secrete insulin as well as pancreatic polypeptide and juxtaspenic islets which secrete both insulin and somatostatin (174).

1.4 Pancreatic Ductal Adenocarcinoma

1.4.1 Concept, Epidemiology and Pathophysiology

Over 90% of all pancreatic cancers are represented by pancreatic ductal adenocarcinoma (PDAC) (175). PDAC affects over 53,000 new cases per year in the USA, and is currently considered as the fourth leading cause of cancer death (176). In fact, it is projected to become the second biggest cancer killer in the United States by 2030 (177). The striking similarity between incidence and fatalities highlights the dismal prognosis of this disease. The median survival is less than 6 months, and the 5-year survival rate is between 3-5%. Across Europe, the 5-year overall survival ranges from 2-9% (178-180).

This low survival rate is multifactorial, mainly attributed to its aggressive biology, its capacity to rapidly disseminate to the lymphatic system and distant organs and its resistance to conventional therapies. Indeed, this disease is almost incurable as patients are commonly diagnosed at a metastatic or locally advanced stage, which is mostly due to PDAC's asymptomatic clinical course (181).

1.4.2 Diagnosis and Staging

As mentioned earlier, one reason that PDAC is a highly lethal disorder is its asymptomatic phenotype, which makes it very hard to diagnose at an early stage. This is partly due to the lack of understanding of the biological behaviour and the ineffective screenings for this disease. Only 15% of patients are eligible for surgical therapy (182), which currently represents the only potentially curative strategy. Significant efforts have been made to find the appropriate serum-and-imaging biomarkers to help early detection and predict response to treatment. Currently, imaging, such as computerised tomography scans, magnetic resonance imaging, ultrasound, cholangiopancreatography, somatostatin receptor scintigraphy, positron emission tomography, and angiography, can be utilised to diagnose PDAC (183). Blood tests and biopsies are also recognised means of diagnosis (183).

Pancreatic Ductal Adenocarcinoma can be categorised into four stages according to the American Joint Committee on Cancer (AJCC) staging system, which is provided in Table 2 below, and whose details were obtained from AJCC's website (183). In many cases, diagnosis takes place at Stage III or IV, complicating attempts at successful treatment (184).

Stage	Description
0	The tumour is confined to the top layers of pancreatic duct cells and has not invaded deeper tissues. Tumour cells have not spread outside the pancreas. These tumours are sometimes referred to as pancreatic carcinoma in situ or pancreatic intraepithelial neoplasia III.
IA	The tumour is confined to the pancreas and is 2 cm across or smaller. The cancer has not spread to nearby lymph nodes or distant sites.
IB	The tumour is confined to the pancreas and is larger than 2 cm across. The cancer has not spread to nearby lymph nodes or distant sites.
IIA	The tumour is growing outside the pancreas but not into major blood vessels or nerves. The cancer has not spread to nearby lymph nodes or distant sites.
IIB	The tumour is either confined to the pancreas or growing outside the pancreas but not into major blood vessels or nerves. The cancer has spread to nearby lymph nodes but not to distant sites.
III	The tumour is growing outside the pancreas and into nearby major blood vessels or nerves. The cancer may or may not have spread to nearby lymph nodes. It has not spread to distant sites.
IV	The cancer has spread to distant sites.

Table 2. Stages of pancreatic cancer as defined by AJCC. Adapted from AJCC (183).

1.4.3 Precursor Lesions

Following genetic reprogramming of normal pancreatic ductal cells is a multi-step, histologically defined progression towards a PDAC diagnosis. Current knowledge postulates that PDAC is not formed *de novo*; but rather, *in situ*, is preceded by distinctly characterised non-invasive precursor lesions. The three major subtypes are pancreatic intraepithelial neoplasia (PanIN), intraductal papillary mucinous neoplasms (IPMNs) and mucinous cystic neoplasms (MCNs) (Figure 6) (185).

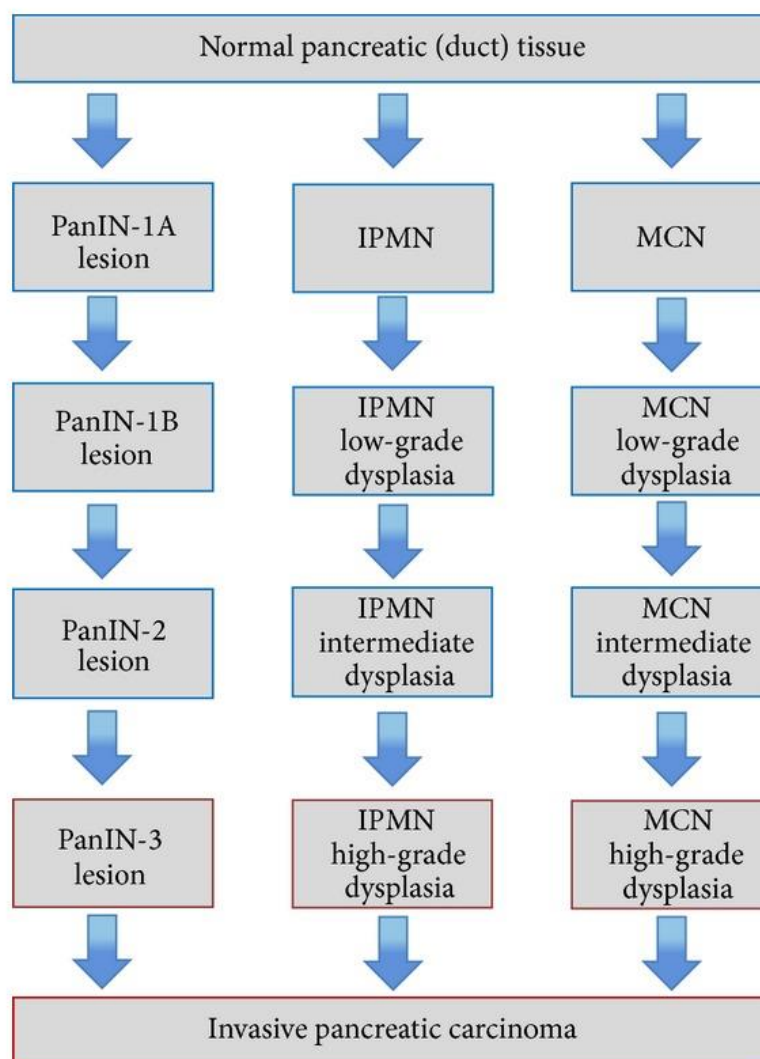


Figure 6. Progression of three distinct precursor lesions preceding PDAC. Image obtained from Distler et al. (185).

PanIN is the most common of the three pre-lesions and is, histologically, situated in the smaller pancreatic ducts and characterised by varying cytological and architectural atypia. Development can be classified into three tiers: low-grade PanIN-1a or 1b, intermediate PanIN-2 or high-grade PanIN-3 lesions. The latter high-grade PanIN-3 lesion has the greatest potential for invasive progression whereas low-grade PanINs can be found in normal pancreatic tissue and in patients with chronic pancreatitis (186). Low to high-grade progression is determined by a compendium of genetic modifications, thought to be driven by KRAS activation, which ultimately gives way to an invasive phenotype (Figure 7) (187).

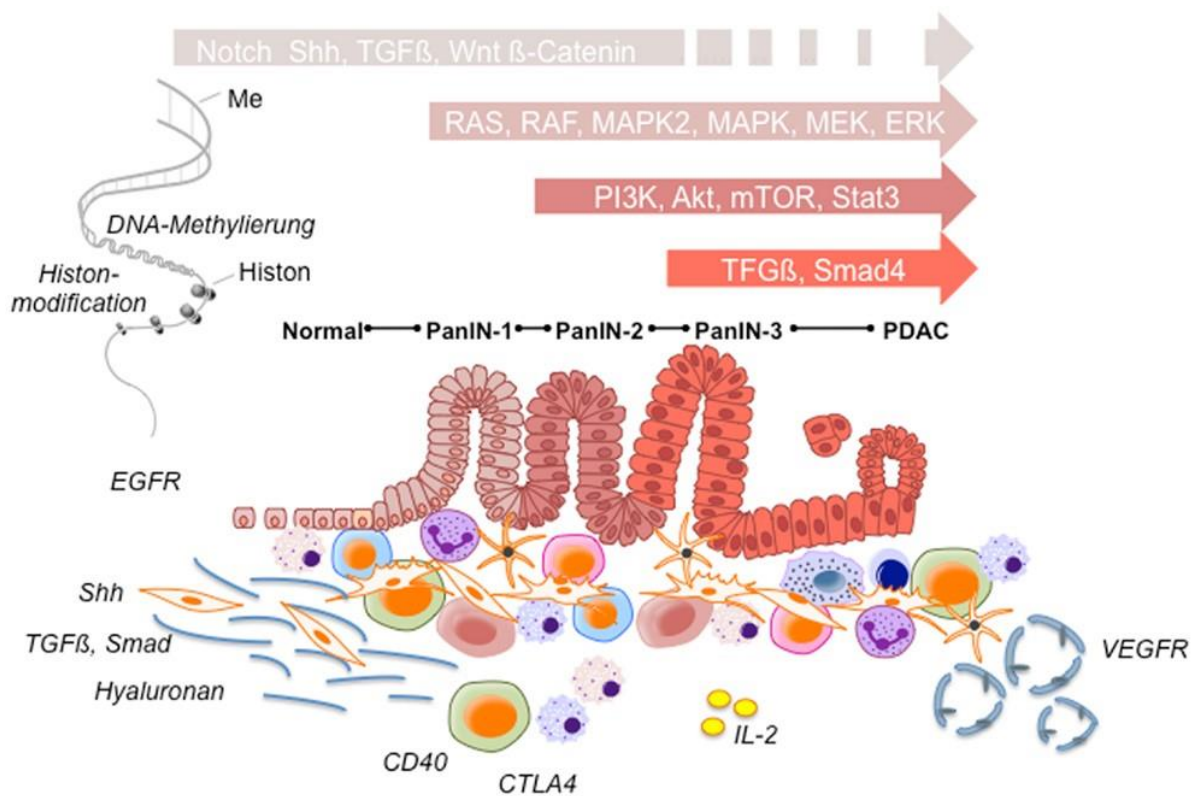


Figure 7. The PanIN precursor lesion model. A Schematic image representing the genetic, morphological and extracellular changes that occur when normal cells progress towards carcinoma. Image obtained from Wörmann and Algül (188).

IPMNs and MCNs are macroscopic cystic lesions and are typically non-invasive (189). Both are associated with high carcinoembryonic antigen (CEA) presence in the cyst fluid (190). IPMNs are mucin-producing tumours of the epithelial duct – main (MD) or branch (BD) type. An estimated third of IPMNs are associated with invasive carcinoma. MCNs are the most infrequent precursor lesion and occur predominantly in females (185). Similar to IPMNs, MCNs are mucinous lesions and about a third become invasive. In contrast, there is no association with the epithelial duct, but rather a single lesion located at the body or tail of the pancreas (191).

1.4.4 Therapies

Therapeutic options are limited, and until recently, there was no standard second-line chemotherapy option. Despite intensive research, the median survival time of patients with PDAC has remained nearly constant during the last four decades (192). Indeed, the majority of PDAC cases are detected at an advanced stage with over half of patients being diagnosed at a metastatic Stage IV (Table 3) (193). Only 9% of patients are detected at a local stage owing to the asymptomatic nature of PDAC and a lack of effective screening modalities for early stage tumours. As mentioned earlier, currently, surgical resection with neoadjuvant treatment presents the only opportunity for a curative outcome; unfortunately, this is not an option for the majority as 80-95% of patients are ineligible for resection at diagnosis (194).

Location	Proportion of cases	Stage	5-year survival rate
Local – primary site	9%	I – IIA	37.4%
Regional – locally advanced to regional lymph nodes	27%	IIB – III	12.4%
Distant – metastasised to other sites in the body	53%	IV	2.9%
Unknown	11%	Unstaged	5.6%

Table 3. Relative Pancreatic Cancer 5-year Survival by Stage. Statistics represent location, proportion of cases, their staging and the 5-year survival rate between the years of 2009-2015 as collected by NIH SEER (193, 195).

The management of PDAC is usually determined according to the tumour-node-metastasis (TNM) classification, i.e. is the cancer localised, regional or metastasised. A diagnosis, by method of imaging (see section 1.4.3) (196), will elucidate the possibility of resection and the most effective therapeutic decision can be determined accordingly. Operative procedures depend on tumour size and location: Whipple procedure, distal pancreatectomy, or total pancreatectomy (197).

The standard for first-line therapy is debatable, but Gemcitabine has proven to be the most promising candidate as a combination therapy for the past decade (198). In 2010, Conroy et al suggested FOLFIRINOX, a combination treatment of 5-FU, leucovorin, irinotecan and oxaliplatin, over Gemcitabine as a first-line standard (199). FOLFIRINOX has since been approved by the National Institute for Health and Care Excellence (or NICE) as a first-line option for locally advanced and metastatic patients well enough to tolerate the toxicities (196). The second-line standard offers Gemcitabine combination chemotherapy or if this has failed first-line then oxaliplatin-based chemotherapy as the second-line treatment (196). Differences in survival rates for Gemcitabine combination therapy or FOLFIRINOX treatment are negligible and the order of administration has an equal outcome for overall survival (OS) (Table 4) (195, 200).

Treatment personalisation could optimise the effective outcome of chemotherapeutics. This is essential for second-line treatment where the tumour responds poorly to first-line treatment. An analysis of the patient response to prior treatment should identify

specific biomarkers to help confront the molecular events that are causing chemoresistance.

Regimen	Description	Median OS VS. Gemcitabine alone (months)	Reference
Gemcitabine + erlotinib	EGFR inhibitor	6.2 vs. 5.9	Moore, M.J. et al, 2007 (12)
Gemcitabine + nab-paclitaxel	Albumin-bound paclitaxel	8.5 vs. 6.7	Von Hoff, D.D. et al, 2016 (13)
Gemcitabine + S-1	Tegafur (5-FU prodrug), gimeracil and oteracil	10.1 vs. 8.8 (vs. 9.7 for S-1 arm)	Uena, H. et al, 2013 (14)
FOLFIRINOX	5-FU, leucovorin, irinotecan and oxaliplatin	11.1 vs. 6.8	Conroy, T. et al, 2010 (10)

Table 4. Multi-drug regimens for treatment of locally advanced and metastatic PDAC. Data compares median overall survival (OS) in months as a measure of effective outcome

1.4.4.1 Localised Surgically Resectable PDAC

Localised surgically resections are the likely procedure in cases of Stage I and IIA diagnosis, where tumour is contained to the pancreas and no bigger than around 4 cm (193). Surgery alone is ineffective; 60-70% of patients experience tumour recurrence due to micrometastases (195) and comorbidities without systemic treatment, i.e. chemotherapy and radiotherapy (197). Adjuvant therapy options include Gemcitabine, fluorouracil (5-FU), Tegafur/gimeracil/oteracil combination (S-1), chemoradiation or chemoradiation plus the aforementioned cytotoxic agents. Chemotherapy with Gemcitabine or 5-FU for 6 months following surgical resection has shown to significantly increase OS (195). NICE guidelines recommend 6 cycles of adjuvant Gemcitabine plus capecitabine for patients once they recover from surgery (196). A recent systematic review reports S-1 adjuvant chemotherapy to have the highest OS (46.5 months) in comparison with other agents, including Gemcitabine combinations (201).

1.4.4.2 Regional Borderline Resectable PDAC

Regional borderline resections are the likely procedure in cases of Stage IIB and in some rare cases Stage III diagnosis. Neoadjuvant therapy is often required for tumours identified as borderline resectable to minimise tumour size prior to surgery. Currently the best options include Gemcitabine plus nab-Paclitaxel, FOLFIRINOX and modified FOLFIRINOX, radiotherapy and chemoradiotherapy (195, 202). Neoadjuvant Gemcitabine, docetaxel, and capecitabine combination has recently been suggested to be the most beneficial with a high OS of over 42 months (201).

1.4.4.3 Regional, Locally Advanced Unresectable PDAC

Approximately one third of diagnoses are Stage III and deemed ineligible for surgical intervention (195). Observed response rates are often poor and so a standard for management is debatable. NICE guidelines suggest systemic combination chemotherapy, e.g. Gemcitabine with nab-paclitaxel or Gemcitabine alone for patients who cannot tolerate the associated high toxicities of other agents (196). Capecitabine is offered as a radiosensitiser for chemoradiotherapy treatment. A meta-analysis suggested the benefit of radiotherapy with 5-FU or Gemcitabine for locally advanced PDAC treatment – about a third of unresectable tumours became resectable cases and OS was improved (203).

1.4.4.4 Distant and Metastatic PDAC – Stage IV

Most PDAC cases are diagnosed as Stage IV metastatic with a low chance of survival (Table 3). For first-line treatment, patients who are deemed tolerable to toxicities are offered FOLFIRINOX or otherwise Gemcitabine in combination with other agents (196). Often a palliative approach is taken for Stage IV diagnoses; treatment focuses on improving patient quality of life rather than a curative outcome, as patients are often not well enough to handle potent cytotoxics.

The high rates of morbidity and disease recurrence across treatment options has caused worldwide uncertainty on the adequacy of current PDAC treatment. Looking ahead to the emergence of randomised clinical trial results and investigations into novel strategies to combat resistance; the standard for PDAC treatment is likely to, and is calling for, a change.

1.4.5 Molecular Genetics

As mentioned before, the fast progression into a metastatic disease is a key feature of PDAC patients, who often succumb from advanced local disease with widespread metastatic burden early after diagnosis. The well-defined histopathological picture and molecular profiles of PDAC have provided the framework for the emergence of both basic and translational research. Novel advances include high-resolution genomic profiles highlighting potential therapeutic targets (Table 5) (204), and new animal models reflecting the histopathological staging of human PDAC (205-208).

The aetiology of PDAC is complex, with multiple genetic-environmental interactions rather than a particular major risk factor (209). At least 5–10% of PDACs can be attributed to a pathogenic sequence variant in familial cancer genes (209). Main targets evaluated include EGFR, KRAS, mTOR, MEK, and VEGF, which are not unusual considering the significant inter-tumour heterogeneity (210-212). In fact, KRAS gene mutations are identified in more than 90% of PDAC tumours and systematically associated with a worse prognosis (211-213).

Moreover, the majority of reports indicate a crucial role for autophagy in PDAC development and survival, more particularly constitutively activated autophagy, as it is believed to provide the necessary ‘fuel’ to PDAC cells in a nutrient-deprived environment (214).

1.4.6 The Tumour Stroma in Pancreatic Cancer

Approximately 90% of PDAC's primary tumour site is comprised of a stromal compartment (215). In fact, PDAC is unique in this term, as over 80% of the actual cancer nodule is accounted for by "scar tissue." This excess tissue is represented by several players including; desmoplasia, activated pancreatic stellate cells (PSCs) and fibroblasts, and inflammatory cells among others (216-222). Similarly, metastatic sites, e.g., liver metastasis, show pathological resemblance to the primary PDAC tumour with analogous ECM components (223). This would suggest the involvement of PDAC cells in recruiting local stromal cells to create an extracellular environment similar to that of its primary tumour (Figure 8). In an animal model, a correlation was established between the size of liver metastases and the stroma recruitment, by employing fluorescent lineage tracing. Another study found that upon the multiplication of tumour cells and as early as in nano-metastases (2-10 cells), myofibroblasts were found to be in contact with tumour cells, and the ECM composition recapitulated that of the primary tumour (224).

Pancreatic stellate cells contribute to both the generation and the embedding of collagens, fibronectin, stem cells, nerve fibres, macrophages and inflammatory cells (217). Thus, pancreatic stellate cells contribute to the development of stroma in which PDAC cells thrive (225). Many factors are involved in the activation of the stellate cells, such as platelet-derived growth factor (PDGF) (226, 227), transforming growth factor beta (TGF β) (226, 227), tumour necrosis factor alpha (TNF α), and interleukins 1, 6, and 10 (IL-1, IL6 and IL10) (228), although the exact mechanism by which PDACs activate PSCs is still not well understood (229).

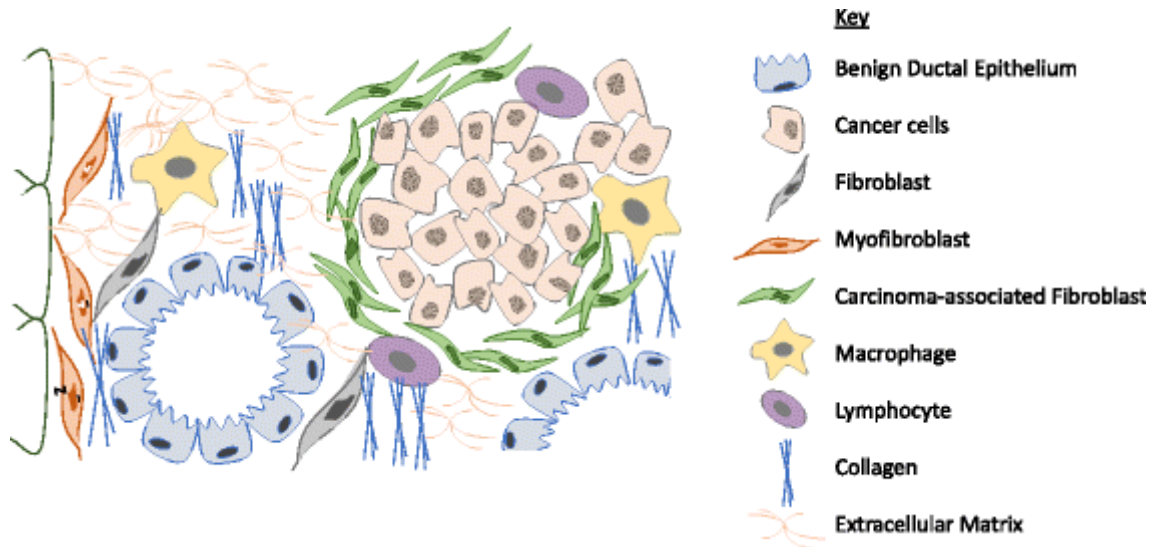


Figure 8. Schematic representation of PDAC stroma. Image obtained from Von Ahrens et al. (230).

Drug Target	Treatment	Phase	Comment	Reference
KRAS (farnesyl transferase)	Tipifarnib + gem vs. gem	R III	Acceptable toxicity profile, but no statistically significant differences in survival parameters	(231)
MAPK	Selumetinib + erlotinib 2nd line	SA II	Modest antitumor activity. Specific molecular subtypes may provide greatest benefit	(232)
mTOR	Everolimus + erlotinib	SA II	Disease progression observed in 15 patients. Study stopped due to impossibility to achieve pre-planned OS of 6 months	(233)
PI3K	Rigosertib + gem vs. gem	R II/III	Study was discontinued due to no significant difference in survival	(234)
EGFR	Erlotinib + gem vs. gem	R III	FDA approved	(235)
EGFR/IGFR	Cixutumumab + erlotinib + gem vs. erlotinib + gem	R Ib/II	Dual inhibition of EGFR and IGFR did not improve OS or PFS	(236)
EGFR	Gefitinib + gem	SA II	Promising results, especially in patients with PTEN expression.	(237)
HER-2	Trastuzumab + cape	SA II	No improvement in mOS or PFS; low number of patients and HER2 expression	(238)
TK	Dasatinib	SA II	No activity of single agent dasatinib in metastatic PDAC, no improvement in OS and PFS	(232)
TK	Lapatinib + gem	SA II	No improvement in survival, small case sample	(239)
IGFR	Ganitumab + gem vs. gem	R III	No improvement in all assessed parameters	(240)
VEGFR	Axitinib + gem vs. gem	R III	No significant survival benefit compared to single agent gem	(241)

VEGF-A	Bevacizumab + gem + erlotinib vs. gem + erlotinib	R III	Despite improvement in PFS could be observed ($p = 0.0002$), no statistically significant difference in OS was achieved	(242)
VEGF	Aflibercept + gem vs. gem	R III	Discontinued due to no improvement in primary end point, OS	(243)
Matrix metalloproteinase	Matrimastat + gem vs. gem	R III	No significant differences in all assessed parameters	(244)
SHH	Vismodegib + gem vs. gem	R Ib/II	No difference in PFS, OS or response rate was noted	(245)
PSCs	Candesartan + gem	SA II	Treatment was well tolerated but failed to show significant activity	(246)
Hyaluronic acid	PEGPH20 + gem	Ib	Well tolerated, may be beneficial, especially for patients with high HA levels (13 months OS)	(247)
PSCs	PEGPH20/Abraxane vs. Abraxane	R II	Ongoing	(248)
JAK/STAT γ-secretase	Ruxolitinib + cape vs. cape	R II	Well tolerated, slight, but significant improvement in OS and PS	(249)
CTLA-4 Telomerase vaccination	Ipilimumab + GVAX vaccine vs. ipilimumab	R Ib/II	Despite the enhancement of the T cell repertoire ($p = 0.031$), no significant increase in OS or PFS was noted	(250)
	GV1001 + gem + cape/gem + cape	R III	No significant improvement in OS has been achieved	(251)

Table 5. Selected targeted therapies and immunotherapies for PDAC. SA, single arm; R, randomized; OS, overall survival; PFS, progression-free survival; RR, response rate; cape, capecitabine; gem, Gemcitabine. Adapted from Adamska et al (198).

1.4.7 Chemoresistance

1.4.7.1 *General Cancer Chemoresistance*

Resistance to chemotherapy treatment causes disease relapse, dissemination and morbid outcomes for patient OS. Chemoresistance arises when there are challenges in the local, cellular and/or molecular delivery of an anticancer agent to its target. The mechanisms promoting a resistance to treatment are related to both pre-existing and acquired phenotypes regulated by intrinsic genetic factors and the extrinsic tumour microenvironment.

Chemoresistance can be generally classified into two broad categories: innate/intrinsic, due to genetic factors, or acquired resistance where cancer cells develop resistance after showing initial sensitivity to treatment. This will often occur within weeks of initiating chemotherapy (252). Genetic factors that regulate signalling pathways, fundamental to cancer cell behaviour, such as growth, differentiation, apoptosis, angiogenesis, and motility will certainly influence sensitivity to treatment. Such include mitogen-activated protein kinase (MAPK), PI3K/Akt, epidermal-growth factor receptor (EGFR), nuclear factor (NF)- κ B and Sonic Hedgehog (SHH) signalling pathways (252-254).

Mechanism of acquired chemoresistance in cancers can be attributed to a rapid accumulation of a number of mutations, giving rise to increasing heterogeneity as the tumour progresses (198). The genotypic variation of the cancer cell subpopulation results in variations in cancer cell sensitivity and resistance to chemotherapeutics. After initial treatment, most of the cells targeted will die and the tumour is likely to show signs of remission. Those cancer cells that survive, having acquired mutations that allow for an adaptive response to treatment, propagate and so the natural selection of a chemoresistant subpopulation gives rise to the formation of a new tumour, which is invulnerable to the treatment.

For treatment to provide therapeutic benefit, it firstly depends on the drugs ability to penetrate into the tumour area to access the cancer target. This can be challenging as stromal changes occur during malignancy to favour chemoresistance and a physical barrier of various cell types is created between the microvasculature and the cancer target (255). After access to the tumour environment has been established, a drug must then prove its metabolic availability and activity to be effective at a cellular and molecular level.

1.4.7.2 Chemoresistance in PDAC

As mentioned earlier, most pancreatic cancers are unresectable at the time of diagnosis and less than 20% of patients are able to undergo surgery as a main treatment option (201) – tumour resection being the only treatment strategy with curative potential (252). Survival for the majority of patients therefore largely depends on the available chemotherapeutic treatments. The current treatments available for pancreatic cancer, however, do not prove to be highly effective (201). Suboptimal effectiveness can be due to limitations in cellular uptake and metabolic activity of the drug. This conveys a clinical crisis for pancreatic cancer treatment. Pancreatic cancer has a 5-year OS rate of <10% worldwide (256), highlighting the unmet need to develop novel treatment strategies.

PDAC is considered one of the cancers most resistant to chemotherapeutic drugs. This, combined with the tendency of a delay in diagnosis, makes pancreatic cancer one of the most fatal cancers (252). The difficulty to treat signifies a poor outcome for patient prognosis and is illustrated by the fact that the majority of available treatments for PDAC are mostly palliative with a focus on improving the quality of life for the patient rather than being able to offer a curative outcome (198).

1.4.7.2.i Metabolism-Associated Chemoresistance to Current PDAC Drug Treatment

The current first-line option for late-stage PDAC treatment is Gemcitabine in combination with other therapeutics (Table 6). The results for survival outcome, OS and progression-free (PFS), for the current available treatments are not overwhelming. A recent systematic review for different combinations of Gemcitabine with other agents reveals the lack of long-term effectiveness in chemotherapy treatment for pancreatic cancer. The median for OS is currently 8.1 months with highest OS of 35.5 months (Gemcitabine and Cisplatin) and PFS ranges from 2.4 to 11.0 months (201).

Despite this, Gemcitabine has proven to be the most promising candidate for chemotherapy treatment since 1997 (257), most effective as a combined therapy. Acquired chemoresistance in initially sensitive tumours has attracted scientific interest in recent years as a primary cause for the suboptimal clinical effect that available treatments for PDAC deliver (Table 7). Genes identified as markers for patient initial sensitivity to Gemcitabine are often related to the intracellular mechanisms governing the cellular uptake and metabolism of Gemcitabine (Table 8). Deeper exploration into the molecular mechanism behind a resistant response to treatment will help pave the way for development of novel strategies with higher survival benefit.

Gemcitabine, a hydrophilic nucleoside cytidine analogue, requires specialised uptake to reach the intracellular target. Low levels of human equilibrative nucleoside transporter (hENT1) expression reduced cellular uptake and has shown to correlate with worse patient survival outcomes following Gemcitabine treatment (252). In comparison, several studies report that high levels of hENT1 expression is associated with increased OS and disease-free survival (DFS) (252, 258).

The regulation of several nucleoside enzymes is considered a principal factor for chemosensitivity. Once inside the cell, deoxycytidine kinase (dCK) metabolically activates Gemcitabine by phosphorylation and so down-regulation correlates to a significant decrease in OS (259). The efficacy of Gemcitabine as an anticancer agent then depends on the incorporation of bio-active metabolites into cancer cell DNA – inhibiting proliferation. This process inhibits the activity of ribonucleotide reductases (RR) which catalyse the *de novo* synthesis of deoxyribonucleotides from ribonucleotides (198). Up-regulation of RRM1 and RRM2 is therefore linked to increased resistance and a worse prognosis as cancer cell proliferation is accelerated (260, 261). Cytidine deaminase metabolically inactivates Gemcitabine metabolites by deamination. Up-regulation relates to increased resistance, whereas a loss in expression restores sensitivity to Gemcitabine (262).

Multidrug resistance-associated proteins (MRPs), i.e. ATP-binding cassette (ABC) pumps, are key regulators of drug efflux. Active outflow of Gemcitabine strongly induces chemoresistance – preventing intracellular accumulation (198). A CD133+ cell subpopulation has shown to correlate with high levels of ABC transporter expression and related to anti-apoptotic protein expression of Bcl2 (254). Moreover, it has been suggested that T2R38, a bitter-taste receptor, may play a potential role in stimulating the up-regulated expression of ABCB1 thereby increasing resistance, while another, T2R10, has shown to induce anticancer activities by down-regulated expression of ABCG2 (263).

Treatment	Phase	n	Outcome	p	Reference
Gem vs. 5-FU	R FL III	126	FDA approved	0.0025	(264)
Gem-5FU vs. gem	FL III	322	No statistically significant improvement in OS	0.09	(265)
FOLFIRINOX	R II/III	342	FDA approved	<0.001	(266)
Abraxane	R III	861	FDA approved	<0.001	(267)
Erlotinib + gem/gem	R III	569	FDA approved	0.038	(235)
Gem + cisplatin/gem	R III	195	Improved survival, but not statistically significant	0.15	(268)
	R III	400	Failed to demonstrate improvement	0.38	(269)
PEFG vs. gem	III	99	Little sample size	0.0008	(270)
Gem + oxaliplatin	III	313	Significant improvement in response rate and PFS, but not statistically significant OS	0.13	(271)
Gem + capecitabine vs. gem	III	319	Not statistically significant improvement in OS	0.234	(272)
	III	533	Alternative treatment for patients with good PS	0.08	(273)
S-1 + gem/gem	III	834	Not inferior to Gemcitabine. Approved in Japan as alternative	<0.001	(274)
Gem + irinotecan	III	360	Good tumour response but no improvement in OS	0.789	(275)

Table 6. Gemcitabine-based combination therapies. FDA, Food and Drug Administration; R, randomized; PS, performance status; OS, overall survival; PFS, progression-free survival; gem, Gemcitabine; PEF, cisplatin, epirubicin, fluorouracil, and Gemcitabine combination. Adapted from Adamska et al (198).

1.4.7.2.ii *Stroma/Microenvironment-Associated Chemoresistance*

Pancreatic cancer is characterised by the presence of a hypovascularised, densely fibrous stroma. The total tumour volume is largely comprised of scar tissue, also known as desmoplasia, which encompasses the malignant epithelial cells (276). Dense stromal fibrosis is characteristic of PDAC and its main component is pancreatic cancer-associated fibroblasts (CAFs). CAFs are the main fibrosis-producing cells and mainly originate from pancreatic stellate cells (PSCs) (277). PSCs encourage a pre-metastatic niche subpopulation while also increasing chemoresistance by preventing perfusion into the tumour (230).

PSCs play an important role in the re-modelling of ECM, activated by the local accumulation of reactive oxygen species, cytokines and growth factors surrounding defective cells to produce hypoxia and fibrosis (278). PSCs secrete factors which encourage a chemoresistant phenotype and so by prevention of H₂O₂-induced apoptosis, chemosensitivity is decreased and PDAC cell survival is increased (253).

An attempt to reduce the number of activated PSCs was achieved in mice models by combination of Gemcitabine with a JAK2 inhibitor. A reduction in fibrosis was shown to be associated with the inhibition of JAK2/STAT3 pathway (188). JAK2/STAT3 signalling is key to stroma modification, tumour growth and resistance to Gemcitabine demonstrated in mice models with loss of p53 function (188). P53 is a tumour suppressor protein directly involved in apoptosis – inactivated in 75% of pancreatic cancers (253).

Extracellular regulated kinases (ERK) mediate pro-survival pathways related to many forms of cancer. ERK1/2 is found to be highly expressed by cancer-associated PSCs and hyperactivity is associated with Gemcitabine resistance in pancreatic cancer (279). This can be via the upstream regulation of immune factors such as IL-6 (280). A significant increase in IL-6 expression is seen in pancreatic cancer cells compared to normal pancreatic cells – receptor blockade combined with chemotherapy in several murine studies has shown to induce cell death resulting in decreased tumour weight and improved OS (281).

Tumour-associated macrophages (TAMs) are the most abundant immune cells in many solid tumours, including pancreatic cancers (198). Promotion of tumour growth is achieved by several phenotypic augmentations. TAMs secrete the enzyme cytidine deaminase which metabolises the bio-active form of Gemcitabine (254). Additionally, TAMs have been found to further promote chemoresistance through enhanced STAT3 signalling and increased IGF production (282).

The accumulating presence of signalling factors (e.g. collagen, integrin), inflammatory cytokines (e.g. IL-6, TNF- α), growth factors (e.g. HGF, EGF, TGF- β) and hypoxia triggers cells to take on an epithelial-mesenchymal transition (EMT). TAMs are also considered a potent EMT inducer (255). Cell-to-cell adhesion and polarity is lost; invasive phenotype gained (253, 283). Observing the effect of mesenchymal transcription factors, such as Snail, Slug, Zeb1, in knockdown studies has shown to enhance the sensitivity of CD133+ pancreatic cancer cells to Gemcitabine (253, 284).

Pathway / Process	Mechanism	Reference
Increasing nucleoside transportation – drug influx	<i>In vivo</i> expression of hENT1 increasing Gemcitabine uptake	(285, 286)
Reducing ATP-bound cassette pump expression – drug efflux	Reduced expression of MRP1 by increased expression of runt-related transcription factor 3 (RUNX3), elevating intracellular accumulation of Gemcitabine	(287, 288)
Nucleoside enzyme activity	Deoxycytidine kinase overexpression restores chemosensitivity in Gemcitabine-resistant cell lines	(289, 290)
Inhibiting epithelial-mesenchymal transition (EMT)	Downstream anti-apoptotic transcription factor, Slug, knockdown enhances CD133 ⁺ pancreatic cancer cells sensitivity to Gemcitabine	(284)
Stromal depletion strategy	Treatment of Gemcitabine with JAK2 inhibitor in mice models forms smaller tumours and improves survival	(188)

Table 7. Key factors influencing increased sensitivity to Gemcitabine.

Pathway / Process	Mechanism	Reference
Nucleoside transporters – drug influx	hENT1 deficiency <i>in vitro</i> reducing cellular uptake	(291)
ATP-bound cassette pumps expression – drug efflux	High levels of ABC transporters related to increased pro-survival proteins, Bcl2	(292)
Nucleoside enzyme activity	Low levels of deoxycytidine kinase (dCK) reduces Gemcitabine bio-activation correlating to decreased overall survival (OS)	(259)
	High levels of ribonucleotide reductase (RRM1 and RRM2) increases rate of ribonucleotide to deoxynucleotide conversion, correlating to cancer cell proliferation and poorer prognosis	(293)
	Cytidine deaminase up-regulation increases catalytic inactivation of Gemcitabine bio-active metabolites	(294)
Epithelial-mesenchymal transition (EMT)	Mesenchymal transcription factors (e.g. slug, snail, Zeb1) increase resistance as PDAC cells take on mesenchymal phenotype	(259)
Extracellular regulated kinase (Erk) activation	Pro-survival pathway activated downstream of MAPK signalling – Erk1/2 activation up-regulates pro-survival proteins, Bcl2, and down-regulates pro-apoptotic proteins, Bax	(295)
Desmoplastic stroma – fibrosis	Loss of p53 function activating JAK2-STAT3 signalling promotes stromal alterations and tumour growth in mouse models	(188)
	Pancreatic stellate cells (PSC) activate Akt and Erk pro-survival pathways via paracrine SDF-1 α /CXCR4 signalling, with subsequent IL-6 up-regulation	(280)

Table 8. Key factors influencing increased resistance to Gemcitabine.

• CHAPTER 2 •

“I shall endeavour still further to prosecute this inquiry, an inquiry I trust not merely speculative, but of sufficient moment to inspire the pleasing hope of its becoming essentially beneficial to mankind.”

- Edward Jenner

2. AIM and OBJECTIVES

2.1 Human Pancreas Decellularisation

2.1.1 Aim

Eliminate cellular and nuclear material from human pancreata, while preserving the ECM protein and microarchitecture.

2.1.2 Objectives

- Assess different options to decellularise human pancreata. I.E. agitation vs. perfusion techniques.
- Achieve no visible cellular material on Sirius red staining after decellularisation.
- Achieve no visible nuclear material on Haematoxylin and Eosin staining and DNA quantification of below 150 ng/mg tissue after decellularisation.
- Maintain ECM proteins and architecture after decellularisation.

2.2 Developing primary and metastatic *in vitro* PDAC models

2.2.1 Aim

Establish 3D PDAC models capable of stimulating the primary cancer, early metastasis and established metastasis *in vitro*.

2.2.2 Objectives

- Reseed decellularised pancreas and liver scaffolds with PANC-1, PK-1 and MIA PaCa-2 cells.
- Assess recellularisation at different time points using histological techniques.

- Investigate key protein expressions and their changes within the different 3D models.
- Explore the effect of the ECM on cancer cells and its progression through changes in cellular transcriptome.
-

2.3 Chemoresistance in PDAC

2.3.1 Aim

Resemble the *in vivo*-like characteristics using the 3D *in vitro* PDAC models to study chemoresistance in cancer.

2.3.2 Objectives

- Assess viability of the PDAC cells in the 3D models after treatment with Gemcitabine.
- Compare changes in viability within the different models and 2D cultures.
- Investigate key protein expressions and their changes due to chemotherapy with the different 3D models
- Explore the effect of ECM on chemoresistance through changes in cellular transcriptome.

• CHAPTER 3 •

“Nothing in life is to be feared, it is only to be understood. Now is the time to understand more, so that we may fear less.”

- **Marie Curie**

3. METHODS & MATERIALS

3.1 Tissue Retrieval and Preparation

The study was approved by the UCL Royal Free Biobank Ethical Review Committee (NRES Rec Reference: 11/WA/0077). Informed consent for research was confirmed via the NHSBT ODT organ retrieval pathway, and the project was also approved by the NHSBT Research Governance Committee. Donor livers were processed in accordance with the UCL Royal Free Biobank protocols under the Research Tissue Bank Human Tissue Act licence, prior to use for research.

Healthy human livers and pancreata, not suitable for transplantation, were obtained, from the Royal Free BioBank. Pancreata and livers were washed and perfused with 1% Phosphate Buffered Saline (PBS; Sigma Aldrich), respectively, to clear them from blood. They were then air dried for 10 minutes and frozen at -80 °C.

Human pancreata and liver right-lobes, which were to be decellularised by agitation, were later partially thawed in a 37 °C water bath and dissected into 5x5x5 mm³ cubes. The cubes were frozen again at -80 °C for future experiments.

Whole human pancreata, which were to be decellularised by perfusion, were partially thawed at 4 °C, for 16 hours. The spleen and excess tissue surrounding the pancreas were carefully removed. The splenic and mesenteric arteries and the superior mesenteric vein were ligated. Excess duodenal-jejunal tissue was removed and the proximal duodenum was stapled closed. Finally, all leakages from the pancreas-duodenum block were ligated and the pancreas was frozen again at -80 °C for future experiments.

3.2 Pancreas and Liver Cubes Decellularisation

Initially, tissue cubes were thawed in a water bath at 37 °C for 1 hour (hr), followed by the addition of 1.2 ml of 1% PBS for 15 minutes. Once thawed the cubes were transferred to 2ml safe-lock tubes (Eppendorf). A standardised 1.5 ml of each solution was added to its respected tube, placed in the middle column of the TissueLyser II (Qiagen) and agitated at 30 Hz for each step. The agitation regime for the decellularization of the liver cubes is shown in Table 9 [Protocol LA1 based on Mazza et al.] (296) and for the pancreas cubes shown in Table 10. The reagent mixture solution was prepared as follows:

Reagent Mixture Solution: 3% Sodium deoxycholate, BioXtra, ≥98.0 (Sigma-Aldrich), 0.5% Sodium dodecyl sulfate, BioXtra, ≥99.0 (Sigma-Aldrich), 0.3% Triton X-100 (Sigma-Aldrich), 0.0025% Gibco® Trypsin-EDTA (Life technologies) and 4.3% of Sodium Chloride (Sigma-Aldrich) in deionized water (MilliQ by Millipore) and stirred for 1 hour using a magnetic stirrer.

Protocol	Reagents	Time	Repetition
LA1	Deionised Water (Milli-Q)	2	10
	Reagent Mixture	2	1
	Reagent Mixture	4	2
	1% PBS solution	5	3

Table 9. Protocol for the decellularisation of human liver cubes by agitation

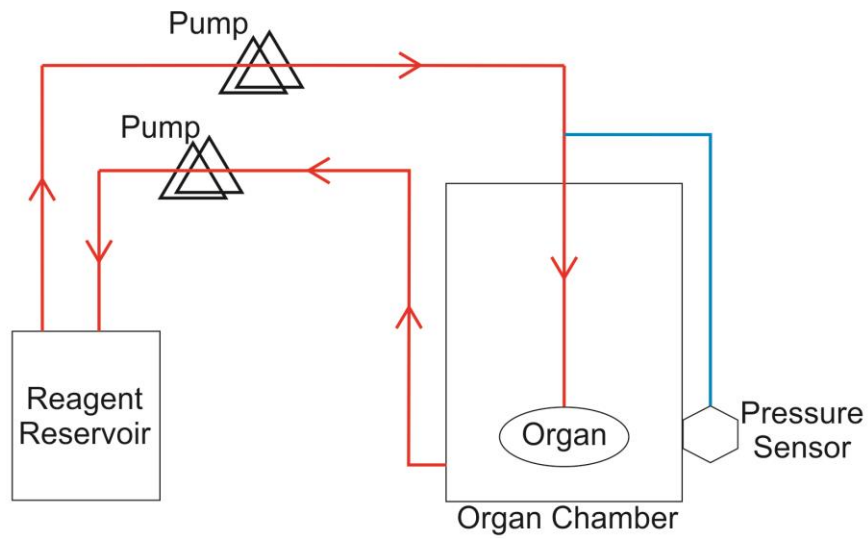
3.3 Pancreas Decellularisation by Perfusion

Initially, pancreata were thawed in 1% PBS (Sigma-Aldrich) at 4 °C, for 16 hours. Before decellularisation, the pancreata were cannulated through the portal vein. At least three pancreata were decellularised; HP1 using a pump and a box without any pressure regulation (Table 11), HP2 and HP3 were decellularised using the

Harvard Apparatus ORCA bioreactor. The bioreactor used for the decellularisation was set up as shown in Figure 6. The software used to control and monitor the perfusion system was HART v1.0.0.0. The perfusion regimes for the decellularization of HP2 and HP3 are shown in Table 12 and Table 13, respectively. After decellularisation was complete, the pancreas was dissected into ~5x5x5 ml cubes and stored in either: 1X HBSS (Thermofisher Scientific) at 4 °C until future experiments or fixed in 4% formaldehyde and assessed by histology and immunohistochemistry.

Protocol	Reagents	Time	Repetition
PA1	Deionised Water (Milli-Q)	2	5
	Reagent Mixture	5	2
	1% PBS solution	1	1
	8.7% NaCl solution	2	5
	Reagent Mixture	10	1
	1% PBS solution	1	1
	8.7% NaCl solution	10	1
	Reagent Mixture	10	1
	1% PBS solution	1	1
	8.7% NaCl solution	10	1
	1% PBS solution	30	2
PA2	Deionised Water	2	15
	Reagent Mixture	2	1
	Reagent Mixture	4	2
	1% PBS solution	1	1
	8.7% NaCl solution	2	5
	Deionised Water	2	5
	Reagent Mixture	2	1
	Reagent Mixture	4	5
	1% PBS solution	5	1
	Reagent Mixture	2	1
	Reagent Mixture	4	5
	1% PBS solution	5	1
	8.7% NaCl solution	2	5
	Deionised Water	2	5
	Reagent Mixture	2	1
Reagent Mixture	4	2	
1% PBS solution	5	3	

Table 10. Protocols for the decellularisation of human pancreas cubes by agitation.



Key:



PharmaMed Opaque Flexible L/S #18



PharmaMed Opaque Flexible L/S #16



Harvard Apparatus Single Channel, Duel Offset head Pump

Organ Chamber

Harvard Apparatus Large Organ Chamber

Reagent Reservoir

DURAN® GLS 80® 10 Litres bottle



PendoTECH PressureMAT Single-Use Sensor

Figure 9. Bioreactor components and setup for decellularisation.

<i>Day</i>	<i>Reagent</i>	<i>Mode of perfusion</i>	<i>Time (hours)</i>	<i>Flow rate (ml/min)</i>
<i>Day 1</i>	Distilled Water (Milli-Q)	Non-Recycle	2.5	100
	0.1 % SDS solution	Non-Recycle	0.5	120
	Distilled Water	Recycle	1	140
	0.1 % SDS solution	Recycle	Overnight	140
<i>Day 2</i>	Distilled Water	Recycle	1	250
	1% SDS solution	Recycle	1	300
	Distilled Water	Recycle	1	400
	1% SDS solution	Recycle	Overnight	400
<i>Day 3</i>	1% SDS solution	Recycle	1	600
	Distilled Water	Recycle	2.5	650
	1% SDS solution	Recycle	Overnight	680
<i>N.B. If the outflow at the start of day 4 is still cloudy, repeat steps from day 3 for another day</i>				
<i>Day 4</i>	Distilled Water	Non-Recycle	1.5	700
	3% Triton X-100 solution	Recycle	Overnight	700
<i>Day 5</i>	Distilled Water	Non-Recycle	1.5	750
	3% Triton X-100 solution	Recycle	4	750
	Distilled Water	Non-Recycle	0.5	800
	3% Triton X-100 solution	Recycle	Overnight	800
<i>Day 6</i>	Distilled Water	Non-Recycle	1.5	850
	Distilled Water	Recycle	3.5	850
	3% Triton X-100 solution	Recycle	Overnight	900
<i>N.B. If the outflow at the start of day 7 is still cloudy, repeat steps from day 6 for another day</i>				
<i>Day 7</i>	Distilled Water	Non-Recycle	1	900
	Distilled Water	Recycle	4	900
	Distilled Water	Recycle	Overnight	900
<i>Day 8</i>	Distilled Water	Non-Recycle	1	1000
	Distilled Water	Recycle	4	1000
	Distilled Water	Recycle	Overnight	1000
<i>Day 9</i>	1% PBS	Recycle	6	1200
	1% PBS	Recycle	Overnight	1200
<i>Day 10</i>	1% PBS	Recycle	6	1200
	1% PBS	Recycle	Overnight	1200
<i>Day 11</i>	PAA solution*	Recycle	1	750
	1% PBS (Sterile)	Recycle	2	750

* PAA solution: 0.1% Peracetic Acid and 4% Absolute Ethanol in distilled water

Table 11. Protocol for the decellularisation of whole human pancreas HP1 by perfusion.

Day	Reagent	Mode of perfusion	Time (hours)	Pressure (mmHg)
Day 1	Distilled Water (Milli-Q)	Non-Recycle	2.5	5
	0.1 % SDS solution	Non-Recycle	0.5	5.5
	Distilled Water	Recycle	1	6.5
	0.1 % SDS solution	Recycle	Overnight	7.5
Day 2	Distilled Water	Recycle	1	10
	1% SDS solution	Recycle	1	10
	Distilled Water	Recycle	1	10
	1% SDS solution	Recycle	Overnight	10
Day 3	1% SDS solution	Recycle	1	15
	Increase pressure to 20 mmHg and continue perfusion for 0.5 hours			
	Distilled Water	Recycle	2.5	20
	1% SDS solution	Recycle	Overnight	20
<i>N.B. If the outflow at the start of day 4 is still cloudy, repeat steps from day 3 for another day</i>				
Day 4	Distilled Water	Non-Recycle	1.5	30
	3% Triton X-100 solution	Recycle	Overnight	30
Day 5	Distilled Water	Non-Recycle	1.5	32.5
	3% Triton X-100 solution	Recycle	4	32.5
	Distilled Water	Non-Recycle	0.5	32.5
	3% Triton X-100 solution	Recycle	Overnight	32.5
Day 6	Distilled Water	Non-Recycle	1.5	35
	Distilled Water	Recycle	3.5	35
	3% Triton X-100 solution	Recycle	Overnight	35
<i>N.B. If the outflow at the start of day 7 is still cloudy, repeat steps from day 6 for another day</i>				
Day 7	Distilled Water	Non-Recycle	1	40
	Distilled Water	Recycle	4	40
	Distilled Water	Recycle	Overnight	40
Day 8	Distilled Water	Non-Recycle	1	40
	Distilled Water	Recycle	4	40
	Distilled Water	Recycle	Overnight	40
Day 9	1% PBS	Recycle	6	30
	1% PBS	Recycle	Overnight	30
Day 10	1% PBS	Recycle	6	30
	1% PBS	Recycle	Overnight	30
Day 11	PAA solution*	Recycle	1	15
	1% PBS (Sterile)	Recycle	2	30

* PAA solution: 0.1% Peracetic Acid and 4% Absolute Ethanol in distilled water

Table 12. Protocol for the decellularisation of whole human pancreas HP2 by perfusion using bioreactor.

<i>Day</i>	<i>Reagent</i>	<i>Mode of perfusion</i>	<i>Time (hours)</i>	<i>Pressure (mmHg)</i>
<i>Day 1</i>	Distilled Water (Milli-Q)	Non-Recycle	2.5	5
	0.1 % SDS solution	Non-Recycle	0.5	5.5
	Distilled Water	Non-Recycle	1	6.5
	0.1 % SDS solution	Recycle	Overnight	7.5
<i>Day 2</i>	Distilled Water	Non-Recycle	1	10
	1% SDS solution	Recycle	1	10
	Distilled Water	Non-Recycle	1	10
	1% SDS solution	Recycle	Overnight	10
<i>Day 3</i>	1% SDS solution	Non-Recycle	1	15
	Increase pressure to 20 mmHg and continue perfusion for 0.5 hours			
	Distilled Water	Recycle	2.5	20
	1% SDS solution	Recycle	Overnight	20
<i>N.B. If the outflow at the start of day 4 is still cloudy, repeat steps from day 3 for another day</i>				
<i>Day 4</i>	Distilled Water	Non-Recycle	1.5	30
	3% Triton X-100 solution	Recycle	Overnight	30
<i>Day 5</i>	Distilled Water	Non-Recycle	1.5	32.5
	3% Triton X-100 solution	Recycle	4	32.5
	Distilled Water	Non-Recycle	0.5	32.5
	3% Triton X-100 solution	Recycle	Overnight	32.5
<i>Day 6</i>	Distilled Water	Non-Recycle	1.5	35
	Distilled Water	Recycle	3.5	35
	3% Triton X-100 solution	Recycle	Overnight	35
<i>N.B. If the outflow at the start of day 7 is still cloudy, repeat steps from day 6 for another day</i>				
<i>Day 7</i>	Distilled Water	Non-Recycle	1	40
	Distilled Water	Recycle	4	40
	Distilled Water	Recycle	Overnight	40
<i>Day 8</i>	Distilled Water	Non-Recycle	1	40
	Distilled Water	Recycle	4	40
	Distilled Water	Recycle	Overnight	40
<i>Day 9</i>	1% PBS	Recycle	6	30
	1% PBS	Recycle	Overnight	30
<i>Day 10</i>	1% PBS	Recycle	6	30
	1% PBS	Recycle	Overnight	30
<i>Day 11</i>	PAA solution*	Recycle	1	15
	1% PBS (Sterile)	Recycle	2	30

* PAA solution: 0.1% Peracetic Acid and 4% Absolute Ethanol in distilled water

Table 13. Protocol for the decellularisation of whole human pancreas HP3 by perfusion using bioreactor.

3.4 DNA Quantification

Fresh and decellularised tissue samples marked for DNA quantification were retrieved from the -80 °C freezer and thawed in a 37 °C water bath for 1 hr. The cubes were then weighed and if necessary, cut to be between 15 and 25 mg in mass. The cubes were then placed in 1.5 ml microcentrifuge tubes. Twenty µl of proteinase K was added to each, and then mixed thoroughly using a vortex. The cubes were then placed into a heating block at 56 °C for at least 16 hrs or until they were completely lysed. The DNA was then extracted using the QIAGEN DNAeasy Blood and Tissue Kit according to the manufacturer's instructions. The extracted DNA was eluted in 200 µl of buffer AE and was quantified using a NanoDrop ND-2000 spectrophotometer.

3.5 Maintenance of Pancreatic Cells in Culture

Three cell lines were used for this study; PANC-1¹, MIA PACA-2 (ATCC) and PK-1¹. The PANC-1 cell line is a well-established primary adenocarcinoma of ductal origin obtained from the head of the pancreas of a 56 year old Caucasian male (297). The MIA PACA-2 cell line is also a primary adenocarcinoma obtained from the head and tail of the pancreas of a 65 year old male (298). The PK-1 cell line was isolated from a liver metastasis of carcinoma originating from the body of the pancreas (299). All cells were cultured in RPMI 1640 Medium (Thermofisher Scientific) supplemented with 2 mM/L glutamine (Thermofisher Scientific), 10% Foetal Bovine Serum (FBS; Thermofisher Scientific) and 1% 1X Gibco® Antibiotic-Antimycotic (Thermofisher Scientific). All cells were cultured under standard conditions in a humidified incubator under 5% CO₂ and at 37°C. Once cells reached ~75% confluence, the culture medium was changed and cells were trypsinised using 0.25% Trypsin-EDTA (Thermofisher Scientific) and passaged at a split ratio 1:3

¹ Kindly provided by Professor Pereira, UCL ILDH.

3.6 Scaffold Sterilisation and Preparation for Bioengineering

To prepare decellularised tissue for cell culture, scaffolds were sterilised using 1.5 ml of 0.1% peracetic acid (Sigma) in 4% absolute ethanol (Fisher Chemical) for 45 minutes in an orbital shaker (Staurt) at 700 rpm. This was followed by replacing the solution with sterile 1X HBSS (Thermofisher Scientific) for 15 minutes in an orbital shaker (Labnet -Orbit™ M60 microtube shaker).

The sterile scaffolds were then placed in individual wells in a 48 well plate 24 hours prior to the additions of cells and 1.4 ml of RPMI 1640 Medium supplemented with 2 mM/L glutamine, 10% FBS and 1% 1X Gibco® Antibiotic-Antimycotic was added.

3.7 3D Cell Cultures in Decellularised Scaffolds

Scaffolds were kept overnight in media as mentioned above [day -1]. Just prior to cell seeding, the scaffolds were transferred to individual wells in a 96 well plate. Cells (PANC-1, MIA PaCa-2 and PK-1) were re-suspended at a concentration of 0.5 million cells per 20 µl per scaffold ($n \geq 4$ per cell line). Cells were drawn up using a pipette and released on top of the decellularized tissue. Seeded scaffolds were kept for 2 hours in a humidified incubator at 37 °C with 5% CO₂ allowing cell attachment. This was followed by addition of 120 µl of culture medium and left in a humidified incubator at 37 °C with 5% CO₂ overnight. On the following day, scaffolds were transferred to individual wells in a 48 well plate and 1.4 ml of culture medium was added. Thereafter, wells and fresh media were changed every 3 days (Figure 10). At days 7 and 14 following seeding, the scaffolds were placed in either; 4% formaldehyde and assessed by histology and immunohistochemistry or snap frozen for further gene expression analysis.

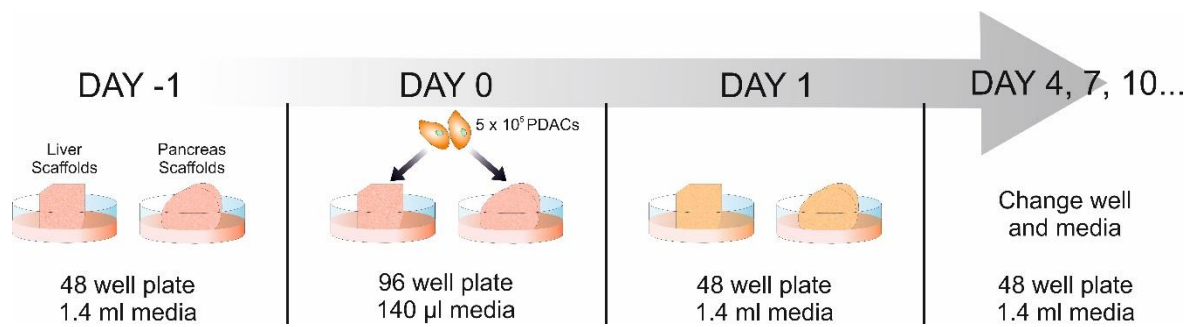


Figure 10. Schematic presenting the timeline for 3D cell culture.

3.8 Histology and Immunohistochemistry

Fresh, decellularised and bioengineered tissue samples, previously fixed in 4% formaldehyde, were retrieved, washed in distilled water, dehydrated in a series of Industrial IDA (Acquascience) and xylene (Acquascience) baths and finally embedded in paraffin. The samples were then sliced into 4 µm sections using a Leica RM2035 microtome (Leica biosystems). All sections were then passed through three histology grade xylene baths for a minimum of 5 minutes, and then through three IDA baths for a minimum of 2 minutes, finally ending up in tap water.

3.8.1 Histology

Sections were stained at room temperature as follows:

Haematoxylin and Eosin: Sections were treated with haematoxylin Harris' formula (Leica biosystems) for 10 minutes and then washed in tap water for 5 minutes. Next, the sections were stained with eosin (Leica biosystems) for 3 minutes, and then washed again with water. The sections were then dehydrated through IDA as quickly as possible and then placed in histology grade xylene until mounted.

Pico-Sirius Red: Sections were treated with freshly filtered pico-sirius red – F38 (R.A.Lamb; CI-35780) for 20 minutes. The sections were then dehydrated through IDA as quickly as possible and then placed in histology grade xylene until mounted.

Elastic Van Gieson: Sections were treated with 0.5% potassium permanganate for 5 minutes and washed thoroughly with distilled water. Next, they were treated with 1% oxalic acid for 1 minute, washed with distilled water followed by absolute alcohol. Sections were then stained with neat Miller's Elastic - (R.A. Lamb; LAMB/080D) for 2 hours, washed thoroughly with 70% industrially methylated spirits (IMS) (Fisher scientific) and then placed in tap water. The sections were checked under the microscope and, if necessary, differentiated in 0.5% acid-alcohol (1% HCl in 70% IDA aq.). As a final step, the sections were stained with van Gieson (Leica biosystems) for 5 minutes. The sections were then dehydrated through IDA as quickly as possible and then placed in histology grade xylene until mounted.

3.8.2 Immunohistochemistry

3.8.2.1. Manual Staining

Manual IHC staining was performed by Mr Andrew Hall² as follows; slides were incubated in 0.5% Trypsin (MP Biomedical) / 0.5% Chymotrypsin (Sigma-Aldrich) / 1% Calcium Chloride (BDH) in 10% Tris buffered saline (TBS) for 30 minutes at 37 °C. Slides were then washed in 10% TBS at pH 7.6 with 0.04% Tween-20 (Sigma-Aldrich) for 5 minutes. The slides were later blocked in peroxide blocking solution (Novocastra) for 5 minutes and incubated for 1 hour in the following primary antibodies; collagen I (Rabbit pAb to coll1 (ab34710), diluted 1:200; abcam), collagen III (Rabbit pAb to coll3 (ab7778), diluted 1:500; abcam), collagen IV (mouse mAb to coll4 (M0785), diluted 1:25; Dako), fibronectin (mouse mAb to fibronectin (MAB1937), diluted 1:100; Millipore) and laminin (mouse mAb to laminin α5-chain (MAB1924), diluted 1:200; Millipore). The slides were then placed for 25 minutes in Novolink™ post primary (Novocastra), 25 minutes in Novolink™ polymer solution (Novocastra) and developed with Novolink™ 3,3' di-amino-benzidine (Novocastra). The slides were finally counterstained with Mayer's Haematoxylin (Sigma-Aldrich) for 1 minute. All sections were mounted with DPX (Leica biosystems) and cover slipped.

² Liver Research Scientist at Royal Free Hampstead NHS Trust. Royal Free Hampstead NHS Trust

3.8.2.2. Automatic Staining

All automated staining was performed on the Leica Bond III Automated Immunostaining platform by UCLPathology³, using Leica Bond Polymer Refine detection with a DAB chromogen (Leica, DS9800).

MMP-9 (Millipore, MAB3309) was diluted 1/1000 and applied at room temp for 15 minutes, following on-board heat-induced epitope retrieval (HIER) using Leica Epitope Retrieval 2 (ER2) solution for 20 minutes (high pH).

ASP175 (Cell Signalling, polyclonal D175, #9661) was diluted 1/300 and applied at room temperature for 40 minutes, following on-board HIER using Leica Epitope Retrieval 1 (ER1) solution for 30 minutes (low pH).

B-catenin (Leica, clone 17C2, NCL-B-CAT) was diluted 1/50 and applied at room temperature for 15 minutes, following HIER using ER2 solution for 30 minutes (high pH).

Ki67 (Dako, clone MIB-1, M7240) was diluted 1/120 and applied at room temperature for 15 minutes, following HIER using ER2 solution for 20 minutes (high pH).

E-cadherin (Dako, clone NCH-38, M3612) is diluted 1/100 and applied at room temperature for 15 minutes following HIER using ER2 for 30 minutes.

CD44 (CD44v6, Leica, clone VFF-7, NCL-CD44v6) is diluted 1/50 and applied at room temperature for 15 minutes following HIER using ER1 for 30 minutes.

γH2A (Cell Signalling, monoclonal Ser139, #9718) is diluted 1/480 and applied at room temperature for 40 minutes, following on-board HIER using Leica Epitope Retrieval 1 (ER1) solution for 30 minutes (low pH).

All slides were observed using a Zeiss Axioskop 40. Images were captured with an AxioCam IcC5 using Zeiss Axiovision (version 4.8.2). All images were analysed and enhanced using Fiji v1.49d (ImageJ Jenkins server).

³ UCLPathology is part of the Pathology Research Department at the UCL Cancer Institute, based at the Rockefeller Building in UCL's Bloomsbury Campus.

3.9 RNA extraction and gene expression analysis

3.9.1 RNA Extraction

Total RNA was extracted from 2D and 3D cultures using TRIzol reagent (Qiagen) and RNeasy Universal Mini Kit (Qiagen) as described by the manufacturer's instructions. Briefly, 3D frozen samples were left to incubate at room temperature with 650 μ l of TRIzol in a 2ml safe-lock Eppendorf tube for 20 minutes and was followed by the addition of 7 mm stainless steel bead. The content was then agitated at 30 Hz for 8 minutes in a TissueLyser II (QIAGEN). The content of the tube (excluding the bead) was then transferred to a new 1.5 ml Eppendorf tube and the manufacturer's protocol was followed from step 4. For 2D samples, 650 μ l of TRIzol was added to the cells and a cell scraper was used to 2 minutes to scrape the cells off the plastic. The content of the plate were then transferred to a new 1.5 ml Eppendorf tube and the manufacturer's protocol was followed from step 4.

3.9.2 Reverse-Transcription

One milligram of total RNA was reverse transcribed with random primers and MultiScribe RT enzymes (Applied Biosystems, Paisley UK) as described by the manufacturer's instructions. Briefly, the volume equivalent to 1 mg of total RNA was mixed with nuclease-free water to make up 10 μ l. A mastermix of MultiScribe RT enzymes were prepared as described in

Table 14 and added to the 10 μ l of RNA. The samples were then run on a QCyler II PCR machine (QuantaBiotech) as described in Table 15.

Component	Volume/Reaction (µl)
10X RT Buffer	2
25X dNTP Mix (100 mM)	0.8
10X RT Random Primers	2
MultiScribe™ Reverse Transcriptase	1
RNase Inhibitor	1
Nuclease-free H2O	3.2
Total per Reaction	10

Table 14. Preparation of 2X reverse transcription master mix.

	Step 1	Step 2	Step 3	Step 4
Temperature (°C)	25	37	85	4
Time	10 mins	120 mins	5 mins	∞

Table 15. Program of the thermal cycler.

3.9.3 Real-Time qPCR

Gene expression was measured using TaqMan gene expression assays with the Applied Biosystems® 7500 Real-Time PCR system. TaqMan array plate genes are presented in Table 16 and additional TaqMan genes are presented in Table 17. Expression levels for each gene were calculated using the delta Ct method (300) and normalized to the Ct of HRPT as reference gene. Graphs depict averages ± SEM of the relative gene expression data (n=3 per group).

Gene Symbol	Assay ID	Gene Symbol	Assay ID
GAPDH	Hs99999905_m1	MAP2K2	Hs00360961_m1
HPRT1	Hs99999909_m1	MAPK1	Hs01046830_m1
GUSB	Hs99999908_m1	MAPK3	Hs00385075_m1
AKT1	Hs00178289_m1	MDM2	Hs99999908_m1
AKT2	Hs01086102_m1	MMP1	Hs00899658_m1
AKT3	Hs00178533_m1	MMP2	Hs01548727_m1
ARHGEF7	Hs00388776_m1	MMP3	Hs00968308_m1
BCL2	Hs999999018_m1	MMP7	Hs01042796_m1
BCL2L1	Hs00236329_m1	MMP9	Hs00234579_m1
BIRC5	Hs00153353_m1	NFKB1	Hs00765730_m1
BRAF	Hs00269944_m1	NFKB2	Hs00174517_m1

BRCA2	Hs01037414_m1	NOTCH1	Hs01062011_m1
CCNA2	Hs00153138_m1	PIK3CA	Hs00180679_m1
CCNB1	Hs99999188_m1	PIK3CB	Hs00927728_m1
CCND1	Hs00765553_m1	PIK3CD	Hs00192399_m1
CCND2	Hs00153380_m1	PIK3R1	Hs00381459_m1
CCNE1	Hs01026536_m1	PIK3R2	Hs00178181_m1
CCNE2	Hs00372959_m1	PTGS2	Hs00153133_m1
CDC42	Hs00741586_mH	RAC1	Hs01025984_m1
CDK2	Hs01548894_m1	RAC2	Hs01032884_m1
CDK4	Hs00175935_m1	RAF1	Hs00234119_m1
CDKN1A	Hs00355782_m1	RB1	Hs01078066_m1
CDKN1B	Hs00153277_m1	REL	Hs00968436_m1
CDKN2A	Hs00923894_m1	RELA	Hs00153294_m1
CDKN2B	Hs00365249_m1	RELB	Hs00232399_m1
CDKN2C	Hs00176227_m1	RHOA	Hs00357608_m1
CDKN2D	Hs00176481_m1	RHOB	Hs00269660_s1
CYP2E1	Hs00559367_m1	SMAD2	Hs00183425_m1
E2F1	Hs00153451_m1	SMAD3	Hs00969210_m1
E2F3	Hs00605457_m1	SMAD4	Hs00929647_m1
E2F4	Hs00608098_m1	SOS1	Hs00362308_m1
EGF	Hs01099999_m1	SRC	Hs00178494_m1
EGFR	Hs01076078_m1	STAT1	Hs01013989_m1
ELK1	Hs00428286_g1	STAT2	Hs01013123_m1
ERBB2	Hs01001580_m1	STAT3	Hs00374280_m1
FIGF	Hs01128659_m1	STAT5B	Hs00273500_m1
GRB2	Hs00157817_m1	STAT6	Hs00598625_m1
HBEGF	Hs00181813_m1	TGFA	Hs00608187_m1
HSP90AA1	Hs00743767_sH	TGFB1	Hs00998133_m1
IGF1	Hs01547656_m1	TGFB2	Hs00234244_m1
IL6	Hs00985639_m1	TGFB3	Hs01086000_m1
JAK1	Hs01026983_m1	TGFBR1	Hs00610318_m1
JAK2	Hs01078136_m1	TGFBR2	Hs00234253_m1
JAK3	Hs00169663_m1	TP53	Hs01034249_m1
KDR	Hs00911700_m1	VEGFA	Hs00900055_m1
KIT	Hs00174029_m1	VEGFB	Hs00173634_m1
KRAS	Hs00364282_m1	VEGFC	Hs01099203_m1
MAP2K1	Hs00605615_mH		

Table 16. List of TaqMan gene in the array plate and their corresponding ID's.

Gene Symbol	Assay ID
HPRT1	Hs02800695_m1
COL1A1	Hs00164004_m1
LOXL2	Hs00234579_m1
MMP9	Hs00171558_m1
TIMP1	Hs00158757_m1
WNT1	Hs00180529_m1
CTNBB1	Hs00355049_m1

Table 17. List of individually tested TaqMan genes and their corresponding ID's.

3.10 Chemotherapy

Drugs were prepared as follows:

Gemcitabine: A stock solution of 1 mM was prepared by solubilising 0.026% (w/v) of Gemcitabine powder (Gemzar) in distilled water. To obtain the desired drug concentrations, the stock solution was diluted in culture media.

Doxorubicin: A stock solution of 1 mM was prepared by solubilising 0.058% (w/v) of Doxorubicin Hydrochloride powder (Sigma-Aldrich) in DMSO (Sigma-Aldrich). To obtain the desired drug concentrations, the stock solution was diluted in culture media.

3.10.1 Determining Suitable Dosage of Chemotherapeutic Drugs on 2D Cultures

To determine the most suitable concentration of Gemcitabine and Doxorubicin for use in future 3D experiments; 3×10^3 cells of PANC-1, 7.5×10^3 cells of MIA PaCa-2 and 7.5×10^3 cells of PK-1 cells were seeded on individual wells in a 96-well-plate (n=6 / condition). Two hundred μL of culture media (see described above) was added to each well and the cells were incubated for 24 hours in a humidified incubator at 37°C with 5% CO_2 . Next, 200 μl of 9 different concentrations of Gemcitabine [0.01, 0.02, 0.04, 0.08, 0.1, 0.2, 0.3, 0.4 and 0.5 μM] and Doxorubicin [0.001, 0.005, 0.01, 0.02, 0.05, 0.1, 0.2, 0.5 and 0.8 μM], as well as a negative control of culture medium, was added to their appropriate wells. Cells were allowed to incubate for an additional 24 hours in a humidified incubator at 37°C with 5% CO_2 . Finally, all solutions were discarded and 200 μl of fresh culture medium was added to each well and the cells were allowed to incubate for 96 hours in a humidified incubator at 37°C with 5% CO_2 . Cells viability was then assessed using Alamar Blue (see section 3.11).

3.10.2 Treatment of 3D Bioengineered Scaffolds with Chemotherapeutics

Both liver and pancreas scaffolds were prepared and seeded with PANC-1, MIA PaCa-2 or PK-1, as described in section 3.7, and cultured for 9 days. On the 9th day the media was discarded and 1.4 ml of 0.5 μ M Gemcitabine or 0.5 μ M Doxorubicin was added to the appropriate scaffolds. As a negative control, 1.4 ml of media and as a positive control, 10% DMSO in culture medium, was added to their respected scaffolds. The scaffolds were then allowed to incubate in the dark for 24 hours in a humidified incubator at 37 °C with 5% CO₂. Next, the scaffolds were moved to fresh wells and washed with 1.4 ml 1X HBSS for 5 minutes and 1.4 ml of fresh media was added to each scaffold. The scaffolds were then allowed to incubate for 96 hours in a humidified incubator at 37°C with 5% CO₂. Cells viability was then assessed using Alamar Blue (see section 3.11).

3.11 Cell Viability Assay

3.11.1 Cells on 2D Cultures

For experiments performed on 2D plastic, culture media was discarded, and the cells were washed three times with 200 μ l 1X HBSS. Residual HBSS was discarded and 200 μ l 10% Alamar Blue (Thermofisher Scientific) in culture media was added to each well. The cells were allowed to incubate with the Alamar Blue in the dark for 2.5 hours in a humidified incubator at 37°C with 5% CO₂.

3.12.2 Cells on 3D Cultures

For experiment performed in 3D scaffolds, culture media was discarded, and the scaffolds were washed three times with 1.4 ml 1X HBSS. Residual HBSS was discarded and 1.4 ml of 10% Alamar Blue in culture media was added to each well. The scaffolds were allowed to incubate with the Alamar Blue in the dark for 2.5 hours in a humidified incubator at 37°C with 5% CO₂.

Fluorescence was read immediately after incubation on a FLUOstar Omega fluorescence microplate reader (BMG Labtech) and fluorescence was quantified using excitation and emission wavelengths of 540 nm and 595 nm, respectively. The data measured in arbitrary units for the treated samples were normalised to the negative control (non-treated samples) and reduction in percent (%) survival was calculated.

3.12 Confirmation of Doxorubicin Uptake

To confirm the uptake of the chemotherapeutic by the cells in 3D scaffolds, Doxorubicin's fluorescence was utilised. PANC-1 and MIA PaCa-2 cells on pancreas scaffolds and PK-1 cells on liver scaffolds were cultured as described in section 3.7 for 9 days. On the 9th day the media was discarded and 1.4 ml of 0.5 μ M Doxorubicin or fresh media was added to 3 samples of each condition. The scaffolds were then allowed to incubate in the dark for 24 hours in a humidified incubator at 37 °C with 5% CO₂. Next, the scaffolds were washed with 1X PBS for 5 minutes, transferred to a mould with OCT (Agarscientific) and snap frozen in liquid nitrogen. Twenty micrometre sections were cut using a CRYOTOME FSE cryostat (Thermofisher Scientific). All sections were then washed 3 times for 5 minutes with 1X PBS and stained with 300 nM DAPI (Thermofisher Scientific) for 1 minutes. Slides had a cover-slip applied and were imaged with a BX63 microscope (Olympus) using excitation/emission of 405/470 nm (DAPI), 480/525 nm (collagen) and 480/590 nm (Doxorubicin). Images were then processed with Fiji (ImageJ 1.52i).

3.13 Analysis of Cell Size

To measure the size of the cells in 3D scaffolds, immunohistochemistry images of MMP9 at 40X were utilised. The images were uploaded into Fiji (ImageJ 1.52i) and processed by converting the images into RGB. This was followed by 'colour deconvolution' using the HE DAB settings which broke down the image into three sub-images: Haematoxylin, DAB and Eosin. The 'threshold' of the DAB image was then changed to 92.5% resulting in a black (cells) and white (background) image. Ten cells

were randomly selected using the 'wand (tracing) tool' and their 'Area' was measured in pixels.

3.14 RNAseq

RNA extracted as described in section 3.9.1 were sent for library preparation and sequencing at the Wellcome Sanger Institute next-generation sequencing facility⁴ (Cambridge, U.K). PolyA purified opposing strand library kit was used, and 4 samples per lane were multiplexed in 6 lanes on Illumina HiSeq 2000, 2x75bp, Paired-End reads. A total of 150/200M reads per sample were mapped to the human genome GRCh38 reference assembly and stored as cram files. Cram were converted into bam keeping only reads with quality score above 10 ($q > 10$) using Samtools view (301). These were then converted into FASTQ files and input into Rosalind (OnRamp). A threshold of 0.05 for statistical significance (p-value) and a log fold change of expression with absolute value of at least 0.5 was chosen.

3.15 RNAseq Data Analysis

RNAseq Data was analysed by Rosalind (<https://rosalind.onramp.bio/>), with a HyperScale architecture developed by OnRamp BioInformatics, Inc. (San Diego, CA). Reads were trimmed using cutadapt (302). Quality scores were assessed using FastQC (303). Reads were aligned to the Homo sapiens genome build hg19 using STAR (304). Individual sample reads were quantified using HTseq (305) and normalized via Relative Log Expression (RLE) using DESeq2 R library (306).

All differentially expressed (DE) genes further were analysed on iPathwayGuide (Advaitabio.com). Methods for pathways analysis (KEGG version 84.0+/10-26 Oct 17), gene ontology (GODb version 2017-Nov6) and upstream regulators (STRING version

⁴ The Vallier research at the Wellcome Sanger Institute, Hinxton, Saffron Walden CB10 1SA

10.5.May14th2017) were automatically processed by the software as described below.

3.15.1 Pathway Analysis

iPathwayGuide scored pathways using the Impact Analysis method (307-309). Impact analysis uses two types of evidence: i) the over-representation of DE genes in a given pathway and ii) the perturbation of that pathway computed by propagating the measured expression changes across the pathway topology. These aspects are captured by two independent probability values, pORA and pAcc, that are then combined in a unique pathway-specific p-value. The underlying pathway topologies, comprised of genes and their directional interactions, are obtained from the KEGG database (310-313).

The first probability, pORA, expresses the probability of observing the number of DE genes in a given pathway that is greater than or equal to the number observed, by random chance (314, 315). Let us consider there are N genes measured in the experiment, with M of these on the given pathway. Based on the user-defined a priori selection of DE genes, K out of M genes were found to be differentially expressed. The probability of observing exactly x DE genes on the given pathway is computed based on the hypergeometric distribution (Figure 11):

$$P(X=x|N,M,K) = \frac{\binom{M}{x} \binom{N-M}{K-x}}{\binom{N}{K}}$$

Figure 11. Hypergeometric distribution. Where x is the DE genes, N is the genes measured in the experiment, M is the genes measured on a given pathway and K is the number of DE genes.

Because the hypergeometric distribution is discrete, the probability of observing fewer than x genes on the given pathway just by chance can be calculated by summing the probabilities of randomly observing 0, 1, 2, ..., up to x-1 DE genes on the pathway (Figure 12):

$$p_u(x-1) = P(X=1)+P(X=2)+\dots+P(X=x-1) = \sum_{i=0}^{x-1} \frac{\binom{M}{i} \binom{N-M}{K-i}}{\binom{N}{K}}$$

Figure 12. Sum of probabilities. Where x is the DE genes, N is the genes measured in the experiment, M is the genes measured on a given pathway and K is the number of DE genes.

iPathwayGuide calculated the probability of randomly observing a number of DE genes on the given pathway that is greater than or equal to the number of DE genes obtained from data, by computing the over-representation p-value: $pORA = p_o(x) = 1 - p_u(x-1)$ (Figure 13):

$$p_o(x) = 1 - \sum_{i=0}^{x-1} \frac{\binom{M}{i} \binom{N-M}{K-i}}{\binom{N}{K}}$$

Figure 13. Over-representation p-value. Where x is the DE genes, N is the genes measured in the experiment, M is the genes measured on a given pathway and K is the number of DE genes.

The second probability, $pAcc$, is calculated based on the amount of total accumulation measured in each pathway. A perturbation factor is computed for each gene on the pathway using (Figure 14):

$$PF(g) = \alpha(g) \cdot \Delta E(g) + \sum_{u \in US_g} \beta_{ug} \frac{PF(u)}{N_{ds}(u)}$$

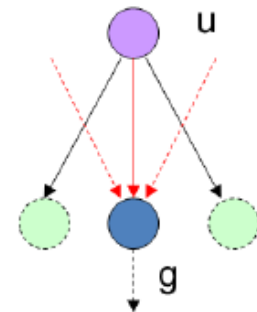


Figure 14. Perturbation factor of an individual gene. Where g represents a given gene and u represents all the genes directly upstream of g .

In Figure 14, $PF(g)$ is the perturbation factor for gene g , the term $\Delta E(g)$ represents the signed normalized measured expression change of gene g , and $\alpha(g)$ is a priori weight based on the type of the gene. The last term is the sum of the perturbation factors of all genes u , directly upstream of the target gene g , normalized by the number of downstream genes of each such gene $N_{ds}(u)$. The value of β_{ug} quantifies the strength of the interaction between genes g and u . The sign of β represents the type of interaction: positive for activation-like signals, and negative for inhibition-like signals. Subsequently, iPathwayGuide calculated the accumulation at the level of each gene, $Acc(g)$, as the difference between the perturbation factor $PF(g)$ and the observed log fold-change:

$$Acc(g_i) = PF(g_i) - \Delta E(g_i)$$

Figure 15. Accumulation of genes. Where g represents a given gene.

All perturbation accumulations are computed at the same time by solving the system of linear equations resulting from combining the equation of Figure 15. For all genes on a given pathway. Once all gene perturbation accumulations are computed, iPathwayGuide computed the total accumulation of the pathway as the sum of all absolute accumulations of the genes in a given pathway. The significance of obtaining a total accumulation ($pAcc$) at least as large as observed, just by chance, is assessed through bootstrap analysis.

The two types of evidence, $pORA$ and $pAcc$, are then combined into an overall pathway score by calculating a p-value using Fisher's method.

3.15.2 Gene Ontology Analysis

For each Gene Ontology (GO) term (316, 317), the number of DE genes annotated to the term is compared to the number of DE genes expected just by chance. iPathwayGuide used an over-representation approach to compute the statistical significance of observing at least the given number of DE genes. The p-value is

computed using the hypergeometric distribution as described for pORA in the Pathway Analysis section.

The classical method used above considers all GO terms to be independent. However, given the nature of gene ontology, consideration of genes multiple times introduces errors. By definition, all the genes annotated to a GO term are also annotated to all its ancestors. To overcome this limitation, several methods were proposed to assess the enrichment of GO terms by considering the structure of the gene ontology. Among these, iPathwayGuide used the proposed elim and weight pruning methods (318). The elim pruning method iteratively eliminates the genes mapped to a significant GO term from more general (higher level) GO terms, while the weight pruning method assigns weight to each gene annotated to a GO term based on the scores of neighbouring GO terms.

3.15.3 Predicted Upstream Regulator Analysis

The prediction of upstream regulators is based on two types of information: i) the enrichment of differentially expressed genes from the experiment and ii) a network of regulatory interactions from iPathwayGuide's proprietary knowledge base. The network is a directed graph in which the nodes represent genes, and the edges represent regulatory interactions between two genes. A signed edge in this graph consists of a source gene, a target gene, and a sign to indicate the type of signal: activation (+) or inhibition (-). To create the network, the analysis selects only those edges observed in the literature with at least a medium confidence (evidence score greater than or equal to 400). The analysis considers two hypotheses: i) HA, the upstream regulator is activated in the condition studied and ii) HI, the upstream regulator is inhibited in the condition studied.

The analysis divides the set of all the genes obtained from NCBI Gene database into several subsets based on the measurements in the experiment and the definitions shown in Figure 16 and Figure 17. Let the sign of a measured DE gene be the sign of the log fold change value: (+) for up-regulated genes and (-) for down-regulated genes. A gene is a target gene if it corresponds to a node in the network that has at least one incoming edge. iPathwayGuide define a consistent gene as a target DE gene such

that the sign of the gene is consistent both with the type of the signal and with the hypothesis considered. Formally, by definition, a target DE gene g is consistent with Hypothesis H_A if and only if an incoming edge e exists such that $\text{sign}(g) = \text{sign}(e)$. In other words, this describes the situation when the upstream regulator is predicted as activated, the signal is activation and the target DE gene is up-regulated, or the signal is inhibition and the target DE gene is down-regulated (see panel A in Figure 16). A target DE gene g is consistent with Hypothesis H_I if and only if an incoming edge e exists such that $\text{sign}(g) \neq \text{sign}(e)$. This second case captures the situation in which the upstream regulator is inhibited, the signal is inhibition and the target DE gene is up-regulated, or the signal is activation and the target DE gene is down-regulated (see panel B in Figure 16).

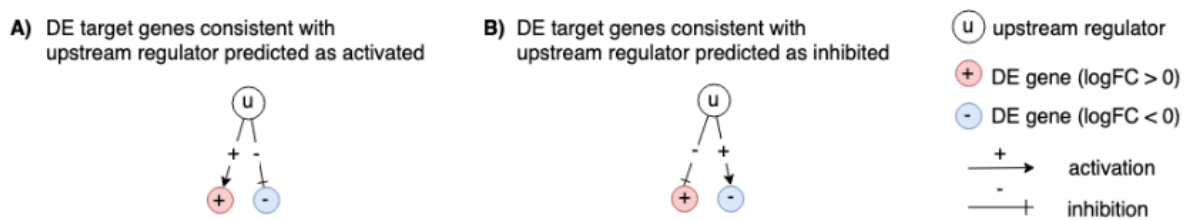


Figure 16. Target genes consistent with the hypothesis considered: In panel A, the signs of the DE genes match the signs of their respective incoming edges, increasing the likelihood that the upstream regulator u is activated. In panel B, the signs of the DE genes are opposite to the signs of their edges, increasing the likelihood that the upstream regulator u is inhibited.

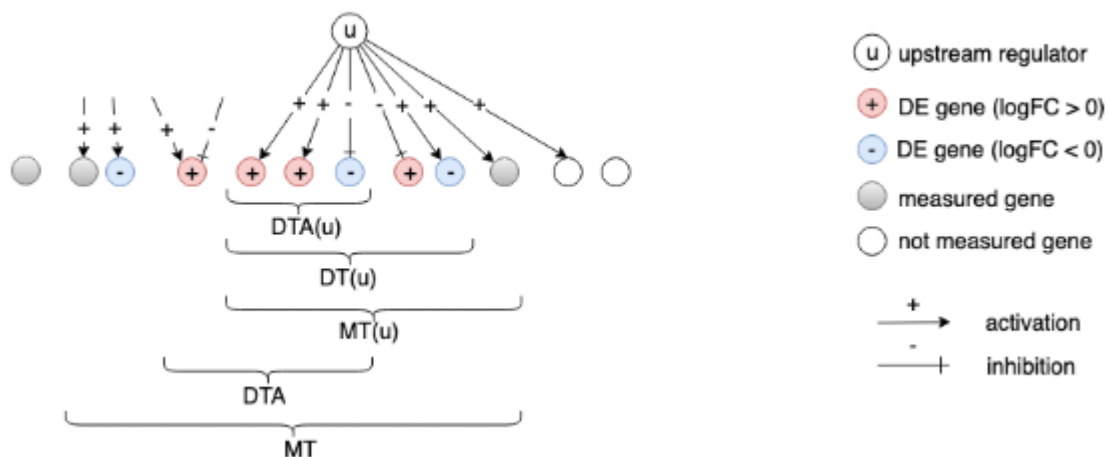
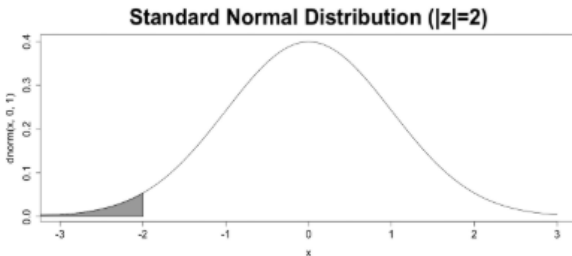


Figure 17. The set of all genes includes the set of measured genes that are also targets in the network, or Measured Targets (MT). *iPathwayGuide* defines the subset of "DE Targets consistent with the first hypothesis that the upstream regulators are Activated", DTA. For a selected upstream regulator u , we have the set of "Measured Targets of u " $MT(u)$, "Differentially expressed Targets downstream of u " $DT(u)$, and the set of "DE targets consistent with the hypothesis H_A that u is

Activated" DTA(u). The equivalent graphic for the hypothesis H1 associated with DTI and DTI(u) is not shown.

Upstream regulators Z-score. For both research hypotheses, the analysis computes a Z-score for each upstream regulator z(u) by iterating over the genes in DT(u) and their incoming edges in(g). iPathwayGuide can then compute the p-value corresponding to the z-score P_z as the one-tailed area under the probability density function for a normal distribution, N(0,1) (Figure 18).

$$z(u) = \frac{\sum_{g \in DT(u)} \sum_{e \in in(g)} sign(e) \times sign(g)}{\sqrt{\sum_{g \in DT(u)} |in(g)|}}$$

$$P_z = \frac{1}{\sqrt{2\pi}} \int_{-\infty}^{-|z|} e^{-\frac{x^2}{2}} dx$$


The figure shows a standard normal distribution curve centered at 0. The x-axis ranges from -3 to 3, and the y-axis (density) ranges from 0.0 to 0.4. A vertical line is drawn at x = -2, and the area under the curve to the left of this line is shaded in gray. The title of the graph is 'Standard Normal Distribution (|z|=2)'.

Figure 18. Upstream regulators Z-score.

Upstream regulators predicted as activated. Here, the research hypothesis considers the upstream regulator as activated. For each upstream regulator u, the number of consistent DE genes downstream of u, DTA(u) is compared to the number of measured target genes expected to be both consistent and DE just by chance. iPathwayGuide uses an over-representation approach to compute the statistical significance of observing at least the given number of consistent DE genes. The p-value P_{act} is computed using the hypergeometric distribution (314, 315).

After computing a p-value for both types of evidence, P_z and P_{act}, we need to combine these two probabilities into one global probability value, P_G that is used to rank the upstream regulators and test the research hypothesis that the upstream regulators are predicted as activated in the condition studied. Since only a positive z-score indicates that the upstream regulator is predicted as activated, we only combine p-values for a positive z-score. Moreover, to avoid introducing false positives, only P_z for significant

z-scores ($z \geq 2$) are combined. The analysis uses the standard Fisher's method to combine p-values into one test statistic.

Upstream regulators predicted as inhibited. In parallel with upstream regulators predicted as activated, we use P_{inh} and P_z to predict upstream regulators that are inhibited. Here, the research hypothesis states that the upstream regulators are inhibited in the conditions studied. For each upstream regulator u , the number of consistent DE genes downstream of u , $DTI(u)$ is compared to the number of measured target genes expected to be both consistent and DE just by chance. Using the Fisher's method as above, the analysis combines P_{inh} and P_z , where P_z is considered only for significant negative z-scores ($z \leq -2$).

3.6 Statistics and Data Analysis

A minimum of three biological replicates were performed for all protocols. Statistical significance was determined using: (i) an ordinary one-way ANOVA followed by a Tukey's multiple comparison test for DNA quantification and qRT-PCR, (ii) a two-way ANOVA followed by a Tukey's multiple comparison test for cell viability analysis and (iii) a Kurskal-Wallis one-way ANOVA followed by a Dunn's multiple comparison test for cell-size analysis. All statistical analyses and graphs were generated on GraphPad Prism (version 8.1.0)

• CHAPTER 4 •

“Never neglect an extraordinary appearance or happening. It may be-usually is, in fact-a false alarm that leads to nothing, but may on the other hand be the clue provided by fate to lead you to some important advance.”

- *Alexander Fleming*

4. RESULTS

4.1 Decellularisation of Human Pancreata

4.1.1 Decellularisation of Pancreas Cubes by Agitation

Discarded healthy human pancreas cubes were initially decellularised-using protocol PA1 as described in the methods and materials section (Methods and Materials; Table 10). This method was loosely based on a well characterised decellularisation protocol for healthy human liver cubes (296) (Methods and Materials; Table 9) and was a reference point on which future improvements would be based on. This protocol utilises a high agitation (40 ms^{-2}); (i) to assist in the destruction of cellular membranes and (ii) to improve the diffusion of reagents through the tissue. The third and final consideration was the order of different reagents during the decellularisation protocol; this was decided according to logical scientific reasoning, which involved starting with deionised water to promote cell lysis through an osmotic shock. Following the exposure of cellular material, a reagent mixture was exploited to disrupt lipid-lipid, lipid-protein, protein-protein bonds, nuclear material and metallic ions. Finally, a highly hypertonic solution (8.7% NaCl) followed by an isotonic solution (1% PBS) was used to flush out the detached cellular material.

After 2 cycles were completed applying the abovementioned reagents, it was macroscopically evident that the tissue was not entirely decellularised. Indeed, the tissue was yellow which commonly indicates the presence of cellular material (Figure not shown). This observation was followed by histological evidence: Sirius Red (SR), which is used to observe cellular material by staining it yellow against a red collagen background. This staining was in perfect agreement with the macroscopic view of the tissue as it showed a vast amount of cellular debris still intact on the ECM (Figure 19; e and f). Additionally, Haemotoxylin and Eosin (H&E) staining, which allows for the identification of nuclear material by staining it blue against a red collagen background, showed the presence of DNA residues (Figure 19; g and h).

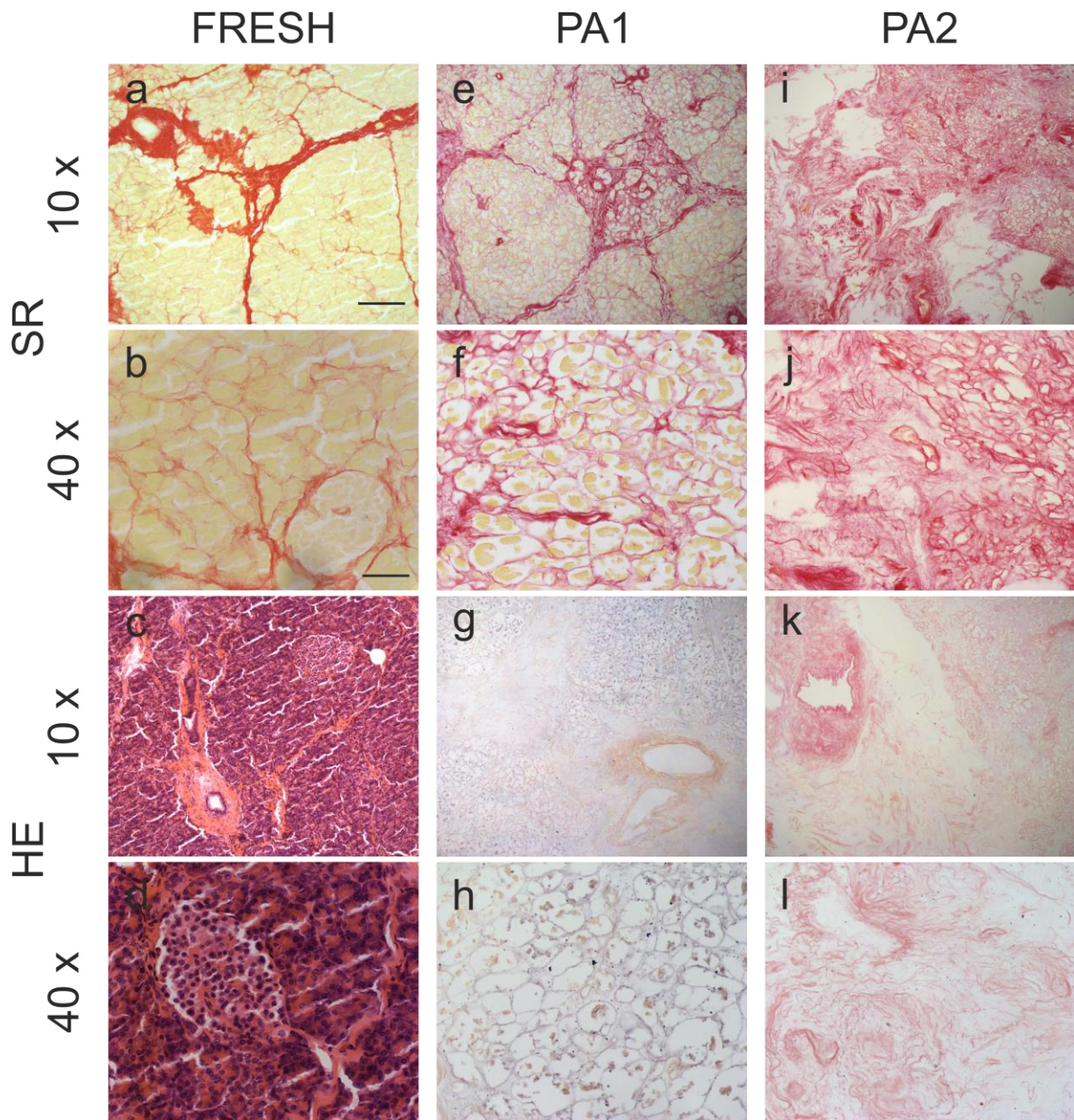


Figure 19. *Histological images of fresh and decellularised pancreas using agitation. SR staining of fresh pancreas distinctly shows cellular material in yellow (a and b). Cellular material is also present on scaffolds decellularised using protocol PA1 (e and f), whereas, no cellular material can be seen in any of the scaffolds decellularised using protocol PA2 (i and j). H&E staining of fresh pancreas is characterised by nuclear material stained in blue (c and d). This material is clearly present in tissue decellularised with protocol PA1 (g and h) but is absent in tissue decellularised using protocol PA2 (k and l). It is also evident that ECM architecture is still preserved in protocols PA1 (e – h) but is not maintained in protocol PA2 (i – l). Scale bar for 10x images is 200 μm and for 40x images 50 μm .*

The next step was to try a longer exposure to the reagents. Therefore, keeping most parameters consistent, 4 cycles of the aforementioned reagents using protocol PA2 was performed (Methods and Materials; Table 10). Macroscopically, there was a significant progress compared to protocol PA1, as the tissue was much clearer, with almost no yellow patches observed (Figure not shown). Additionally, there was a loss to the bulk structure of the decellularised tissue. Microscopically, there was no cellular debris observed on the SR slides (Figure 19; i and j) and no nuclear material observed on the H&E slides (Figure 19; k and l). However, the decellularisation of the pancreas cubes using this protocol was achieved at the expense of the ECM, which was visibly destroyed. Both H&E and SR staining showed no retention of the ECM architecture (Figure 19).

4.1.2 Decellularisation of Whole Human Pancreas by Perfusion

Following unsatisfactory results using agitation, the next approach was to attempt decellularisation of whole pancreata by perfusion. The pancreata were prepared for decellularisation using the same protocol as for transplantation (Methods and Materials; Section 3.3). This procedure was performed by a surgeon to ensure no damage to the pancreas was incurred. Furthermore, to enhance perfusion to the superficial parenchyma of the pancreas, the duodenum and pancreas were decellularised en-bloc to allow for the flow of reagents via the pancreaticoduodenal veins.

Decellularisation of the en-bloc pancreata was achieved within 2 weeks of perfusion. The protocol used for decellularisation was loosely based on the well-characterised protocol used for healthy human liver decellularisation (319). During and following decellularisation the pancreas gradually turned translucent white with the dissolution of cells (Figure 20). The decellularisation protocol, based on a retrograde perfusion through the portal vein, utilised the combination of four different cell elimination factors: i) physical cell-damaging by freezing and thawing, ii) osmotic shock to allow cell lysis, iii) detergents to destruct chemical bonds; and iv) flow shear stress to allow the penetration into the parenchyma of the pancreas to eliminate cellular remnants.

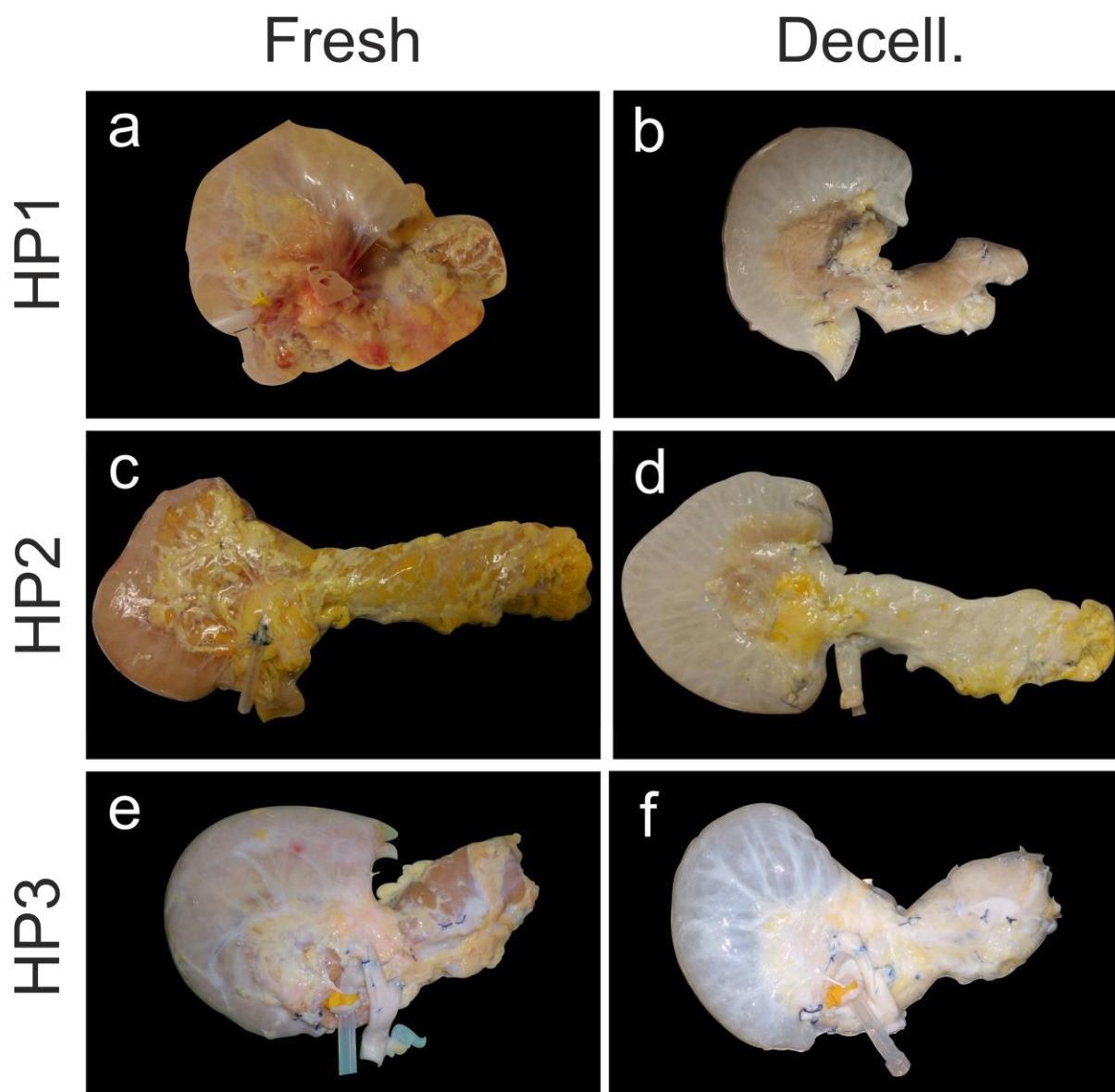


Figure 20. Macroscopic view of pancreata decellularised using different perfusion protocols. Yellow/pink tissue is a representative of cellular material, which is the colour of fresh pancreata (**a, c and e**). The translucent-white colour usually represents decellularised tissue (**b, d and f**). HP1 is the first pancreas decellularised using no pressure regulation (**a and b**). HP2 is the first pancreas decellularised using a bioreactor (**c and d**), HP3 is the pancreas decellularised using the most optimal perfusion protocol within a bioreactor (**e and f**).

4.1.2.1 Protocol Development for the Decellularisation of the First Human Pancreas

The first attempt at decellularising of a pancreas, HP1 (Figure 20; a and b) was performed with no sensors for pressure measurements. The flow rate was incremental throughout decellularisation and was determined according to the formula used for

healthy human liver decellularisation (319). Initially, deionised water was perfused for several hours to cause an osmotic shock to the cells, thereby disrupting the cell membrane. This allowed the cellular material to be exposed to further degradation. Due to the exaggerated amount of cellular material released into the solution from the pancreas, a low concentration of SDS (0.1%) was initially used. SDS further assists in lysing the cell membranes as well as the destruction of the nuclear membranes. Once the excreted cellular content was saturated, the concentration of SDS was increased to 1% for 2 consecutive days. Again, when the dissolution was further saturated, the pancreas was perfused with a high concentration of Triton X-100 (3%) indefinitely until the organ appeared macroscopically decellularised. Triton X-100 is used to; i) neutralise the SDS and ii) disrupt lipid–lipid and lipid-protein interactions, while leaving protein-protein interactions intact. The main macroscopic criteria were: i) the whole organ turned translucent white and ii) the outflow solution was consistently transparent for one day. Once these standards were satisfied, the pancreas was washed with deionised water for 2 days followed by 2 days of 1% PBS.

Characterisation for Cellular Elimination

Following decellularisation of HP1, the next step was to evaluate cellular elimination and ECM preservation of the head, body, and tail of the pancreas. It was important to analyse all three segments separately as the flow of reagents differs within the pancreas due to its natural anatomy. The first step was to assess the elimination of cellular material histologically. H&E staining showed slight evidence of nuclear material and SR staining was negative for cell remnants in all three segments (Head, Figure 21 a - d; Body, Figure 21 e - h and Tail Figure 21 i - l). Also, quantification of DNA using a DNeasy Blood and Tissue kit showed a significant reduction of nuclear material in all three segments of the pancreas when compared to the fresh pancreas. Furthermore, there were no significant differences in the quantity of nuclear material between the three-decellularised segments (Figure 24). However, the quantity of DNA was still above the standardised criteria of our lab, stated as 100 ng/mg wet tissue.

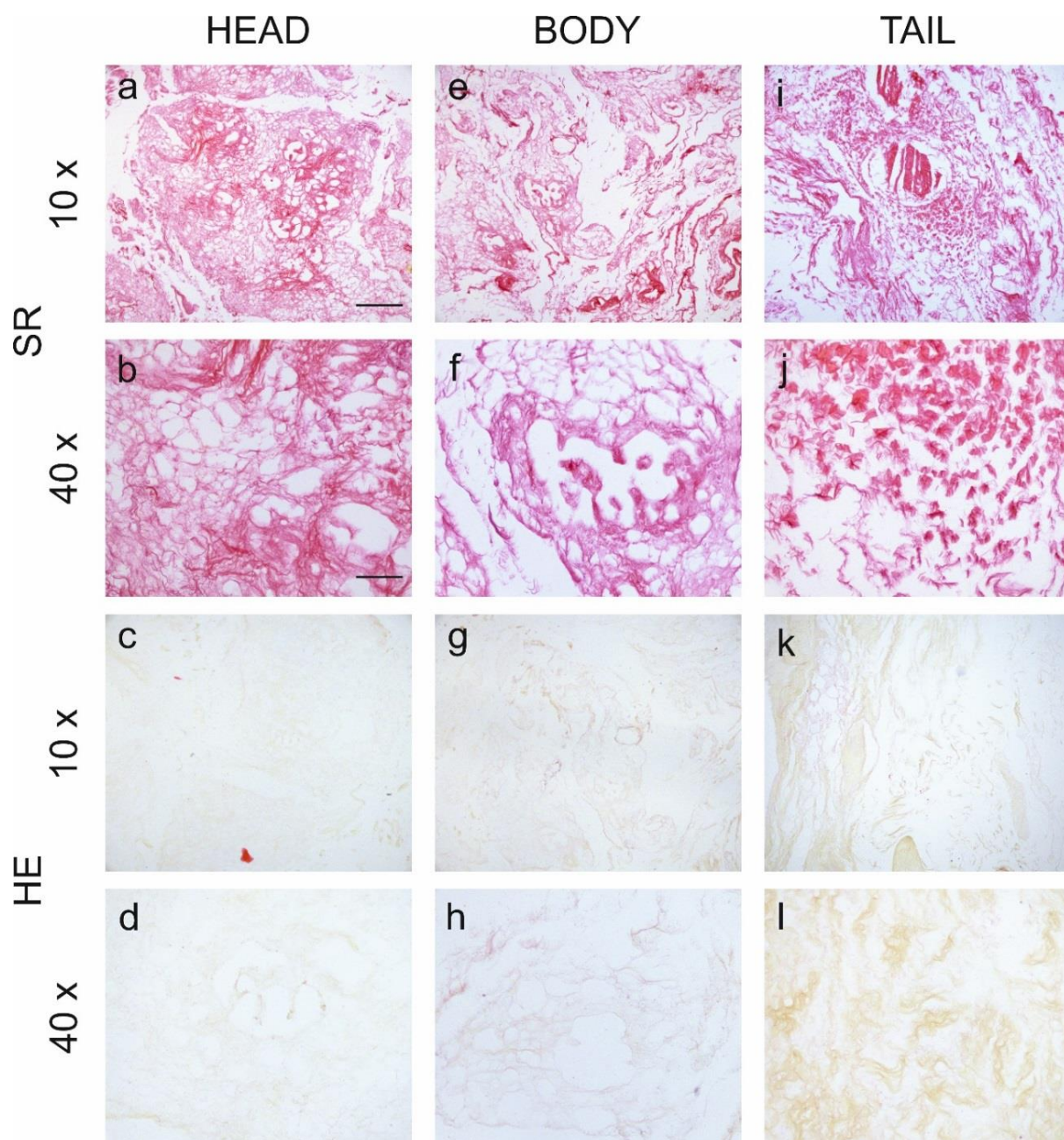


Figure 21. Histological images of pancreas HP1 decellularised by perfusion. SR staining of the head (**a and b**), body (**e and f**) and tail (**i and j**) show no indication of cellular material (yellow). Similarly, H&E staining show almost no remaining nuclear material in the head (**c and d**) and tail (**k and l**) of the pancreas. There is some blue complexion observed in the body of the pancreas which could indicate residual nuclear material (**g and h**). Both SR and H&E staining show an extent of ECM microarchitectural destruction, which is more evident in the parenchyma of the tissue. Scale bar for 10x images is 200 μm and for 40x images 50 μm .

Characterisation for ECM Preservation

As previously mentioned, it is of primary importance for this study to produce decellularised scaffolds that could be tissue-specific for disease modelling and regenerative medicine. Thus, it is vital to preserve as much of the ECM as possible, as it would be inadequate if the decellularised tissue is unable to: (i) re-attach cells or (ii) represent the native environment. The first step was to analyse the retention of the ECM architecture, by employing both H&E and SR stainings. The three main features considered for ECM preservation were the presence of: (i) islets of Langerhans, (ii) exocrine ECM and (iii) blood vessels. Only the body of the pancreas showed maintenance of all three structures (Figure 21 e – h); whereas, the head showed compression of the blood vessels and exocrine ECM (Figure 21 a – d), and the tail presented deformation and destruction of the exocrine ECM (Figure 21 i – l).

To further investigate the retention of specific ECM proteins, namely: collagen I, collagen III, collagen IV, fibronectin and laminin, immunohistochemistry was performed on the body of the pancreas, as it was considered unnecessary to evaluate tissue from the destroyed sections of the pancreas. All stains showed similar patterns to the native pancreas tissue. Collagen I (Figure 25f), collagen III (Figure 25g) and fibronectin (Figure 25h) stained positive for the exocrine ECM, whereas collagen IV (Figure 25i) was not strongly evident in the exocrine tissue but was found lining the ducts. Finally, laminin was present around blood vessels and islets of Langerhans (Figure 25j).

4.1.2.2 Perfusion - Decellularisation using a Bioreactor

To improve on the promising results obtained by perfusion, the next decellularisation (HP2) was performed in an ORCA Harvard Apparatus perfusion bioreactor. The bioreactor can monitor the pressure within the pancreas, and therefore the flow rate used was in correlation to an incremental pressure gradient. The pressure was increased gradually to substitute the loss of pressure from the cells. An identical reagent regime, as to the previous HP1 perfusion decellularisation, was used.

The elimination of cellular material was histologically evaluated by H&E (Figure 22 c, d, g, h, k and l) and SR (Figure 22 a, c, e, f, i and j), which showed no signs of nuclear material or cellular content, respectively. DNA quantification supported the histological analysis and presented DNA content above 150 ng/mg-wet tissue in all three segments of the pancreas (Figure 24). This was found to be not significant compared to native and HP1 pancreas.

Further, for HP3, it was decided to increase the number of fresh reagents used, instead of recycling them, in order to reduce the amount of cellular material being re-perfused back into the organ.

The elimination of cellular material was histologically evaluated by H&E (Figure 23 c, d, g, h, k and l) and SR (Figure 23 a, c, e, f, i and j), which showed no signs of nuclear material or cellular content, respectively. DNA quantification supported the histological analysis and presented DNA content below 150 ng/mg-wet tissue in all three segments of the pancreas (Figure 24). This was found to be significantly lower compared to HP1 and HP2 ($p < 0.05$).

HP3 ECM architecture was notably superior to HP1. The head, body, and tail were preserved as all three features showed the presence of 1) islets of Langerhans (Figure 25 k – o; red arrow), 2) exocrine ECM, ducts (Figure 25 n; green arrow) and 3) blood vessels which were well maintained. Additionally, there were no notable differences in ECM protein content and distribution of the body of the pancreas in HP3 (Figure 25 k - o) when compared to native tissue or HP1.

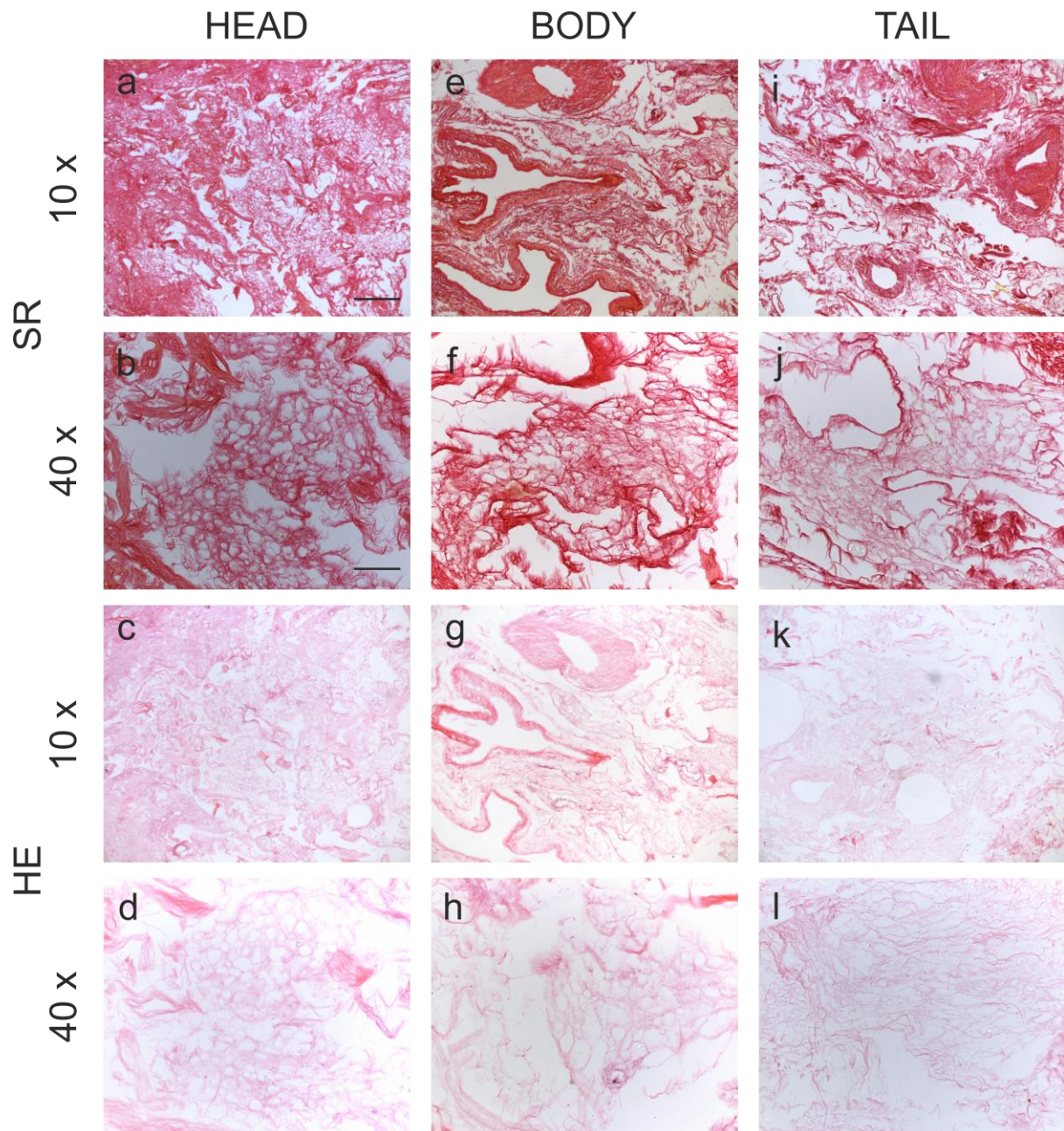


Figure 22. *Histological images of pancreas HP2 decellularised by perfusion using a bioreactor. SR staining of the head (a and b), body (e and f) and tail (i and j) show no indication of cellular material (yellow). Similarly, H&E staining show no residual nuclear material in the head (c and d), body (g and h) and tail (k and l) of the pancreas. Both SR and H&E staining show preservation of ECM microarchitecture in the head (a – d) and body (e – h) of the pancreas but indicated some collapse in the tail (i – l). Scale bar for 10x images is 200 μ m and for 40x images 50 μ m.*

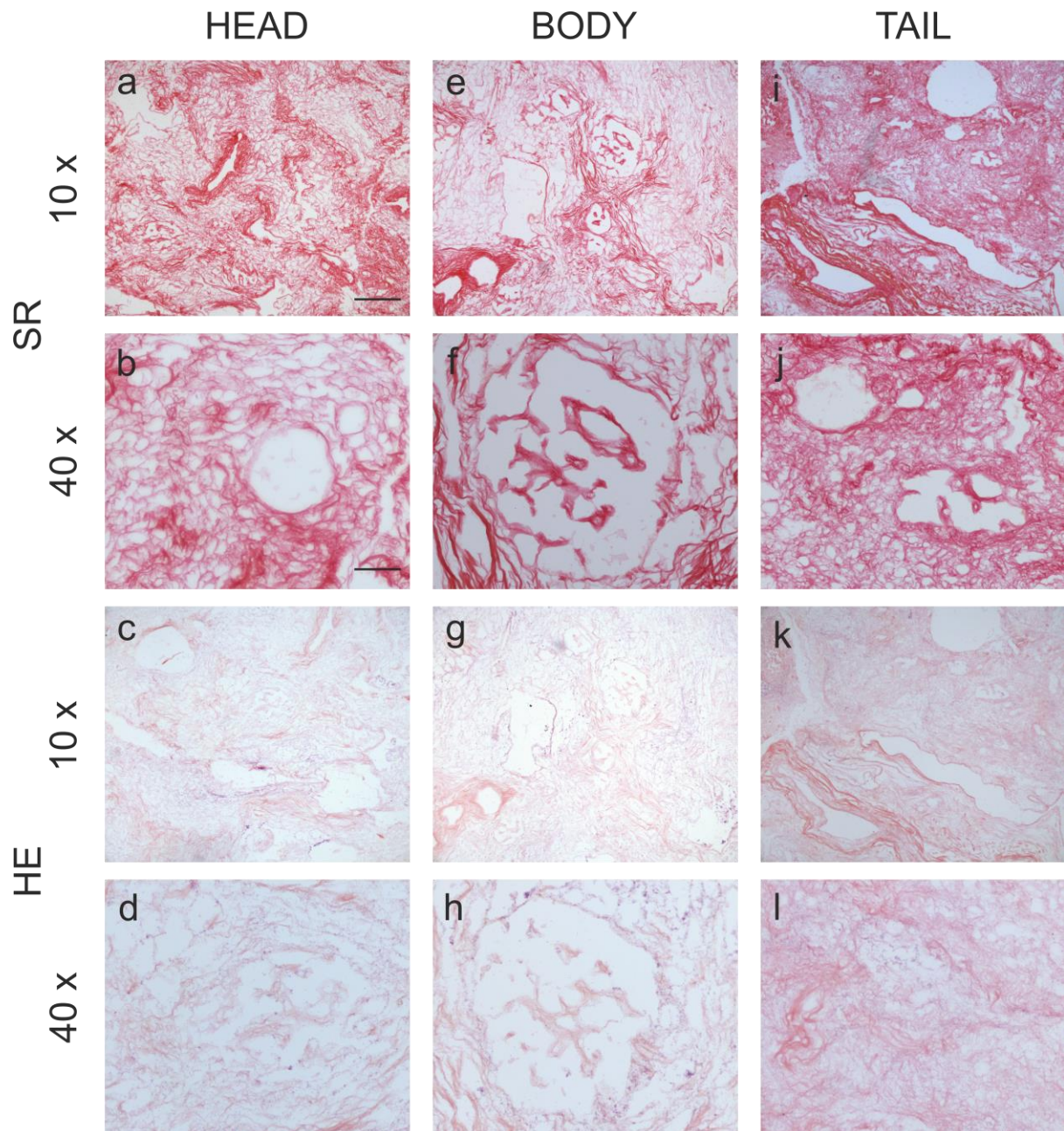


Figure 23. *Histological images of pancreas HP3 decellularised by perfusion using a bioreactor. SR staining of the head (a and b), body (e and f) and tail (i and j) show no indication of cellular material (yellow). Similarly, H&E staining show no residual nuclear material in the head (c and d), body (g and h) and tail (k and l) of the pancreas. Both SR and H&E staining show preservation of ECM microarchitecture in the head (a – d) and body (e – h) of the pancreas. SR staining of the tail of the pancreas (i – l) demonstrates break down of the ECM. Scale bar for 10x images is 200 μm and for 40x images 50 μm .*

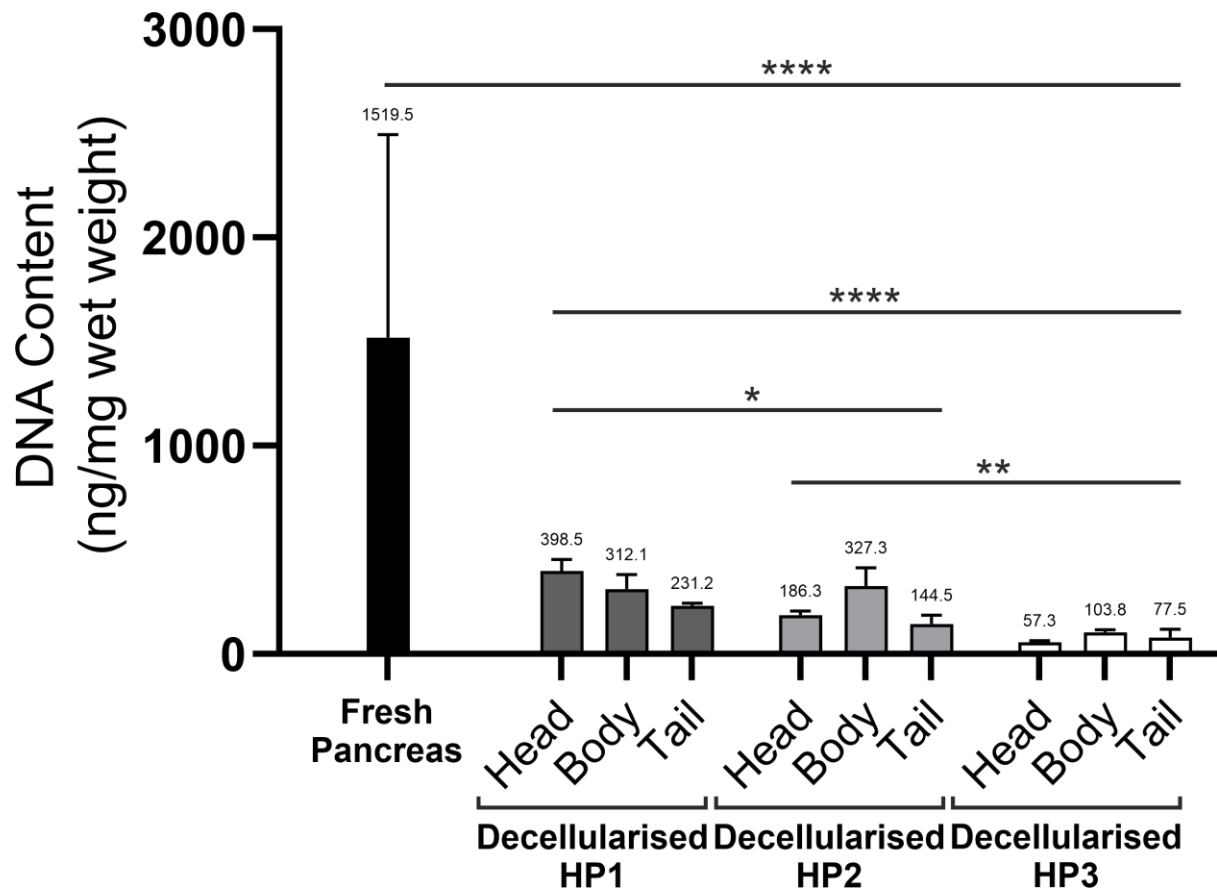


Figure 24. DNA quantification of fresh and decellularised pancreas. All decellularised tissue had a significant decrease in DNA content compared to fresh tissue. Additionally, there is a significant decrease in DNA content between HP3 and both HP1 and HP2. Data are expressed as mean \pm s.d. * $p < 0.05$, ** $p < 0.01$ and **** $p < 0.0001$.

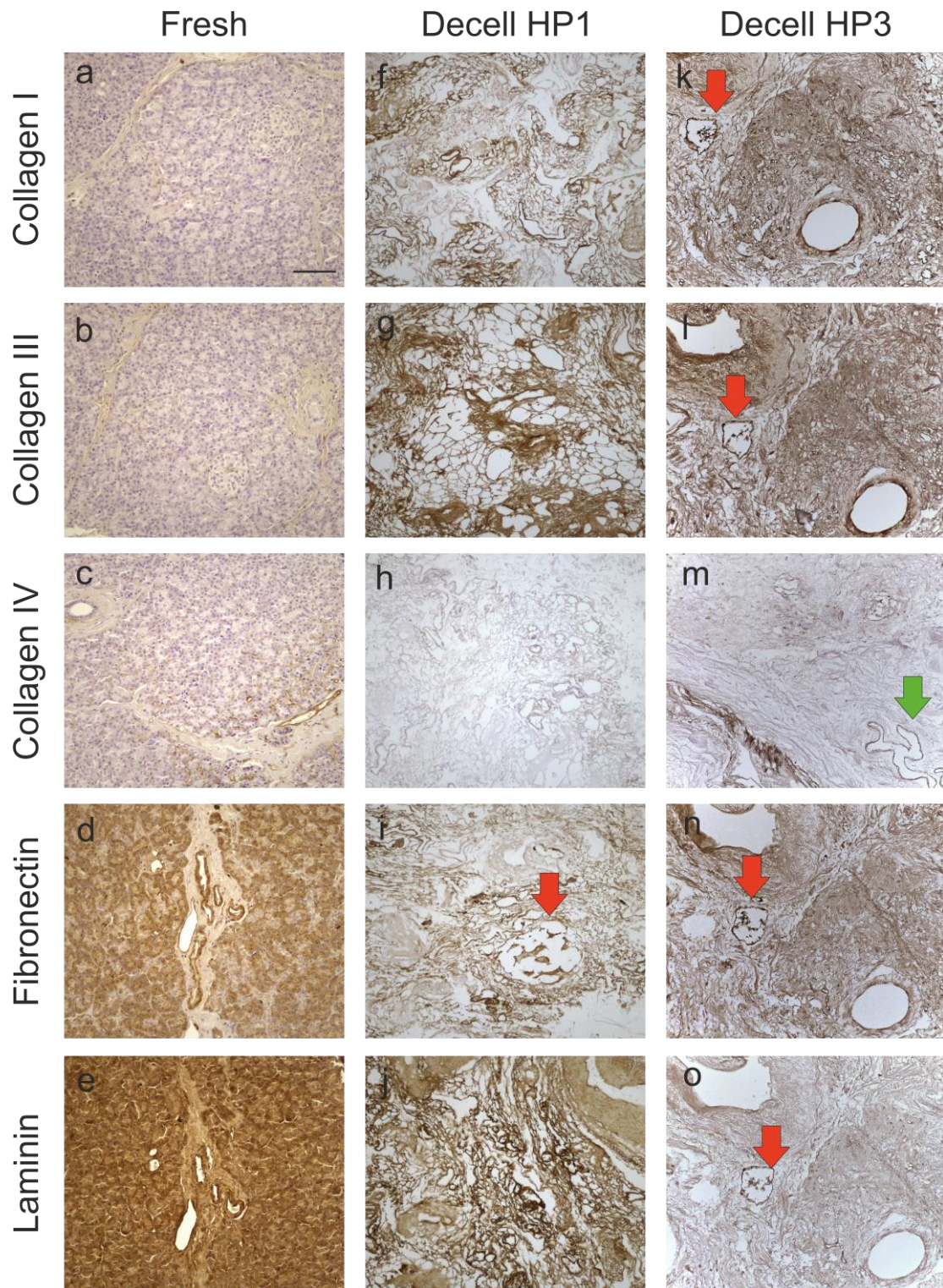


Figure 25. Immunohistochemistry images of fresh and decellularised pancreas. All proteins are stained dark brown. Fresh pancreas was stained as a positive control and all proteins showed appropriate staining (a – e). Both pancreata HP1 (f – j) and HP3 (k – o) showed positive staining for all 5 proteins with some degree of difference between the protocols, particularly laminin (k and o). Additionally, preserved Islets (red arrows) and ducts (green arrow) can be seen on some slides. All images were obtained using a 20x objective. Scale bar: 100 µm.

4.2 PDAC Cell Cultures

4.2.1 Histological Characterisation

4.2.1.1 Histopathological Analysis of the Effect of Tissue-Specificity on PDAC

Following successful decellularisation of pancreas tissue, the next step was to investigate the ability of pancreas and liver scaffolds to accommodate PDAC cells. Three cell types were chosen due to their anatomical site of derivation and metastatic potential; PANC-1 (primary non-metastatic isolated from the pancreas), MIA PaCa-2 (primary metastatic isolated from the pancreas) and PK-1 (metastatic isolated from the liver).

After 7 days in culture, PANC-1 cells were observed to attach to both pancreas (Figure 26 a - c) and liver scaffolds (Figure 26 d - f), without extended migration into the scaffolds. After 14 days, PANC-1 cells on the pancreas scaffolds invaded deeper into the parenchymal space as well as the walls of the ducts (Figure 26 g - i). This was not observed on liver scaffolds, as the cells only partially invaded inwards (Figure 26 j - l).

MIA PaCa-2 cells invaded both tissue types similarly. After 7 days, cells migrated as singular units into the parenchyma (Figure 27 a - f). Similarly, after 14 days of culture, cells appeared to maintain their singular invasive behaviour. (Figure 27 g - l).

Finally, PK-1 cells showed similar cell numbers at both day 7 and 14 of culture (Figure 28). There was a distinct difference in behaviour between the liver and pancreas tissue. PK-1 cells on the liver scaffolds migrated and attached to all major vessels as well as some smaller vessels (Figure 28 d – f and j – l). This was not observed on the pancreas scaffolds as the cells created thick layers on the outer layer of the scaffold, attaching in aggregates (Figure 28 a – c and g – i).

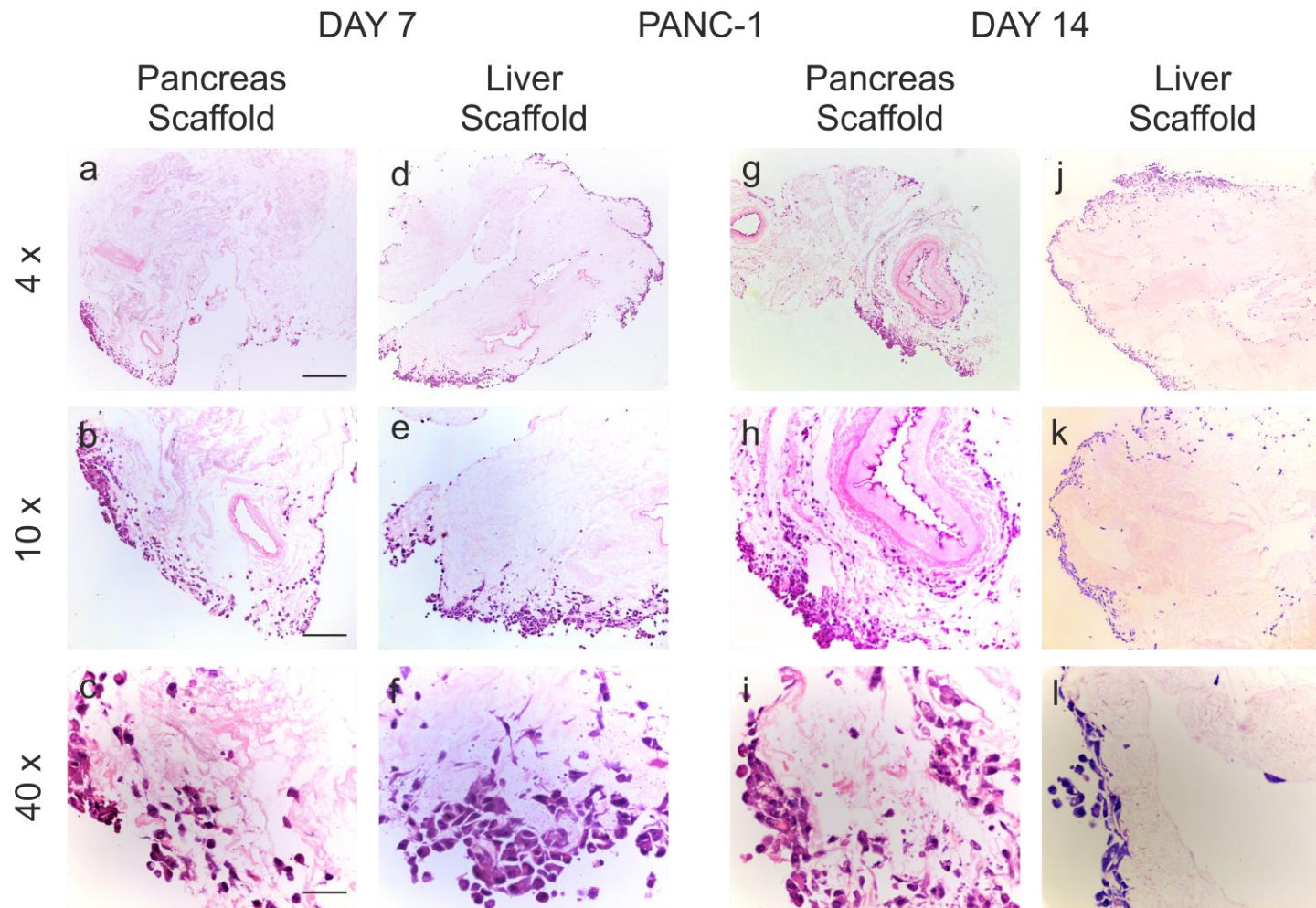


Figure 26. PANC-1 cells cultured on pancreas and liver scaffolds. After 7 days in culture, H&E staining showed that PANC-1 cells attached to both pancreas (a – c) and liver scaffolds (d – f), without extended migration into the scaffolds. After 14 days, PANC-1 cells on the pancreas scaffolds invaded deeper into the parenchymal space as well as the walls of the ducts (g – i). On liver scaffolds, the cells only partially invaded inwards (j – l). Scale bar for 4x images is 500 μ m, 10x images is 200 μ m and 40x images 50 μ m.

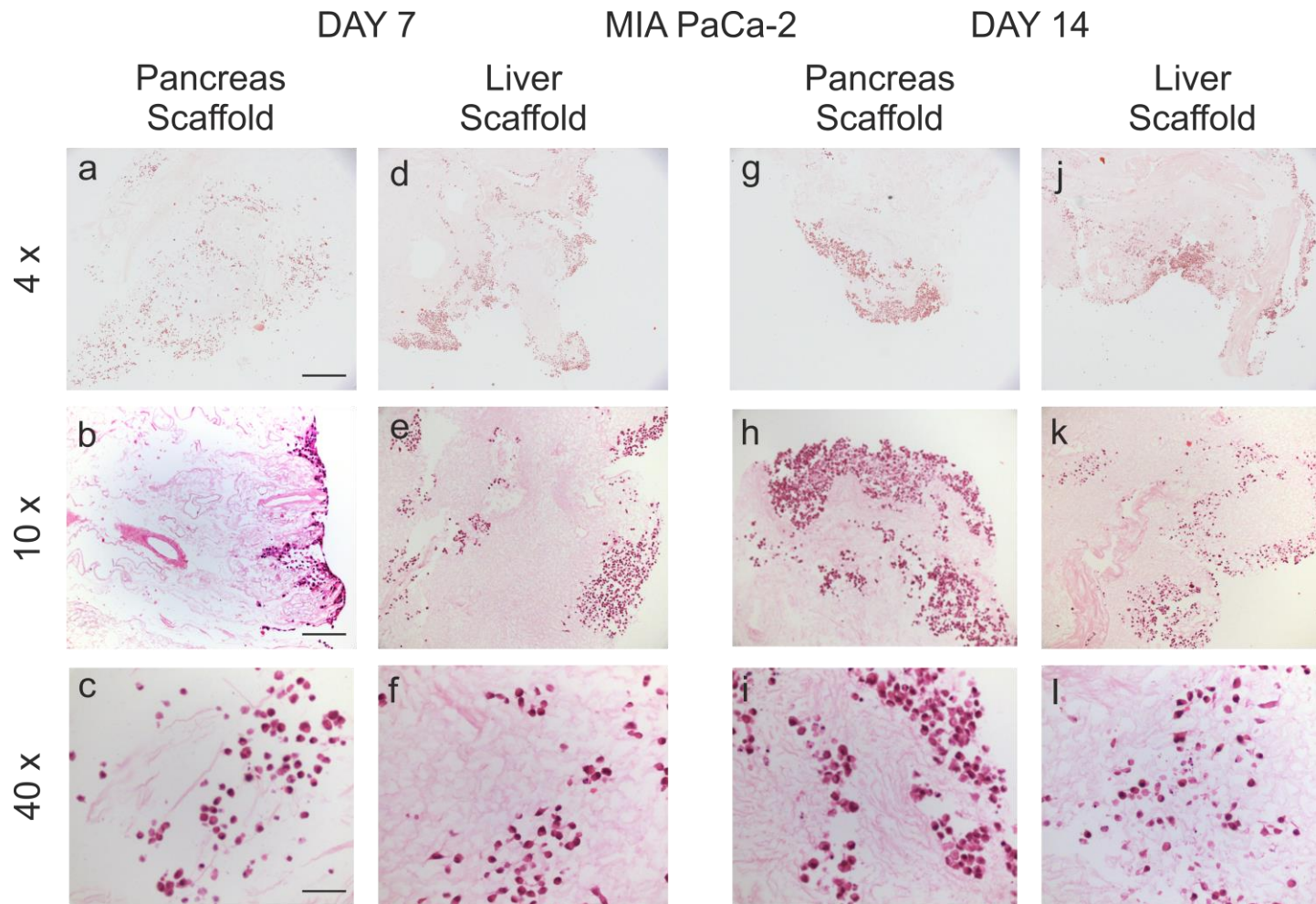


Figure 27. MIA PaCa-2 cells cultured on pancreas and liver scaffolds. After 7 and 14 days in culture, H&E staining showed that MIA PaCa-2 cells attached to both pancreas (**a – c and g – i**) and liver scaffolds (**d – f and j – l**) similarly as singular units. Although, after 14 days (**g – l**), the number of MIA PaCa-2 cells appear to be greater than after 7 days (**a – f**). Scale bar for 4x images is 500 μm , 10x images is 200 μm and 40x images 50 μm .

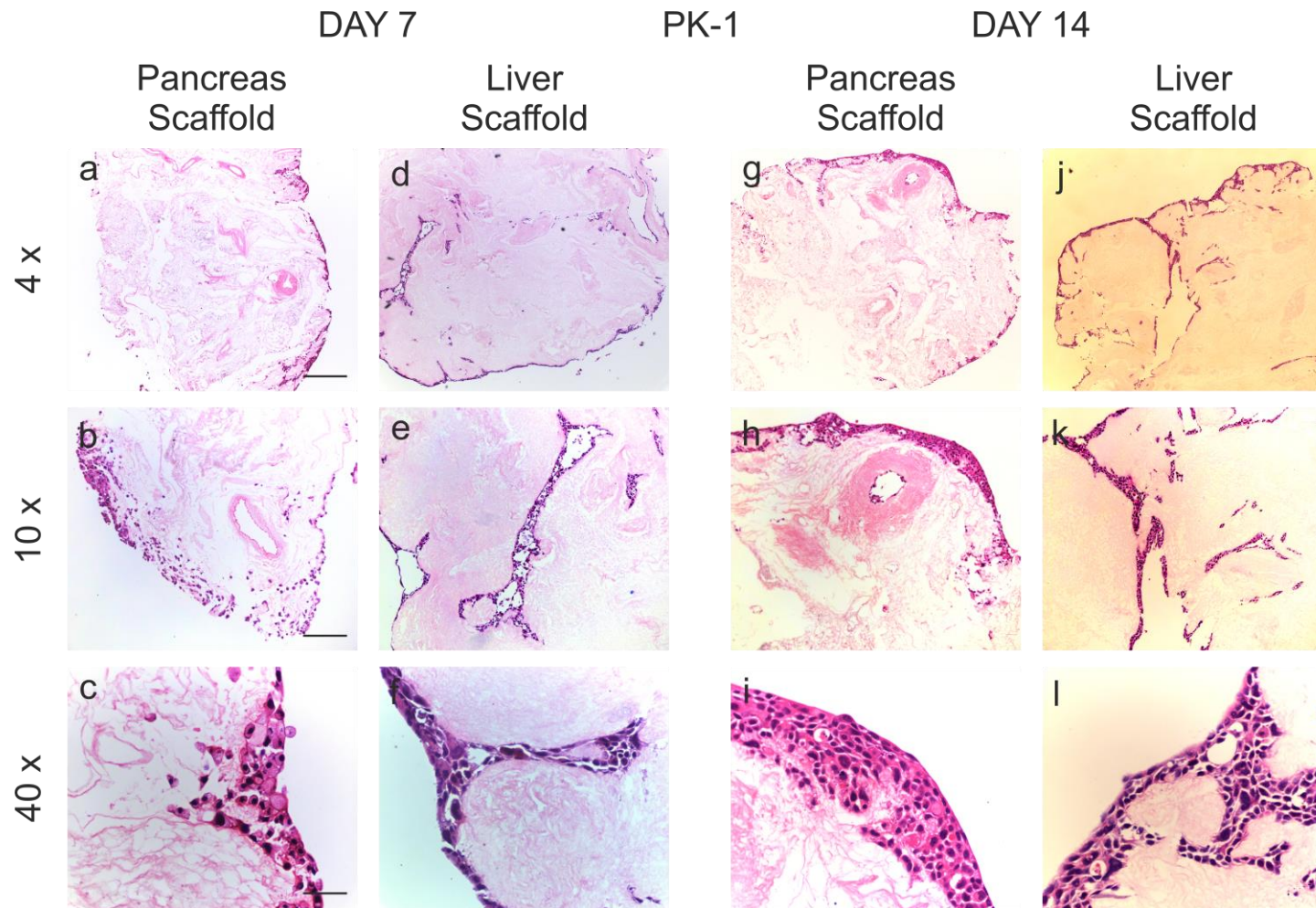


Figure 28. PK-1 cells cultured on pancreas and liver scaffolds. H&E staining showed that PK-1 cells on the pancreas scaffolds created thick layers on the outer surface of the scaffolds, attaching in aggregates (a – c and g – i). Whereas, after 7 and 14 days in culture, PK-1 cell on the liver migrated and attached to all major vessels as well as some smaller vessels (d – f and j – l). Scale bar for 4x images is 500 μ m, 10x images is 200 μ m and 40x images 50 μ m.

4.2.1.2 Immunohistological Analysis of the Effect of Tissue-Specificity on PDAC

To further investigate the role of tissue-specific ECM on the PDAC cells, IHC staining was used to study changes in cellular characteristics of PANC-1 and PK-1 cells in pancreas and liver scaffolds. PANC-1 cells stained for Ki-67, a marker for proliferation, presented a moderate intensity on both Day 7 (Figure 29a) and Day 14 (Figure 29g) on pancreas scaffolds. Whereas, a high Ki-67 intensity was seen on liver scaffolds on both day 7 (Figure 30a) and 14 (Figure 30g), which indicated a more proliferative status of these cells on a metastatic ECM material. ASP175 (cleaved caspase-3), a marker for apoptosis, was overall not present on neither day 7 or 14 on either the pancreas (Figure 29 b and h) or liver scaffolds (Figure 30.b and h), although there were more ASP175 positive cells on day 14 compared to day 7 on both tissues.

To investigate changes in migratory potential of the PANC-1 cells on the different tissue types, MMP9 (Matrix metalloproteinase 9) staining was performed. MMP9 showed a moderate intensity on all conditions (Figure 29 c and i and Figure 30 c and i); tissue type (pancreas and liver) and time point (day 7 and 14).

Furthermore, EMT and stemness markers were examined. E-Cadherin, a marker of “epithelial” cells, was mildly positive on both pancreas (Figure 29d) and liver scaffolds (Figure 30d) on day 7 but was lost on day 14 (Figure 29j and Figure 30j). Whereas, β -catenin, a promoter of mobility and a mesenchymal phenotype, was moderately expressed in all conditions (Figure 29 e and k and Figure 30 e and k); tissue type (pancreas and liver) and time point (day 7 and 14).

Finally, CD44, a cancer stem cell marker, was not detected in any of the conditions (Figure 29 f and l and Figure 30 f and l); tissue type (pancreas and liver) and time point (day 7 and 14).

PK-1 cells stained for Ki-67, presented a moderate intensity on both day 7 (Figure 31a) and a high intensity on day 14 on pancreas scaffolds (Figure 31g), whereas a high intensity was seen on liver scaffolds on day 7 (Figure 32a) and a decreased intensity on day 14 (Figure 32g). ASP175 was not detected on any of the sample

conditions (Figure 31 b and h and Figure 32 b and h); tissue type (pancreas and liver) and time point (day 7 and 14).

The migratory marker MMP9 presented a moderate to high intensity on PK-1 cells on the pancreas scaffolds on both time points; day 7 (Figure 31c) and 14 (Figure 31i) but a very high intensity of MMP9 staining on the liver scaffolds on both time points; day 7 (Figure 32c) and day 14 (Figure 32i).

The EMT marker, E-Cadherin (Figure 31 d and j and Figure 32 d and j) and β -catenin (Figure 31 e and k and Figure 32 e and k) were shown to be highly expressed in all conditions; tissue type (pancreas and liver) and time point (day 7 and 14). Finally, CD44 was moderately expressed on all conditions (Figure 31 f and l and Figure 32 f and l); tissue type (pancreas and liver) and time point (day 7 and 14).

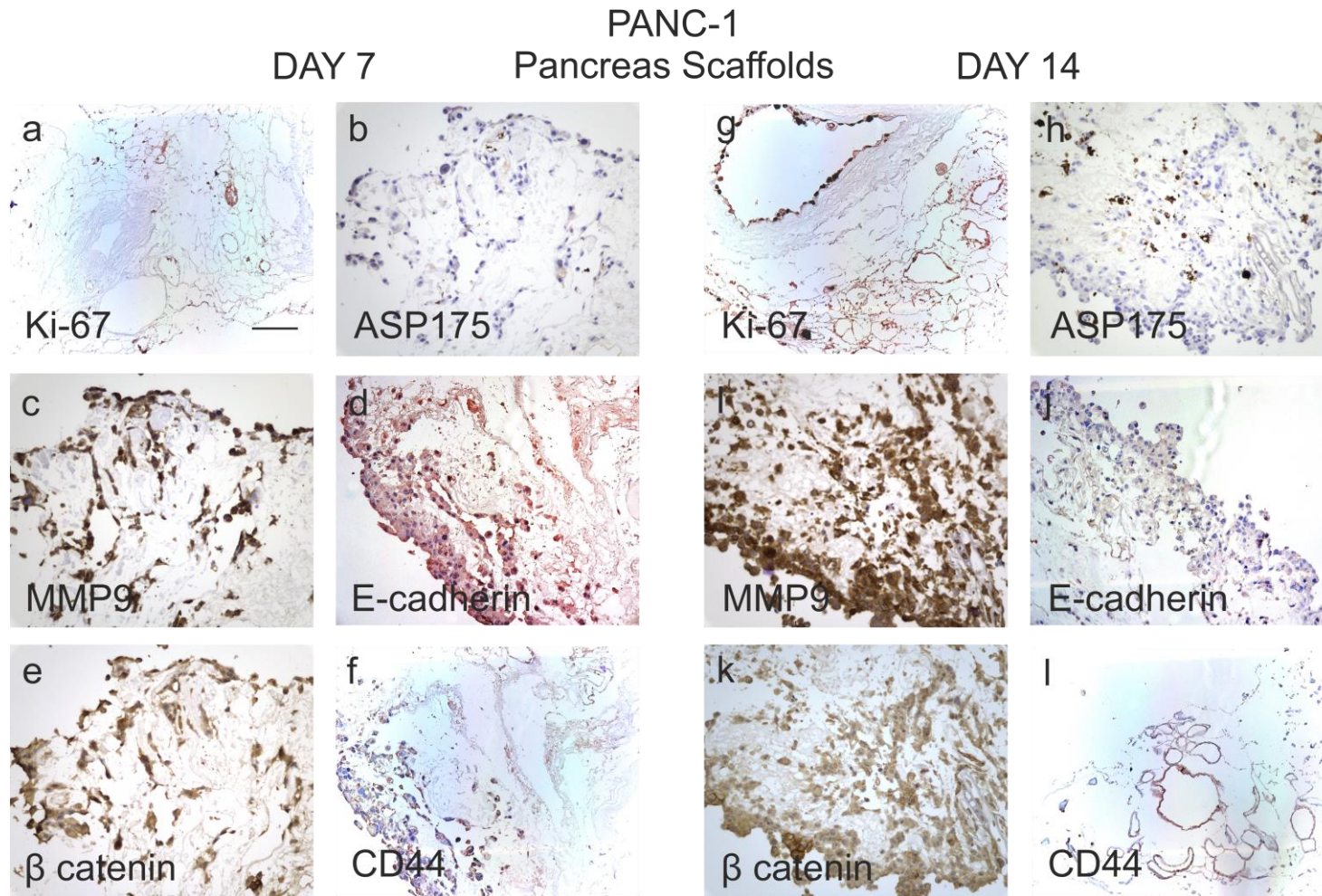


Figure 29. Immunohistochemistry analysis of PANC-1 cells cultured on pancreas scaffolds. PANC-1 cells stained for Ki-67 showed a moderate intensity on both day 7 (a) and day 14 (g). Staining for ASP175 was negative for the majority of the cells; with only a few number of cells presenting a positive stain on day 7 (b) and a greater amount on day 14 (h). Staining for MMP9 was positive with a high intensity on both day 7 (c) and day 14 (i). E-cadherin presented a mild positive staining on day 7 (d) but was negative on day 14 (j). Staining for β catenin presented a moderate expression on both day 7 (e) and day 14 (k). CD44 staining was negative on both day 7 (f) and day 14 (l). All images were obtained using a 20x objective. Scale bar: 100 μ m.

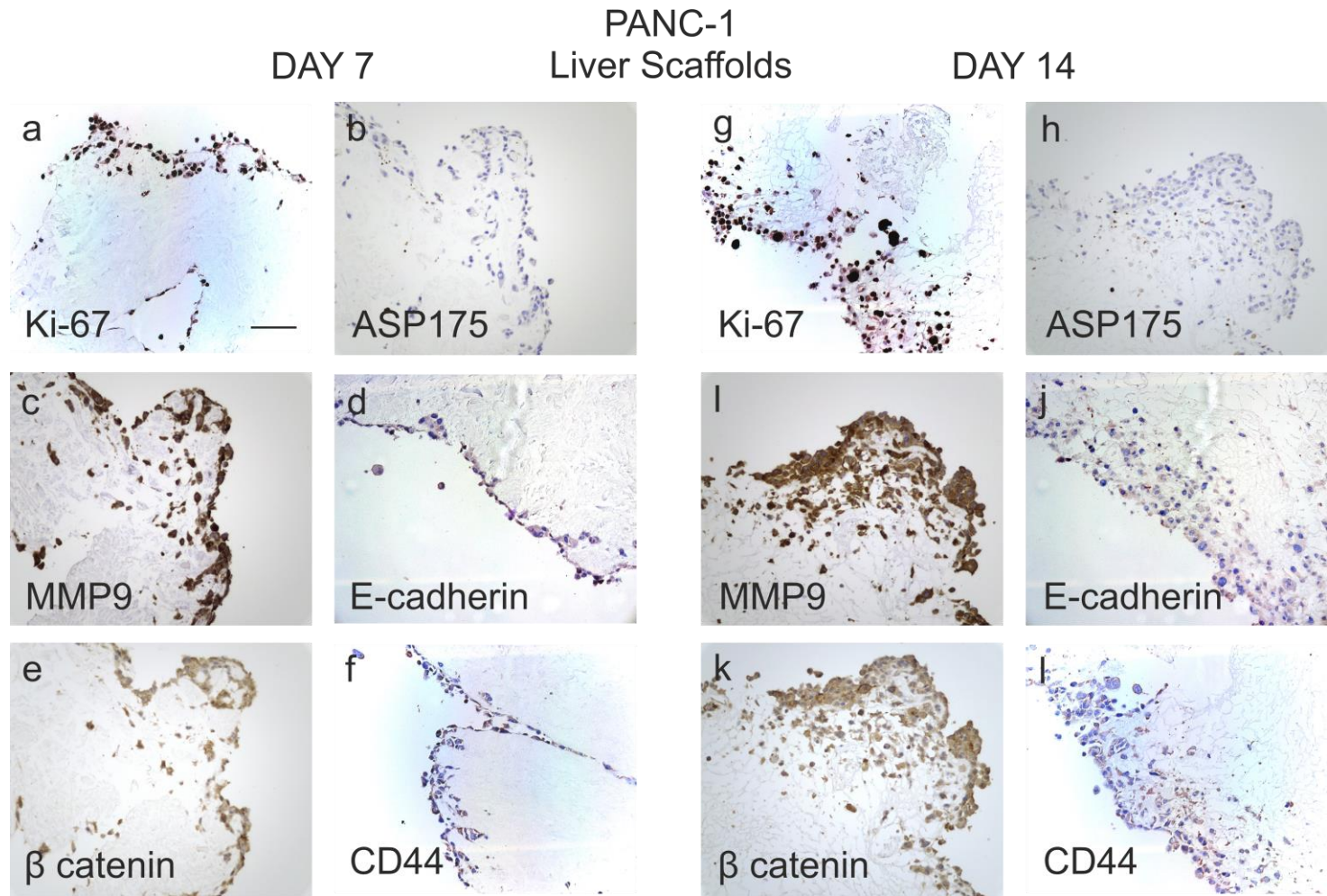


Figure 30. Immunohistochemistry analysis of PANC-1 cells cultured on liver scaffolds. PANC-1 cells stained for Ki-67 showed a high intensity on both day 7 (a) and day 14 (g). Staining for ASP175 was negative for the majority of the cells; with only a few number of cells presenting a positive stain on day 7 (b) and a greater amount on day 14 (h). Staining for MMP9 was positive with a high intensity on both day 7 (c) and day 14 (i). E-cadherin presented a mild positive staining on day 7 (d) but was negative on day 14 (j). Staining for β catenin presented a moderate expression on both day 7 (e) and day 14 (k). CD44 staining was negative on both day 7 (f) and day 14 (l). All images were obtained using a 20x objective. Scale bar: 100 μ m.

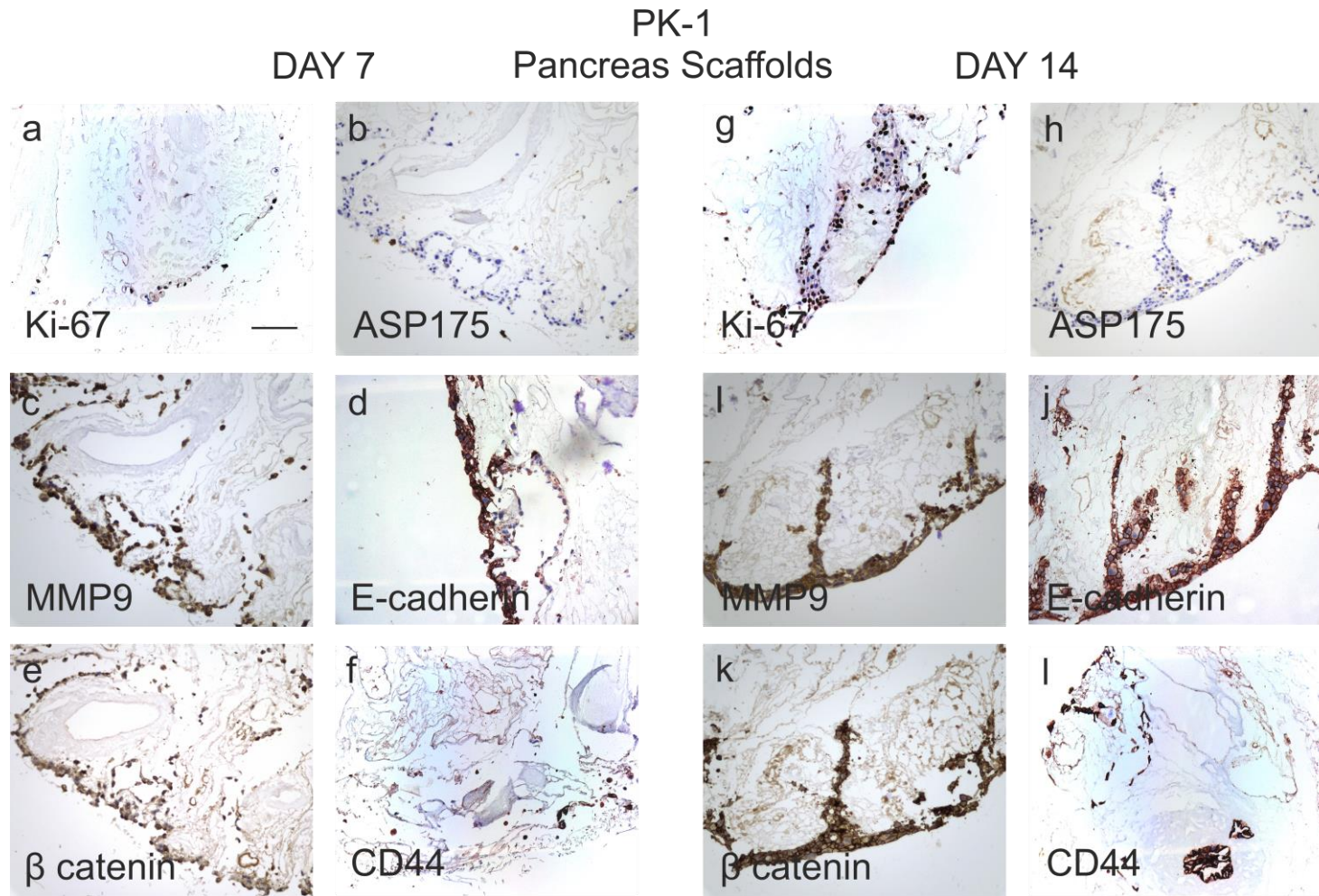


Figure 31. Immunohistochemistry analysis of PK-1 cells cultured on pancreas scaffolds. PK-1 cells stained for Ki-67 showed a moderate intensity on day 7 (**a**) and a higher intensity on day 14 (**g**). Staining for ASP175 was negative for the majority of the cells; with only a few number of cells presenting a positive stain on day 7 (**b**) and day 14 (**h**). Staining for MMP9 was positive with a moderate/high intensity on both day 7 (**c**) and day 14 (**i**). E-cadherin presented a high intensity staining on both day 7 (**d**) and day 14 (**j**). Staining for β catenin presented a high expression on both day 7 (**e**) and day 14 (**k**). CD44 staining was highly expressed on both day 7 (**f**) and day 14 (**l**). All images were obtained using a 20x objective. Scale bar: 100 μ m.

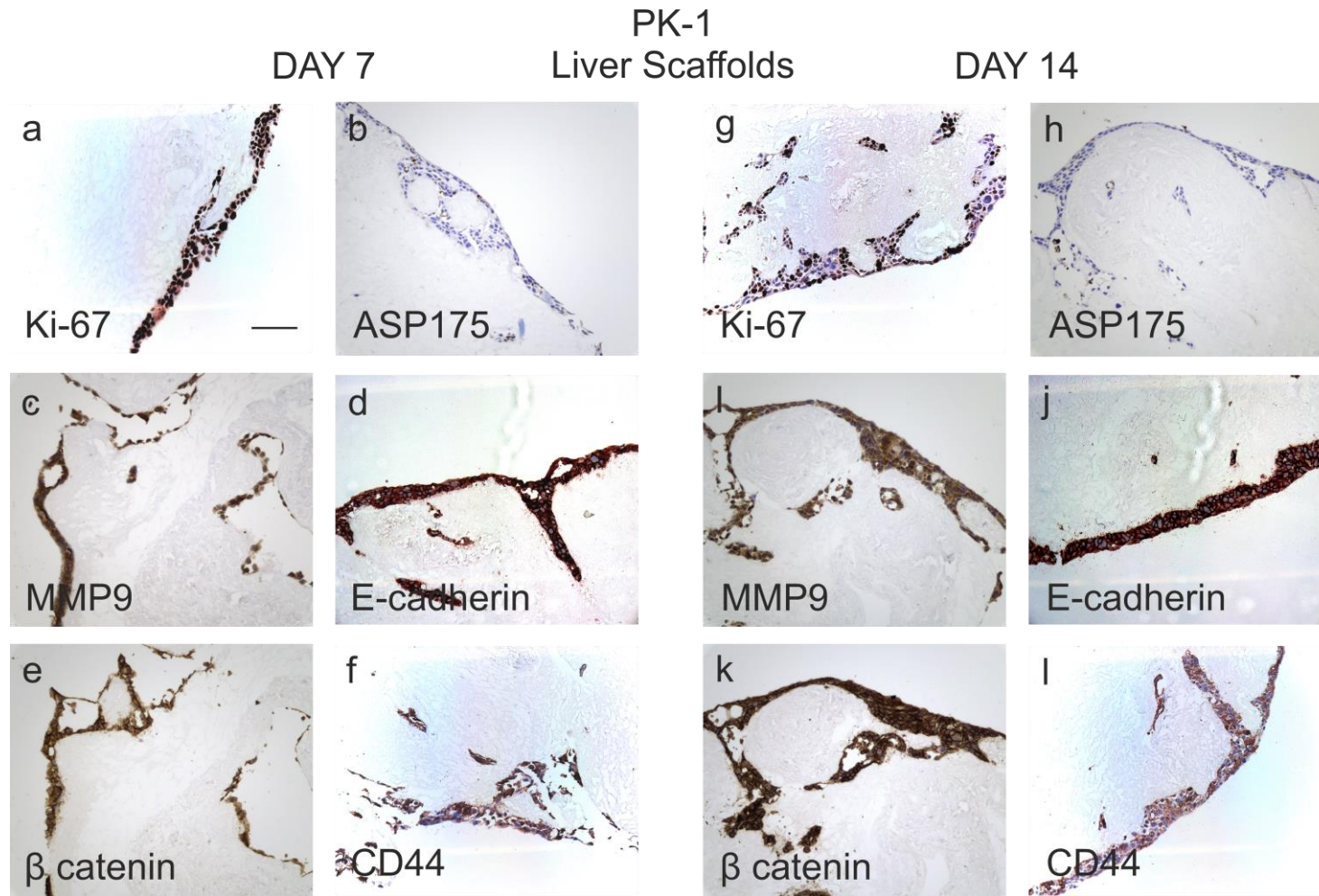


Figure 32. Immunohistochemistry analysis of PK-1 cells cultured on liver scaffolds. PK-1 cells stained for Ki-67 showed a high intensity on day 7 (**a**) and a moderate intensity on day 14 (**g**). Staining for ASP175 was negative for the majority of the cells; with only a few number of cells presenting a positive stain on day 7 (**b**) and day 14 (**h**). Staining for MMP9 was positive with a very high intensity on both day 7 (**c**) and day 14 (**i**). E-cadherin presented a very high intensity staining on both day 7 (**d**) and day 14 (**j**). Staining for β catenin presented a very high expression on both day 7 (**e**) and day 14 (**k**). CD44 staining was highly expressed on both day 7 (**f**) and day 14 (**l**). All images were obtained using a 20x objective. Scale bar: 100 μ m.

4.2.2 Genetic Profiling of PDAC Cell Lines in their Natural Tissue

To better understand the gene expression profiles of the three cell lines, qPCR of 93 genes were analysed, using TaqMan™ Arrays for human pancreas adenocarcinoma. For the purpose of this experiment, four technical replicates were pooled from cells cultured on scaffolds of tissue of their origin, i.e. (i) PANC-1 cells cultured in pancreas scaffolds, (ii) MIA PACA-2 cells cultured on pancreas scaffolds and (iii) PK-1 cells cultured on liver scaffolds. The genes of the array were grouped into 9 categories for optimisation of analysis, namely: Tissue Remodelling and Angiogenesis, Cytokines/Growth Factors and Receptors, Oncogenes and Tumour Suppressors, Cell Cycle Regulators, AKT/PKB Signalling Pathways, TGF/SMAD Signalling Pathways, JAK/STAT Signalling Pathways, RAS/MAPK Signalling Pathways, and Other PDAC-Related Genes.

Analyses of the “tissue remodelling and angiogenesis” related genes showed that GUSB, a hydrolase that degrades glycosaminoglycans, was similar in all three cells lines. MMP1, a protease that breaks down interstitial collagen, showed similar expression in MIA PACA-2 and PK-1 cells but a ~5-fold lower expression in PANC-1 cells. MMP2, a protease that denatures type IV and V collagen and elastin, was similarly expressed in PANC-1 and PK-1 cells but expressed ~500 fold less in MIA PACA-2 cells. MMP3, a protease that degrades fibronectin, laminin, collagens III, IV, IX, and X, and cartilage proteoglycans, had a low expression on all three cell lines. MMP7, a protease the degrades proteoglycans, fibronectin, elastin and casein, was not expressed in MIA PACA-2, mildly expressed in PANC-1 cells and moderately expressed in PK-1 cells, in comparison to the expression of the other metalloproteinases. MMP9, an enzyme that degrades type IV and V collagens, had a similar pattern to MMP7 but with higher expression in all three cell lines. VEGFA, VEGFB and VEGFC, growth factors that regulate the formation of blood vessels and involved in endothelial cell physiology, were highly expressed in all cell lines, even though, VEGFA and VEGFB were higher in PANC-1 and PK-1 compared to MIA PACA-2 cells. FIGF (VEGFD) was expressed much less than the other VEGFs in all three cell lines. Finally, it is important to note that the metastatic cells, PK-1, has similar or higher expression of all of the tissue remodelling and angiogenesis related genes;

GUSB, MMP1, MMP2, MMP3, MMP7, MMP9, VEGFA, VEGFB and VEGFB except for FIGF (Figure 33).

Analyses of the “cytokines/growth factor and receptors” related genes presented a similar pattern to those of “tissue remodelling and angiogenesis” where the metastatic cells, PK-1, had an equal or higher expression in comparison to PANC-1 and MIA PACA-2 of all genes tested; EGF, EGFR, HBEGF, ERBB2, IGF1, IL6 KDR, NOTCH1 AND KIT. Additionally, the primary PDAC cell line, MIA PACA-2, had a gene expression profile that was either not present, lower or equal to the other two cell lines PANC-1 and PK-1. In fact, IGF1, a hormone similar in molecular structure to insulin and known to be produced by the liver, was not expressed in neither of the primary tumour cell lines, PANC-1 and MIA PACA-2, whereas IL6, a pro-inflammatory cytokine, KDR, a VEGF receptor, and KIT, Mast/stem cell growth factor receptor, were only expressed in PANC-1 and PK-1 but not in MIA PACA-2. EGF, a potent mitogenic factor that plays an important role in the growth, proliferation and differentiation, and its receptor, EGFR, has a similar expression pattern between the three cell lines even though EGF had ~1000-fold lower expression. HBEGF, Heparin Binding EGF Like Growth Factor, and its receptor, ERBB2, has similar pattern and expression between the three cell lines. Finally, NOTCH1, a receptor involved in the Notch signalling pathway, had a similar expression in all three cells (Figure 34).

Analyses of the “oncogenes and tumour suppressors” related genes, similarly, showed an equal or lower expression of all genes; E2F1, E2F3, E2F4, TP53, MDM2, RB1, BRCA2, BRAF, BIRC5, BCL2 and BCL2L1, in MIA PACA-2 cells in comparison to PANC-1 and PK-1 cells. The oncogenes, E2F1, E2F3 and E2F4, transcription factors that play a crucial role in the control of cell cycle and action of tumour suppressor proteins, and MDM2, a tumour formation promoter, were found to be higher in the metastatic cell line PK-1 than the primary cell line PANC-1. Whereas, the tumour suppressor genes, TP53 and BRCA2, and the apoptosis inhibitor genes, BIRC2 and BCL2, presented higher expression in PANC-1 than in PK-1 cells. It is important to note that BCL2 was expressed more than 15-fold higher in PANC-1 than PK-1 and MIA PACA-2 (Figure 35).

Analysis of the “cell cycle regulators” genes, like the above gene groups, showed that MIA PACA-2 cells had a similar or lower expression of all genes, CCNA2, CCNB1, CCND1, CCND2, CCNE1, CCNE2, CDC42, CDK2, CDK4, CDKN1A, CDKN1B, CDKN2A, CDKN2B and CDKN2D, in comparison to the other two cell lines, except for CDKN2C, which was lowest in PK-1. The cyclin dependent kinase inhibitors, CDKN2A and CDKN2B, were not expressed in any of the three cell lines. The largest differences in expression were observed in CCNA2, a cyclin, and CDKN2C, a cyclin depended kinase inhibitor, which were more than 4-fold higher in PANC-1 in comparison to PK-1. Whereas, the cyclin, CCND2, was expressed >10 fold higher in PK-1 cells in comparison to PANC-1 cells (Figure 36).

Analyses of the “AKT/PKB signalling pathways” related genes also showed MIA PACA-2 cells had a similar or lower expression of all genes tested, AKT1, AKT2, PIK3CA, PIK3CB, PIK3CD, PIK3R1 and PIK3R2 in comparison to the other two cell lines, except for AKT3 that was lowest in PANC-1 cells. The highlight of this group was in fact, AKT3 that was >30 fold higher in the metastatic cell line PK-1 in comparison to the primary cell line PANC-1 (Figure 37).

Analyses of the “TGF/SMAD signalling pathways” related genes also showed that MIA PACA-2 cells had a similar or lower expression of all genes tested, TGFA, TGFB1, TGFB2, TGFB3, TGFBR1, TGFBR2, SMAD2 and SMAD3 in comparison to the other two cell lines, except for SMAD4, which was lowest in PK-1 cells. The highlight of this group where TGFA and TGFB, which were >200 and >8 fold higher, respectively, in the metastatic cell line PK-1 in comparison to the primary cell line PANC-1 (Figure 38).

Analyses of the “JAK/STAT signalling pathways” related genes also showed that MIA PACA-2 cells had a similar or lower expression of all genes tested, JAK1, JAK2, STAT1, STAT2, STAT3, STAT5B, STAT6 and CYP2E1 in comparison to the other two cell lines, except for JAK3, which was lowest in PK-1 cells. The highlight of this group was JAK2, which was >8 fold higher in the metastatic cell line PK-1 in comparison to the primary cell line PANC-1 (Figure 39).

Analyses of the “RAS/MAPK signalling Pathways” related genes also showed that MIA PACA-2 cells had a similar or lower expression of all genes tested, GRB2, SOS1,

SRC, RAF1, KRAS, MAP2K1, MAP2K2, MAPK1, MAPK3 and ELK1 in comparison to the other two cell lines. The highlight of this group was SRC, a proto-oncogene that promotes survival, angiogenesis, proliferation and invasion was ~8 fold higher in the metastatic cell line PK-1 in comparison to the primary cell line PANC-1 (Figure 40).

Finally, further analyses of “other PDAC related genes” additionally showed that MIA PACA-2 cells had a similar or lower expression of all genes tested, HSP90AA1, PTGS2, NFKB1, NFKB2, REL, RELA, RELB, RAC1, RHOA, RHOB and ARHGEF7, in comparison to the other two cell lines, except for RAC2 that was lowest in PANC-1 cells. The highlight of this group was PTGS2, a cyclooxygenase not usually expressed in healthy cells but elevated during inflammation, was ~1000 fold higher in the metastatic cell line PK-1 in comparison to the primary cell line PANC-1 (Figure 41).

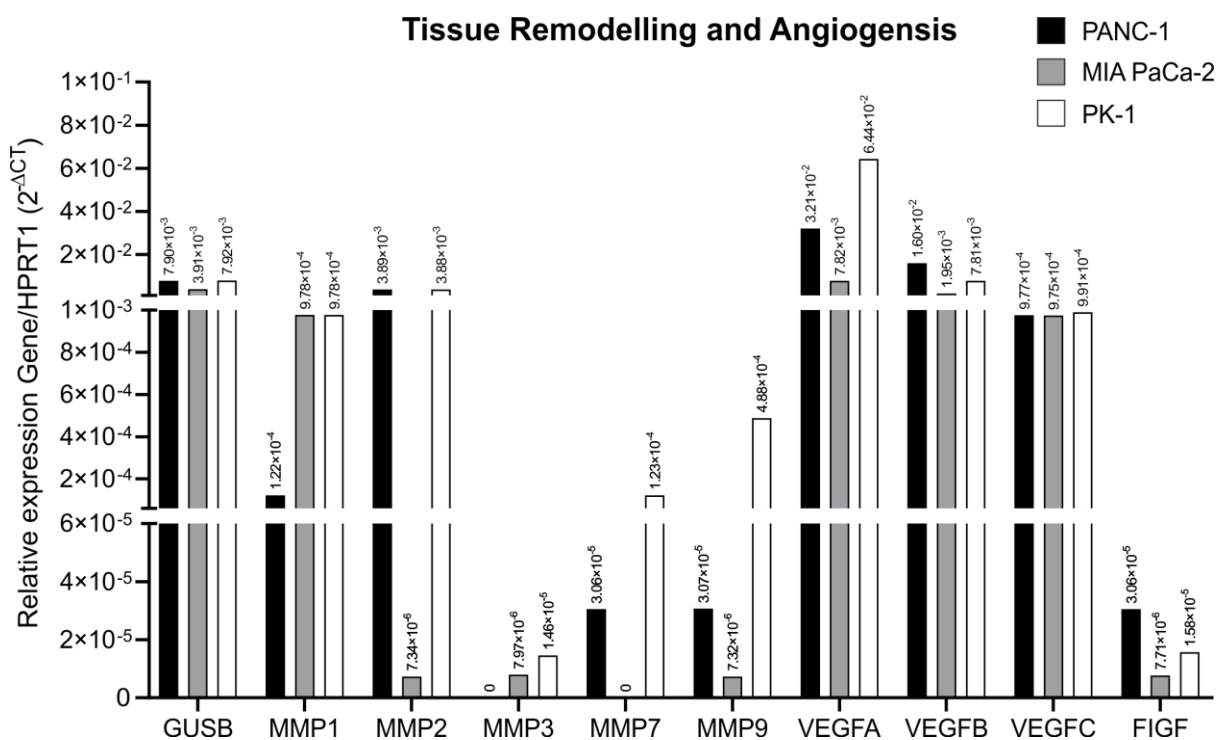


Figure 33. Quantitative comparison of genes related to “tissue remodelling and angiogenesis”. RNA extracted from PANC-1 on pancreas scaffolds, MIA PaCa-2 on pancreas scaffolds and PK-1 on liver scaffolds were tested for the relative expression of GUSB, MMP1, MMP2, MMP3, MMP7, MMP9, VEGFA, VEGFB, VEGFC and FIGF. Numerals over bars represent value of the relative expression ($2^{-\Delta CT}$).

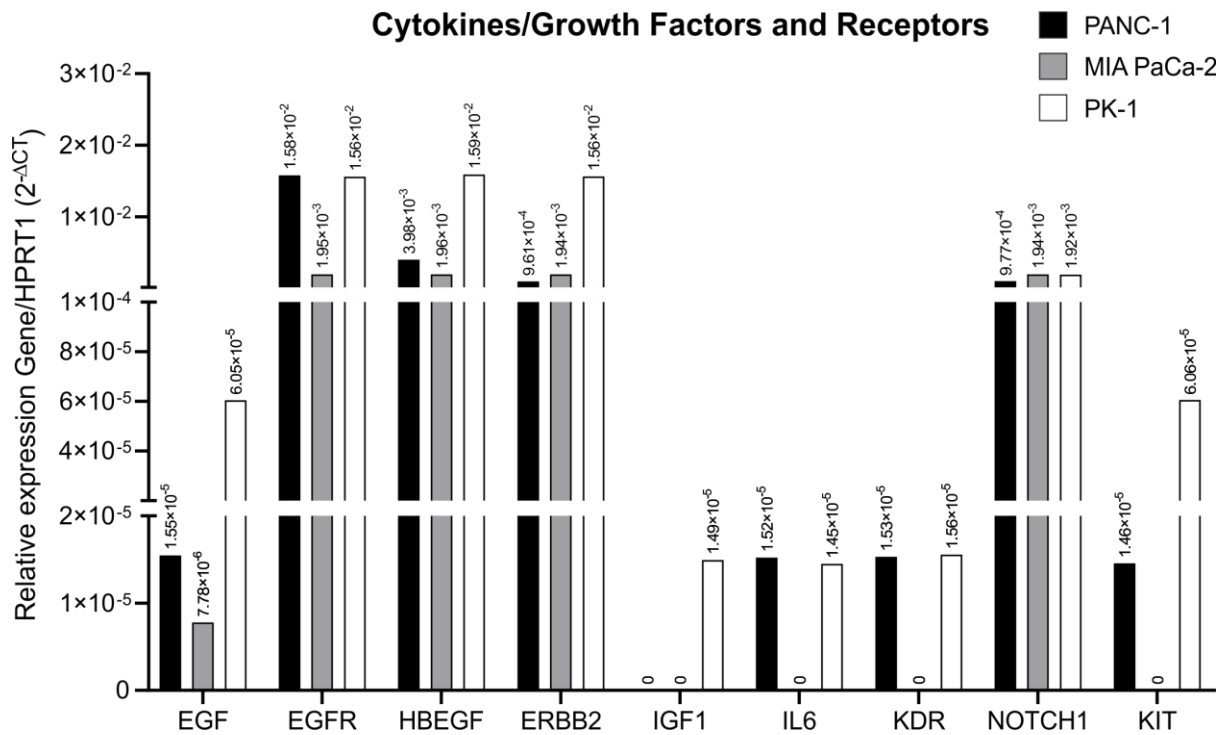


Figure 34. Quantitative comparison of genes related to “cytokines/growth factors and receptors”. RNA extracted from PANC-1 on pancreas scaffolds, MIA PaCa-2 on pancreas scaffolds and PK-1 on liver scaffolds were tested for the relative expression of EGF, EGFR, HBEGF, ERBB2, IGF1, IL6, KDR, NOTCH1 and KIT. Numerals over bars represent value of the relative expression ($2^{-\Delta CT}$).

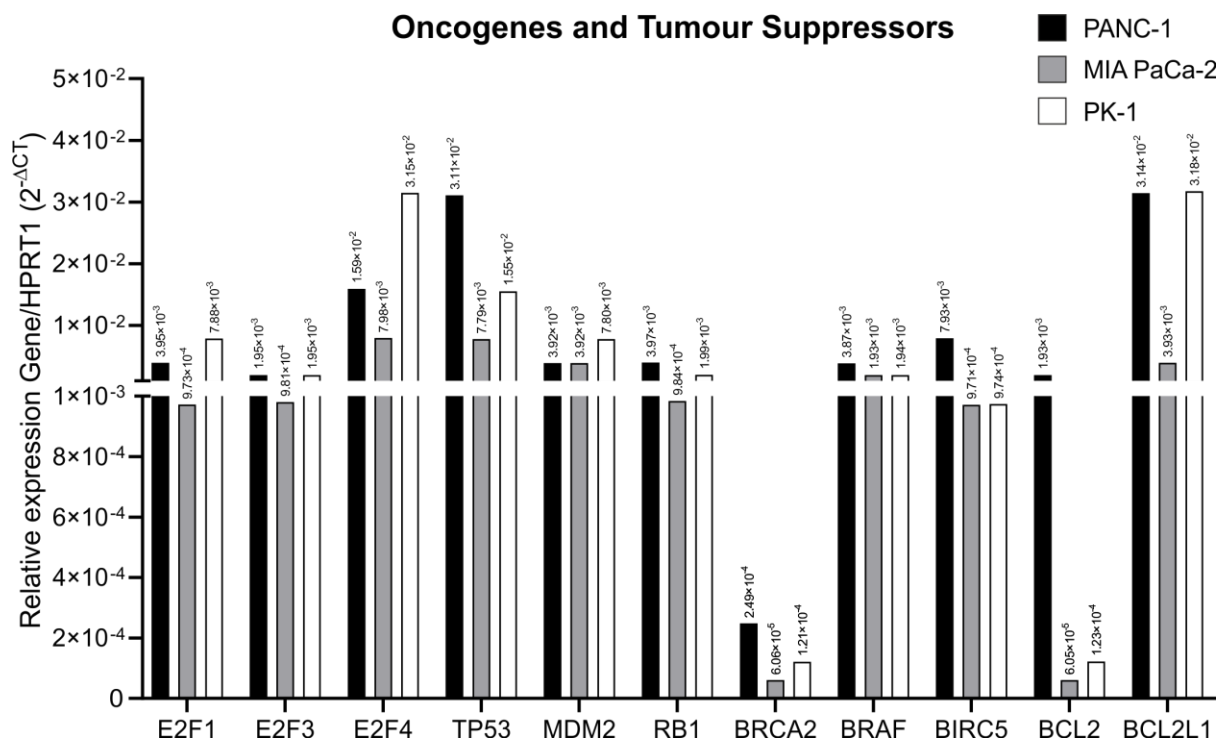


Figure 35. Quantitative comparison of genes related to “oncogenes and tumour suppressors”. RNA extracted from PANC-1 on pancreas scaffolds, MIA PaCa-2 on pancreas scaffolds and PK-1 on liver scaffolds were tested for the relative expression of E2F1, E2F3, E2F4, TP53, MDM2, RB1, BRCA2, BRAF, BIRC5, BCL2 and BCL2L1. Numerals over bars represent value of the relative expression ($2^{-\Delta CT}$).

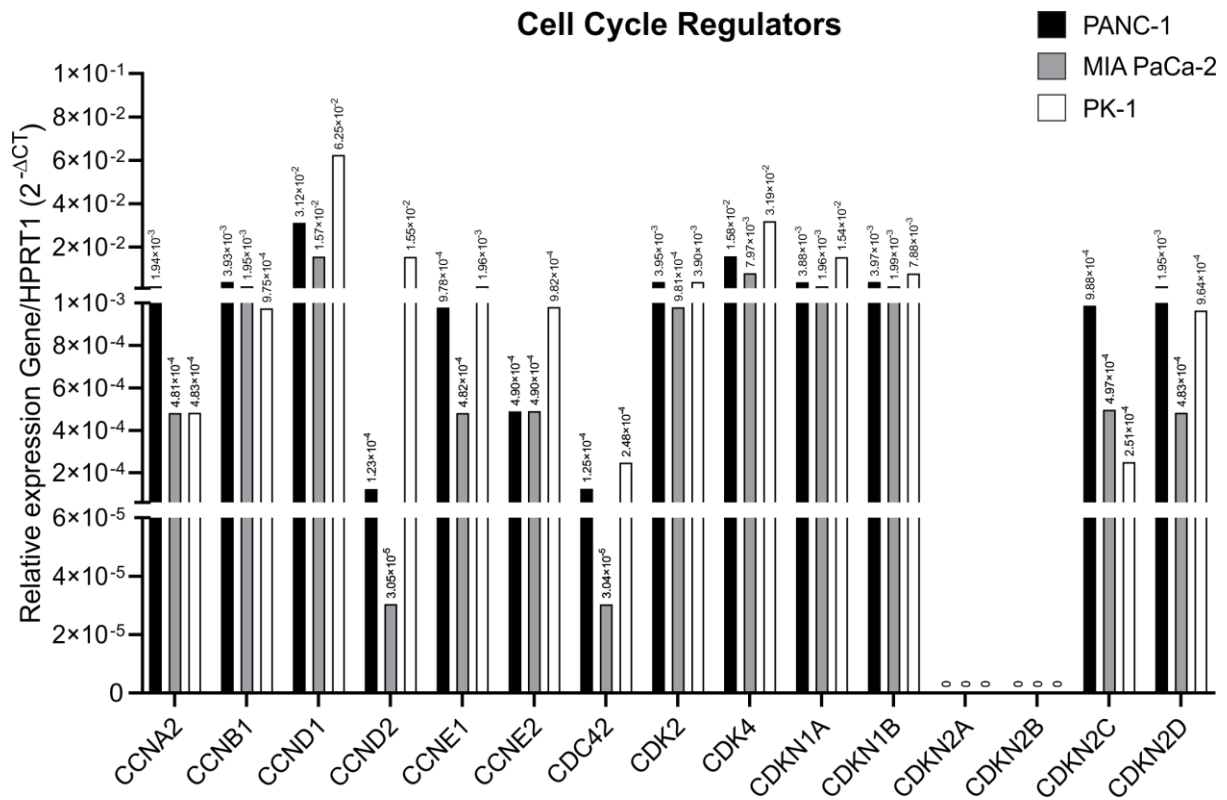


Figure 36. Quantitative comparison of genes related to “cell cycle regulators”. RNA extracted from PANC-1 on pancreas scaffolds, MIA PaCa-2 on pancreas scaffolds and PK-1 on liver scaffolds were tested for the relative expression of CCNA2, CCNB1, CCND1, CCND2, CCNE1, CCNE2, CDC42, CDK2, CDK4, CDKN1A, CDKN1B, CDKN2A, CDKN2B, CDKN2C and CDKN2D. Numerals over bars represent value of the relative expression ($2^{-\Delta CT}$).

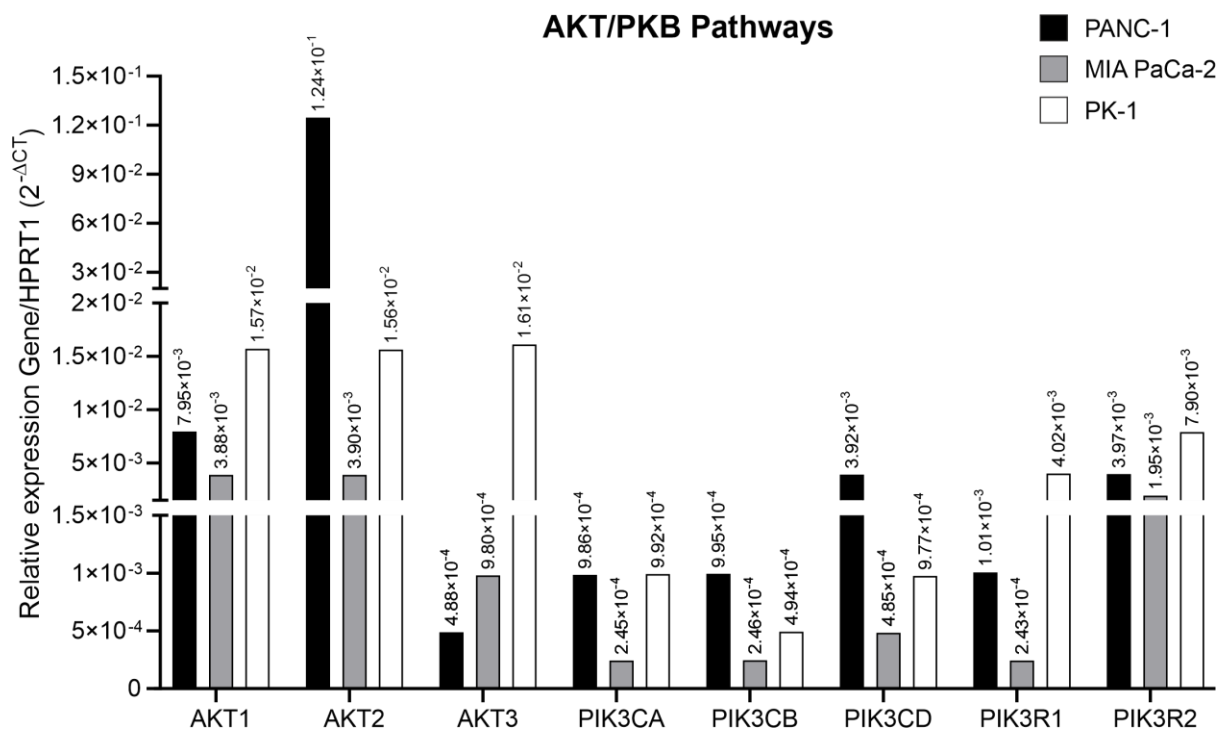


Figure 37. Quantitative comparison of genes related to “AKT/PKB signalling pathways”. RNA extracted from PANC-1 on pancreas scaffolds, MIA PaCa-2 on pancreas scaffolds and PK-1 on liver scaffolds were tested for the relative expression of AKT1, AKT2, AKT3, PIK3CA, PIK3CB, PIK3CD, PIK3R1 and PIK3R2. Numerals over bars represent value of the relative expression ($2^{-\Delta CT}$).

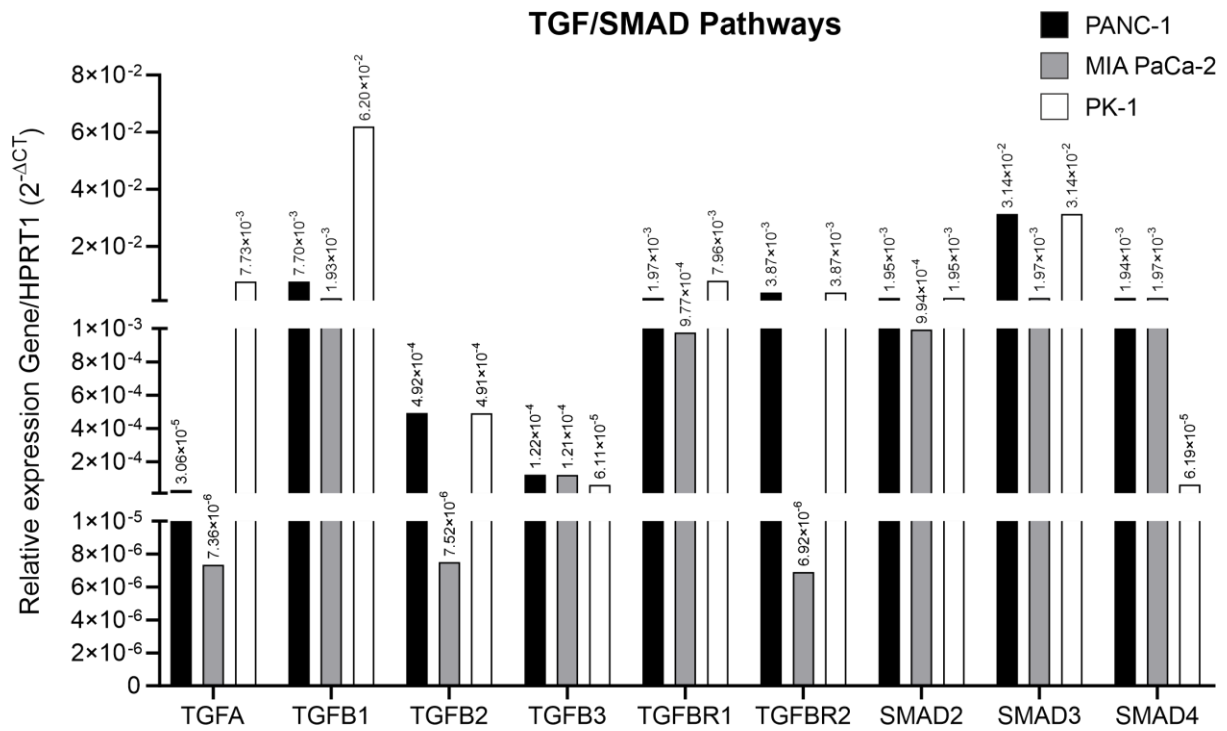


Figure 38. Quantitative comparison of genes related to “TGF/SMAD signalling pathways”. RNA extracted from PANC-1 on pancreas scaffolds, MIA PaCa-2 on pancreas scaffolds and PK-1 on liver scaffolds were tested for the relative expression of TGFA, TGFB1, TGFB2, TGFB3, TGFBR1, TGFBR2, SMAD2, SMAD3 and SMAD4. Numerals over bars represent value of the relative expression ($2^{-\Delta CT}$).

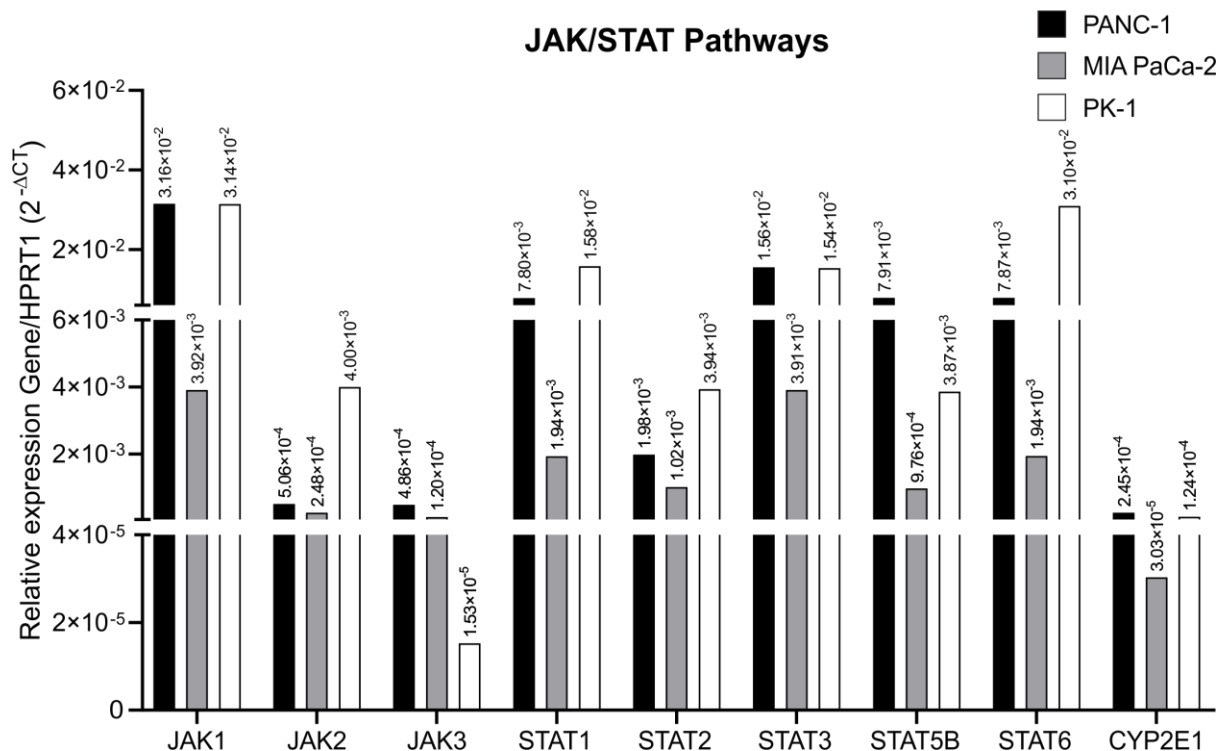


Figure 39. Quantitative comparison of genes related to “JAK/STAT signalling pathways”. RNA extracted from PANC-1 on pancreas scaffolds, MIA PaCa-2 on pancreas scaffolds and PK-1 on liver scaffolds were tested for the relative expression of JAK1, JAK2, JAK3, STAT1, STAT2, STAT3, STAT5B, STAT6 and CYP2E1. Numerals over bars represent value of the relative expression ($2^{-\Delta CT}$).

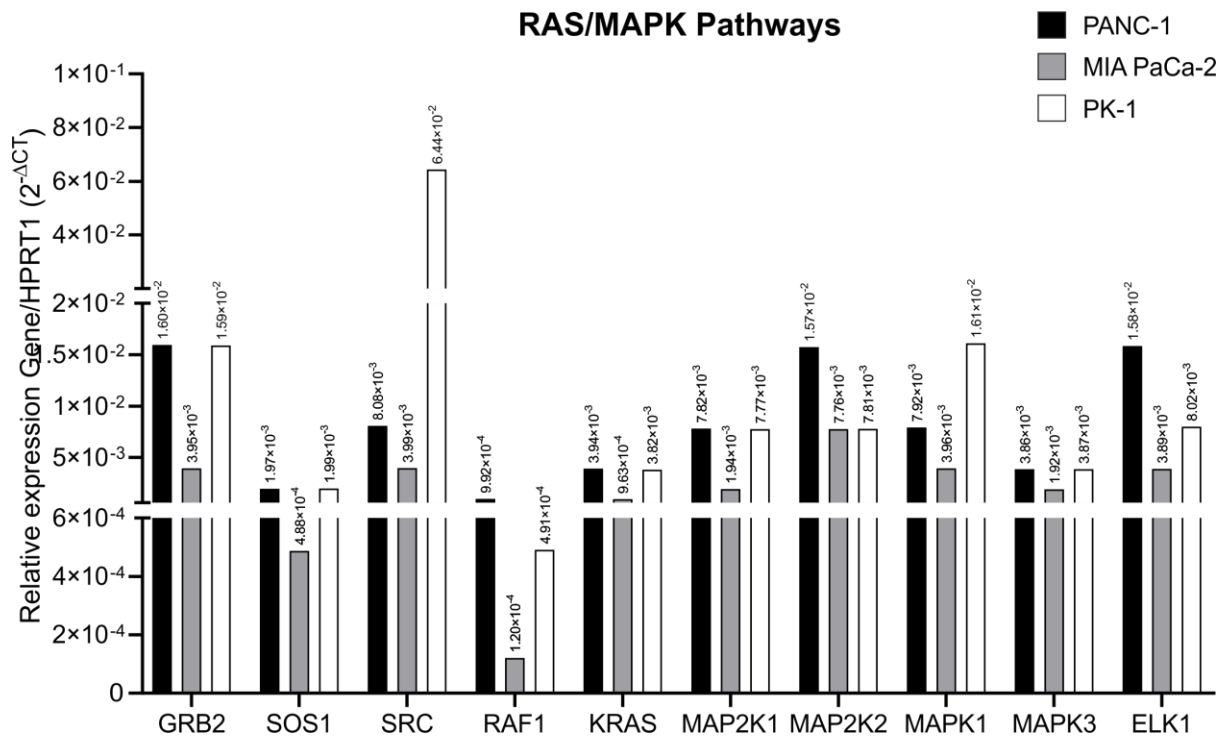


Figure 40. Quantitative comparison of genes related to “RAS/MAPK signalling pathways”. RNA extracted from PANC-1 on pancreas scaffolds, MIA PaCa-2 on pancreas scaffolds and PK-1 on liver scaffolds were tested for the relative expression of GRB2, SOS1, SRC, RAF1, KRAS, MAP2K1, MAP2K2, MAPK1, MAPK3 and ELK1. Numerals over bars represent value of the relative expression ($2^{-\Delta CT}$).

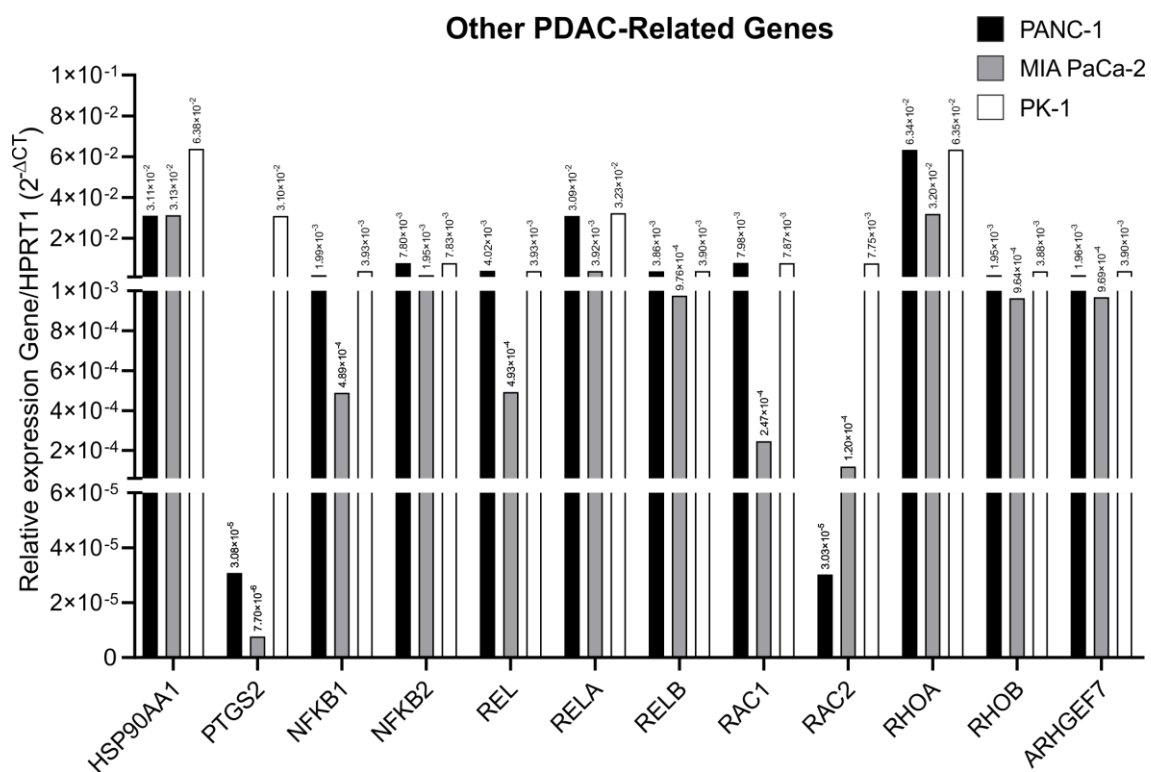


Figure 41. Quantitative comparison of “other PDAC related to genes”. RNA extracted from PANC-1 on pancreas scaffolds, MIA PaCa-2 on pancreas scaffolds and PK-1 on liver scaffolds were tested for the relative expression of HSP90AA1, PTGS2, NFKB1, NFKB2, REL, RELA, RELB, RAC1, RAC2, RHOA, RHOB and ARHGEF7. Numerals over bars represent value of the relative expression ($2^{-\Delta CT}$).

4.2.3 qRT-PCR Analysis of the effect of Tissue-Specificity and 2D Plastic on PDAC

Following the analyses of the qPCR array, PANC-1 and PK-1 cells were chosen to further investigate the influence of the environment on the cells i.e. pancreas scaffolds, liver scaffolds and 2D plastic plates. Two genes were selected from three different categories (i) ECM proteins, COL1A1 and LOXL2, (ii) ECM remodelling and migration, MMP9 and TIMP1, and (iii) Proto-oncogenes of the WNT pathway, WNT1 and CTNNB1.

Both PANC-1 (Figure 42a) and PK-1 cells (Figure 43a) showed no significant change in COL1A1 expression when cultured on the different materials; pancreas scaffolds, liver scaffolds and 2D plastic plates. LOXL2 expression was not changed in PANC-1 cells cultured on the different material (Figure 42b). Whereas, PK-1 cells in liver scaffolds presented a significant up regulation of LOXL2 compared to PK-1 cells cultured in pancreas scaffolds ($p < 0.005$) and 2D plastic ($p < 0.005$), but no significant change was observed between cells in pancreas scaffolds and 2D plastic (Figure 43b).

PANC-1 MMP9 expression was significantly up-regulated in both the pancreas ($p < 0.005$) and liver scaffolds ($p < 0.001$) in comparison to 2D plastic, but no significant change was observed between the pancreas and liver scaffolds (Figure 42c). On the other hand, interestingly, PK-1 cells in liver scaffolds presented a significant up regulation of MMP9 compared to PK-1 cells cultured in pancreas scaffolds ($p < 0.0001$) and 2D plastic ($p < 0.0001$), but no significant change was observed between cells in pancreas scaffolds and 2D plastic (Figure 43c). PANC-1 TIMP1 expression was significantly different between all conditions. The highest expression was present in pancreas scaffolds, which was significantly higher than in liver scaffolds ($p = 0.0001$) and 2D plastic ($p < 0.0001$). Additionally, the expression of TIMP1 in liver scaffolds was significantly higher than in 2D plastic ($p < 0.0001$) (Figure 42d). PK-1 TIMP1 expression was significantly up-regulated in the pancreas scaffolds in comparison to 2D plastic ($p < 0.01$) but not in comparison to liver scaffolds ($p > 0.05$). Furthermore, no significant change was observed between the liver scaffolds and 2D plastic (Figure 43d).

PANC-1 WNT1 expression was significantly different between all conditions. The highest expression was present in pancreas scaffolds, which was significantly higher

than in liver scaffolds ($p < 0.005$) and 2D plastic ($p < 0.0001$). Moreover, the expression of WNT1 in liver scaffolds was significantly higher than in 2D plastic ($p < 0.005$) (Figure 42e). PK-1 WNT1 expression was significantly up-regulated in the both pancreas ($p < 0.005$) and liver scaffolds ($p < 0.005$) in comparison to 2D plastic, but no significant change was observed between the pancreas and liver scaffolds (Figure 43e). PANC-1 CTNNB1 expression was significantly up-regulated in the pancreas scaffolds in comparison to 2D plastic ($p < 0.05$) but not in comparison to liver scaffolds. In addition, no significant change was observed between the liver scaffolds and 2D plastic (Figure 42f). PK-1 cells showed no significant change in CTNNB1 expression when cultured on the different materials (Figure 43f).

4.2.4 Next Generation Sequencing Evaluation of the Effect of Tissue-Specificity on PDAC

To thoroughly examine the influence of the ECM on PDAC cells and to justify the importance of tissue-specificity, total RNA from the primary cell line, PANC-1, and the metastatic cell line, PK-1, cultured on both pancreas and liver scaffolds were sequenced using the RNAseq technique.

When compared PANC-1 cells between pancreas and liver scaffolds, 1,081 differentially expressed (DE) genes were identified out of a total of 20,970 genes with measured expression. In this experiment, we chose a threshold of $p < 0.05$ for statistical significance and a log fold change (LogFC) of expression $> 0.5x$. Out of these DE genes, 600 genes were up-regulated, and 481 genes were down-regulated in the PANC-1 cells on liver scaffolds when compared to those cultured on pancreas scaffolds. These data were further analysed in the context of pathways obtained from the Kyoto Encyclopaedia of Genes and Genomes (KEGG) database, gene ontologies (GO) from the Gene Ontology Consortium database and network of regulatory relations from Biological General Repository for Interaction Datasets (BioGRID). In summary, 42 pathways were found to be significantly impacted. In addition, 1,425 GO terms and 144 upstream regulators, were found to be significantly ($p < 0.05$) enriched.

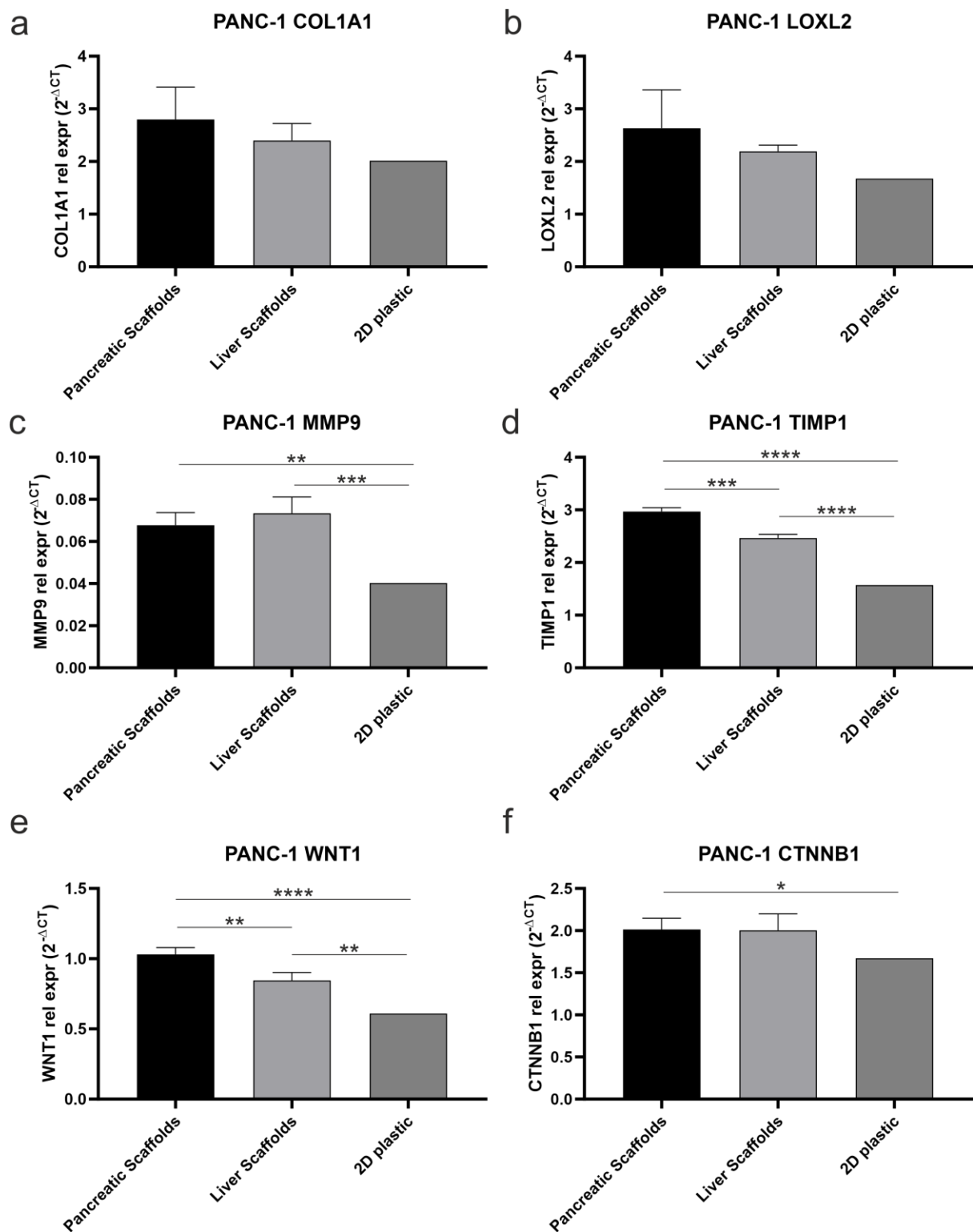


Figure 42. Quantitative gene expression comparison of PANC-1 cells on different materials. PANC-1 cells on pancreas scaffolds, liver scaffolds and 2D plastic were compared for their relative gene expression of (a) COL1A1, (b) LOXL2, (c) MMP9, (d) TIMP1, (e) WNT1 and (f) CTNNB1. Data are expressed as mean \pm s.d. * $p < 0.05$, ** $p < 0.01$, *** $p < 0.001$ and **** $p < 0.0001$.

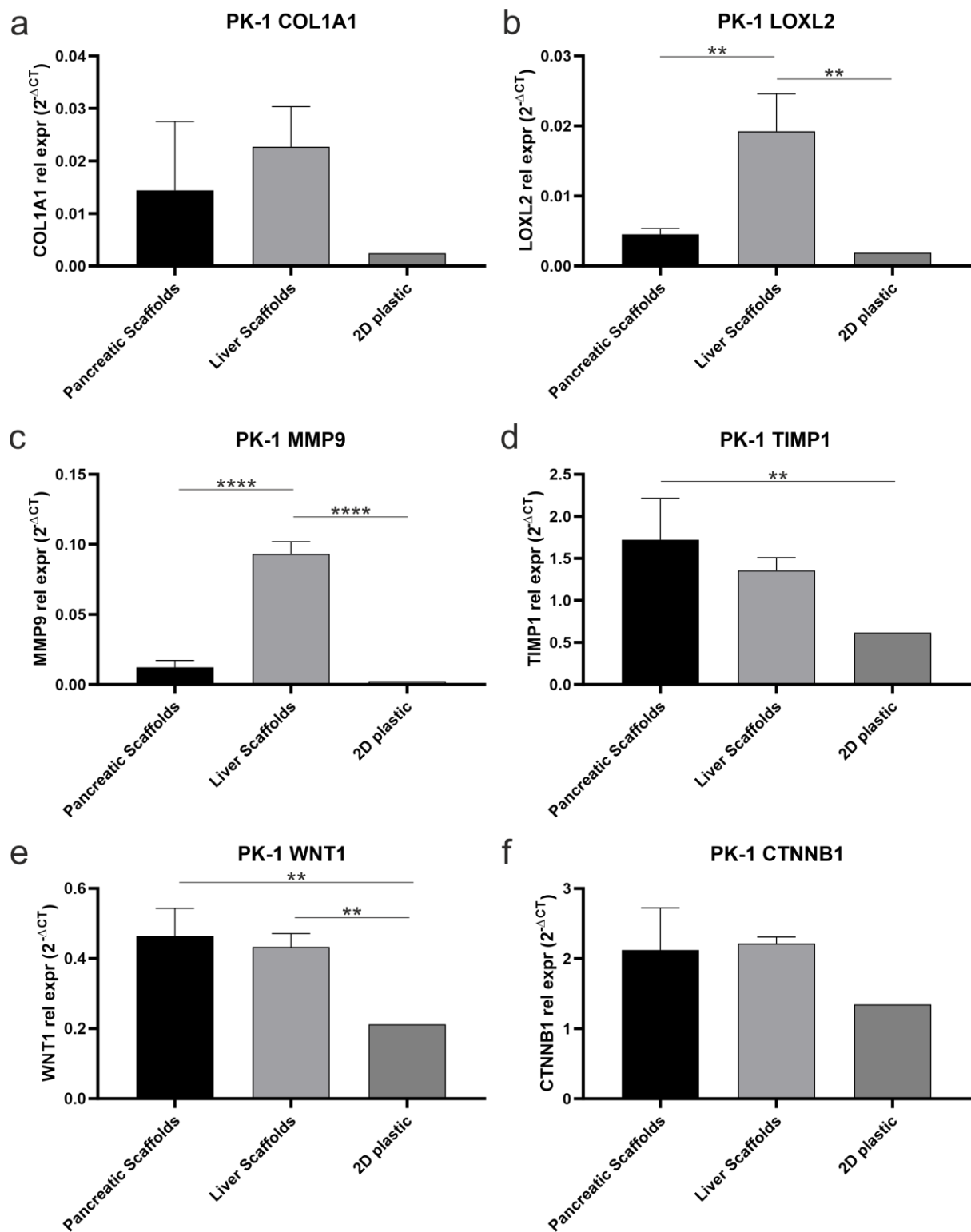


Figure 43. Quantitative gene expression comparison of PK-1 cells. PK-1 cells on pancreas scaffolds, liver scaffolds and 2D plastic were compared for their relative gene expression of (a) COL1A1, (b) LOXL2, (c) MMP9, (d) TIMP1, (e) WNT1 and (f) CTNNB1. Data are expressed as mean \pm s.d. ** $p < 0.01$ and **** $p < 0.0001$.

To best demonstrate the overall impact of tissue-specific ECM on PANC-1 cells, the 1,425 significantly affected GO terms were broken down (Table 18), in order of significance, into (i) the top 10 most significantly impacted GO terms (Table 18a), (ii) the GO terms directly related to cell adhesion (Table 18b), (iii) the GO terms directly related to motility and migration (Table 18c) and (iv) the GO terms directly related to tissue organisation and angiogenesis (Table 18d).

It was found that 28 GO terms were significantly impacted that directly involved cell adhesion. Out of these 28 GO terms, “cell-cell adhesion” (Table 18b) and “cell-matrix adhesion” were studied in further details. Analysis of the “cell-cell adhesion” GO term showed that there were 90 significantly ($p < 0.05$) DE genes out of a total 765 genes involved. Of these genes, 69 genes had a LogFC of > 0.5 in the liver scaffolds compared to the pancreas scaffolds (Supplementary Table 1). In contrast, 21 genes had a LogFC of > 0.5 in the pancreas scaffolds compared to the liver scaffolds (Supplementary Table 1). Analysis of the “cell-matrix adhesion” GO term showed that there were 28 significantly ($p < 0.05$) DE genes out of a total 196 genes involved. Of these genes, 20 genes had a LogFC of > 0.5 in the liver scaffolds compared to the pancreas scaffolds (Supplementary Table 2). In contrast, 8 genes had a LogFC of > 0.5 in the pancreas scaffolds compared to the liver scaffolds (Supplementary Table 2).

Furthermore, it was found that 21 GO terms were significantly impacted that directly involved motility and migration (Table 18c). Out of these 21 GO terms, “cell motility” and “tissue migration” were studied in further details. Analysis of the “cell motility” GO term showed that there were 115 significantly ($p < 0.05$) DE genes out of a total 1350 genes involved. Of these genes, 87 genes had a LogFC of > 0.5 in the liver scaffolds compared to the pancreas scaffolds (Supplementary Table 3). In contrast, 28 genes had a LogFC of > 0.5 in the pancreas scaffolds compared to the liver scaffolds (Supplementary Table 3). Analysis of the “tissue migration” GO term showed that there were 28 significantly ($p < 0.05$) DE genes out of a total 256 genes involved. Of these genes, 21 genes had a LogFC of > 0.5 in the liver scaffolds compared to the pancreas scaffolds (Supplementary Table 4). In contrast, 7 genes had a LogFC of > 0.5 in the pancreas scaffolds compared to the liver scaffolds (Supplementary Table 4).

(a) Top 10 Gene Ontology

GO ID	GO Name	Count DE	Count All	p-value	GO ID	GO Name	Count DE	Count All	p-value
GO:0022610	biological adhesion	148	1296	8.60E-19	GO:0007154	cell communication	409	5652	1.80E-13
GO:0007155	cell adhesion	147	1290	1.40E-18	GO:0009888	tissue development	162	1740	2.20E-12
GO:0032501	multicellular organismal process	466	6388	3.00E-17	GO:0098609	cell-cell adhesion	90	765	2.50E-12
GO:0048731	system development	331	4261	2.40E-14	GO:0007275	multicellular organism development	353	4779	2.90E-12
GO:0023052	signalling	411	5640	4.20E-14	GO:0007166	cell surface receptor signalling pathway	216	2566	4.70E-12

(b) Cell Adhesion Related Gene Ontology

GO ID	GO Name	Count DE	Count All	p-value	GO ID	GO Name	Count DE	Count All	p-value
GO:0022610	biological adhesion	148	1296	8.60E-19	GO:0007157	heterophilic cell-cell adhesion via plasma membrane cell adhesion molecules	8	46	0.00311
GO:0007155	cell adhesion	147	1290	1.40E-18	GO:0034113	heterotypic cell-cell adhesion	8	47	0.00357
GO:0098609	cell-cell adhesion	90	765	2.50E-12	GO:0010810	regulation of cell-substrate adhesion	19	178	0.00391
GO:0098742	cell-cell adhesion via plasma-membrane adhesion molecules	36	228	7.70E-09	GO:0034111	negative regulation of homotypic cell-cell adhesion	4	14	0.00565
GO:0007156	homophilic cell adhesion via plasma membrane adhesion molecules	28	151	1.00E-08	GO:0034110	regulation of homotypic cell-cell adhesion	5	24	0.0085
GO:0034332	adherens junction organization	22	122	6.30E-07	GO:0033634	positive regulation of cell-cell adhesion mediated by integrin	2	3	0.00858
GO:0030155	regulation of cell adhesion	62	633	0.0000051	GO:0007162	negative regulation of cell adhesion	22	234	0.00905
GO:0031589	cell-substrate adhesion	35	300	0.000018	GO:0001952	regulation of cell-matrix adhesion	11	97	0.01636
GO:0007160	cell-matrix adhesion	28	196	0.000065	GO:0022409	positive regulation of cell-cell adhesion	21	233	0.01647
GO:0007229	integrin-mediated signalling pathway	15	95	0.00018	GO:0048041	focal adhesion assembly	9	73	0.01733
GO:0045785	positive regulation of cell adhesion	36	363	0.00038	GO:0033627	cell adhesion mediated by integrin	7	53	0.02417
GO:0034109	homotypic cell-cell adhesion	12	74	0.00061	GO:0051893	regulation of focal adhesion assembly	7	54	0.02651
GO:0022407	regulation of cell-cell adhesion	35	392	0.00285	GO:1903037	regulation of leukocyte cell-cell adhesion	25	315	0.03849
GO:0051040	regulation of calcium-independent cell-cell adhesion	2	2	0.00297	GO:0033630	positive regulation of cell adhesion mediated by integrin	3	15	0.04494

(c) Motility and Migration Related Gene Ontology

GO ID	GO Name	Count DE	Count All	p-value	GO ID	GO Name	Count DE	Count All	p-value
GO:0016477	cell migration	110	1227	1.00E-07	GO:2000147	positive regulation of cell motility	43	431	0.000094

GO:0030334	regulation of cell migration	71	710	4.70E-07	GO:0090130	tissue migration	28	256	0.00036
GO:0048870	cell motility	115	1350	7.20E-07	GO:0010631	epithelial cell migration	24	248	0.00463
GO:0051674	localization of cell	115	1350	7.20E-07	GO:0090132	epithelium migration	24	251	0.00538
GO:0040012	regulation of locomotion	78	822	0.000001	GO:1903115	regulation of actin filament-based movement	7	41	0.00618
GO:0040011	locomotion	128	1569	0.0000016	GO:0030048	actin filament-based movement	14	127	0.00933
GO:2000145	regulation of cell motility	72	756	0.0000024	GO:2000146	negative regulation of cell motility	22	244	0.01427
GO:0006928	movement of cell or subcellular component	141	1821	0.0000076	GO:0030336	negative regulation of cell migration	21	232	0.01576
GO:0090131	mesenchyme migration	4	5	0.000042	GO:0040013	negative regulation of locomotion	23	273	0.02554
GO:0040017	positive regulation of locomotion	46	461	0.000054	GO:0010634	positive regulation of epithelial cell migration	12	117	0.02571
GO:0030335	positive regulation of cell migration	42	417	0.000092					

(d) Tissue Organisation and Angiogenesis Related Gene Ontology

GO ID	GO Name	Count DE	Count All	p-value	GO ID	GO Name	Count DE	Count All	p-value
GO:0043062	extracellular structure organization	48	324	2.30E-10	GO:0001763	morphogenesis of a branching structure	20	185	0.00269
GO:0009653	anatomical structure morphogenesis	196	2387	5.90E-10	GO:0061138	morphogenesis of a branching epithelium	19	173	0.00285
GO:0030198	extracellular matrix organization	47	323	6.60E-10	GO:0002011	morphogenesis of an epithelial sheet	8	50	0.00528
GO:0009887	animal organ morphogenesis	93	947	1.70E-08	GO:0035239	tube morphogenesis	30	337	0.00571
GO:0048729	tissue morphogenesis	62	605	1.1E-06	GO:0043542	endothelial cell migration	18	174	0.00677
GO:0001568	blood vessel development	61	603	2.1E-06	GO:0072132	mesenchyme morphogenesis	7	44	0.00915
GO:0048646	anatomical structure formation involved in morphogenesis	87	970	2.5E-06	GO:0097755	positive regulation of blood vessel diameter	8	55	0.00943
GO:0000904	cell morphogenesis involved in differentiation	60	642	0.00003	GO:0010595	positive regulation of endothelial cell migration	10	78	0.00959
GO:0000902	cell morphogenesis	78	902	0.000031	GO:0060562	epithelial tube morphogenesis	26	300	0.01329
GO:0048514	blood vessel morphogenesis	51	522	0.000038	GO:0010769	regulation of cell morphogenesis involved in differentiation	22	251	0.01918
GO:0050880	regulation of blood vessel size	19	125	0.000045	GO:0022603	regulation of anatomical structure morphogenesis	67	955	0.0194
GO:0097746	regulation of blood vessel diameter	18	118	0.000068	GO:0022617	extracellular matrix disassembly	10	87	0.01973
GO:0001525	angiogenesis	44	439	0.00007	GO:0043534	blood vessel endothelial cell migration	10	88	0.02121
GO:0048858	cell projection morphogenesis	54	587	0.00011	GO:0010770	positive regulation of cell morphogenesis involved in differentiation	13	134	0.03114

GO:0120039	plasma membrane bounded cell projection morphogenesis	53	584	0.00018	GO:0022604	regulation of cell morphogenesis	32	423	0.03811
GO:0002009	morphogenesis of an epithelium	46	506	0.00046	GO:0043536	positive regulation of blood vessel endothelial cell migration	5	36	0.04417
GO:0022612	gland morphogenesis	16	115	0.0005	GO:0030947	regulation of vascular endothelial growth factor receptor signalling pathway	4	25	0.0445
GO:0097756	negative regulation of blood vessel diameter	12	74	0.00061	GO:0048754	branching morphogenesis of an epithelial tube	13	142	0.04637

Table 18. Gene Ontology terms of RNAseq data of PANC-1 cells on pancreas vs liver scaffolds. The analysis is represented as follows: (a) the top 10 most significantly impacted GO terms, (b) the significantly impacted GO terms directly related to cell adhesion, (c) the significantly impacted GO terms directly related to motility and migration and (d) the significantly impacted GO terms directly related to tissue organisation and angiogenesis. Included in the table are the total number of genes involved in each GO Name (Count All) and the number of differentially expressed genes of each GO Name (Count DE). The GO terms are ordered in terms of significance (lowest p-value to highest).

Finally, it was found that 36 GO terms were significantly impacted that directly involved tissue organisation and angiogenesis (Table 18d). Out of these 36 GO terms, “extracellular structure organisation” and “angiogenesis” were studied in further details. Analysis of the “extracellular structure organisation” GO term showed that there were 48 significantly ($p < 0.05$) DE genes out of a total 324 genes involved. Of these genes, 39 genes had a LogFC of > 0.5 in the liver scaffolds compared to the pancreas scaffolds (Supplementary Table 5). In contrast, 7 genes had a LogFC of > 0.5 in the pancreas scaffolds compared to the liver scaffolds (Supplementary Table 5). Analysis of the “angiogenesis” GO term showed there were 44 significantly ($p < 0.05$) DE genes out of a total 439 genes involved. Of these genes, 33 genes had a LogFC of > 0.5 in the liver scaffolds compared to the pancreas scaffolds (Supplementary Table 6). In contrast, 11 genes had a LogFC of > 0.5 in the pancreas scaffolds compared to the liver scaffolds (Supplementary Table 6).

Next, we investigated the cellular pathways that were impacted in PANC-1 cells on the different scaffold environment. The pathways were scored on iPathwayGuide according to the Impact Analysis method (see methods and materials). Briefly, impact analysis uses two types of evidence: i) the over-representation of DE genes in a given pathway and ii) the perturbation of that pathway computed by propagating the measured expression changes across the pathway topology. These aspects are captured by two independent probability values, pORA and pAcc, that are then combined in a unique pathway-specific p-value. There were 275 pathways that presented at least one DE gene, of which 42 pathways showed a pathway-specific p-value of < 0.05 (Table 19).

The most significant pathway was “ECM-receptor interaction” ($p = 2.8E-8$) (Table 19). Further investigation showed that all DE genes associated with this pathway were up-regulated in the liver compared to the pancreas (Figure 44). Of these DE genes, 2 were collagens (COL6A2 and COL9A3), 4 were laminins (LAMA3, LAMA5, LAMB1 and LAMC2) and 6 were integrins (ITGA3, ITGAV, ITGB3, ITGB4, ITGB8 and ITGA10) among other genes.

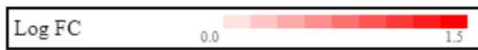
Pathway Name	p-value	Pathway Name	p-value
ECM-receptor interaction	2.85E-08	Phenylalanine metabolism	0.007766242
Axon guidance	4.0919E-06	Hypertrophic cardiomyopathy (HCM)	0.009369155
Arrhythmogenic right ventricular cardiomyopathy (ARVC)	1.43731E-05	Platelet activation	0.009700176
Focal adhesion	2.46856E-05	Tyrosine metabolism	0.013171641
PI3K-Akt signalling pathway	2.65091E-05	Basal cell carcinoma	0.015017373
Cell adhesion molecules (CAMs)	3.06003E-05	Phagosome	0.015903648
Cytokine-cytokine receptor interaction	7.23695E-05	Herpes simplex infection	0.016643962
Proteoglycans in cancer	0.000118577	Dilated cardiomyopathy (DCM)	0.019786764
Pathways in cancer	0.000198155	Asthma	0.020820893
Regulation of actin cytoskeleton	0.000510981	Transcriptional misregulation in cancer	0.020995067
Rheumatoid arthritis	0.001574304	Malaria	0.024534235
Protein digestion and absorption	0.002602373	Melanogenesis	0.027219514
Small cell lung cancer	0.002661597	Biosynthesis of unsaturated fatty acids	0.028405508
Hematopoietic cell lineage	0.002874205	Adherens junction	0.031509676
Rap1 signalling pathway	0.003108315	Thiamine metabolism	0.039060021
cGMP-PKG signalling pathway	0.00346881	TNF signalling pathway	0.041205411
Neuroactive ligand-receptor interaction	0.003600339	Hepatocellular carcinoma	0.041258291
Human papillomavirus infection	0.003885796	Cardiac muscle contraction	0.041581419
MicroRNAs in cancer	0.004604068	Vascular smooth muscle contraction	0.044344645
Salivary secretion	0.006003662	Amphetamine addiction	0.047527816
Cocaine addiction	0.006465214	Vasopressin-regulated water reabsorption	0.049595291

Table 19. Significantly impacted pathways from RNAseq data of PANC-1 cells on pancreas vs liver scaffolds. Pathways are ordered by significance (lowest p-value to highest).

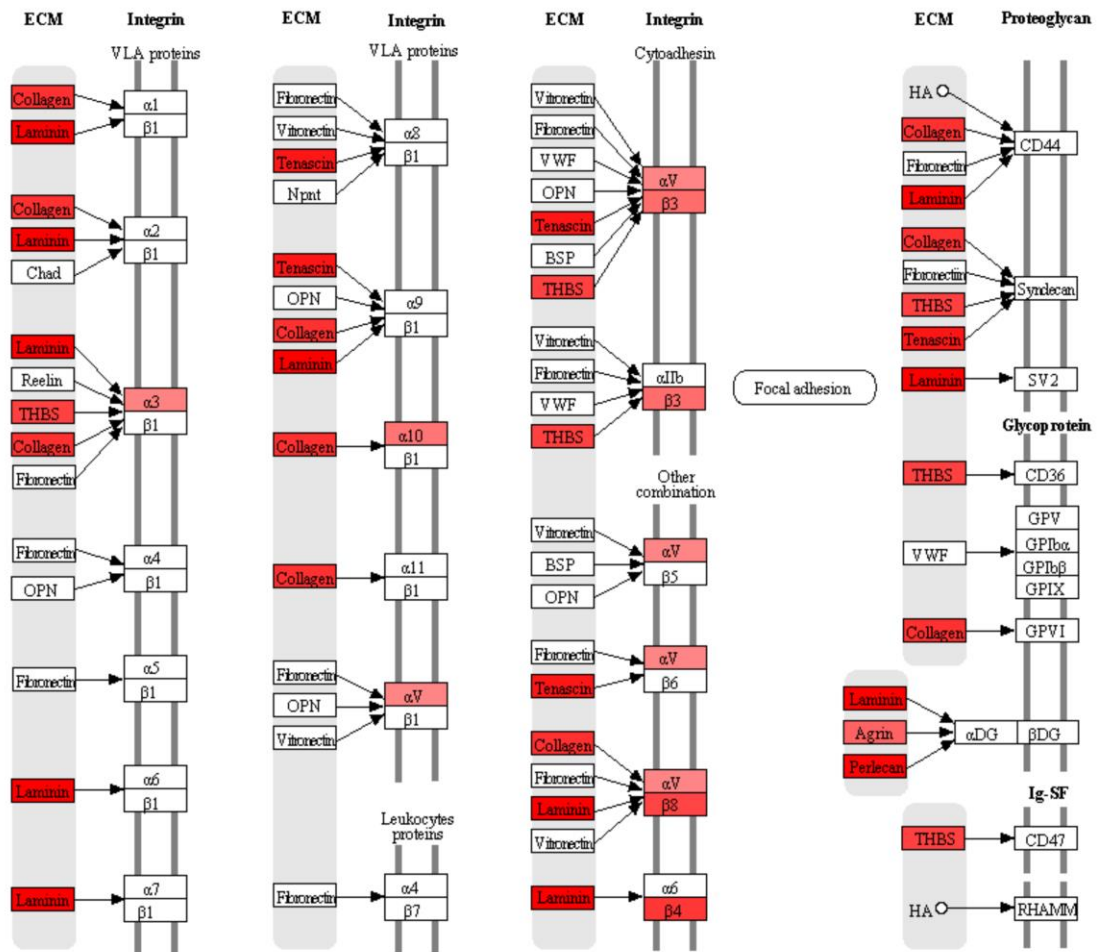
The final aspect investigated relating to the RNAseq data of PANC-1 on the different environments was the prediction of upstream regulators (see methods and material). Briefly, it is based on two types of information: i) the enrichment of DE genes from the experiment and ii) a network of regulatory interactions from iPathwayGuide's proprietary knowledge base. To create the network, the analysis selects only those edges observed in the literature with at least a medium confidence (evidence score greater than or equal to 400). The analysis considers two hypotheses: i) The upstream regulator is activated in the condition studied and ii) The upstream regulator is inhibited in the condition studied.

To that note, the top ten hypothesised “activated” upstream regulators were listed in order of significance (Figure 45a), PCOLCE2 (Figure 45b), PCOLCE (Figure 45c), HSPA4 (Figure 45d), TP63 (Figure 45e), GLI1 (Figure 45f), ESR1 (Figure 45g), CXCL12 (Figure 45h), IL13 (Figure 45i), KDM3A (Figure 45j) and LIF (Figure 45k). Additionally, the top ten hypothesised “inhibited” upstream regulators were listed in order of significance (Figure 46a), PNPLA2 (Figure 46b), GHSR (Figure 46c), GHITM (Figure 46d), CEBPD (Figure 46e), PRKG1 (Figure 46f), MAF (Figure 46g), OPRM1 (Figure 46h), NKX3-1 (Figure 46i), TXLNG (Figure 46j) and CRH (Figure 46k).

Further, when comparing between PK-1 cells on pancreas and liver scaffolds, 1,757 DE genes were identified out of a total of 20,860 genes with measured expression. Similar to the PANC-1 experiment, we chose a threshold of $p < 0.05$ for statistical significance and a LogFC of expression $> 0.5x$. Out of these DE genes, 467 genes were up-regulated, and 1,290 genes were down-regulated in the PK-1 cells on liver scaffolds when compared to those cultured on pancreas scaffolds. Further, these were then analysed in the context of GO, KEGG pathways and network of regulatory relations. In summary, 42 pathways were found to be significantly impacted. In addition, 1,445 GO terms and 220 upstream regulators, were found to be significantly ($p < 0.05$) enriched.



ECM-RECEPTOR INTERACTION



04512 11/25/15
(c) Kanehisa Laboratories

(c) Advaita Corporation 2019

Figure 44. Pathway map for ECM-receptor interaction representing the significantly differentially expressed genes from RNAseq of PANC-1 cells cultured on pancreas vs liver scaffolds. ECM-receptor interaction (KEGG: 04512) was the most significantly impacted pathway. The pathway diagram is overlaid with the computed perturbation of each gene. The perturbation accounts both for the gene's measured fold change and for the accumulated perturbation propagated from any upstream genes (accumulation). The highest negative perturbation (up-regulated in pancreas scaffolds) would be shown in dark blue (non-present), while the highest positive perturbation (up-regulated in liver scaffolds) in dark red. The legend describes the values on the gradient. One gene may be represented in multiple places in the diagram and one box may represent multiple genes in the same gene family. A gene is highlighted in all locations it occurs in the diagram. For each gene family, the colour corresponding to the gene with the highest absolute perturbation is displayed.

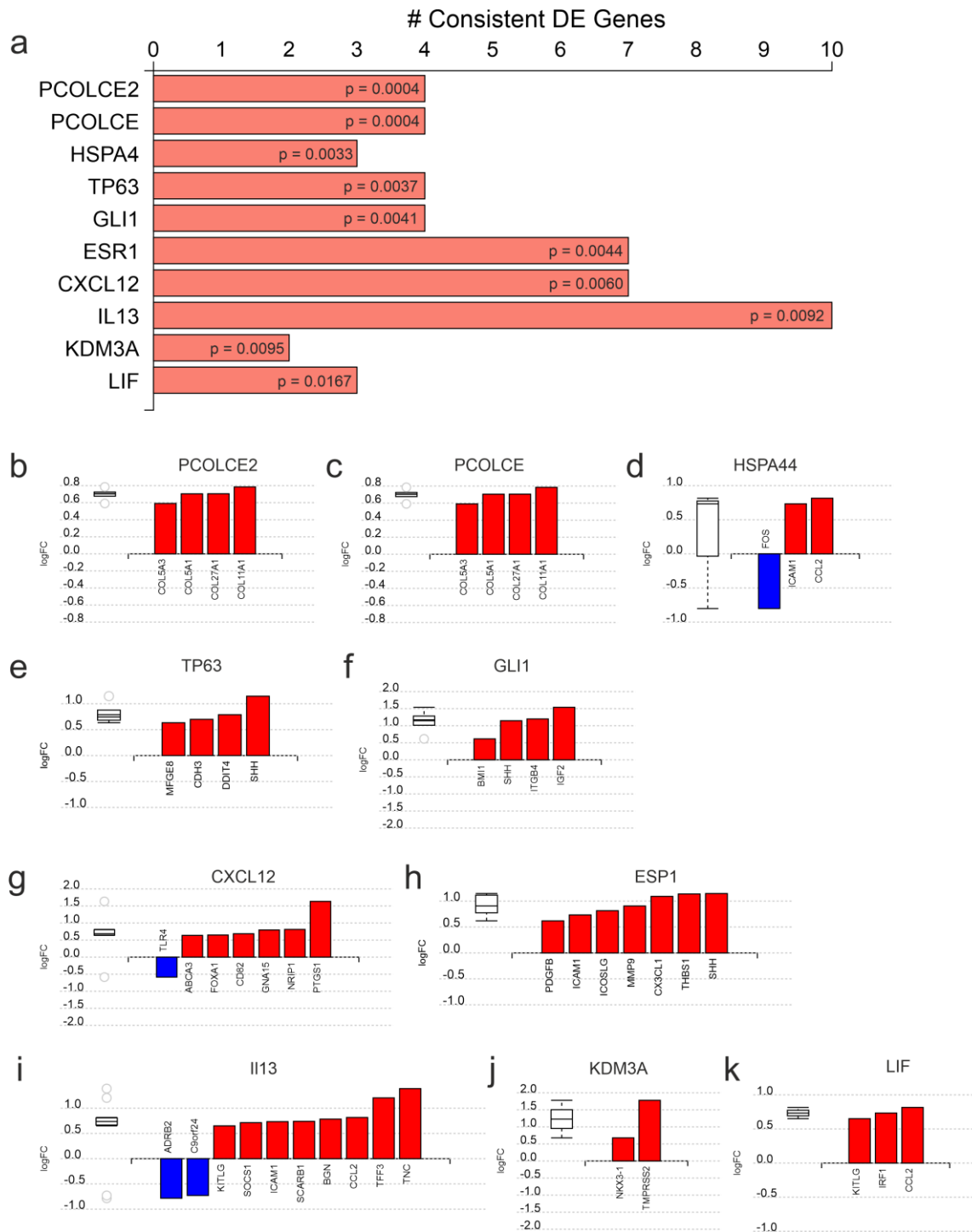


Figure 45. Predicted activated upstream regulators of RNAseq data of PANC-1 cells on pancreas vs liver scaffolds. (a) Top 10 significant upstream regulators predicted as activated. The x axis represented the number of DE genes downstream of the regulator. The gene measured expression bar plot: All the consistent differentially expressed genes that are targeted by (b) PCOLCE2, (c) PCOLCE, (d) HSPA44, (e) TP63, (f) GLI1, (g) CXCL12, (h) ESP1, (i) IL13, (j) KDM3A and (k) LIF are ranked based on their measured expression change from most down-regulated (in blue) to up-regulated (in red) in liver scaffolds compared to pancreas scaffolds. The box and whisker plot on the left summarises the distribution of all the consistent differentially expressed genes targeted by this upstream regulator. The box shows the 1st quartile, the median and the 3rd quartile, while the outliers are represented by circles.

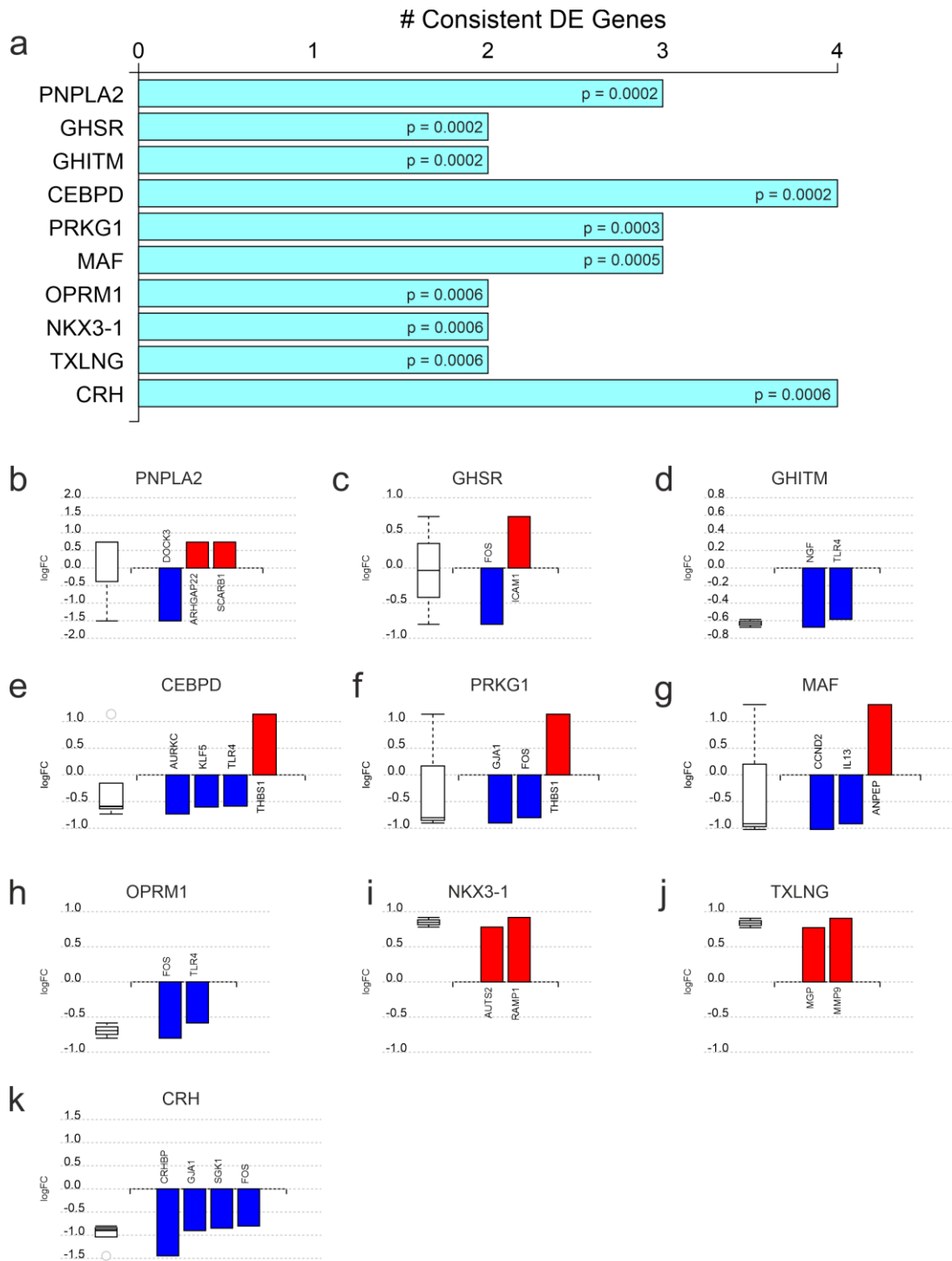


Figure 46. Predicted inhibited upstream regulators of RNAseq data of PANC-1 cells on pancreas vs liver scaffolds. (a) Top 10 significant upstream regulators predicted as inhibited. The x axis represented the number of DE genes downstream of the regulator. The gene measured expression bar plot: All the consistent differentially expressed genes that are targeted by (b) PNPLA2, (c) GHSR, (d) GHITM, (e) CEBPD, (f) PRKG1, (g) MAF, (h) OPRM1, (i) NKX3-1, (j) TXLNG and (k) CRH are ranked based on their measured expression change from most down-regulated (in blue) to up-regulated (in red) in liver scaffolds compared to pancreas scaffolds. The box and whisker plot on the left summarises the distribution of all the consistent differentially expressed genes targeted by this upstream regulator. The box shows the 1st quartile, the median and the 3rd quartile, while the outliers are represented by circles.

The 1,445 significantly affected GO terms, were broken down, in order of significance, as demonstrated before, into (i) the top 10 most significantly impacted GO terms (Table 20a), (ii) the GO terms directly related to cell adhesion (Table 20b), (iii) the GO terms directly related to motility and migration (Table 20c) and (iv) the GO terms directly related to tissue organisation and angiogenesis (Table 20d).

It was found that 20 GO terms were significantly impacted that directly involved cell adhesion (Table 20b). Out of these 20 GO terms, “cell-cell adhesion” and “negative regulation of cell-matrix adhesion” were studied in further details. Analysis of the “cell-cell adhesion” GO term showed that there were 95 significantly ($p < 0.05$) DE genes out of a total 759 genes involved. Of these genes, 30 genes had a LogFC of >0.5 in the liver scaffolds compared to the pancreas scaffolds (Supplementary Table 7). In contrast, 65 genes had a LogFC of >0.5 in the pancreas scaffolds compared to the liver scaffolds (Supplementary Table 7). Analysis of the “cell-matrix adhesion” GO term showed that there were 6 significantly ($p < 0.05$) DE genes out of a total 28 genes involved. Of these genes, 3 genes had a LogFC of >0.5 in the liver scaffolds compared to the pancreas scaffolds (Supplementary Table 8). In contrast, 3 genes had a LogFC of >0.5 in the pancreas scaffolds compared to the liver scaffolds (Supplementary Table 8).

Furthermore, it was found that 12 GO terms were significantly impacted that directly involved motility and migration (Table 20c). Out of these 12 GO terms, “cell motility” and “tissue migration” were studied in further details. Analysis of the “cell motility” GO term showed that there were 147 significantly ($p < 0.05$) DE genes out of a total 1350 genes involved. Of these genes, 51 genes had a LogFC of >0.5 in the liver scaffolds compared to the pancreas scaffolds (Supplementary Table 9). In contrast, 96 genes had a LogFC of >0.5 in the pancreas scaffolds compared to the liver scaffolds (Supplementary Table 9). Analysis of the “tissue migration” GO term showed that there were 32 significantly ($p < 0.05$) DE genes out of a total 254 genes involved. Of these genes, 10 genes had a LogFC of >0.5 in the liver scaffolds compared to the pancreas scaffolds (Supplementary Table 10). In contrast, 23 genes had a LogFC of >0.5 in the pancreas scaffolds compared to the liver scaffolds (Supplementary Table 10).

Top 10 Gene Ontology									
GO ID	GO Name	Count DE	Count All	p-value	GO ID	GO Name	Count DE	Count All	p-value
GO:0000819	sister chromatid segregation	56	228	2.40E-13	GO:0000278	mitotic cell cycle	141	971	1.30E-10
GO:0007059	chromosome segregation	71	338	6.70E-13	GO:0140014	mitotic nuclear division	54	250	1.30E-10
GO:0098813	nuclear chromosome segregation	63	290	2.90E-12	GO:1903047	mitotic cell cycle process	122	809	2.40E-10
GO:0000070	mitotic sister chromatid segregation	40	142	6.60E-12	GO:0000280	nuclear division	71	382	2.60E-10
GO:0051301	cell division	96	562	2.60E-11	GO:0008283	cell proliferation	229	1839	7.70E-10

Cell Adhesion Related Gene Ontology									
GO ID	GO Name	Count DE	Count All	p-value	GO ID	GO Name	Count DE	Count All	p-value
GO:0007155	cell adhesion	156	1276	1.8E-06	GO:0033631	cell-cell adhesion mediated by integrin	4	12	0.01503
GO:0022610	biological adhesion	156	1283	2.5E-06	GO:0033632	regulation of cell-cell adhesion mediated by integrin	3	8	0.02512
GO:0030155	regulation of cell adhesion	86	631	8.7E-06	GO:0022408	negative regulation of cell-cell adhesion	20	147	0.02526
GO:0098609	cell-cell adhesion	95	759	0.000089	GO:0010812	negative regulation of cell-substrate adhesion	9	51	0.0273
GO:0022407	regulation of cell-cell adhesion	53	391	0.00051	GO:0001953	negative regulation of cell-matrix adhesion	6	28	0.0283
GO:0007162	negative regulation of cell adhesion	33	229	0.00205	GO:0034110	regulation of homotypic cell-cell adhesion	5	22	0.03489
GO:0033627	cell adhesion mediated by integrin	11	54	0.00528	GO:0034115	negative regulation of heterotypic cell-cell adhesion	3	9	0.03533
GO:0098742	cell-cell adhesion via plasma-membrane adhesion molecules	30	223	0.0086	GO:0033634	positive regulation of cell-cell adhesion mediated by integrin	2	4	0.03895
GO:0033628	regulation of cell adhesion mediated by integrin	8	38	0.01343	GO:0045785	positive regulation of cell adhesion	41	364	0.04119
GO:0007155	cell adhesion	156	1276	1.8E-06	GO:0033631	cell-cell adhesion mediated by integrin	4	12	0.01503

Motility and Migration Related Gene Ontology									
GO ID	GO Name	Count DE	Count All	p-value	GO ID	GO Name	Count DE	Count All	p-value
GO:0016477	cell migration	137	1219	0.00043	GO:0090130	tissue migration	32	254	0.01699
GO:0048870	cell motility	147	1350	0.00103	GO:0010631	epithelial cell migration	31	245	0.01757
GO:0006935	chemotaxis	66	528	0.00107	GO:2000147	positive regulation of cell motility	49	431	0.02393
GO:0060326	cell chemotaxis	32	235	0.0057	GO:0030335	positive regulation of cell migration	47	415	0.02817
GO:0090132	epithelium migration	32	248	0.01231	GO:2000145	regulation of cell motility	79	757	0.03534

GO:0030334	regulation of cell migration	77	705	0.01456	GO:0040017	positive regulation of locomotion	50	460	0.04561
------------	------------------------------	----	-----	---------	------------	-----------------------------------	----	-----	---------

Tissue Organisation Related Gene Ontology

GO ID	GO Name	Count DE	Count All	p-value	GO ID	GO Name	Count DE	Count All	p-value
GO:0009653	anatomical structure morphogenesis	261	2315	5.00E-07	GO:0001936	regulation of endothelial cell proliferation	17	104	0.00685
GO:0048646	anatomical structure formation involved in morphogenesis	117	942	0.000019	GO:0001935	endothelial cell proliferation	19	121	0.00686
GO:0001568	blood vessel development	77	589	0.0001	GO:1903670	regulation of sprouting angiogenesis	9	43	0.00932
GO:0002040	sprouting angiogenesis	18	82	0.00016	GO:0045765	regulation of angiogenesis	31	238	0.01198
GO:0043062	extracellular structure organization	46	321	0.00035	GO:0061138	morphogenesis of a branching epithelium	23	167	0.01518
GO:0048514	blood vessel morphogenesis	66	509	0.0004	GO:0009887	animal organ morphogenesis	97	917	0.01539
GO:0030198	extracellular matrix organization	45	320	0.00061	GO:0010594	regulation of endothelial cell migration	19	131	0.0156
GO:0001937	negative regulation of endothelial cell proliferation	10	36	0.00065	GO:1905332	positive regulation of morphogenesis of an epithelium	7	32	0.01649
GO:0001525	angiogenesis	56	426	0.00077	GO:0022603	regulation of anatomical structure morphogenesis	97	924	0.01858
GO:0043537	negative regulation of blood vessel endothelial cell migration	9	31	0.00084	GO:0001763	morphogenesis of a branching structure	24	180	0.01922
GO:0043535	regulation of blood vessel endothelial cell migration	14	67	0.00136	GO:1901202	negative regulation of extracellular matrix assembly	2	3	0.02064
GO:2000181	negative regulation of blood vessel morphogenesis	17	90	0.00144	GO:0120039	plasma membrane bounded cell projection morphogenesis	62	566	0.02494
GO:0002043	blood vessel endothelial cell proliferation involved in sprouting angiogenesis	6	16	0.00145	GO:0048754	branching morphogenesis of an epithelial tube	19	138	0.02569
GO:0016525	negative regulation of angiogenesis	16	88	0.00295	GO:0048858	cell projection morphogenesis	62	569	0.02745
GO:0043534	blood vessel endothelial cell migration	16	88	0.00295	GO:0043536	positive regulation of blood vessel endothelial cell migration	7	36	0.0304
GO:0043542	endothelial cell migration	26	173	0.00328	GO:2000351	regulation of endothelial cell apoptotic process	7	37	0.03482
GO:0035239	tube morphogenesis	42	324	0.00427	GO:0060562	epithelial tube morphogenesis	34	289	0.03502
GO:0002042	cell migration involved in sprouting angiogenesis	9	39	0.00477	GO:1903587	regulation of blood vessel endothelial cell proliferation involved in sprouting angiogenesis	3	9	0.03533
GO:0035767	endothelial cell chemotaxis	7	26	0.00505	GO:0000904	cell morphogenesis involved in differentiation	66	621	0.03713
GO:0090049	regulation of cell migration involved in sprouting angiogenesis	7	26	0.00505	GO:0042118	endothelial cell activation	3	10	0.04734
GO:0090051	negative regulation of cell migration involved in sprouting angiogenesis	5	15	0.00655	GO:2000352	negative regulation of endothelial cell apoptotic process	5	24	0.04893

GO:1903671	negative regulation of sprouting angiogenesis	6	21	0.0068
------------	---	---	----	--------

Table 20. Gene Ontology terms of RNAseq data of PK-1 cells on pancreas vs liver scaffolds. The analysis is representing as (a) the top 10 most significantly impacted GO terms, (b) the significantly impacted GO terms directly related to cell adhesion, (c) the significantly impacted GO terms directly related to motility and migration and (d) the significantly impacted GO terms directly related to tissue organisation and angiogenesis. Included in the table are the total number of genes involved in each GO Name (Count All) and the number of differentially expressed genes of each GO Name (Count DE). The GO terms are ordered in terms of significance (lowest p-value to highest).

Finally, it was found that 45 GO terms were significantly impacted that directly involved tissue organisation and angiogenesis (Table 20d). Out of these 45 GO terms, “extracellular structure organisation” and “angiogenesis” were studied in further details. Analysis of the “extracellular structure organisation” GO term showed that there were 46 significantly ($p < 0.05$) DE genes out of a total 321 genes involved. Of these genes, 20 genes had a LogFC of > 0.5 in the liver scaffolds compared to the pancreas scaffolds (Supplementary Table 11). In contrast, 26 genes had a LogFC of > 0.5 in the pancreas scaffolds compared to the liver scaffolds (Supplementary Table 11). Analysis of the “angiogenesis” GO term showed that there were 56 significantly ($p < 0.05$) DE genes out of a total 426 genes involved. Of these genes, 18 genes had a LogFC of > 0.5 in the liver scaffolds compared to the pancreas scaffolds (Supplementary Table 12). In contrast, 38 genes had a LogFC of > 0.5 in the pancreas scaffolds compared to the liver scaffolds (Supplementary Table 12).

Next, we investigated the cellular pathways that were impacted in PK-1 cells on the different scaffold environment. There were 300 pathways that presented at least one DE gene, of which 42 showed a pathway-specific p-value of < 0.05 (Table 21). The most significant pathway was “cell cycle” ($p = 8.7e-6$) (Table 21). Further investigation showed that all but one DE genes associated with this pathway were down-regulated in the liver compared to the pancreas (Figure 47).

The final aspect investigated relating to the RNAseq data of PK-1 on the different environments was the prediction of upstream regulators. The top ten hypothesised “activated” upstream regulators were listed in order of significance (Figure 48a); E2F4 (Figure 48b), RBL2 (Figure 48c), RBL1 (Figure 48d), SNAI1 (Figure 48e), IL1RN (Figure 48f), CD151 (Figure 48g), EFS (Figure 48h), LMX1A (Figure 48i), FBLN5 (Figure 48j) and TRIP6 (Figure 48k). Additionally, the top ten hypothesised “inhibited” upstream regulators were listed in order of significance (Figure 49a); PLK1 (Figure 49b), AURKB (Figure 49c), INCENP (Figure 49d), CENPS (Figure 49e), MAPRE1 (Figure 49f), CDCA8 (Figure 49g), CENPH (Figure 49h), MIS12 (Figure 49i), CENPO (Figure 49j) and B9D2 (Figure 49k).

Pathway Name	p-value	Pathway Name	p-value
Cell cycle	8.68191E-06	Osteoclast differentiation	0.015326962
p53 signalling pathway	5.12703E-05	Progesterone-mediated oocyte maturation	0.020629802
IL-17 signalling pathway	0.000115478	Endocrine resistance	0.021092397
Transcriptional misregulation in cancer	0.000126724	Amoebiasis	0.022011991
Cytokine-cytokine receptor interaction	0.000362604	Gastric acid secretion	0.023341329
Oocyte meiosis	0.000782943	Phospholipase D signalling pathway	0.023469257
Inflammatory mediator regulation of TRP channels	0.001604745	Glycolysis / Gluconeogenesis	0.023519443
Metabolism of xenobiotics by cytochrome P450	0.001986479	Ether lipid metabolism	0.025369858
Amphetamine addiction	0.002167773	GABAergic synapse	0.026881783
MAPK signalling pathway	0.003588865	Small cell lung cancer	0.027421959
Chemokine signalling pathway	0.003600825	Bladder cancer	0.028993073
Pancreas secretion	0.005666768	Legionellosis	0.02931204
Drug metabolism - cytochrome P450	0.006345172	Complement and coagulation cascades	0.030661074
Rheumatoid arthritis	0.009127538	Malaria	0.032292848
Regulation of actin cytoskeleton	0.009353737	HTLV-I infection	0.033049413
NF-kappa B signalling pathway	0.010417211	Type II diabetes mellitus	0.036519325
Cellular senescence	0.013900067	Epithelial cell signalling in Helicobacter pylori infection	0.038771937
Estrogen signalling pathway	0.014275862	Arachidonic acid metabolism	0.039085026
MicroRNAs in cancer	0.014914344	Phenylalanine metabolism	0.04019851
TNF signalling pathway	0.015003101	NOD-like receptor signalling pathway	0.040456618
Leukocyte transendothelial migration	0.015305753	Starch and sucrose metabolism	0.048147514

Table 21. Significantly impacted pathways from RNAseq data of PK-1 cells on pancreas vs liver scaffolds. Pathways are ordered by significance (lowest p-value to highest)

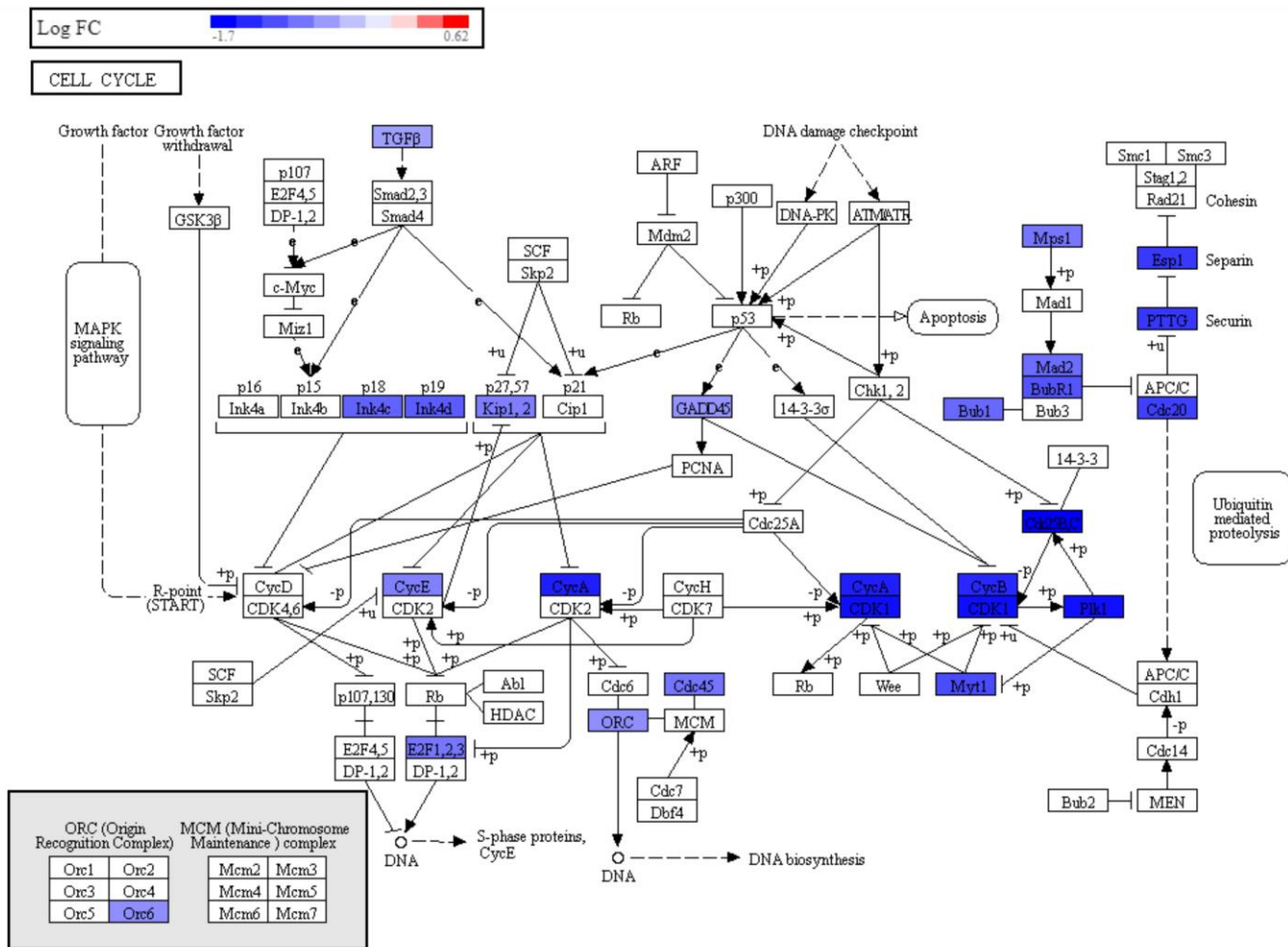


Figure 47. Pathway map for cell cycle representing the significantly differentially expressed genes from RNAseq of PANC-1 cells cultured on pancreas vs liver scaffolds. Cell cycle (KEGG: 04110) was the most significantly impacted pathway. The pathway diagram is overlaid with the computed perturbation of each gene. The perturbation accounts both for the gene's measured fold change and for the accumulated perturbation propagated from any upstream genes (accumulation). The highest negative perturbation (up-regulated in pancreas scaffolds) is shown in dark blue, while the highest positive perturbation (up-regulated in liver scaffolds) would be in dark red (non-present). The legend describes the values on the gradient. One gene may be represented in multiple places in the diagram and one box may represent multiple genes in the same gene family. A gene is highlighted in all locations it occurs in the diagram. For each gene family, the colour corresponding to the gene with the highest absolute perturbation is displayed.

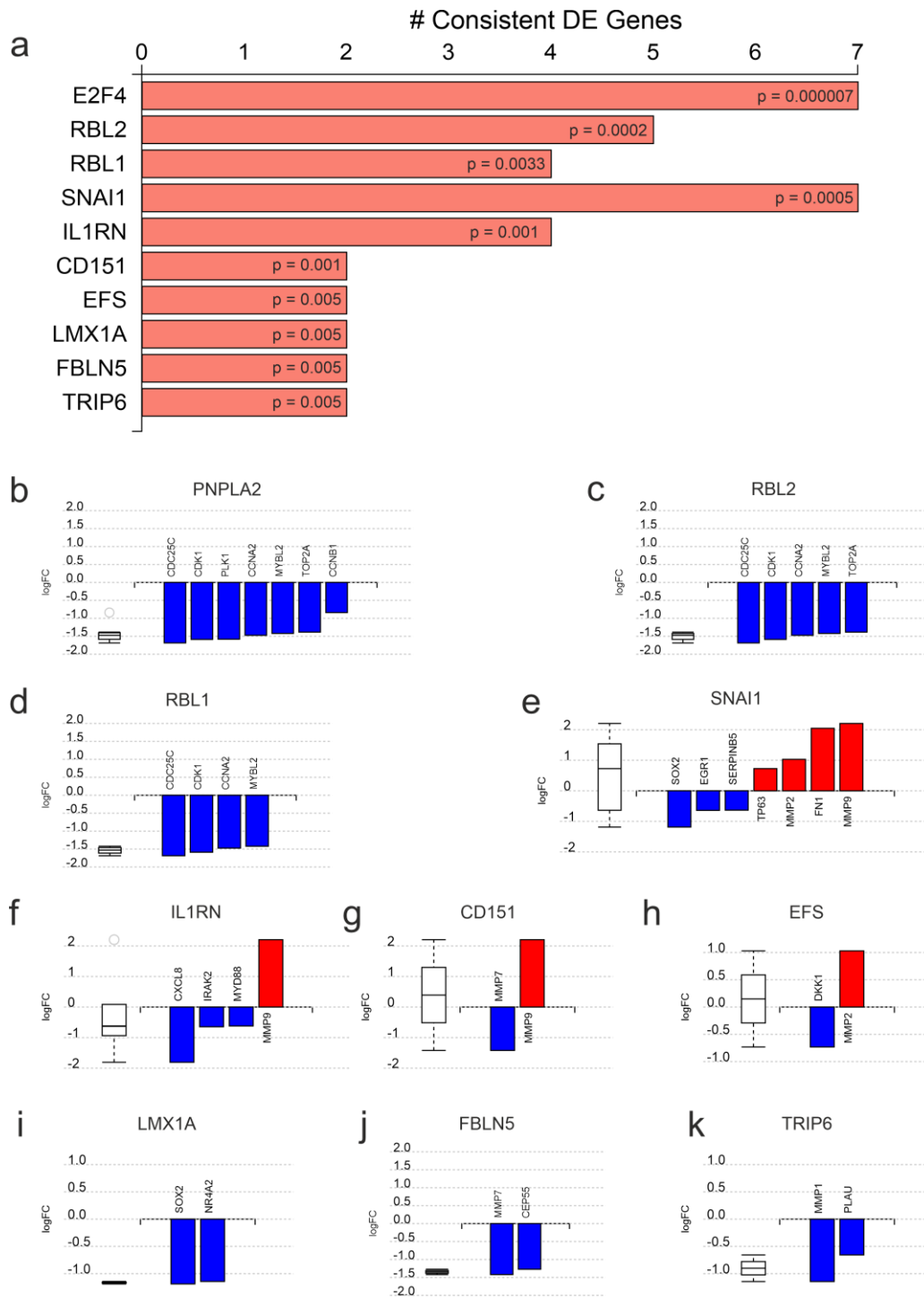


Figure 48. Predicted activated upstream regulators of RNAseq data of PK-1 cells on pancreas vs liver scaffolds. (a) Top 10 significant upstream regulators predicted as activated. The x axis represented the number of DE genes downstream of the regulator. The gene measured expression bar plot: All the consistent differentially expressed genes that are targeted by (b) PNPLA2, (c) RBL2, (d) RBL1, (e) SNAI1, (f) IL1RN, (g) CD151, (h) EFS, (i) LMX1A, (j) FBLN5 and (k) TRIP6 are ranked based on their measured expression change from most down-regulated (in blue) to up-regulated (in red) in liver scaffolds compared to pancreas scaffolds. The box and whisker plot on the left summarises the distribution of all the consistent differentially expressed genes targeted by this upstream regulator. The box shows the 1st quartile, the median and the 3rd quartile, while the outliers are represented by circles.

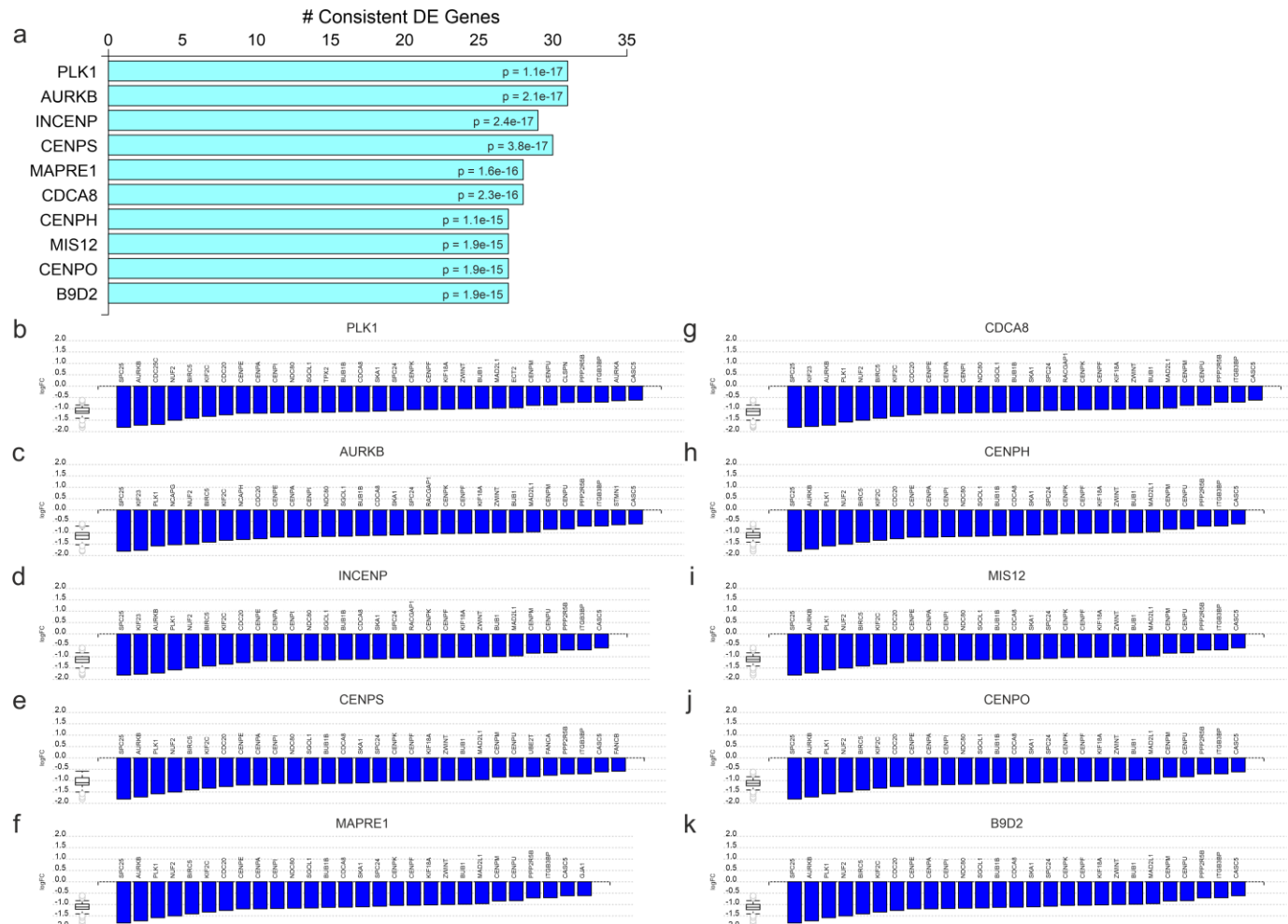


Figure 49. Predicted inhibited upstream regulators of RNAseq data of PK-1 cells on pancreas vs liver scaffolds. (a) Top 10 significant upstream regulators predicted as inhibited. The x axis represented the number of DE genes downstream of the regulator. The gene measured expression bar plot: All the consistent differentially expressed genes that are targeted by **(b) PLK1, (c) AURKB, (d) INCENP, (e) CENPS, (f) MAPRE1, (g) CDCA8, (h) CENPH, (i) MIS12, (j) CENPO** and **(k) B9D2** are ranked based on their measured expression change from most down-regulated (in blue) to up-regulated (in red) in liver scaffolds compared to pancreas scaffolds. The box and whisker plot on the left summarises the distribution of all the consistent differentially expressed genes targeted by this upstream regulator. The box shows the 1st quartile, the median and the 3rd quartile, while the outliers are represented by circles.

4.3 Tissue-Specific PDAC Models to Evaluate Chemotherapeutics

4.3.1 Evaluation of PDAC Response to Different Chemotherapy Drug Dose on 2D Plastic

To be able to investigate and validate the PDAC models for drug screening and chemoresistance studies, it was important to confirm the ability of these models to mimic an “*in vivo*-like” behaviour when treated with established drugs. To that effect, two chemotherapeutics were chosen (i) Gemcitabine, the most acknowledged chemotherapy for PDAC patients and (ii) Doxorubicin, one of the most potent and widely used chemotherapeutic agents, but not recognised for PDAC patients.

The three cell lines, PANC-1, MIA PaCa-2 and PK-1, were first cultured in 2D and a series of drug concentrations were tested; for Gemcitabine 0.01, 0.02, 0.04, 0.08, 0.1, 0.2, 0.3, 0.4 and 0.5 μm and for Doxorubicin 0.001, 0.005, 0.01, 0.02, 0.05, 0.1, 0.2, 0.5 and 0.8 μm . The survival of these cells was measured using Alamar Blue and as a percentage of a control (media with no treatment). PANC-1 cells presented no significant cell death with Gemcitabine beyond 0.1 μm between the incremental drug concentration and cell survival was at ~60% at the max dose of 0.5 μm (Figure 50a, blue line). This was also very similar with Doxorubicin, that showed no significant change in cell death from 0.1 μm to 0.5 μm , although a significant increase was present between 0.5 and 0.8 μm (Figure 50b, blue line). MIA PaCa-2 cells presented no significant cell death with Gemcitabine beyond 0.2 μm between the incremental drug concentration and cell survival was at ~15% at the max dose of 0.5 μm (Figure 50a, green line). This was also very similar with Doxorubicin, which showed no significant cell death beyond 0.05 μm between the incremental drug concentrations, reaching a cell survival of ~10% at a concentration of 0.8 μm (Figure 50b, green line). PK-1 cells presented no significant cell death with Gemcitabine beyond 0.2 μm between the incremental drug concentration and cell survival was at ~20% at the max dose of 0.5 μm (Figure 50a, red line). Although, when treated with Doxorubicin, cell death kept increasing significantly with the incremental concentration of the drug, reaching a cell survival of ~15% at a concentration of 0.8 μm (Figure 50a, red line).

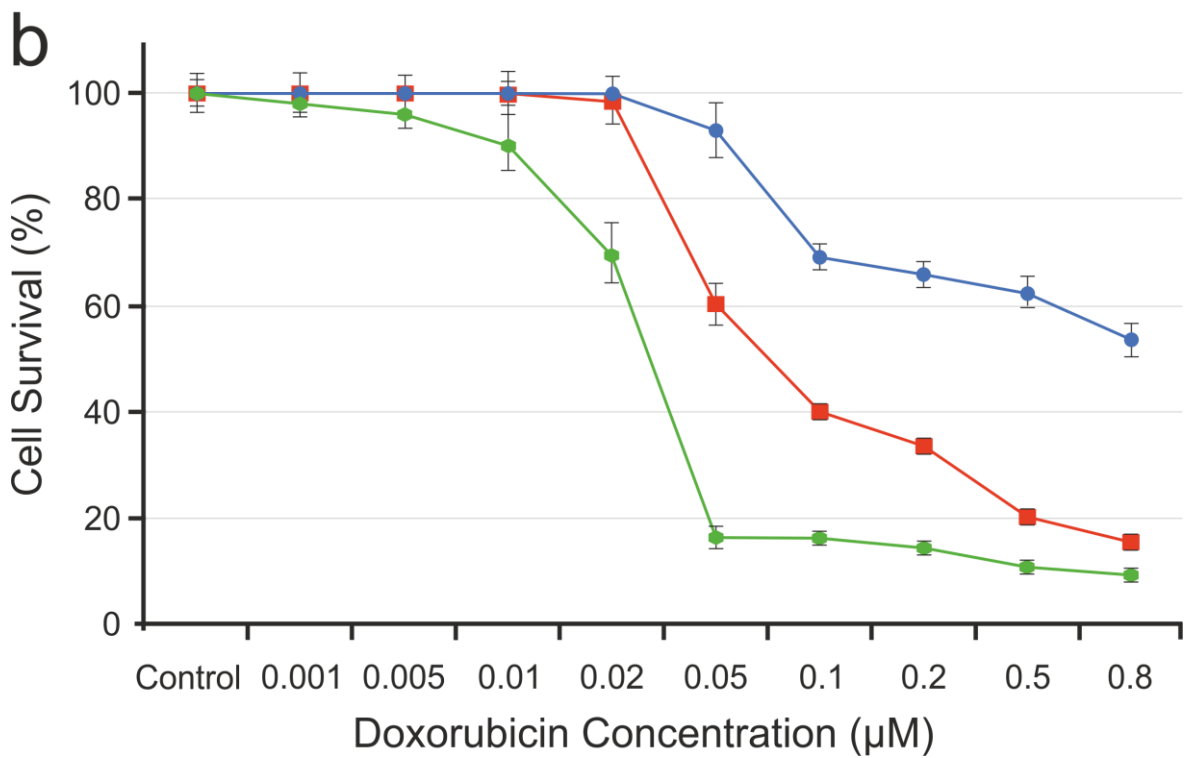
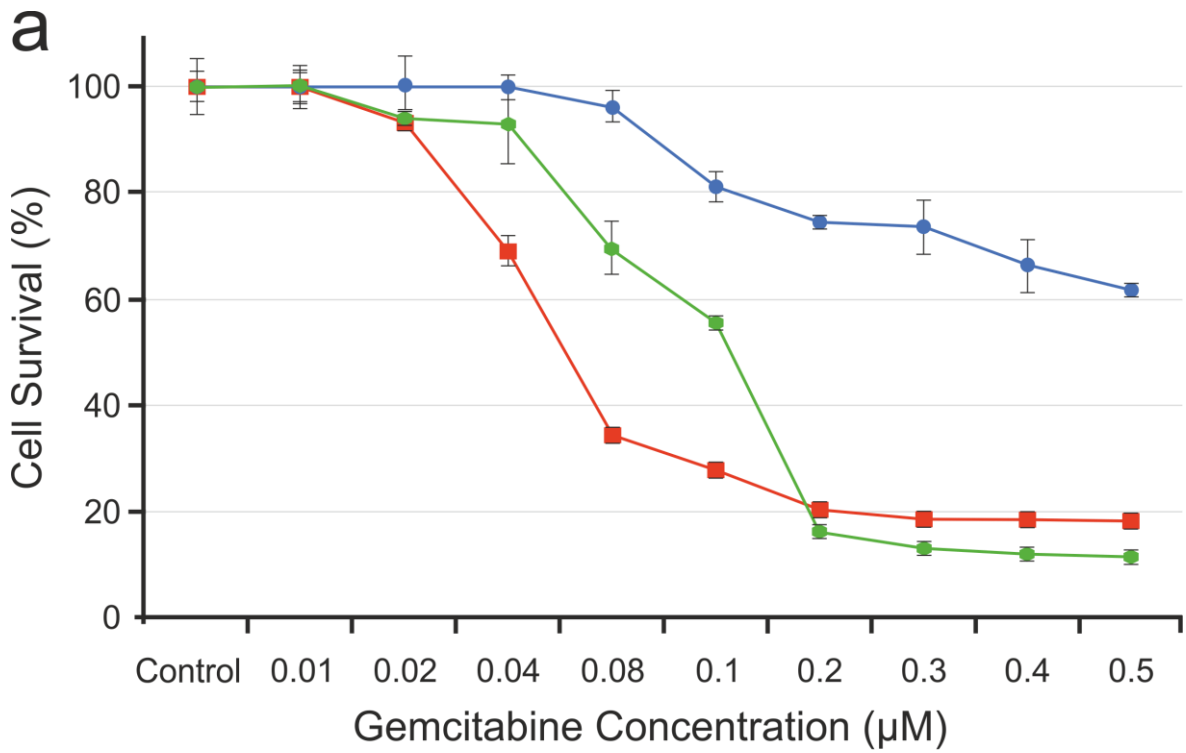


Figure 50. 2D cultured PDAC cell treated with chemotherapeutics. PANC-1 (blue), MIA PaCa-2 (green) and PK-1 (blue) were cultured on 2D plastic and treated with a series of incremental concentrations of (a) Gemcitabine and (b) Doxorubicin.

4.3.2 Analysis of Cell Response to Chemotherapy in Tissue-Specific PDAC models

4.3.2.1 Evaluation of Cell Viability

Reflecting on the analyses of the 2D drug concentration results, it was decided, for consistency, to use 0.5 μm for both Gemcitabine and Doxorubicin on all the 3D model experiments (PANC-1, PK-1 and MIA PaCa-2 on both pancreas and liver scaffolds). Like the 2D experiments, the survival of these cells was measured using Alamar Blue and as a percentage of a control (media with no treatment).

Initially, a proof-of-concept experiment was run to assess feasibility of using Alamar Blue for the 3D scaffolds (n=3). All conditions, PANC-1 on pancreas (Figure 51a) and liver scaffolds (Figure 52a), MIA PaCa-2 on pancreas (Figure 53a) and liver scaffolds (Figure 54a) and PK-1 on pancreas (Figure 55a) and liver scaffolds (Figure 56a), presented a large standard deviation within the individual conditions and no significance ($p < 0.05$) was observed between any of the treated vs control samples. It was also observed that there was a big diversity of scaffold size within each condition, and there was macroscopic correlation between scaffold size and Alamar Blue's colour change.

To improve on the previous results, and to reduce the large variation observed, scaffolds were preselected and organised by macroscopic size prior to cell seeding, e.g. all pancreas scaffolds for "PANC-1" cell seeding had a macroscopically similar size and this was the case for all the models. Additionally, the replicate size was increased to n=5. For this experiment, only Gemcitabine was used as a treatment.

This method revealed to be successful in reducing the standard deviation. Indeed, PANC-1 on pancreas scaffolds showed a significant reduction in cell survival ($p < 0.01$) between the treated and untreated models, with the average survival being 89.03% when treated (Figure 51b). PANC-1 on liver scaffolds also showed a significant reduction in cell survival ($p < 0.05$) between the treated and untreated models, with the average survival being 89.19% when treated (Figure 52b).

MIA PaCa-2 on pancreas scaffolds showed a significant reduction in cell survival ($p < 0.05$) between the treated and untreated models, with the average survival being 85.44% when treated (Figure 53b). MIA PaCa-2 on liver scaffolds also showed a significant reduction in cell survival ($p < 0.05$) between the treated and untreated models, with the average survival being 82.92% when treated (Figure 54b).

PK-1 on pancreas scaffolds showed no significant reduction in cell survival ($p > 0.05$) between the treated and untreated models, with the average survival increasing to 101.5% when treated (Figure 55b). Whereas, PK-1 on liver scaffolds showed a significant reduction in cell survival ($p < 0.01$) between the treated and untreated models, with the average survival being 71.02% when treated (Figure 56b).

To confirm the success of our results, the previous experiment was repeated with the exact conditions, but the cells were from a different batch and the pancreas and liver scaffolds were from different donors. Additionally, Doxorubicin was added again as a condition and 10% DMSO as a positive control.

PANC-1 cells cultured on pancreas scaffolds presented a significant reduction of 7.960 ± 2.076 in cell survival when treated with Gemcitabine compared to the control ($p < 0.05$). This was also observed with Doxorubicin, with a significant reduction of 8.443 ± 1.457 in cell survival in treated vs control ($p < 0.05$). There was no significant ($p > 0.05$) difference between samples treated Gemcitabine or Doxorubicin. The positive control, samples treated with DMSO, showed a significant reduction in cell survival compared to the control ($p < 0.05$), Gemcitabine ($p < 0.05$) and Doxorubicin ($p < 0.05$) (Figure 51c).

PANC-1 cells cultured on liver scaffolds presented no significant reduction in cell survival when treated with Gemcitabine compared to the control ($p > 0.05$). This was also observed with Doxorubicin ($p < 0.05$). There was no significant ($p > 0.05$) difference between samples treated Gemcitabine or Doxorubicin. The positive control, samples treated with DMSO, showed a significant increase in cell survival compared to the control ($p < 0.01$) and Gemcitabine ($p < 0.05$) but no significant change compared to Doxorubicin ($p > 0.05$) (Figure 52c).

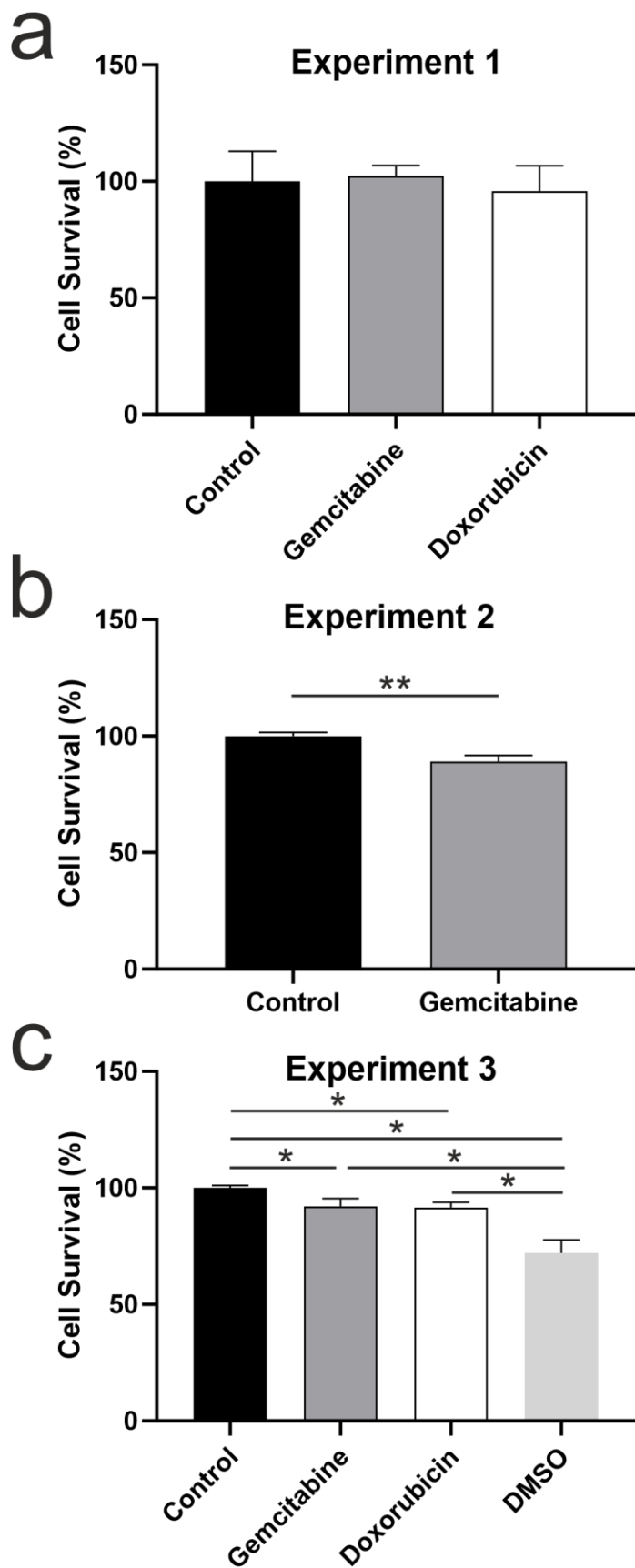


Figure 51. Chemotherapeutics treatment of PANC-1 cell cultured on pancreas scaffolds. Alamar blue viability test of PANC-1 cells cultured on pancreas scaffolds; in the first experiment (a) treated with 0.5 μ M Gemcitabine or 0.5 μ M Doxorubicin, in the second experiment (b) treated with 0.5 μ M Gemcitabine, and in the third experiment (c) treated with 0.5 μ M Gemcitabine, 0.5 μ M Doxorubicin or 10% DMSO. All results are represented as a percentage of cell survival in comparison to untreated cells (control). Data are expressed as mean \pm s.d. * $p < 0.05$ and ** $p < 0.01$.

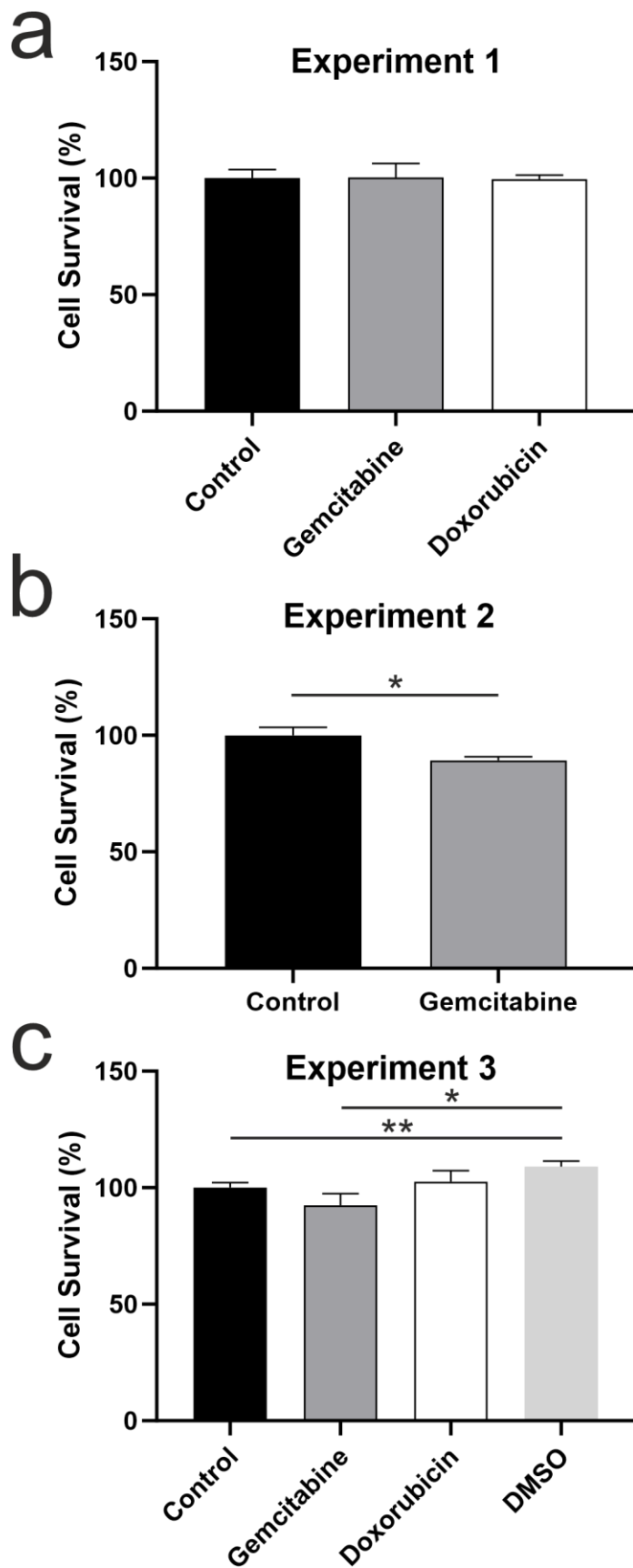


Figure 52. Chemotherapeutics treatment of PANC-1 cell cultured on liver scaffolds. Alamar blue viability test of PANC-1 cells cultured on liver scaffolds; in the first experiment (a) treated with 0.5 μ M Gemcitabine or 0.5 μ M Doxorubicin, in the second experiment (b) treated with 0.5 μ M Gemcitabine, and in the third experiment (c) treated with 0.5 μ M Gemcitabine, 0.5 μ M Doxorubicin or 10% DMSO. All results are represented as a percentage of cell survival in comparison to untreated cells (control). Data are expressed as mean \pm s.d. * $p < 0.05$ and ** $p < 0.01$.

MIA PaCa-2 cells cultured on pancreas scaffolds presented a significant reduction of 29.22 ± 1.997 in cell survival when treated with Gemcitabine compared to the control ($p < 0.0005$). This was also observed with Doxorubicin, with a significant reduction of 21.78 ± 3.915 in cell survival in treated vs control ($p < 0.05$). There was no significant ($p > 0.05$) difference between samples treated Gemcitabine or Doxorubicin. The positive control, samples treated with DMSO, showed a significant reduction in cell survival compared to the control ($p < 0.0005$), Gemcitabine ($p < 0.05$) and Doxorubicin ($p < 0.05$) (Figure 53c).

MIA PaCa-2 cells cultured on liver scaffolds presented a significant reduction of 20.67 ± 3.460 in cell survival when treated with Gemcitabine compared to the control ($p < 0.005$). This was also observed with Doxorubicin, with a significant reduction of 18.64 ± 3.095 in cell survival in treated vs control ($p < 0.01$). There was no significant ($p > 0.05$) difference between samples treated Gemcitabine or Doxorubicin. The positive control, samples treated with DMSO, showed a significant reduction in cell survival compared to the control ($p < 0.0001$), Gemcitabine ($p < 0.0001$) and Doxorubicin ($p < 0.0001$) (Figure 54c).

PK-1 cells cultured on pancreas scaffolds presented no significant reduction in cell survival when treated with Gemcitabine compared to the control ($p > 0.05$). This was also observed with Doxorubicin ($p > 0.05$). There was no significant ($p > 0.05$) difference between samples treated Gemcitabine or Doxorubicin. The positive control, samples treated with DMSO, showed a significant reduction in cell survival compared to the control ($p < 0.05$) and Gemcitabine ($p < 0.05$) but no significant change compared to Doxorubicin ($p > 0.05$) (Figure 55c).

PK-1 cells cultured on liver scaffolds presented a significant reduction of 33.90 ± 5.653 in cell survival when treated with Gemcitabine compared to the control ($p < 0.01$). This was not observed with Doxorubicin, which presented no significant change ($p > 0.05$). There was also a significant reduction of 42.56 ± 4.093 in cell survival when cells were treated with Gemcitabine compared to those treated with Doxorubicin ($p < 0.01$). The positive control, samples treated with DMSO, showed a significant reduction in cell survival compared to the control ($p < 0.05$) and Doxorubicin ($p < 0.01$) but a significant increase in cell survival compared to Gemcitabine ($p < 0.05$) (Figure 56c).

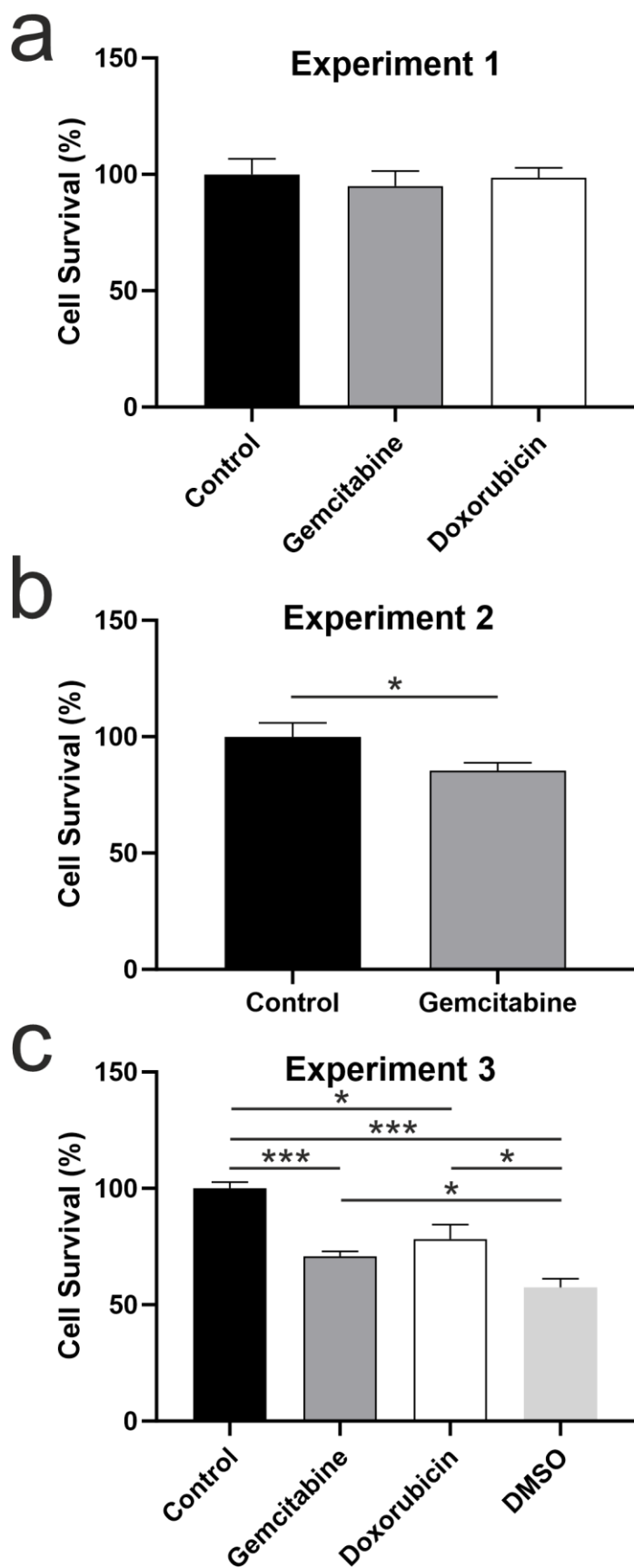


Figure 53. Chemotherapeutics treatment of MIA PaCa-2 cell cultured on pancreas scaffolds. Alamar blue viability test of MIA PaCa-2 cells cultured on pancreas scaffolds; in the first experiment (a) treated with 0.5 μ M Gemcitabine or 0.5 μ M Doxorubicin, in the second experiment (b) treated with 0.5 μ M Gemcitabine, and in the third experiment (c) treated with 0.5 μ M Gemcitabine, 0.5 μ M Doxorubicin or 10% DMSO. All results are represented as a percentage of cell survival in comparison to untreated cells (control). Data are expressed as mean \pm s.d. * $p < 0.05$ and *** $p < 0.001$.

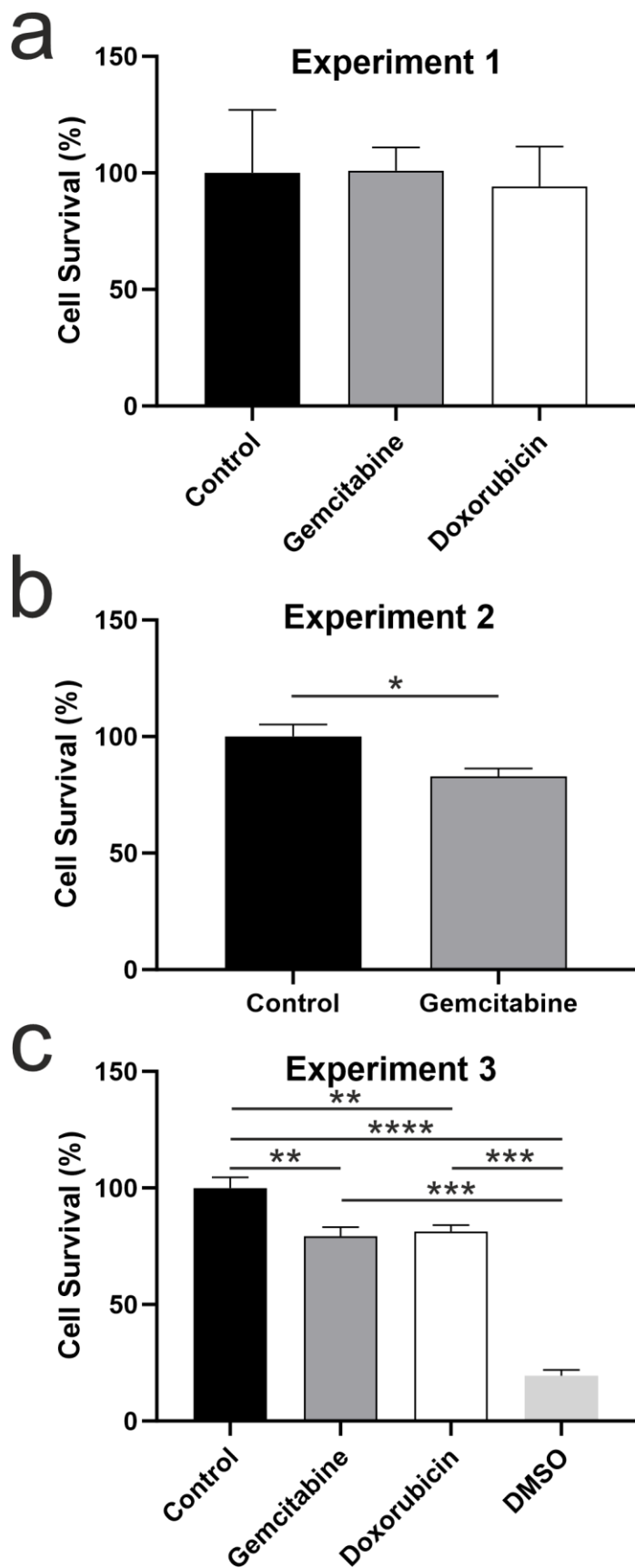


Figure 54. Chemotherapeutics treatment of MIA PaCa-2 cell cultured on liver scaffolds. Alamar blue viability test of MIA PaCa-2 cells cultured on liver scaffolds; in the first experiment (a) treated with 0.5 μ M Gemcitabine or 0.5 μ M Doxorubicin, in the second experiment (b) treated with 0.5 μ M Gemcitabine, and in the third experiment (c) treated with 0.5 μ M Gemcitabine, 0.5 μ M Doxorubicin or 10% DMSO. All results are represented as a percentage of cell survival in comparison to untreated cells (control). Data are expressed as mean \pm s.d. * $p < 0.05$, ** $p < 0.01$, *** $p < 0.001$ and **** $p < 0.0001$.

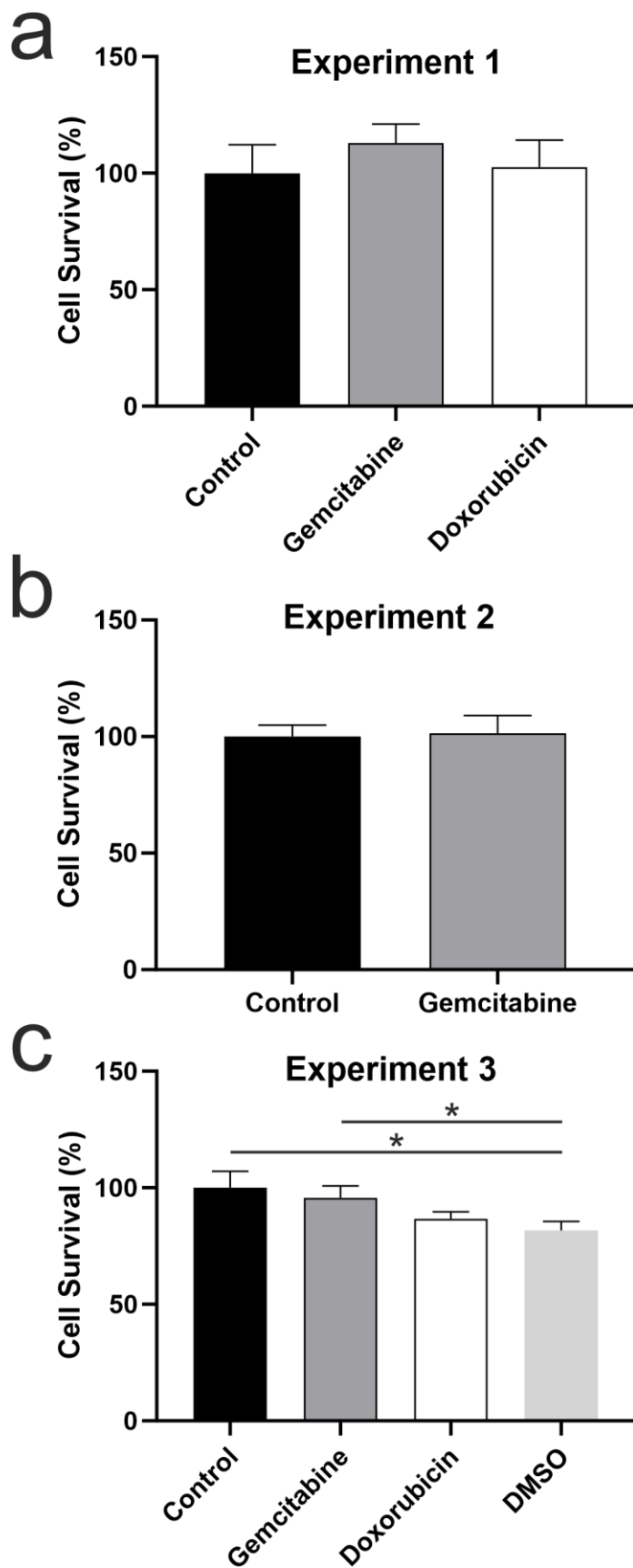


Figure 55. Chemotherapeutics treatment of PK-1 cell cultured on pancreas scaffolds. Alamar blue viability test of PK-1 cells cultured on pancreas scaffolds; in the first experiment (a) treated with 0.5 μ M Gemcitabine or 0.5 μ M Doxorubicin, in the second experiment (b) treated with 0.5 μ M Gemcitabine, and in the third experiment (c) treated with 0.5 μ M Gemcitabine, 0.5 μ M Doxorubicin or 10% DMSO. All results are represented as a percentage of cell survival in comparison to untreated cells (control). Data are expressed as mean \pm s.d. * $p < 0.05$.

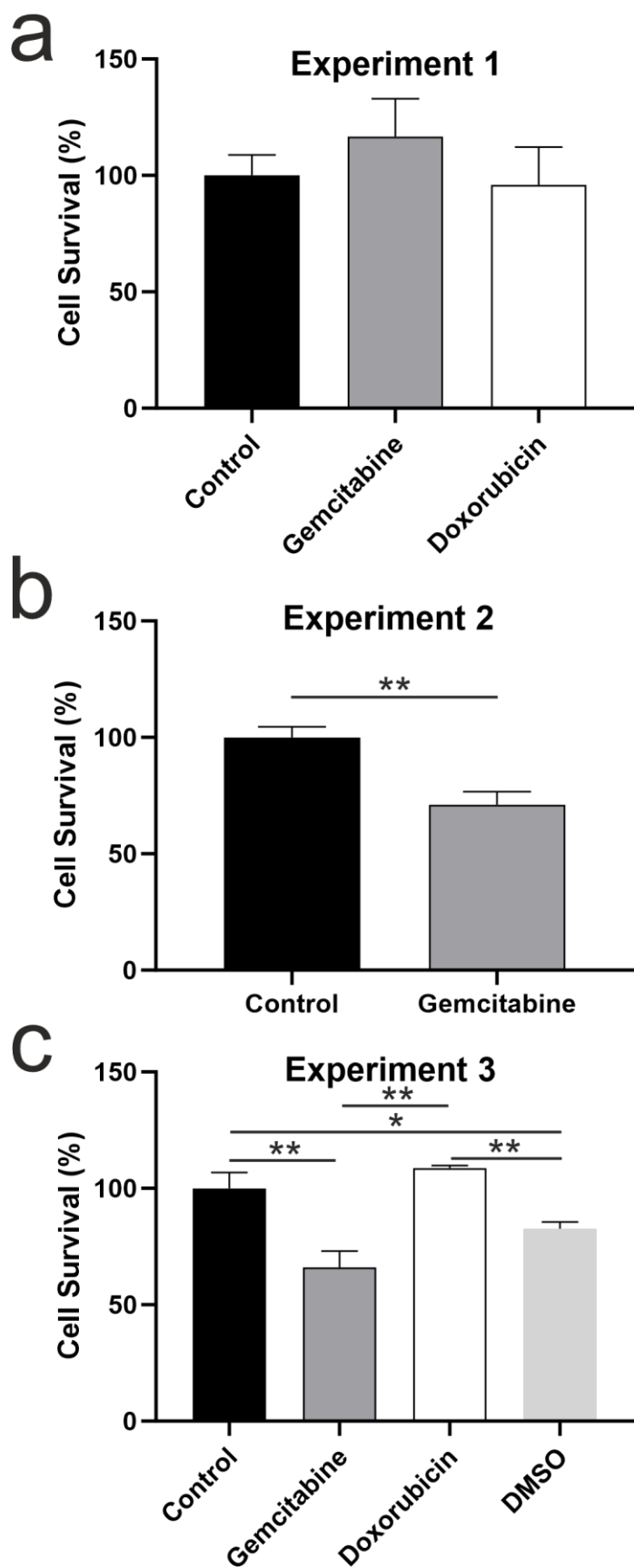


Figure 56. Chemotherapeutics treatment of PK-1 cell cultured on liver scaffolds. Alamar blue viability test of PK-1 cells cultured on liver scaffolds; in the first experiment (a) treated with 0.5 μ M Gemcitabine or 0.5 μ M Doxorubicin, in the second experiment (b) treated with 0.5 μ M Gemcitabine, and in the third experiment (c) treated with 0.5 μ M Gemcitabine, 0.5 μ M Doxorubicin or 10% DMSO. All results are represented as a percentage of cell survival in comparison to untreated cells (control). Data are expressed as mean \pm s.d. * $p < 0.05$ and ** $p < 0.01$.

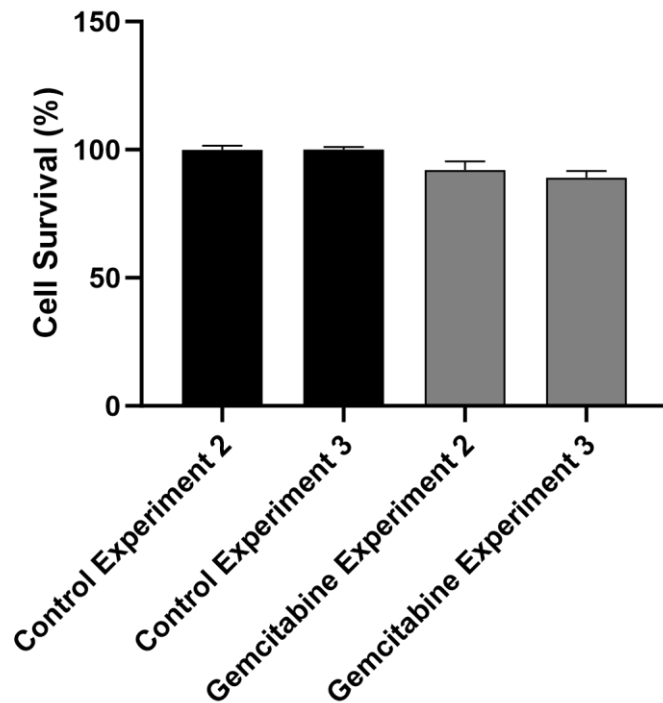
To investigate consistency and reproducibility of using decellularised scaffold PDAC for drug testing, the results of the previous two experiments were statically compared for the Gemcitabine treatment. It was observed that there was no significant difference ($p>0.05$) between the Gemcitabine treated samples from the experiment 1 and experiment 2 in PANC-1 cells on pancreas scaffolds (Figure 57a) and liver scaffolds (Figure 57b), MIA PaCa-2 cells on liver scaffolds (Figure 58b) and PK-1 cells on pancreas scaffolds (Figure 59a) and liver scaffolds (Figure 59b) and. The only condition to have a significant difference inter-experiments when treated with Gemcitabine was MIA PaCa-2 cells on pancreas scaffolds ($p<0.01$) (Figure 58a).

Finally, the results of the chemotherapy treatments were accumulated to examine the impact of the material (pancreas scaffolds, liver scaffolds and 2D) on chemoresistance. PANC-1 cells treated with Gemcitabine had no significant change in cell survival between the pancreas and liver scaffolds ($p>0.05$), whereas, there was a significant reduction in 2D plastic cell survival of 31.10 ± 2.529 in comparison to pancreas scaffolds ($p<0.0001$) and a significant reduction of 31.46 ± 2.529 in comparison to liver scaffolds ($p<0.0001$) (Figure 60a).

PANC-1 cells treated with Doxorubicin had a significant reduction of 10.98 ± 2.529 in cell survival in the pancreas scaffolds compared to liver scaffolds ($p<0.001$). Additionally, there was a significant reduction in 2D plastic cell survival of 38.54 ± 2.529 in comparison to pancreas scaffolds ($p<0.0001$) and a significant reduction of 49.52 ± 2.529 in comparison to liver scaffolds ($p<0.0001$) (Figure 60a).

PANC-1 cells treated with DMSO, as a positive control, had a significant reduction of 36.97 ± 2.529 in cell survival in the pancreas scaffolds compared to liver scaffolds ($p<0.001$). Additionally, there was a significant reduction in 2D plastic cell survival of 36.71 ± 2.529 in comparison to pancreas scaffolds ($p<0.0001$) and a significant reduction of 73.68 ± 2.529 in comparison to liver scaffolds ($p<0.0001$) (Figure 60a).

a PANC-1 on Pancreas Scaffolds



b PANC-1 on Liver Scaffolds

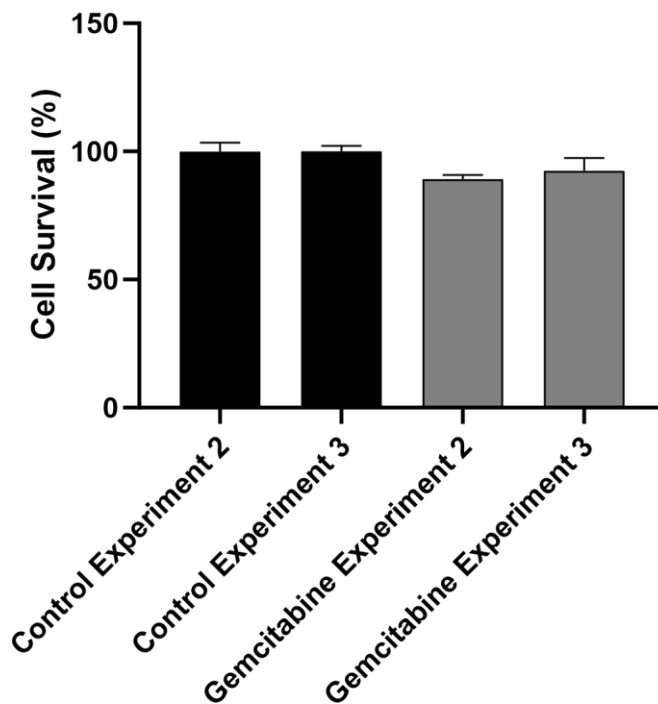
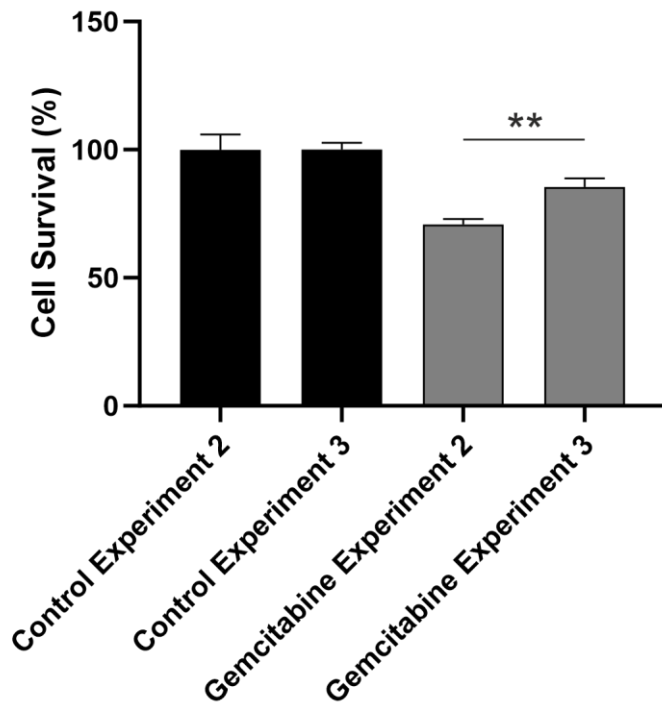


Figure 57. Inter-experiment comparison of Gemcitabine treated PANC-1 cell cultured on 3D scaffolds. Alamar blue viability test of PANC-1 cells cultured on (a) pancreas scaffolds and (b) liver scaffolds from two separate experiment (experiment 2 and 3) presented no significant difference ($p > 0,05$) in percentage of cell survival after treatment with $0.5 \mu\text{M}$ Gemcitabine. Data are expressed as mean \pm s.d.

a MIA PaCa-2 on Pancreas Scaffolds



b MIA PaCa-2 on Liver Scaffolds

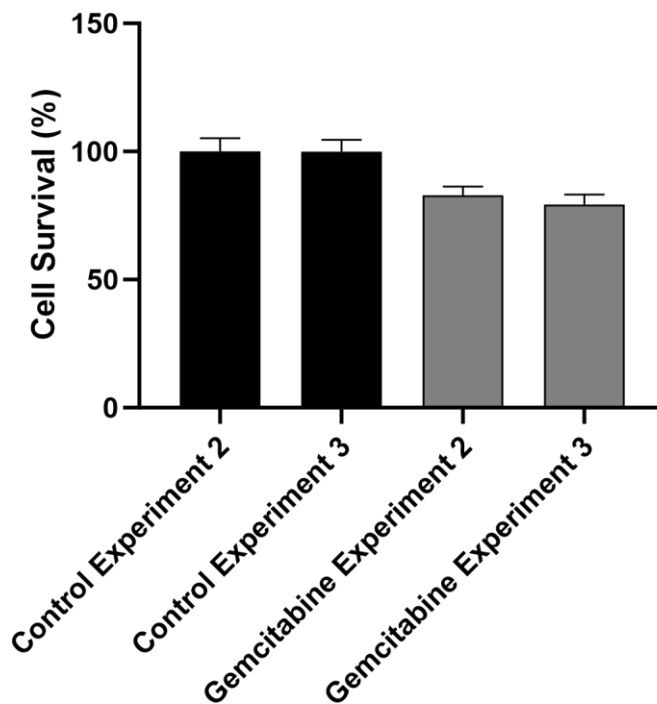
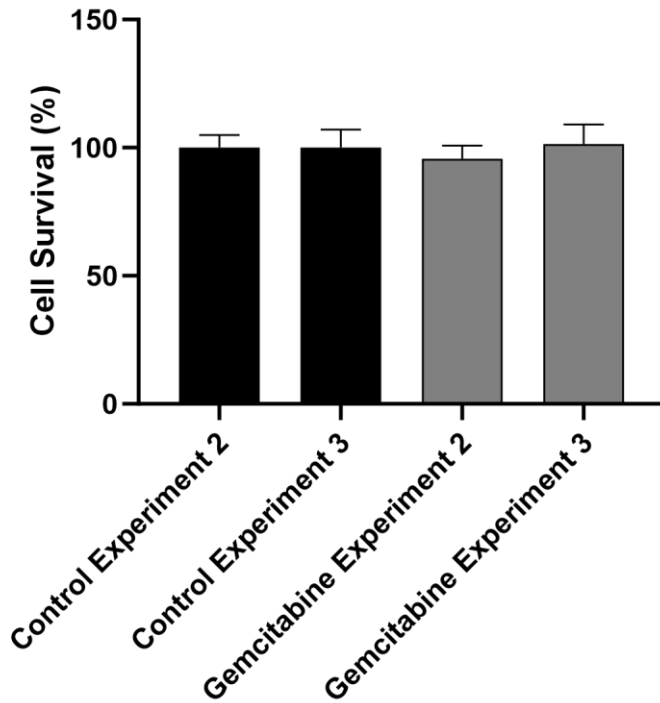


Figure 58. Inter-experiment comparison of Gemcitabine treated MIA PaCa-2 cell cultured on 3D scaffolds. Alamar blue viability test of MIA PaCa-2 cells from two separate experiment (experiment 2 and 3) presented a significant difference in percentage of cell survival after treatment with 0.5 μ M Gemcitabine when cultured on (a) pancreas scaffolds but no significant difference ($p>0.05$) when cultured on (b) liver scaffolds. Data are expressed as mean \pm s.d. ** $p<0.01$.

a PK-1 on Pancreas Scaffolds



b PK-1 on Liver Scaffolds

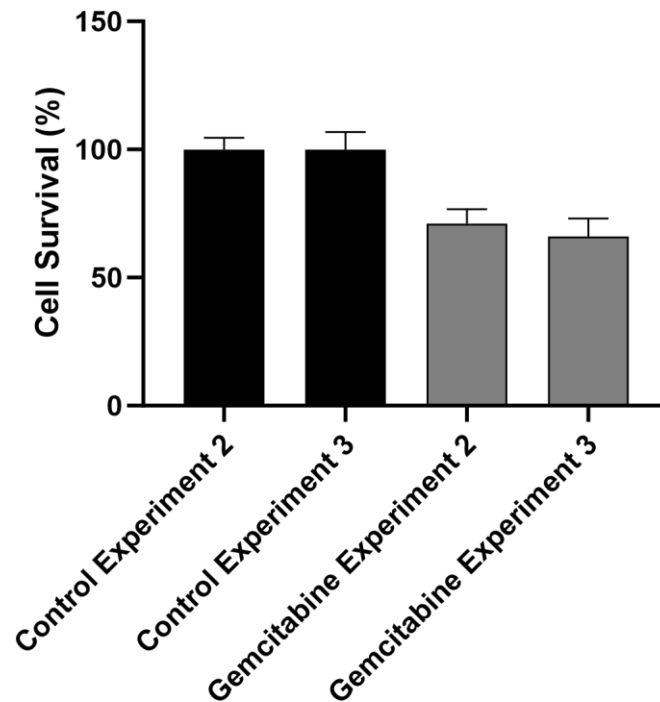


Figure 59. Inter-experiment comparison of Gemcitabine treated PK-1 cell cultured on 3D scaffolds. Alamar blue viability test of PK-1 cells cultured on (a) pancreas scaffolds and (b) liver scaffolds from two separate experiment (experiment 2 and 3) presented no significant difference ($p > 0,05$) in percentage of cell survival after treatment with $0.5 \mu\text{M}$ Gemcitabine. Data are expressed as mean \pm s.d.

MIA PaCa-2 cells treated with Gemcitabine had no significant change in cell survival between the pancreas and liver scaffolds ($p>0.05$), whereas, there was a significant reduction in 2D plastic cell survival of 37.09 ± 3.440 in comparison to pancreas scaffolds ($p<0.0001$) and a significant reduction of 45.64 ± 2.529 in comparison to liver scaffolds ($p<0.0001$) (Figure 60b).

MIA PaCa-2 cells treated with Doxorubicin had no significant change in cell survival between the pancreas and liver scaffolds ($p>0.05$), whereas, there was a significant reduction in 2D plastic cell survival of 50.93 ± 3.440 in comparison to pancreas scaffolds ($p<0.0001$) and a significant reduction of 54.07 ± 2.529 in comparison to liver scaffolds ($p<0.0001$) (Figure 60b).

MIA PaCa-2 cells treated with DMSO, as a positive control had a significant reduction of 38.04 ± 3.440 in cell survival in the liver scaffolds compared to pancreas scaffolds ($p<0.001$). Additionally, there was a significant reduction in 2D plastic cell survival of 46.65 ± 3.440 in comparison to pancreas scaffolds ($p<0.0001$) and a significant reduction of 8.610 ± 3.440 in comparison to liver scaffolds ($p<0.05$) (Figure 60b).

PK-1 cells treated with Gemcitabine had a significant reduction of 29.58 ± 3.411 in cell survival in the liver scaffolds compared to pancreas scaffolds ($p<0.001$). Additionally, there was a significant reduction in 2D plastic cell survival of 64.74 ± 3.411 in comparison to pancreas scaffolds ($p<0.0001$) and a significant reduction of 35.16 ± 3.411 in comparison to liver scaffolds ($p<0.0001$) (Figure 60c).

PK-1 cells treated with Doxorubicin had a significant reduction of 21.93 ± 3.411 in cell survival in the pancreas scaffolds compared to liver scaffolds ($p<0.001$). Additionally, there was a significant reduction in 2D plastic cell survival of 52.99 ± 3.411 in comparison to pancreas scaffolds ($p<0.0001$) and a significant reduction of 74.92 ± 3.411 in comparison to liver scaffolds ($p<0.0001$) (Figure 60c).

PK-1 cells treated with DMSO, as a positive control, had no significant change in cell survival between the pancreas and liver scaffolds ($p>0.05$). Whereas, there was a significant reduction in 2D plastic cell survival of 67.46 ± 3.411 in comparison to

pancreas scaffolds ($p < 0.0001$) and a significant reduction of 68.40 ± 3.411 in comparison to liver scaffolds ($p < 0.0001$) (Figure 60c).

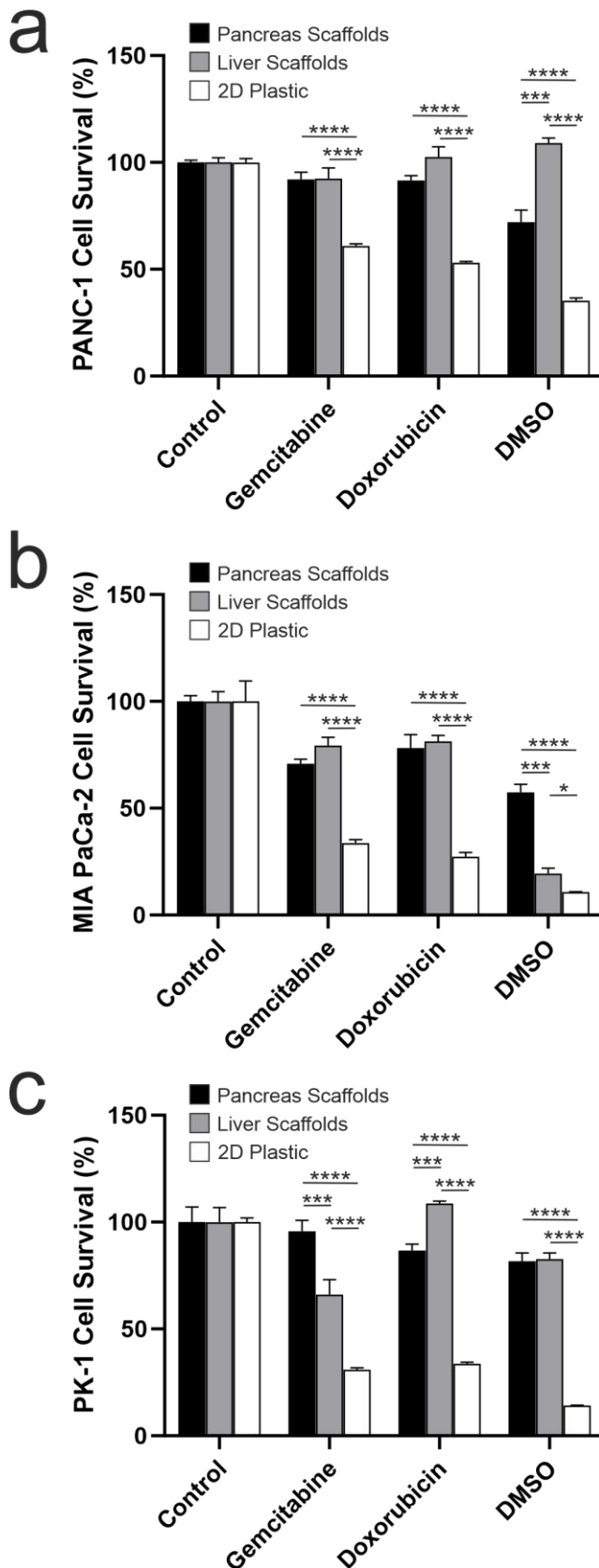


Figure 60. Comparison of PDAC cells' response to chemotherapeutic treatments in 3D scaffolds vs 2D plastic. Alamar blue viability test of (a) PANC-1, (b) MIA PaCa-2 and (c) PK-1 cells cultured on pancreas scaffolds (black bars), liver scaffolds (grey bars) and 2D plastic, treated with 0.5 μ M Gemcitabine, 0.5 μ M Doxorubicin and 10% DMSO. Data are expressed as mean \pm s.d. * $p < 0.05$, ** $p < 0.01$, *** $p < 0.001$ and **** $p < 0.0001$.

4.3.2.2 *Validation of Chemotherapy Uptake by PDAC Cells*

To prove that the chemotherapy drugs were able to reach the cells, the natural fluorescence of Doxorubicin was utilised. PANC-1, MIA PaCa-2 and PK-1 cells cultured on pancreas scaffolds were treated with one μm for 24 hours. The samples were then directly frozen and cryo-sectioned. As a control, untreated samples were also imaged; PANC-1 (Figure 61a; top panel), MIA PaCa-2 (Figure 61b; top panel) and PK-1 (Figure 61c; top panel) samples did not present any fluorescence in the Doxorubicin channel (TRITC; red) but did present a positive signal for nuclei (DAPI; blue) and collagen (FITC; green). On the other hand, all treated samples, PANC-1 (Figure 61a; bottom panel), MIA PaCa-2 (Figure 61b; bottom panel) and PK-1 (Figure 61c; bottom panel) presented a fluorescence for Doxorubicin (TRITC; red), nuclei (DAPI; blue) and collagen (FITC, green). When the three channels were merged together, it was evident that Doxorubicin had reached the nuclei (MERGE; purple).

4.3.2.3 *Immunohistochemistry Analysis of Treated PDAC Cells*

To further investigate the effect of the chemotherapy drugs on the PDAC cells, immunohistochemical staining for MMP9 (for invasiveness), γH2A (for nuclear damage) and ASP175 (for apoptosis) was performed. PANC-1 cells on pancreas scaffolds presented no observable difference in staining intensity for MMP9 between the control (untreated) sample and Gemcitabine or Doxorubicin treated samples (Figure 62a; top panel). γH2A staining was negative on the control samples but was positive on the Gemcitabine treated samples and additionally a high intensity of staining was present on the Doxorubicin treated samples (Figure 62a; middle panel). ASP175 staining was also negative in the control samples, which was also the case in the many cells in the Gemcitabine treated sample and in almost all the cell in the Doxorubicin treated sample (Figure 62a; bottom panel).

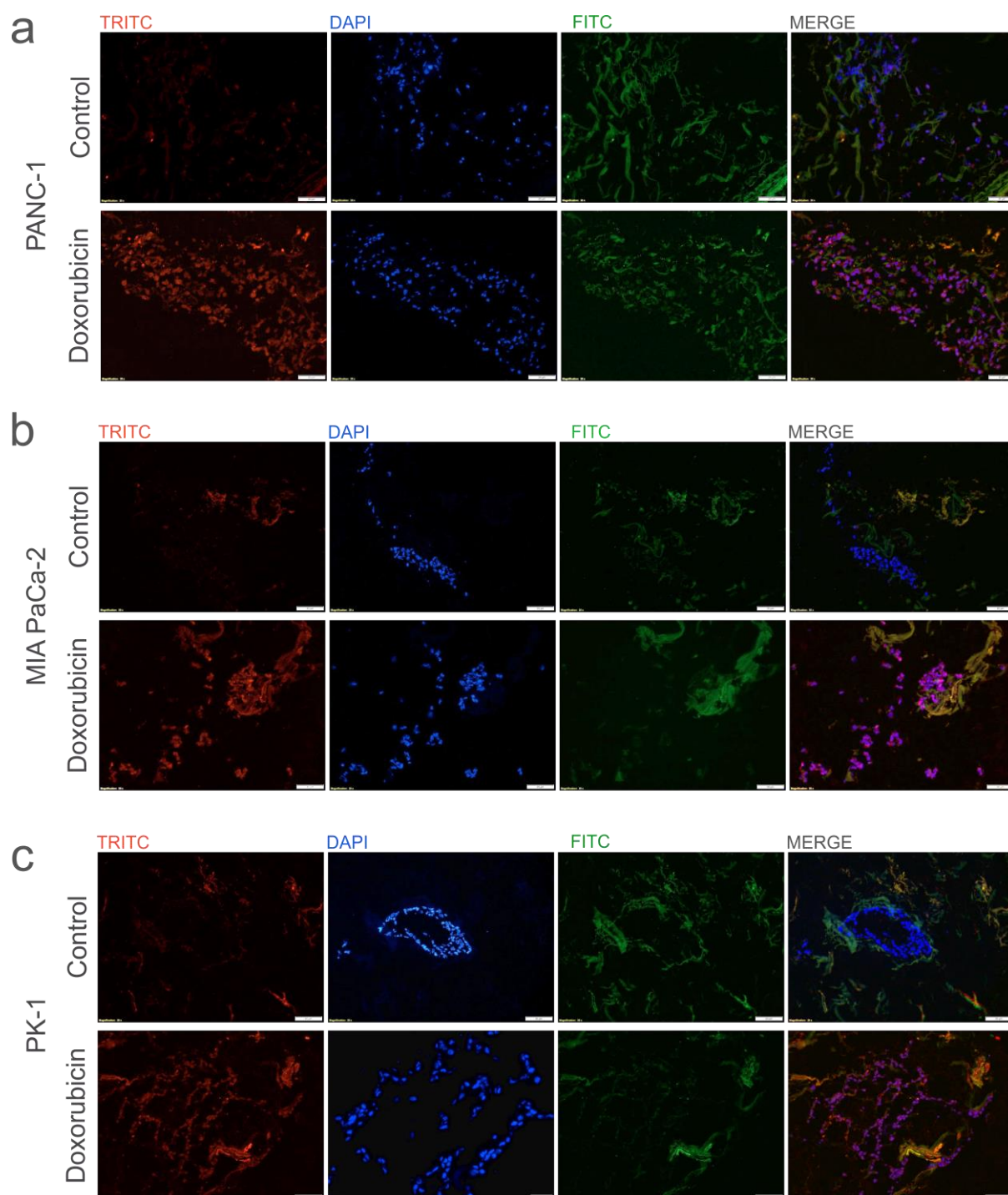


Figure 61. Validation of Doxorubicin uptake by PDAC cells. Fluorescent imaging of **(a)** PANC-1, **(b)** MIA PaCa-2 and **(c)** PK-1 cultured on pancreas scaffolds that were not treated (control; top panel) did not present any fluorescence in the Doxorubicin channel (TRITC; red) but presented a positive fluorescence for nuclei (DAPI; blue) and collagens (FITC; green). All doxorubicin treated samples (bottom panel), presented a fluorescence on the Doxorubicin channel (TRITC; red), nucleus channel (DAPI, blue) and collagen channel (FITC, green). When the three channels were merged together, it is evident that Doxorubicin had reached the nucleus (purple). All images were obtained using a 20x objective. Scale bar: 100 μ m.

PANC-1 cells on liver scaffolds similarly presented no observable difference in staining intensity for MMP9 between the control (untreated) sample and Gemcitabine or Doxorubicin treated samples (Figure 62b; top panel). γ H2A (Figure 62b; middle panel) and ASP175 (Figure 62b; bottom panel) staining's were both negative on all conditions (control, Gemcitabine and Doxorubicin). It was additionally notable that there was a difference in cell morphology between the PANC-1 cells on the pancreas (Figure 62a) vs liver scaffolds (Figure 62b), where they appeared to be larger and more spherical in the former and more spindle-like in the latter.

MIA PaCa-2 cells on pancreas scaffolds presented no observable difference in staining intensity for MMP9 between the control (untreated) samples and Gemcitabine or Doxorubicin treated samples (Figure 63a; top panel). γ H2A staining was dominantly negative on the control samples but was positive on the Gemcitabine and Doxorubicin treated samples (Figure 63a; middle panel). ASP175 staining was also negative in the control samples, which was also the case for most cells in the Gemcitabine and Doxorubicin treated samples (Figure 63a; bottom panel).

MIA PaCa-2 cells on liver scaffolds similarly presented no observable difference in staining intensity for MMP9 between the control (untreated) sample and Gemcitabine or Doxorubicin treated samples (Figure 63b; top panel). γ H2A (Figure 63b; middle panel) and ASP175 (Figure 63b; bottom panel) staining's were both negative on all conditions (control, Gemcitabine and Doxorubicin). It was additionally notable that there was a difference in cell morphology between the MIA PaCa-2 cells on the pancreas (Figure 63a) vs liver scaffolds (Figure 63b), where they appeared to be larger, spherical and more dispersed in the former and more cubical and clustered in the latter.

PK-1 cells on pancreas scaffolds presented no observable difference in staining intensity for MMP9 between the control (untreated) sample and Gemcitabine or Doxorubicin treated samples (Figure 64a; top panel). γ H2A staining was negative on the control samples but was faintly positive on the Gemcitabine treated samples and a moderate intensity of staining was observed on the Doxorubicin treated samples (Figure 64a; middle panel). ASP175 staining was negative in all samples (Figure 64a; bottom panel).

PK-1 cells on liver scaffolds showed an obvious difference in intensity of staining of MMP9, where cells treated with Gemcitabine had a lighter intensity of staining the control samples. There was also a mix of MMP9 intensity in the Doxorubicin treated sample (Figure 64b; top panel). Both, γ H2A (Figure 64b; middle panel) and ASP175 (Figure 64b; bottom panel) staining's were negative on all conditions (control, Gemcitabine and Doxorubicin). Additionally, there was a clear change in cell morphology from a spherical-shape in the control sample to a smaller more spindle-like shape in the Gemcitabine treated cells, and similarly with the Doxorubicin treated cells (Figure 64b). Furthermore, there was a difference in cell morphology between the PK-1 cells on the pancreas (Figure 64a) vs liver scaffolds (Figure 64b), where they appeared to be larger and more cubical in the former.

4.3.2.4 Evaluation of Changes in PDAC Cell Size

After observing the immunohistochemistry staining, it was noticeable qualitatively that in many conditions there were differences in cell size and shape, therefore, we proceeded to investigate this quantitatively. The immunohistochemistry images of MMP9 were computed into Fiji (v1.49d (ImageJ Jenkins server) and processed as described in the methods and materials. The average surface area of ten randomly selected cells was measured.

There was significantly greater cell size ($p < 0.005$) in PANC-1 cells cultured in pancreas vs liver scaffolds in the control (untreated) group (Figure 65a). Additionally, there was a significant ($p < 0.05$) increase in size in the PANC-1 cells treated with Gemcitabine vs the control in the liver scaffold group (Figure 65a). There was no significant change in cell size in the MIA PaCa-2 cells within any condition (Figure 65b). Finally, for the PK-1 cells, a notable change was observed in the Gemcitabine treatments, where the cells in the liver scaffold group were significantly ($p < 0.0005$) smaller than those in the pancreas scaffolds (Figure 65c).

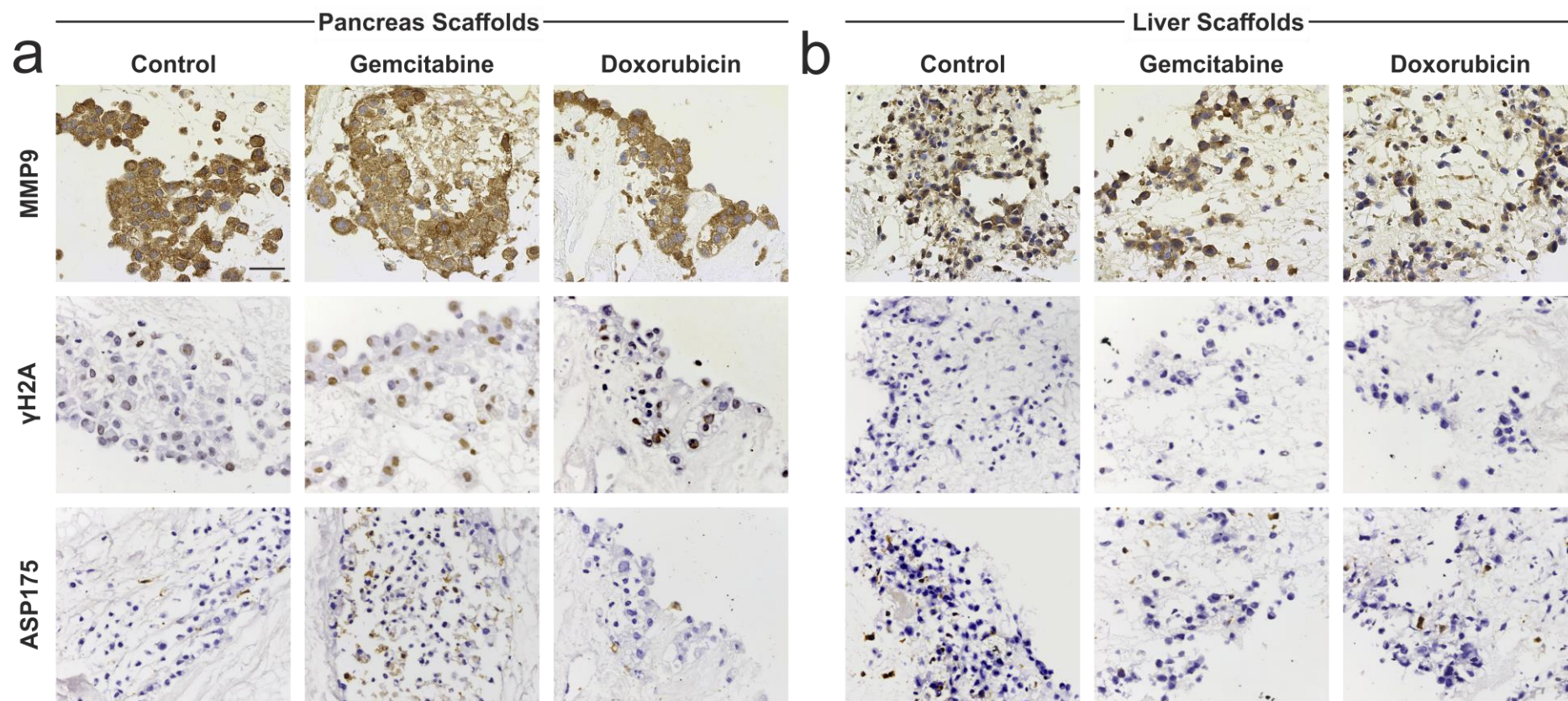


Figure 62. Immunohistochemistry analysis of chemotherapy treated PANC-1 cells cultured on 3D scaffolds. PANC-1 cells cultured on 3D scaffolds, were left untreated (control) or treated with 0.5 μ M Gemcitabine and 0.5 μ M Doxorubicin, were stained for MMP9 (top panel), γ H2A (middle panel) or ASP175 (bottom panel). Cells on **(a)** pancreas scaffolds stained positive for MMP9 in all condition. γ H2A staining was negative on the control sample but was positive on the Gemcitabine and Doxorubicin treated sample. There was no difference in staining of ASP175 between the different conditions. Cells on **(b)** liver scaffolds stained positive for MMP9 in all condition. γ H2A and ASP175 staining was negative in all conditions. All images were obtained using a 20x objective. Scale bar: 100 μ m.

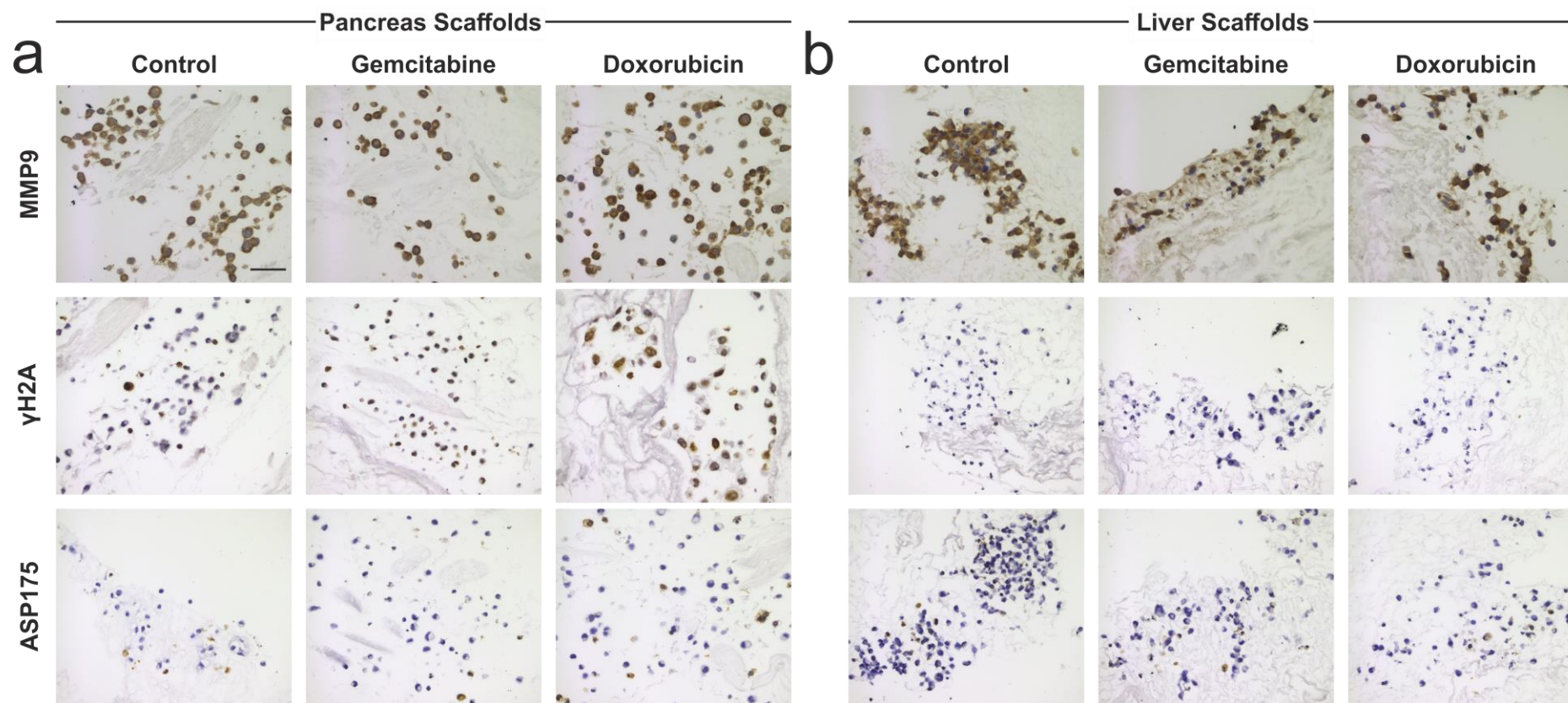


Figure 63. Immunohistochemistry analysis of chemotherapy treated MIA PaCa-2 cells cultured on 3D scaffolds. MIA PaCa-2 cells cultured on 3D scaffolds, were left untreated (control) or treated with 0.5 μ M Gemcitabine and 0.5 μ M Doxorubicin, were stained for MMP9 (top panel), γ H2A (middle panel) or ASP175 (bottom panel). Cells on **(a)** pancreas scaffolds stained positive for MMP9 in all condition. γ H2A staining was negative on the control sample but was positive on the Gemcitabine and Doxorubicin treated sample. There was no difference in staining of ASP175 between the different conditions. Cells on **(b)** liver scaffolds stained positive for MMP9 in all condition. γ H2A and ASP175 staining was negative in all conditions. All images were obtained using a 20x objective. Scale bar: 100 μ m.

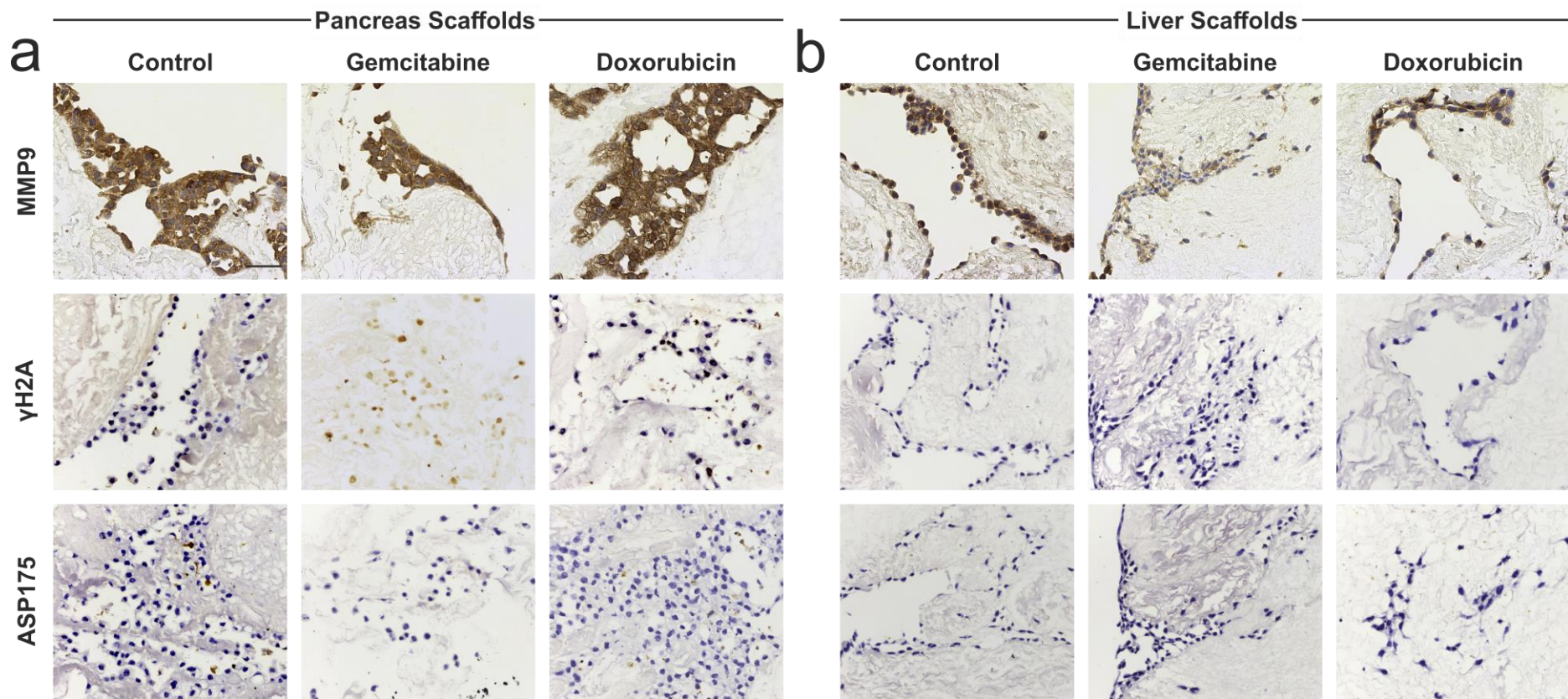


Figure 64. Immunohistochemistry analysis of chemotherapy treated PK-1 cells cultured on 3D scaffolds. PK-1 cells cultured on 3D scaffolds, were left untreated (control) or treated with 0.5 μ M Gemcitabine and 0.5 μ M Doxorubicin, were stained for MMP9 (top panel), γ H2A (middle panel) or ASP175 (bottom panel). Cells on **(a)** pancreas scaffolds stained positive for MMP9 in all condition. γ H2A staining was negative on the control sample but was faintly positive on the Gemcitabine and moderately positive on the Doxorubicin treated sample. There was no difference in negative staining of ASP175 between the different conditions. Cells on **(b)** liver scaffolds stained positive for MMP9 in all condition but showed a milder intensity on the Gemcitabine treated sample. γ H2A and ASP175 staining was negative in all conditions. All images were obtained using a 20x objective. Scale bar: 100 μ m.

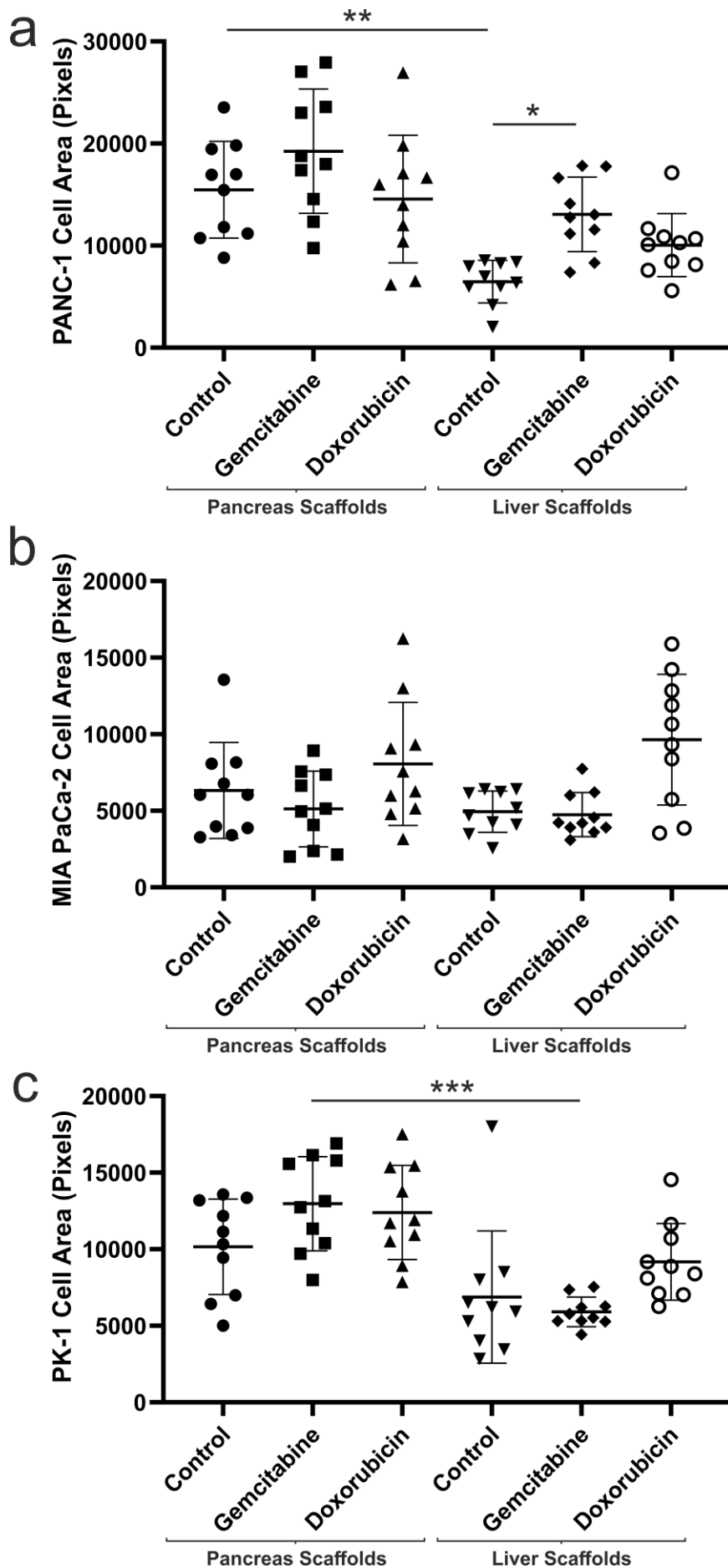


Figure 65. Computational quantification of treated and untreated PDAC cell size in 3D scaffolds. Immunohistochemistry images of MMP9 from treated and untreated (a) PANC-1, (b) MIA PaCa-2 and (c) PK-1 cells cultured on pancreas and liver scaffolds were processed to obtain the average surface area of ten randomly selected cells. Data are expressed as mean \pm s.d. * $p < 0.05$, ** $p < 0.01$ and *** $p < 0.001$

4.3.2.5 Next Generation Sequencing Evaluation of the Effect of Gemcitabine Chemotherapy on Tissue-Specific PDAC Models

To fully examine the influence of the ECM on chemoresistance of PDAC cells. mRNA from Gemcitabine treated PANC-1 cells cultured on pancreas scaffolds and PK-1 cells cultures on liver scaffolds were sequenced using the RNAseq technique.

When comparing between Gemcitabine treated and untreated (control) PANC-1 cells on pancreas scaffolds, 2879 DE genes were identified out of a total of 21,350 genes with measured expression. In this experiment, we chose a threshold of $p < 0.05$ for statistical significance and a LogFC of expression > 0.5 . Out of these DE genes, 2,220 genes were up-regulated, and 659 genes were down-regulated in the Gemcitabine treated PANC-1 cells when compared to those that were left untreated. These data were further analysed in the context of pathways obtained from the KEGG database, GO from the Gene Ontology Consortium database and network of regulatory relations from BioGRID. In summary, 42 pathways were found to be significantly impacted. In addition, 1,308 GO terms and 278 upstream regulators, were found to be significantly ($p < 0.05$) enriched.

To best demonstrate the overall impact Gemcitabine treatment has on PANC-1 cells cultured on pancreas scaffolds, the 1,308 significantly affected GO terms, were broken down, in order of significance, (as previously described) into (i) the top 10 most significantly impacted GO terms (Table 18a), (ii) the GO terms directly related to cell adhesion (Table 18b), (iii) the GO terms directly related to motility and migration (Table 18c) and (iv) the GO terms directly related to tissue organisation and angiogenesis (Table 18d).

It was found that 17 GO terms were significantly impacted that directly involved cell adhesion (Table 18b). Out of these 17 GO terms, “cell-cell adhesion” and “cell-matrix adhesion” were studied in further details. Analysis of the “cell-cell adhesion” GO term showed that there were 159 significantly ($p < 0.05$) DE genes out of a total 774 genes involved. Of these genes, 104 genes had a LogFC of > 0.5 in Gemcitabine treated samples compared to untreated samples (Supplementary Table 13). In contrast, 55

genes had a LogFC of >0.5 in the untreated samples compared to the Gemcitabine treated samples (Supplementary Table 13). Analysis of the “cell-matrix adhesion” GO term showed that there were 41 significantly ($p<0.05$) DE genes out of a total 199 genes involved. Of these genes, 34 genes had a LogFC of >0.5 in Gemcitabine treated samples compared to untreated samples (Supplementary Table 14). In contrast, 7 genes had a LogFC of >0.5 in the untreated samples compared to the Gemcitabine treated samples (Supplementary Table 14).

Furthermore, it was found that 14 GO terms were significantly impacted that directly involved motility and migration (Table 18c). Out of these 14 GO terms, “cell motility” and “leukocyte migration” were studied in further details. Analysis of the “cell motility” GO term showed that there were 229 significantly ($p<0.05$) DE genes out of a total 1368 genes involved. Of these genes, 189 genes had a LogFC of >0.5 in Gemcitabine treated samples compared to untreated samples (Supplementary Table 15). In contrast, 46 genes had a LogFC of >0.5 in the untreated samples compared to the Gemcitabine treated samples (Supplementary Table 15). Analysis of the “leukocyte migration” GO term showed that there were 78 significantly ($p<0.05$) DE genes out of a total 379 genes involved. Of these genes, 63 genes had a LogFC of >0.5 in Gemcitabine treated samples compared to untreated samples (Supplementary Table 16). In contrast, 15 genes had a LogFC of >0.5 in the untreated samples compared to the Gemcitabine treated samples (Supplementary Table 16).

Finally, it was found that 20 GO terms were significantly impacted that directly involved tissue organisation and angiogenesis (Table 18d). Out of these 20 GO terms, “extracellular structure organisation” and “sprouting angiogenesis” were studied in further details. Analysis of the “extracellular structure organisation” GO term showed that there were 86 significantly ($p<0.05$) DE genes out of a total 327 genes involved. Of these genes, 73 genes had a LogFC of >0.5 in Gemcitabine treated samples compared to untreated samples (Supplementary Table 17). In contrast, 15 genes had a LogFC of >0.5 in the untreated samples compared to the Gemcitabine treated samples (Supplementary Table 17). Analysis of the “sprouting angiogenesis” GO term showed that there were 20 significantly ($p<0.05$) DE genes out of a total 84 genes involved. Of these genes, 18 genes had a LogFC of >0.5 in Gemcitabine treated samples compared to untreated samples (Supplementary Table 18). In contrast, 2

genes had a LogFC of >0.5 in the untreated samples compared to the Gemcitabine treated samples (Supplementary Table 18).

Next, we investigated the cellular pathways that were impacted by Gemcitabine treatment of PANC-1 cells on pancreas scaffold. There were 275 pathways that presented at least one DE gene, of which 42 showed a pathway-specific p-value of <0.05 (Table 19). The most significant pathway was “Cytokine-cytokine receptor interaction” ($p = 8.59E-06$) (Table 19). Further investigation showed that all, but one (CCR6), DE cytokine receptor genes associated with this pathway were up-regulated in the Gemcitabine treated samples (Figure 66).

The final aspect investigated relating to the RNAseq data of Gemcitabine treated PANC-1 cells on pancreas scaffold was the prediction of upstream regulators. The top ten hypothesised “activated” upstream regulators were listed in order of significance (Figure 67a); RBL2 (Figure 67b), RBL1 (Figure 67c), CPSM1 (Figure 67d), E2F4 (Figure 67e), HDAC1 (Figure 67f), E2F5 (Figure 67g), SPDEF (Figure 67h), E2F7 (Figure 67i), FGFR4 (Figure 67j) and RBBP4 (Figure 67k). Additionally, the top ten hypothesised “inhibited” upstream regulators were listed in order of significance (Figure 68a); PLK1 (Figure 68b), AURKB (Figure 68c), CDCA8 (Figure 68d), INCENP (Figure 68e), CENPS (Figure 68f), ZW10 (Figure 68g), BUB3 (Figure 68h), CKAP5 (Figure 68i), NUDC (Figure 68j) and CLASP2 (Figure 68k).

Top 10 Gene Ontology

GO ID	GO Name	Count DE	Count All	p-value	GO ID	GO Name	Count DE	Count All	p-value
GO:0032501	multicellular organismal process	1094	6498	1.70E11	GO:0043062	extracellular structure organization	86	327	1.70E08
GO:0007155	cell adhesion	267	1307	1.40E09	GO:0006261	DNA-dependent DNA replication	47	142	2.10E08
GO:0022610	biological adhesion	268	1313	1.40E09	GO:0032502	developmental process	945	5673	2.60E08
GO:0048856	anatomical structure development	892	5279	4.70E09	GO:0098813	nuclear chromosome segregation	78	290	2.80E08
GO:0007059	chromosome segregation	88	337	1.70E08	GO:0030198	extracellular matrix organization	85	326	3.20E08

Cell Adhesion Related Gene Ontology

GO ID	GO Name	Count DE	Count All	p-value	GO ID	GO Name	Count DE	Count All	p-value
GO:0007155	cell adhesion	267	1307	1.40E09	GO:0022407	regulation of cell-cell adhesion	75	402	0.01368
GO:0022610	biological adhesion	268	1313	1.40E09	GO:0034113	heterotypic cell-cell adhesion	13	49	0.02072
GO:0007156	homophilic cell adhesion via plasma membrane adhesion molecules	46	150	3.70E07	GO:0030155	regulation of cell adhesion	113	646	0.0209
GO:0098609	cell-cell adhesion	159	774	0.0000027	GO:0007159	leukocyte cell-cell adhesion	65	351	0.02378
GO:0098742	cell-cell adhesion via plasma-membrane adhesion molecules	58	228	0.000011	GO:1900025	negative regulation of substrate adhesion-dependent cell spreading	5	13	0.03064
GO:0007229	integrin-mediated signalling pathway	30	94	0.000016	GO:0061756	leukocyte adhesion to vascular endothelial cell	8	27	0.03432
GO:0016339	calcium-dependent cell-cell adhesion via plasma membrane cell adhesion molecules	11	28	0.00121	GO:1903037	regulation of leukocyte cell-cell adhesion	59	322	0.0362
GO:0031589	cell-substrate adhesion	63	304	0.00218	GO:1903039	positive regulation of leukocyte cell-cell adhesion	40	209	0.04162
GO:0007160	cell-matrix adhesion	41	199	0.01289					

Motility and Migration Related Gene Ontology

GO ID	GO Name	Count DE	Count All	p-value	GO ID	GO Name	Count DE	Count All	p-value
GO:0050900	leukocyte migration	78	379	0.00087	GO:0097530	granulocyte migration	25	112	0.0181
GO:0071621	granulocyte chemotaxis	24	99	0.00738	GO:0071622	regulation of granulocyte chemotaxis	13	49	0.02072
GO:0006928	movement of cell or subcellular component	304	1839	0.00742	GO:0016477	cell migration	206	1242	0.02252
GO:0030593	neutrophil chemotaxis	20	79	0.00839	GO:0090131	mesenchyme migration	3	5	0.02466
GO:0040011	locomotion	263	1585	0.01049	GO:0002523	leukocyte migration involved in inflammatory response	5	13	0.03064
GO:0048870	cell motility	229	1368	0.01133	GO:0051546	keratinocyte migration	5	14	0.04208

GO:1990266	neutrophil migration	21	89	0.01584	GO:0030595	leukocyte chemotaxis	36	186	0.04431
Tissue Organisation and Angiogenesis Related Gene Ontology									
GO ID	GO Name	Count DE	Count All	p-value	GO ID	GO Name	Count DE	Count All	p-value
GO:0043062	extracellular structure organization	86	327	1.70E08	GO:0072132	mesenchyme morphogenesis	12	45	0.02472
GO:0030198	extracellular matrix organization	85	326	3.20E08	GO:0048646	anatomical structure formation involved in morphogenesis	164	978	0.02767
GO:0097755	positive regulation of blood vessel diameter	18	54	0.00042	GO:0035924	cellular response to vascular endothelial growth factor stimulus	11	41	0.02954
GO:0050880	regulation of blood vessel size	30	124	0.00308	GO:0045776	negative regulation of blood pressure	11	41	0.02954
GO:0097746	regulation of blood vessel diameter	28	117	0.00487	GO:0001568	blood vessel development	105	606	0.0319
GO:0022617	extracellular matrix disassembly	21	86	0.01076	GO:0010575	positive regulation of vascular endothelial growth factor production	8	27	0.03432
GO:0008015	blood circulation	88	478	0.01144	GO:0061756	leukocyte adhesion to vascular endothelial cell	8	27	0.03432
GO:0085029	extracellular matrix assembly	10	32	0.01293	GO:0008217	regulation of blood pressure	32	161	0.04036
GO:0002040	sprouting angiogenesis	20	84	0.01658	GO:0010574	regulation of vascular endothelial growth factor production	9	33	0.0424
GO:0010573	vascular endothelial growth factor production	10	35	0.02444	GO:0048514	blood vessel morphogenesis	91	525	0.04286

Table 22. Gene Ontology terms of RNAseq data of Gemcitabine treated vs untreated PANC-1 cells on pancreas scaffolds. The analysis is representing as (a) the top 10 most significantly impacted GO terms, (b) the significantly impacted GO terms directly related to cell adhesion, (c) the significantly impacted GO terms directly related to motility and migration and (d) the significantly impacted GO terms directly related to tissue organisation and angiogenesis. Included in the table are the total number of genes involved in each GO Name (Count All) and the number of differentially expressed genes of each GO Name (Count DE). The GO terms are ordered in terms of significance (lowest p-value to highest).

Pathway Name	P-value	Pathway Name	P-value
Cytokine-cytokine receptor interaction	8.59E-06	Leukocyte transendothelial migration	0.008339
Systemic lupus erythematosus	6.26E-05	Graft-versus-host disease	0.008471
Hematopoietic cell lineage	7.76E-05	Glutathione metabolism	0.009317
Fanconi anemia pathway	0.000107	Phagosome	0.009439
Natural killer cell mediated cytotoxicity	0.000159	Bladder cancer	0.009886
Arginine and proline metabolism	0.000359	Mineral absorption	0.011683
Alcoholism	0.000372	Intestinal immune network for IgA production	0.011726
Regulation of actin cytoskeleton	0.000481	PI3K-Akt signalling pathway	0.013832
Cell adhesion molecules (CAMs)	0.000512	p53 signalling pathway	0.014713
Staphylococcus aureus infection	0.000515	Focal adhesion	0.014719
DNA replication	0.000529	Protein digestion and absorption	0.015031
Amoebiasis	0.00058	Rheumatoid arthritis	0.01515
Type I diabetes mellitus	0.000651	Cocaine addiction	0.020657
Mucin type O-glycan biosynthesis	0.001215	Human papillomavirus infection	0.022005
MicroRNAs in cancer	0.002283	Nicotinate and nicotinamide metabolism	0.022364
ECM-receptor interaction	0.002483	Fc gamma R-mediated phagocytosis	0.027582
Cell cycle	0.002658	Homologous recombination	0.031093
Neuroactive ligand-receptor interaction	0.002928	Cellular senescence	0.033801
Endocrine and other factor-regulated calcium reabsorption	0.003161	Histidine metabolism	0.034583
Antigen processing and presentation	0.003554	Arrhythmogenic right ventricular cardiomyopathy (ARVC)	0.034761
Autoimmune thyroid disease	0.005108	Viral carcinogenesis	0.036202

Table 23. Significantly impacted pathways from RNAseq data of Gemcitabine treated vs untreated PANC-1 cells on pancreas scaffolds. Pathways are ordered by significance (lowest p-value to highest).

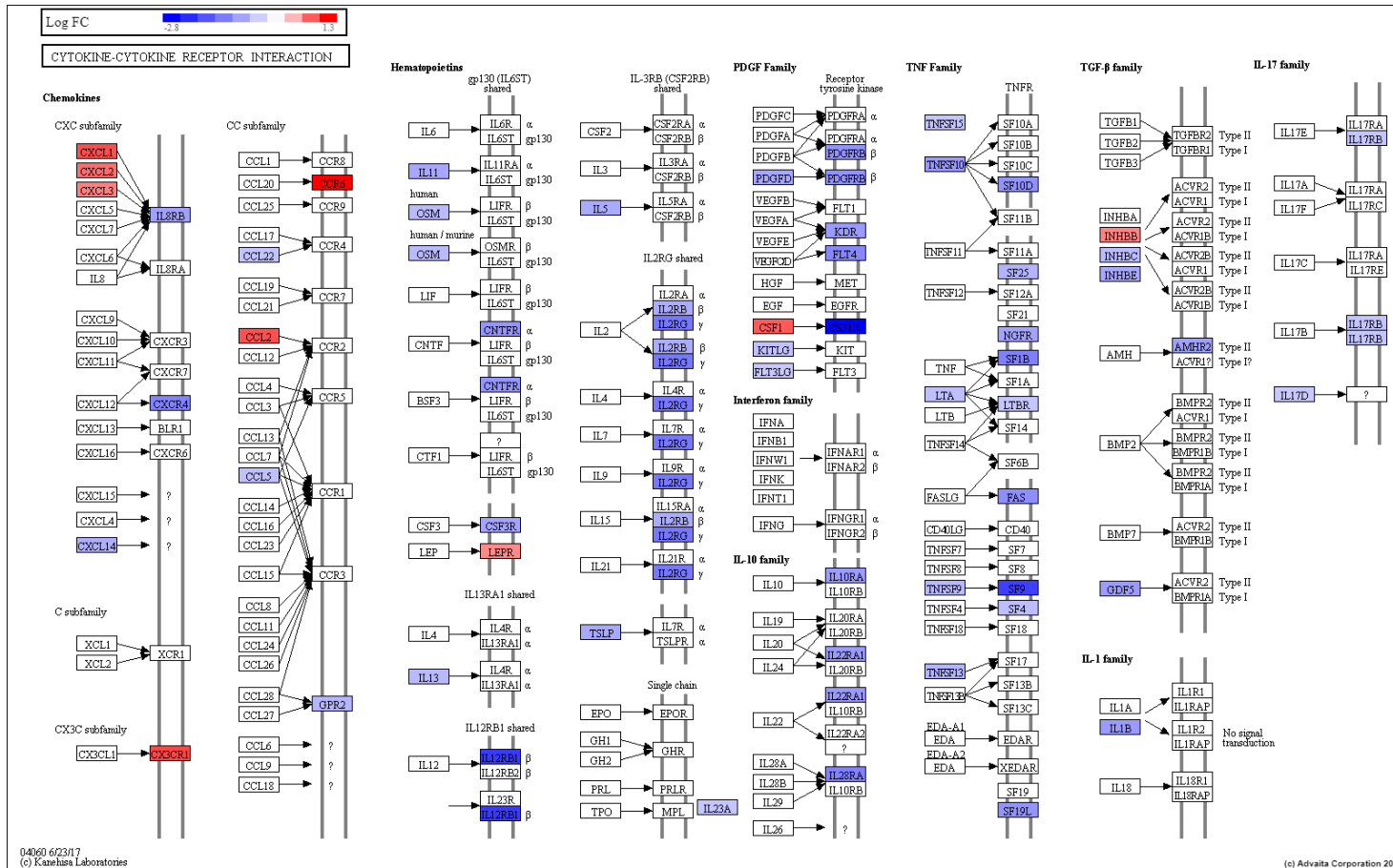


Figure 66. Pathway map for cytokine-cytokine receptor interactions representing the significantly differentially expressed genes from RNAseq of untreated vs Gemcitabine treated PANC-1 cells cultured on pancreas scaffolds. Cytokine-cytokine receptor interactions (KEGG: 04060) was the most significantly impacted pathway. The pathway diagram is overlaid with the computed perturbation of each gene. The perturbation accounts both for the gene's measured fold change and for the accumulated perturbation propagated from any upstream genes (accumulation). The highest negative perturbation (up-regulated in Gemcitabine treated samples) is shown in dark blue, while the highest positive perturbation (down-regulated in Gemcitabine treated samples) is shown in dark red. The legend describes the values on the gradient. One gene may be represented in multiple places in the diagram and one box may represent multiple genes in the same gene family. A gene is highlighted in all locations it occurs in the diagram. For each gene family, the colour corresponding to the gene with the highest absolute perturbation is displayed.

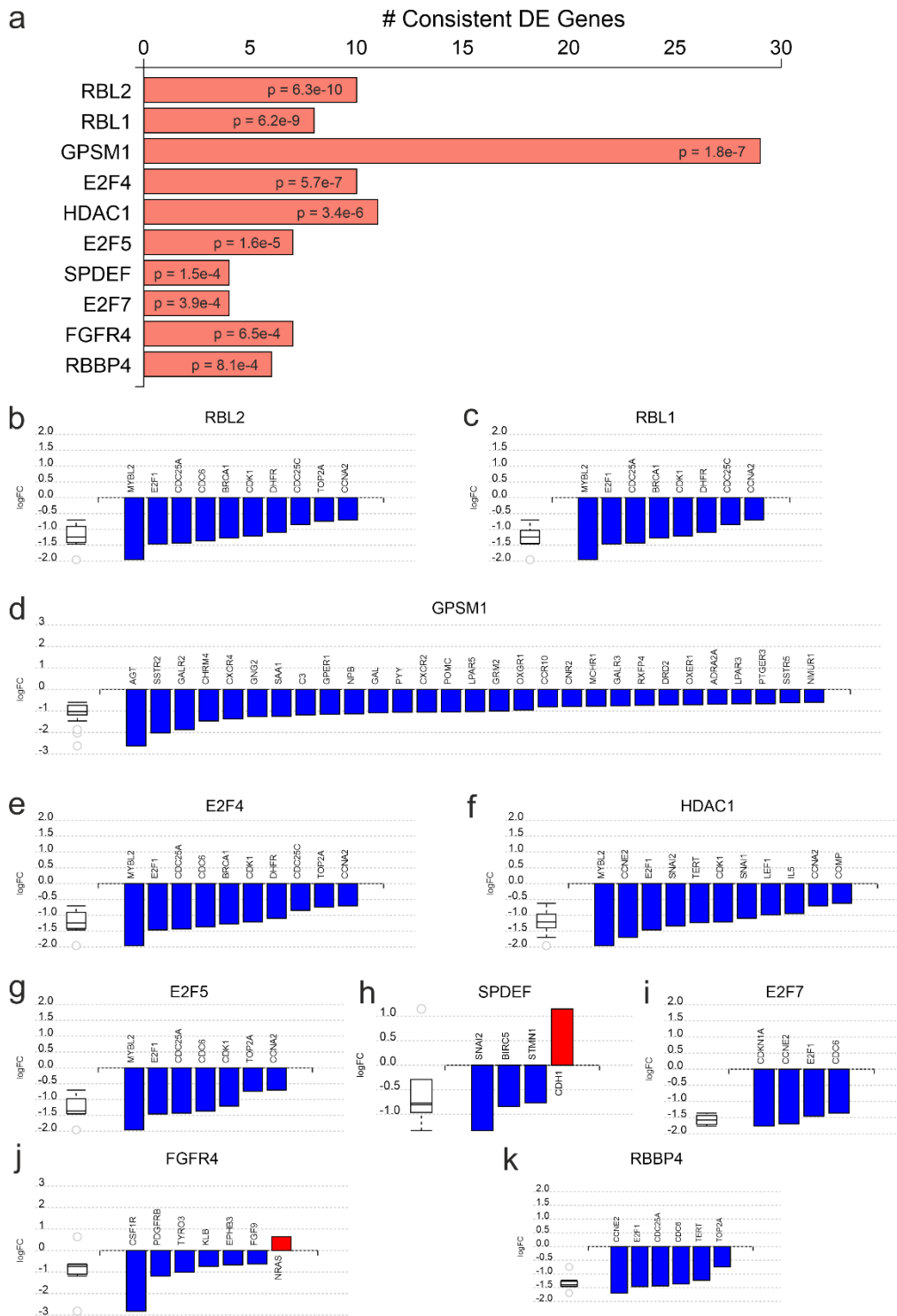


Figure 67. Predicted activated upstream regulators of RNAseq data of untreated vs Gemcitabine treated PANC-1 cells cultured on pancreas scaffolds. (a) Top 10 significant upstream regulators predicted as activated. The x axis represented the number of DE genes downstream of the regulator. The gene measured expression bar plot: all the consistent differentially expressed genes that are targeted by (b) RBL2, (c) RBL1, (d) GPSM1, (e) E2F4, (f) HDAC1, (g) E2F5, (h) SPDEF, (i) E2F7, (j) FGFR4 and (k) RBBP4 are ranked based on their measured expression change from most down-regulated (in blue) to up-regulated (in red) in untreated samples compared to Gemcitabine treated samples. The box and whisker plot on the left summarises the distribution of all the consistent differentially expressed genes targeted by this upstream regulator. The box shows the 1st quartile, the median and the 3rd quartile, while the outliers are represented by circles.

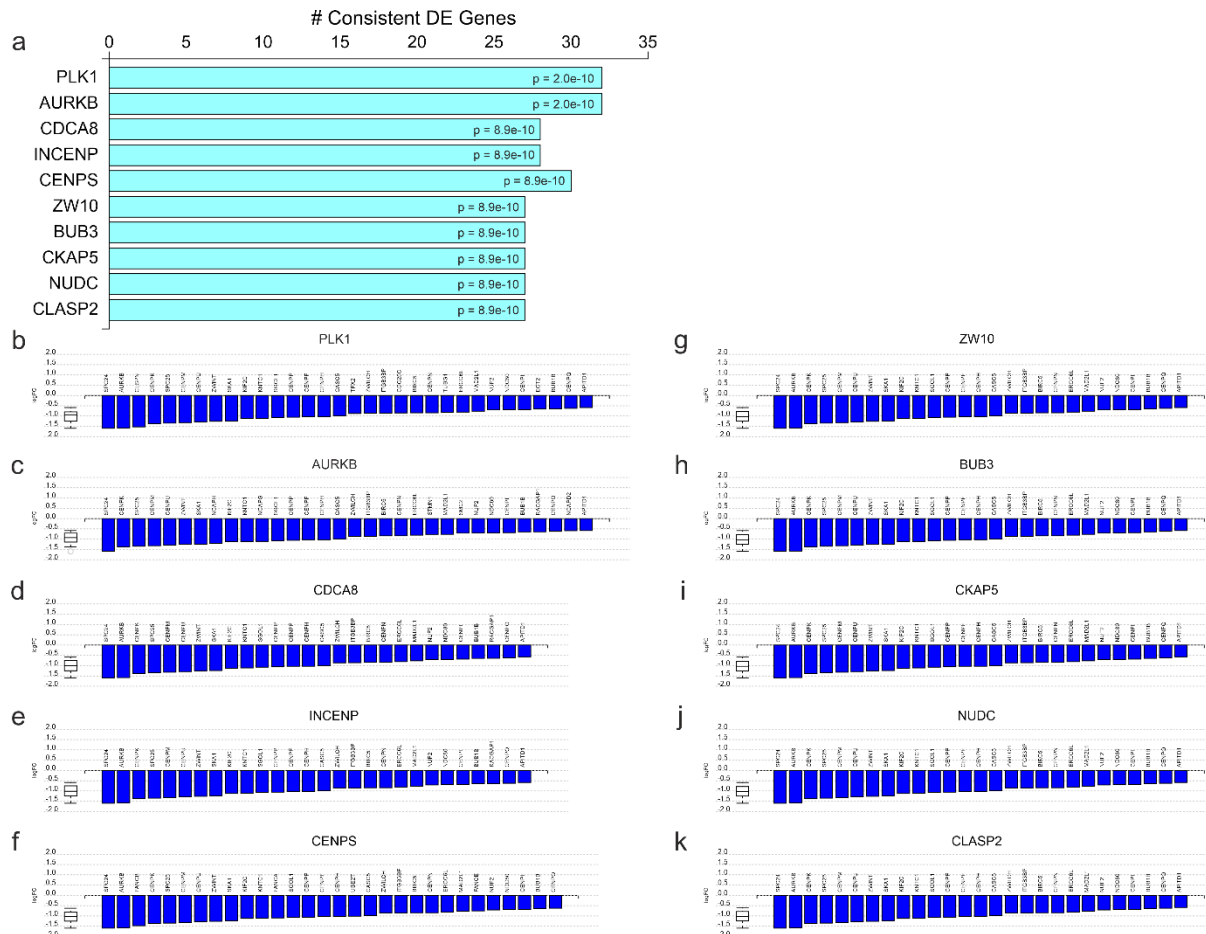


Figure 68. Predicted inhibited upstream regulators of RNAseq data of untreated vs Gemcitabine treated PANC-1 cells cultured on pancreas scaffolds. (a) Top 10 significant upstream regulators predicted as inhibited. The x axis represented the number of DE genes downstream of the regulator. The gene measured expression bar plot: all the consistent differentially expressed genes that are targeted by (b) PLK1, (c) AURKB, (d) CDC48, (e) INCENP, (f) CENPS, (g) ZW10, (h) BUB3, (i) CKAP5, (j) NUDC and (k) CLAP2 are ranked based on their measured expression change from most down-regulated (in blue) to up-regulated (in red) in untreated samples compared to Gemcitabine treated samples. The box and whisker plot on the left summarises the distribution of all the consistent differentially expressed genes targeted by this upstream regulator. The box shows the 1st quartile, the median and the 3rd quartile, while the outliers are represented by circles.

Further, when comparing between Gemcitabine treated and untreated (control) PK-1 cells on liver scaffolds, 1587 DE genes were identified out of a total of 21,259 genes with measured expression. In this experiment, we chose a threshold of $p < 0.05$ for statistical significance and a LogFC of expression $> 0.5x$. Out of these DE genes, 1,242 genes were up-regulated, and 343 genes were down-regulated in the Gemcitabine treated PK-1 cells when compared to those that were left untreated. These data were further analysed in the context of pathways obtained from the KEGG database, GO from the Gene Ontology Consortium database and network of regulatory relations from BioGRID. In summary, 57 pathways were found to be significantly impacted. In addition, 1,692 GO terms and 418 upstream regulators, were found to be significantly ($p < 0.05$) enriched.

To best demonstrate the overall impact Gemcitabine treatment has on PK-1 cells cultured on liver scaffolds, the 1,692 significantly affected GO terms, were broken down, in order of significance, (as previously described) into (i) the top 10 most significantly impacted GO terms (Table 24a), (ii) the GO terms directly related to cell adhesion (Table 24b), (iii) the GO terms directly related to motility and migration (Table 24c) and (iv) the GO terms directly related to tissue organisation and angiogenesis (Table 24d).

It was found that 14 GO terms were significantly impacted that directly involved cell adhesion (Table 24b). Out of these 14 GO terms, “cell-cell adhesion” and “leukocyte cell-cell adhesion” were studied in further details. Analysis of the “cell-cell adhesion” GO term showed that there were 79 significantly ($p < 0.05$) DE genes out of a total 776 genes involved. Of these genes, 61 genes had a LogFC of > 0.5 in Gemcitabine treated samples compared to untreated samples (Supplementary Table 19). In contrast, 18 genes had a LogFC of > 0.5 in the untreated samples compared to the Gemcitabine treated samples (Supplementary Table 19). Analysis of the “leukocyte cell-cell adhesion” GO term showed that there were 43 significantly ($p < 0.05$) DE genes out of a total 352 genes involved. Of these genes, 38 genes had a LogFC of > 0.5 in Gemcitabine treated samples compared to untreated samples (Supplementary Table 20). In contrast, 5 genes had a LogFC of > 0.5 in the untreated samples compared to the Gemcitabine treated samples (Supplementary Table 20).

Furthermore, it was found that 20 GO terms were significantly impacted that directly involved motility and migration (Table 24c). Out of these 20 GO terms, “cell motility” and “leukocyte migration” were studied in further details. Analysis of the “cell motility” GO term showed that there were 131 significantly ($p < 0.05$) DE genes out of a total 1373 genes involved. Of these genes, 113 genes had a LogFC of >0.5 in Gemcitabine treated samples compared to untreated samples (Supplementary Table 21). In contrast, 18 genes had a LogFC of >0.5 in the untreated samples compared to the Gemcitabine treated samples (Supplementary Table 21). Analysis of the “leukocyte migration” GO term showed that there were 43 significantly ($p < 0.05$) DE genes out of a total 382 genes involved. Of these genes, 38 genes had a LogFC of >0.5 in Gemcitabine treated samples compared to untreated samples (Supplementary Table 22). In contrast, 5 genes had a LogFC of >0.5 in the untreated samples compared to the Gemcitabine treated samples (Supplementary Table 22).

Finally, it was found that 22 GO terms were significantly impacted that directly involved tissue organisation and angiogenesis (Table 24d). Out of these 22 GO terms, “extracellular structure organisation” and “sprouting angiogenesis” were studied in further details. Analysis of the “extracellular structure organisation” GO term showed that there were 44 significantly ($p < 0.05$) DE genes out of a total 324 genes involved. Of these genes, 33 genes had a LogFC of >0.5 in Gemcitabine treated samples compared to untreated samples (Supplementary Table 23). In contrast, 11 genes had a LogFC of >0.5 in the untreated samples compared to the Gemcitabine treated samples (Supplementary Table 23). Analysis of the “sprouting angiogenesis” GO term showed that there were 18 significantly ($p < 0.05$) DE genes out of a total 83 genes involved. Of these genes, 12 genes had a LogFC of >0.5 in Gemcitabine treated samples compared to untreated samples (Supplementary Table 24). In contrast, 6 gene had a LogFC of >0.5 in the untreated samples compared to the Gemcitabine treated samples (Supplementary Table 24).

Top 10 Gene Ontology

GO ID	GO Name	Count DE	Count All	p-value	GO ID	GO Name	Count DE	Count All	p-value
GO:0007049	cell cycle	333	1786	1.00E-24	GO:0000819	sister chromatid segregation	87	227	1.00E-24
GO:0022402	cell cycle process	269	1284	1.00E-24	GO:0098813	nuclear chromosome segregation	97	292	1.00E-24
GO:1903047	mitotic cell cycle process	195	811	1.00E-24	GO:0051301	cell division	138	568	1.00E-24
GO:0000278	mitotic cell cycle	212	974	1.00E-24	GO:0006260	DNA replication	90	283	1.00E-24
GO:0007059	chromosome segregation	108	339	1.00E-24	GO:0000280	nuclear division	106	385	1.00E-24

Cell Adhesion Related Gene Ontology

GO ID	GO Name	Count DE	Count All	p-value	GO ID	GO Name	Count DE	Count All	p-value
GO:1904996	positive regulation of leukocyte adhesion to vascular endothelial cell	5	7	0.000064	GO:0007159	leukocyte cell-cell adhesion	43	352	0.00449
GO:0022610	biological adhesion	139	1308	0.00046	GO:0061756	leukocyte adhesion to vascular endothelial cell	7	29	0.00725
GO:0007155	cell adhesion	138	1301	0.00052	GO:1903039	positive regulation of leukocyte cell-cell adhesion	26	208	0.01793
GO:1904994	regulation of leukocyte adhesion to vascular endothelial cell	6	16	0.00111	GO:0098609	cell-cell adhesion	79	776	0.0203
GO:0030155	regulation of cell adhesion	74	646	0.0015	GO:0071603	endothelial cell-cell adhesion	2	4	0.03531
GO:1903037	regulation of leukocyte cell-cell adhesion	41	322	0.00261	GO:0098742	cell-cell adhesion via plasma-membrane adhesion molecules	26	228	0.0485
GO:0022407	regulation of cell-cell adhesion	48	402	0.00436	GO:0022409	positive regulation of cell-cell adhesion	27	239	0.04964

Motility and Migration Related Gene Ontology

GO ID	GO Name	Count DE	Count All	p-value	GO ID	GO Name	Count DE	Count All	p-value
GO:0030335	positive regulation of cell migration	50	421	0.00408	GO:0006935	chemotaxis	57	535	0.02022
GO:2000147	positive regulation of cell motility	50	436	0.00798	GO:1990266	neutrophil migration	13	86	0.0208
GO:0040017	positive regulation of locomotion	52	466	0.01153	GO:2000145	regulation of cell motility	78	770	0.02333
GO:0002687	positive regulation of leukocyte migration	17	116	0.01219	GO:0048870	cell motility	131	1373	0.02563
GO:0002685	regulation of leukocyte migration	22	164	0.01327	GO:1902624	positive regulation of neutrophil migration	6	30	0.03093
GO:0016477	cell migration	122	1243	0.01413	GO:0002042	cell migration involved in sprouting angiogenesis	7	39	0.0353

GO:0060326	cell chemotaxis	30	244	0.01447	GO:0002689	negative regulation of leukocyte chemotaxis	4	16	0.03562
GO:0050900	leukocyte migration	43	382	0.01766	GO:0002688	regulation of leukocyte chemotaxis	14	103	0.03836
GO:0030593	neutrophil chemotaxis	12	76	0.01879	GO:0071621	granulocyte chemotaxis	13	95	0.04282
GO:0040011	locomotion	151	1589	0.01957	GO:0030334	regulation of cell migration	71	719	0.04707

Tissue Organisation Related Gene Ontology

GO ID	GO Name	Count DE	Count All	p-value	GO ID	GO Name	Count DE	Count All	p-value
GO:0043062	extracellular structure organization	44	324	0.0005	GO:0097756	negative regulation of blood vessel diameter	12	77	0.02067
GO:0045601	regulation of endothelial cell differentiation	9	31	0.00058	GO:0001955	blood vessel maturation	3	8	0.02186
GO:0030198	extracellular matrix organization	43	323	0.00086	GO:0009653	anatomical structure morphogenesis	217	2363	0.02227
GO:0045602	negative regulation of endothelial cell differentiation	4	8	0.00231	GO:0001935	endothelial cell proliferation	17	124	0.02246
GO:0048646	anatomical structure formation involved in morphogenesis	100	961	0.00537	GO:0072132	mesenchyme morphogenesis	8	44	0.02353
GO:0001568	blood vessel development	66	597	0.006	GO:0001569	branching involved in blood vessel morphogenesis	6	29	0.0265
GO:0045603	positive regulation of endothelial cell differentiation	5	16	0.00713	GO:0001937	negative regulation of endothelial cell proliferation	7	37	0.02717
GO:0001936	regulation of endothelial cell proliferation	16	107	0.01228	GO:0001763	morphogenesis of a branching structure	23	187	0.02936
GO:0009887	animal organ morphogenesis	95	937	0.01299	GO:0002042	cell migration involved in sprouting angiogenesis	7	39	0.0353
GO:0010574	regulation of vascular endothelial growth factor production	7	33	0.01494	GO:0071603	endothelial cell-cell adhesion	2	4	0.03531
GO:0048514	blood vessel morphogenesis	56	516	0.01523	GO:0045446	endothelial cell differentiation	13	93	0.03691
GO:0002040	sprouting angiogenesis	13	83	0.0158	GO:0035924	cellular response to vascular endothelial growth factor stimulus	7	40	0.0399
GO:0010575	positive regulation of vascular endothelial growth factor production	6	27	0.01896	GO:1902337	regulation of apoptotic process involved in morphogenesis	3	10	0.04146
GO:0010573	vascular endothelial growth factor production	7	35	0.02042	GO:0035239	tube morphogenesis	36	332	0.04504
GO:0043062	extracellular structure organization	44	324	0.0005	GO:0097756	negative regulation of blood vessel diameter	12	77	0.02067
GO:0045601	regulation of endothelial cell differentiation	9	31	0.00058	GO:0001955	blood vessel maturation	3	8	0.02186
GO:0030198	extracellular matrix organization	43	323	0.00086	GO:0009653	anatomical structure morphogenesis	217	2363	0.02227
GO:0045602	negative regulation of endothelial cell differentiation	4	8	0.00231	GO:0001935	endothelial cell proliferation	17	124	0.02246

GO:0048646	anatomical structure formation involved in morphogenesis	100	961	0.00537	GO:0072132	mesenchyme morphogenesis	8	44	0.02353
GO:0001568	blood vessel development	66	597	0.006	GO:0001569	branching involved in blood vessel morphogenesis	6	29	0.0265
GO:0045603	positive regulation of endothelial cell differentiation	5	16	0.00713	GO:0001937	negative regulation of endothelial cell proliferation	7	37	0.02717
GO:0001936	regulation of endothelial cell proliferation	16	107	0.01228	GO:0001763	morphogenesis of a branching structure	23	187	0.02936

Table 24 . Gene Ontology terms of RNAseq data of Gemcitabine treated vs untreated PK-1 cells on liver scaffolds. The analysis is represented as followed (a) the top 10 most significantly impacted GO terms, (b) the significantly impacted GO terms directly related to cell adhesion, (c) the significantly impacted GO terms directly related to motility and migration and (d) the significantly impacted GO terms directly related to tissue organisation and angiogenesis. Included in the table are the total number of genes involved in each GO Name (Count All) and the number of differentially expressed genes of each GO Name (Count DE). The GO terms are ordered in terms of significance (lowest p-value to highest).

Next, we investigated the cellular pathways that were impacted by Gemcitabine treatment of PK-1 cells on liver scaffold. There were 294 pathways that presented at least one DE gene, of which 57 showed a pathway-specific p-value of <0.05 (Table 25). The most significant pathway was “DNA replication” ($p = 1.92e-16$) (Table 25). Further investigation showed that all 22 DE genes associated with this pathway were up-regulated in the Gemcitabine treated samples (Figure 69).

The final aspect investigated relating to the RNAseq data of Gemcitabine treated PK-1 cells on pancreas scaffold was the prediction of upstream regulators. The top ten hypothesised “activated” upstream regulators were listed in order of significance (Figure 70a); RBL2 (Figure 70b), E2F4 (Figure 70c), RBL1 (Figure 70d), E2F5 (Figure 70e), E2F7 (Figure 70f), TFDP2 (Figure 70g), LIN52 (Figure 70h), LIN37 (Figure 70i), LIN54 (Figure 70j) and HDAC1 (Figure 70k). Additionally, the top ten hypothesised “inhibited” upstream regulators were listed in order of significance (Figure 71a); AURKB (Figure 71b), PLK1 (Figure 71c), CENPS (Figure 71d), INCENP (Figure 71e), CDCA8 (Figure 71f), CENPC (Figure 71g), KIF2A (Figure 71h), PPP2R1B (Figure 71i), PPP2R5B (Figure 71j) and PPP2R5C (Figure 71k).

Pathway Name	P-value	Pathway Name	P-value
DNA replication	1.92E-16	B cell receptor signalling pathway	0.006719
Cell cycle	3.66E-07	Pathways in cancer	0.007415
Fanconi anemia pathway	5.67E-07	Influenza A	0.007508
Cytokine-cytokine receptor interaction	9.76E-07	NOD-like receptor signalling pathway	0.009052
Homologous recombination	4.04855E-06	Hepatitis B	0.011463
p53 signalling pathway	4.96104E-06	Human papillomavirus infection	0.013208
HTLV-I infection	7.03032E-06	Salmonella infection	0.014771
IL-17 signalling pathway	1.61597E-05	Chemokine signalling pathway	0.015359
Mismatch repair	2.19759E-05	Salivary secretion	0.016771
Cellular senescence	0.000123291	Bladder cancer	0.019312
MicroRNAs in cancer	0.000137791	Hepatitis C	0.019455
Rheumatoid arthritis	0.000162283	Toxoplasmosis	0.020918
Oocyte meiosis	0.000240853	FoxO signalling pathway	0.021999
NF-kappa B signalling pathway	0.000399501	Antifolate resistance	0.025327
Transcriptional misregulation in cancer	0.000485984	Chemical carcinogenesis	0.028776
Breast cancer	0.000547547	Pyrimidine metabolism	0.030232
TNF signalling pathway	0.000892742	Fluid shear stress and atherosclerosis	0.033095
Nucleotide excision repair	0.001776978	Mineral absorption	0.033322
Primary immunodeficiency	0.001971155	Jak-STAT signalling pathway	0.035286
Small cell lung cancer	0.002321373	Metabolism of xenobiotics by cytochrome P450	0.03626
Base excision repair	0.002434071	Prostate cancer	0.037277
Basal cell carcinoma	0.003186599	Leishmaniasis	0.037779
TGF-beta signalling pathway	0.004003428	Non-small cell lung cancer	0.038832
Progesterone-mediated oocyte maturation	0.004516997	Pancreatic cancer	0.040143
Pertussis	0.004703916	Alcoholism	0.042775
Ovarian steroidogenesis	0.005899033	Non-alcoholic fatty liver disease (NAFLD)	0.043216
Legionellosis	0.006203242	Gastric acid secretion	0.04749
Malaria	0.006244667	Amoebiasis	0.049675
Apoptosis	0.006408973		

Table 25. Significantly impacted pathways from RNAseq data of Gemcitabine treated vs untreated PK-1 cells on liver scaffolds. Pathways are ordered by significance (lowest p-value to highest).

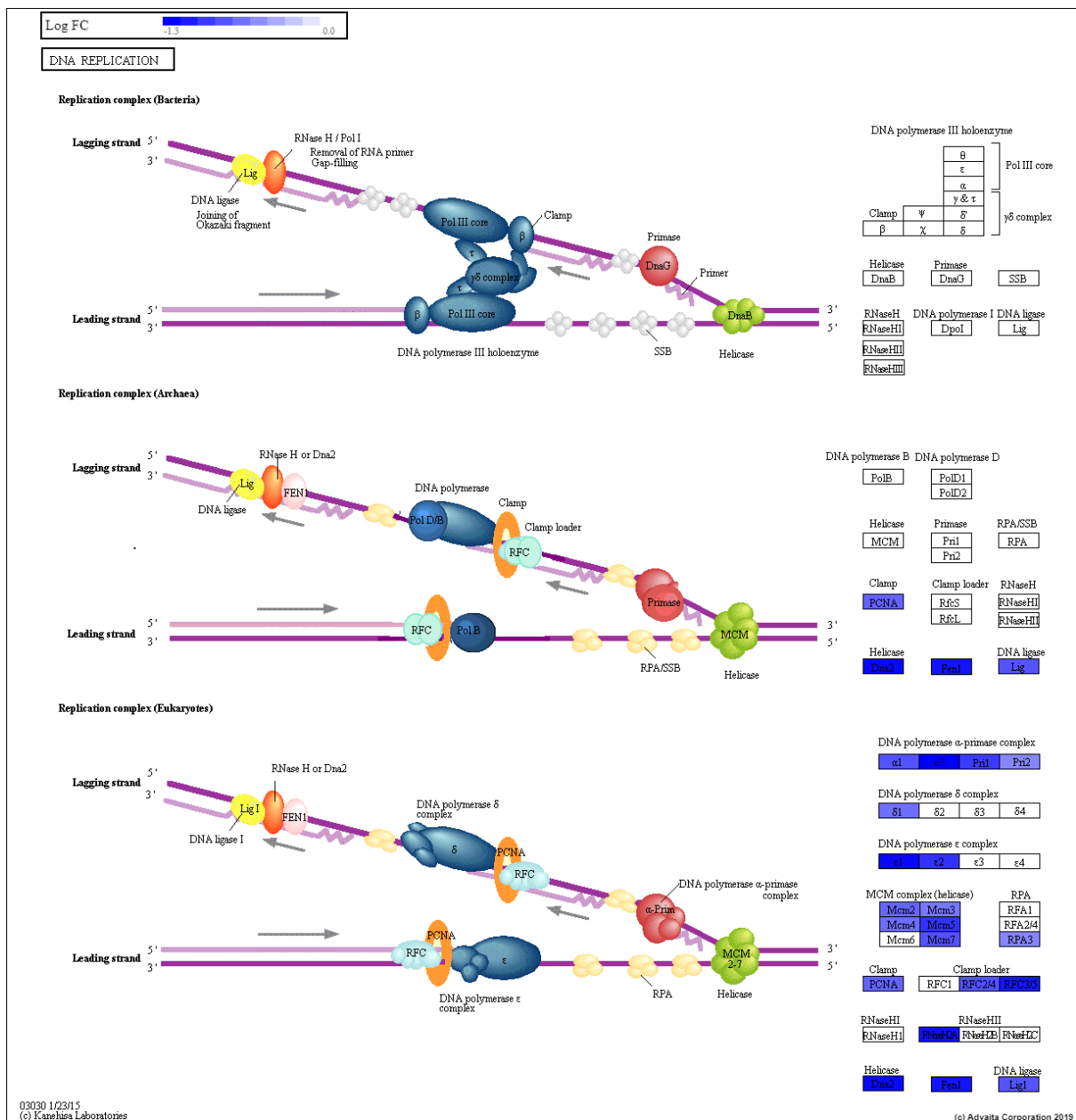


Figure 69. Pathway map for DNA replication representing the significantly differentially expressed genes from RNAseq of untreated vs Gemcitabine treated PK-1 cells cultured on liver scaffolds. DNA replication (KEGG: 03030) was the most significantly impacted pathway. The pathway diagram is overlaid with the computed perturbation of each gene. The perturbation accounts both for the gene's measured fold change and for the accumulated perturbation propagated from any upstream genes (accumulation). The highest negative perturbation (up-regulated in Gemcitabine treated samples) is shown in dark blue, while the highest positive perturbation (down-regulated in Gemcitabine treated samples) in dark red. The legend describes the values on the gradient. One gene may be represented in multiple places in the diagram and one box may represent multiple genes in the same gene family. A gene is highlighted in all locations it occurs in the diagram. For each gene family, the colour corresponding to the gene with the highest absolute perturbation is displayed.

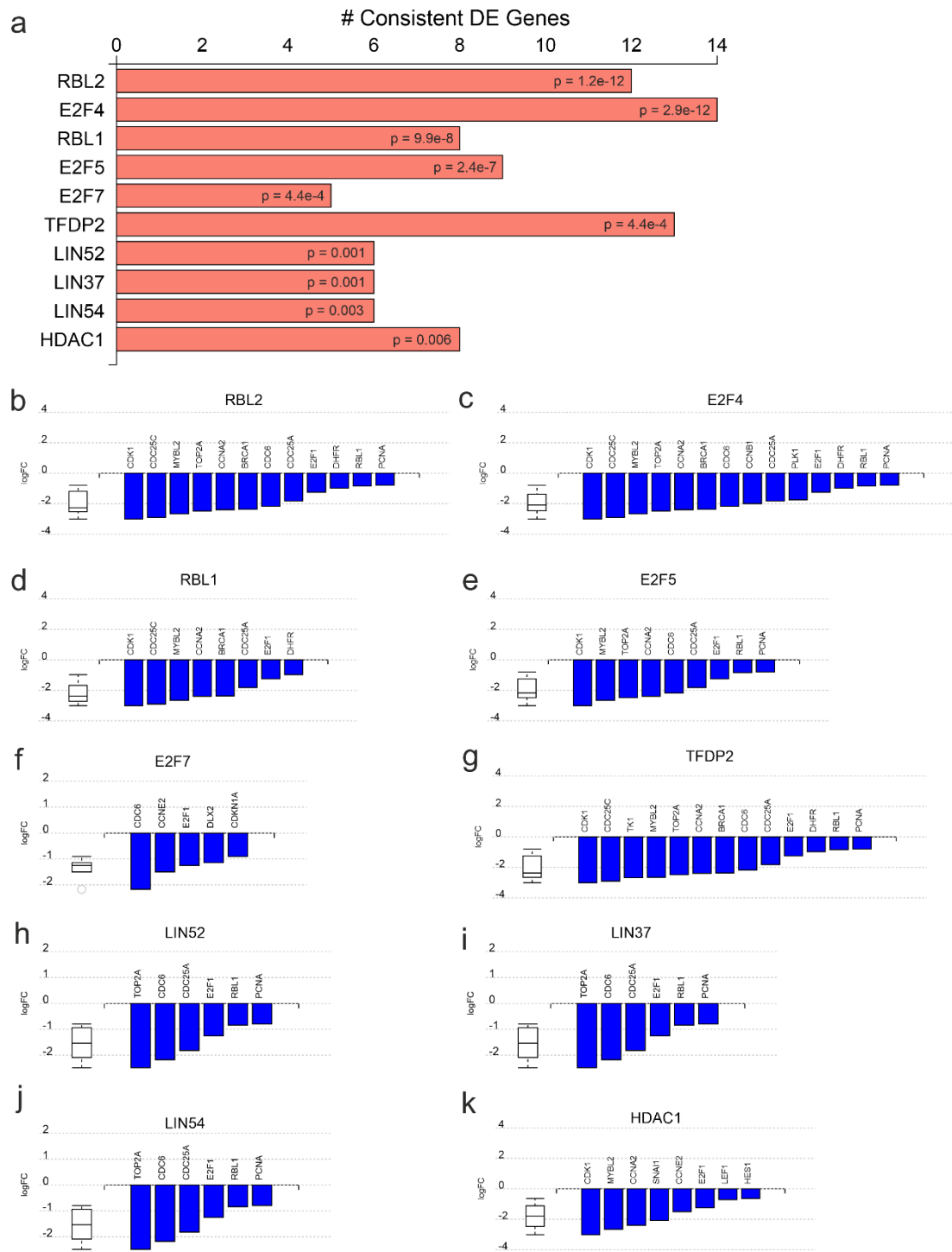


Figure 70. Predicted activated upstream regulators of RNAseq data of untreated vs Gemcitabine treated PK-1 cells cultured on pancreas scaffolds. (a) Top 10 significant upstream regulators predicted as activated. The x axis represented the number of DE genes downstream of the regulator. The gene measured expression bar plot: All the consistent differentially expressed genes that are targeted by ((b) RBL2, (c) E2F4, (d) RBL1, (e) E2F5, (f) E2F7, (g) TFDP2, (h) LIN52, (i) LIN37, (j) LIN54 and (k) HDAC1 are ranked based on their measured expression change from most down-regulated (in blue) to up-regulated (in red) in untreated samples compared to Gemcitabine treated samples. The box and whisker plot on the left summarises the distribution of all the consistent differentially expressed genes targeted by this upstream regulator. The box shows the 1st quartile, the median and the 3rd quartile, while the outliers are represented by circles.

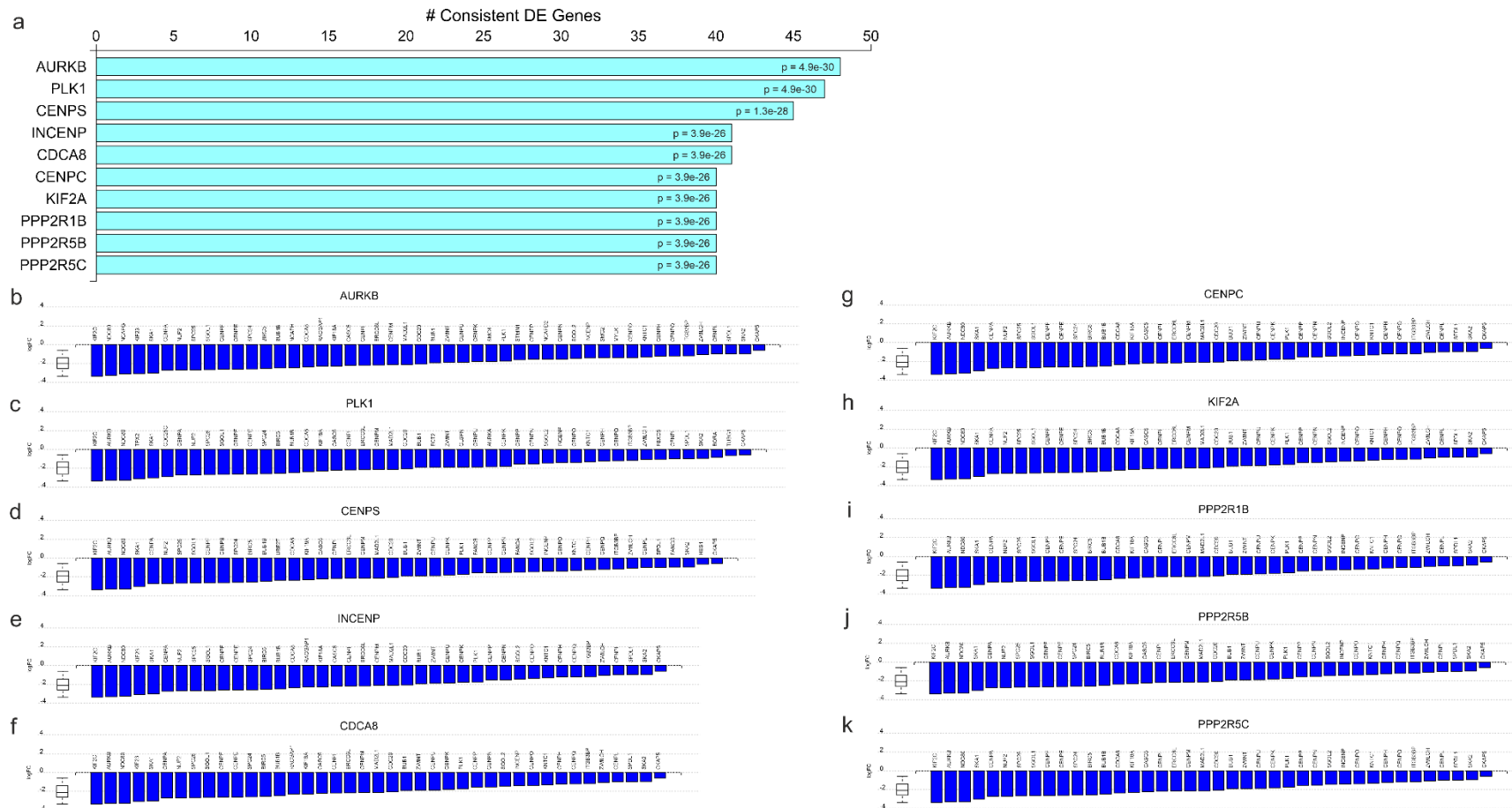


Figure 71. Predicted inhibited upstream regulators of RNAseq data of untreated vs Gemcitabine treated PK-1 cells cultured on pancreas scaffolds. (a) Top 10 significant upstream regulators predicted as inhibited. The x axis represented the number of DE genes downstream of the regulator. The gene measured expression bar plot: All the consistent differentially expressed genes that are targeted by (b) AURKB, (c) PLK1, (d) CENPS, (e) INCENP, (f) CDCA8, (g) CENPC, (h) KIF2A, (i) PPP2R1B, (j) PPP2R5B and (k) PPP2R5C are ranked based on their measured expression change from most down-regulated (in blue) to up-regulated (in red) in untreated samples compared to Gemcitabine treated samples. The box and whisker plot on the left summarises the distribution of all the consistent differentially expressed genes targeted by this upstream regulator. The box shows the 1st quartile, the median and the 3rd quartile, while the outliers are represented by circles.

• **CHAPTER 5** •

“If knowledge can create problems, it is not through ignorance that we can solve them.”

- Isaac Asimov

5. DISCUSSION

Decellularised tissue from other organs have previously been utilized as *in vitro* 3D scaffolds for human tumour modelling, e.g., liver (320, 321), lung (322, 323), breast and adipose tissue (324, 325), and intestinal tissue (326, 327). These studies showed a clear benefit in using decellularised scaffolds to predict *in vivo* outcomes. Indeed, Dunne et al., demonstrated that decellularised human adipose scaffolds presented a more suitable environment for the growth, migration/invasion, morphology, and drug response of breast cancer cells, MCF-7 and BT474, compared to both Matrigel and 2D plastic cultures (324). In this study, both cell types were resistant to a) doxorubicin, a drug that does not present positive results in humans, and b) sensitive to lapatinib, a drug that presents a positive impact in humans. Furthermore, Miyauchi et al., demonstrated the use of fibrotic mouse liver scaffolds to model hepatocellular carcinoma (HCC) (320). This study is the first published work to prove the direct involvement of the ECM in promoting an EMT phenotype and increasing the proliferation and chemoresistance of HCC cells.

The novel PDAC platforms presented in this thesis, both the primary and metastatic, present a perfect model to encourage the principles of the National Centers' 3Rs (the replacement, refinement, and reduction of animals in research). The mission of the National Center, as stated on their website, is to "use the 3Rs principles to accelerate scientific discovery, support innovation, and technological developments, and address societal concerns about animal research (328)." These decellularised liver cubes would, without a doubt, (i) accelerate scientific discovery, (ii) support innovation and (iii) reduce and replace animal use in much scientific research. Lessons learned from experience in our laboratory showed the difficulty of trying to organise experiments that involve both cell culture and tissue decellularisation, as both procedures were time-consuming and difficult to coordinate. The fact that a fresh pancreas can now be decellularised and further sterilised in less than 10 days would allow many research groups to develop these decellularised tissue and use them to better predict *in vivo* results before the use of animals.

5.1 Pancreas Decellularisation

The first aim of this thesis was to perform the decellularisation of human pancreata, as opposed to animal pancreatic tissue. To do so, two approaches were investigated: agitation and perfusion. Both methods have their advantages and limitations; agitation is a much faster technique of decellularisation, and only a small portion of the pancreas is needed. On the other hand, for the perfusion decellularisation technique, the whole pancreas en-bloc with duodenum is required, as all vessels need to be preserved but would eventually allow for a much greater number of scaffolds to be available for use.

5.1.1 Elimination of Cellular Debris and Preservation of the ECM

The first piece of pancreas obtained was a small chunk from a pancreaticoduodenectomy. Therefore, we initially aimed to investigate our successful liver agitation decellularisation technique on 5x5x5 mm cubes from this pancreas (296). After the completion of protocol PA1, the cubes have gained size and remained yellow, which are both negative macroscopic indicators for ECM preservation and decellularisation, respectively. These observations were confirmed by histology. The next protocol, PA2, attempted to address these observations by (i) reducing the frequency of agitation; to preserve the bulk structure and (ii) prolonging the exposure to reagents; to improve cellular elimination. Similarly, the pancreatic cubes were either decellularised but destroyed or preserved but not decellularised. On further investigation, it was found that the human pancreas has thin connective tissue separating the parenchyma (329, 330). This connective tissue is unable to withstand the agitating force, thereby causing the bulk structure to disseminate. Additionally, the use of a mild shaking/mixing instead of agitation i.e. to decellularise pancreatic cubes, would result in a very lengthy protocol, with longer time points to respect than for perfusion.

The next step was to examine perfusion as an option of decellularisation. The first protocol was a preliminary method of decellularisation and was based on a 'pump and a box' technique, with no additional monitoring equipment. After 7 days of decellularisation, the pancreas appeared white microscopically and therefore all reagents were halted, and the organ was washed for several days with distilled water and 1X PBS. Histological analysis proved the cell remnants, excluding nuclear material, were eliminated from the decellularised pancreas. Additionally, IHC staining for vital ECM proteins was consistent with fresh pancreatic tissue. Finally, the most consistent protocol for decellularisation that resulted in complete decellularisation and the best preservation of both the bulk structure and microarchitecture of the ECM was achieved by replicating protocol PA1 with minor modifications; (i) monitoring the pressure of the tissue and increasing this during the course of decellularisation, (ii) increasing the flow rate, and (iii) increasing the number of non-recycled reagents. DNA quantification was lowest in the head of the pancreas (mean 57.3 ng/mg wet tissue), which is the closest area to the point of in-flow. Immunohistochemistry staining has also presented a consistent preservation of the vital ECM proteins and indicative architecture of the pancreas.

Although the phrase "complete decellularisation" was used, it is very hard to define what "complete" stands for, as it is impossible to remove all cellular debris. Up-to-date there has been no study that determined what quantity of cellular material or DNA content remaining within a scaffold would be accepted as "complete" decellularization with preservation of the ECM and microarchitecture. Although these tissue scaffolds will only be used for disease modelling and won't be implanted, it is still essential to understand how much cellular debris is deemed satisfactory; thereby not interfering with experimental integrity. To elaborate; there is no published work that truly determines the effect of cellular debris and nuclear material on viable cells in culture; therefore the only indication we have is to decellularise the scaffolds for a standard fitting for implantation. It is very well understood that membrane-bound antigens cause a host response, but awareness needs to be raised that cytoplasmic fractions, as well as DNA, does result in an untoward host response. For example, Nagata et al., demonstrated that DNA fragments over 180 bp accumulate in macrophages resulting in the activation of the innate immune system (331). Furthermore, Zheng et al.,

showed that DNA remaining in porcine small intestine submucosa caused an inflammatory response in both mice and rabbits (332). Mitochondria have also been demonstrated to cause an inflammatory response by the host; this has been verified by Zhang et al., who showed that impaired mitochondria release damage-associated molecular patterns which also triggers the innate immune system (333). Therefore, it is essential to remove as much cellular material as possible from tissue cubes intended for disease modelling, as these cellular remnants will (i) hinder future cellular attachment of the reseeded cells and (ii) produce false results during experimentation.

When initiating this project there were no published work related to the decellularisation of human pancreata, but since then there have been two published articles related to this matter. In 2016, Peloso et al., decellularised whole human pancreata using an antegrade perfusion system through three in-flows, namely the pancreatic duct, the superior mesenteric artery and the proximal stump of the splenic artery (334). In comparison, the pancreas decellularisation protocol described in this thesis uses only one in-flow through the portal vein (retrograde), which allows for the same vascular coverage of the entire organ but reducing the complexity of the system, e.g. the number of pumps, pressure sensors and surgical skills. Additionally, our protocol allows for the decellularisation of the pancreas en-bloc with the duodenum in comparison to Peloso et al. whom remove the duodenum. This allows for better perfusion through the head of the pancreas as well as obtaining a decellularised duodenum for other possible studies.

Further, Peloso et al had superior nuclear material elimination in comparison to the protocol described here (40 ± 30 ng/mg vs 81 ± 31 ng/mg), but Peloso's protocol involved the use of DNase, which was avoided in our protocol due to its difficulty to remove from tissue and its possible effect on future cell culture experiments. Peloso et al carried out further extensive ECM characterisation experiments that were not performed in this thesis and should be carried out as future work including (i) Scanning electron microscopy to visualise the microarchitecture of the ECM, (ii) CAM assay to study the induction of vascularisation by the scaffold, (iii) quantitative array to investigate the retention of growth factors, and (iv) biomechanical studies to

investigate the retention of stiffness properties of the scaffold in comparison to native pancreas tissue (334).

The second article published also detailing the decellularisation of human pancreata is that by Sachett et al., in 2018. It provided novel decellularisation methods for the production human pancreas-derived hydrogels (335). The first protocol involved is the decellularization of 1 cm³ pieces of human pancreata by using agitation but the article fails to detail the g-force of the agitation making it hard to compare with the agitation protocols mentioned in this thesis. The decellularised scaffolds produced by this method showed a significant reduction of nuclear material content in comparison to native tissue but ~ 5x fold higher than the scaffolds produced by the perfusion-protocol of this thesis. The second protocol detailed by Sachett et al is truly novel but could only be used to manufacture hydrogels as it involved the complete homogenisation of native tissue prior to decellularisation (335).

5.1.2 Reseeding with PDAC cells

Over 50% of patients with pancreatic cancer are diagnosed at the metastatic stage and die due to the debilitating metabolic effects of their unrestrained growth (1) making this fast progression into a metastatic disease a key feature of PDAC patients. Therefore, in addition to the pancreatic scaffolds, liver scaffolds were introduced to culture PDAC cells. Three cell lines were chosen, PANC-1, MIA PaCa-2, and PK-1. Interestingly, each cell line presented a distinct cell behaviour profile on the different scaffolds. PANC-1 cells appeared to invade deeper into the pancreatic tissue than in the liver scaffolds. PANC-1 cells are defined metastatic, as these cells were isolated from a patient which was presented with local invasion to the duodenal wall and metastasis to one lymph node (297). Upon further investigation, many publications have defined and used PANC-1 cells as their non-metastatic models. Indeed, there is a correlation with the observed pattern in our models compared to *in vivo* results from other groups (336-338). Suemizu et al. tested the metastatic behaviour of 7 PDAC cell

line in NOG mice. Liver metastasis was evaluated 6 weeks after the inoculation of 1×10^4 cells, and although PANC-1 cells did attach to the livers, they presented the lowest surface area increase when compared to the other cell lines (339). Additionally, PANC-1 cells in both pancreatic and liver scaffolds presented, through IHC, positive Ki67 and negative ASP17 stainings', which indicated their proliferative status and the lack of apoptotic cells, respectively.

MIA PaCa-2 cells showed a similar pattern of invasion in both the pancreatic and liver scaffolds. Cells seem to migrate in single units rather than groups of aggregates. When compared to *in vivo* results in NOG mice MIA PaCa-2 cells showed more than 2 folds increase in liver surface area when compared to any other cell line and had invaded over 60% of the livers (339). Indeed, other groups have also reported the ability of MIA PaCa-2 cells to easily metastasise the liver (192, 340, 341), which correlates with our *in vitro* model.

PK-1 cells presented very different behaviour between the liver and pancreas scaffolds. When seeded onto the liver scaffolds, these cells managed to invade and attach onto all large vessels and many smaller vessels, but not when seeded onto the pancreas as cells formed thick aggregates on the outer surface of the scaffold, with no indication of deep invasion. PK-1 cells were isolated from a liver metastasis that originated from the body of the pancreas (299). Since its isolation by Kobari et al., in 1984, there have only been 13 publications that have used PK-1 in their studies (342-354). Although, the interesting and obvious difference in behaviour of PK-1 cells between the liver and pancreas scaffolds makes it a perfect cell line to be studied in our model. A possible explanation for the specific attachment of these cells to the vessels of the liver scaffolds and not the pancreas scaffolds is the difference in fibronectin, laminin and collagen IV content within the vessel matrix. As seen in the IHC staining of the decellularised scaffolds (Figure 25). It appears that fibronectin, laminin and collagen IV are more expressed on the vessels of the liver scaffolds than the pancreas scaffolds. Amikura et al. found that PK-1 cells preferred to attach to fibronectin compared to other ECM proteins (352). Additionally, PK-1 cells in both pancreatic and liver scaffolds presented, through IHC, positive Ki67 and negative

ASP17 stainings', which indicated their proliferative status and the lack of apoptotic cells, respectively.

5.2 Retention of Tissue-Specificity within the 3D PDAC Models

5.2.1 Importance of Tissue-specificity for the Accurate Study of PDAC Biology

Secondary hepatic cancer account for 95% of all hepatic malignancies and the major cause of death of PDAC is related to the rapid development of liver metastasis. Bhagwandin et al. perfectly summed up the difficulty of studying metastasis by stating "The utility of cell lines derived from human PDAC, however, has been compromised by the failure of tumours produced with such cells to display the robust metastasis that is so typical of the clinical disease" (338). There is a lack of options available to study metastasis *in vitro* but with the emergence of 3D cultures, several assays have been developed to address the distinct steps of the metastatic cascade. For example invasion assays commonly use Matrigel, a reconstructed ECM, to monitor cell movement through the matrix, usually measured in transwell filters (355). Matrigel is a mixture of laminin, type IV collagen, entactin and heparin sulfate (356), which makes it an inappropriate *in vitro* model to study the interactions that determine cancer development and metastasis. PDACs are epithelial carcinomas, whereas Matrigel is developed from EHS sarcomas (357), thereby the ECM composition within the tumour niche would be relatively different, if not extensively unlike. For example, Matrigel is rich with laminin LM-111, which is absent in most epithelial basement membranes (358).

The importance of the ECM in dictating cellular behaviour and its role in metastasis has been previously well documented (3, 4). Our knowledge of the ECM is still novice but with the emerging techniques and technologies (e.g. decellularisation) we are now able to build a more defined picture of the heterogeneity of the "inter-organ" ECM. By reducing the signal to noise ratio, i.e. eliminating the noise produced by cellular material through decellularisation, Ma et al., were able to identify through proteomics, that in a healthy human pancreas the seven most abundant ECM proteins were (in

order of abundance): COL1A1, COL1A2, COL3A1, COL5A2, COL5A2, COL5A1 and COL6A1 (359). In another study using similar techniques, Versteegen et al., showed that the seven most abundant ECM proteins in a healthy human liver were (in order of abundance): COL3A1, COL1A1, COL1A2, COL6A3, COL5A2, COL4A2 and COL6A2 (360). Due to the vast amount of ECM proteins, which currently stand at 1066 proteins (361), and their possible combinations and quantities, the cues received by cells can lead to very different outcomes. Therefore, following the evident microscopical difference in cell behaviour on the different ECM (pancreas and liver) observed in our models; we investigated the effect of this in further detail.

In our NGS comparative studies, analysis of the “extracellular structure organisation” GO term of PANC-1 cells in pancreas vs liver scaffolds showed that there were 48 significantly DE genes. Of these genes, 39 genes had a LogFC of >0.5 in the liver scaffolds compared to the pancreas scaffolds. In contrast, 7 genes had a LogFC of >0.5 in the pancreas scaffolds compared to the liver scaffolds. Ten collagen subtypes, four laminin subtypes and four proteoglycans were up-regulated in the liver scaffolds. Similarly, the most significantly affected pathway was “ECM-receptor interaction” with further investigation showing that all DE genes associated with this pathway were up-regulated in the liver compared to the pancreas.

These findings are in agreement with the theory that when tumour cells metastasise to distant organs, they are dependent on the successful interaction with the new microenvironment they enter (362). As explained earlier, the structure and composition of microenvironments in the distant organs (which in the case of PANC-1 cells is the liver) are different than in the organ that is the “home” of the primary tumour (which in the case of PANC-1 cells is the pancreas). An increasing amount of evidence suggests that the ECM, and modifications thereof, are key factors determining whether metastatic tumours will develop or not (363). Therefore, comparison with PK-1 cells are necessary to determine the strength of this theory.

Analysis of the “extracellular structure organisation” GO term of PK-1 cells on pancreas vs liver scaffolds showed that there were 46 significantly DE genes. Of these, 20 genes had a LogFC of >0.5 in the liver scaffolds compared to the pancreas scaffold. In contrast, 26 genes had a LogFC of >0.5 in the pancreas scaffolds

compared to the liver scaffolds. It is therefore easily noticeable that there is a difference with PANC-1 cells, as the number of DE genes in this particular GO is more even in the PK-1 cells. In addition, there were only six collagens that were DE, with COL9A3 being up-regulated in the pancreas rather than the liver scaffolds. When investigating significantly impacted pathways, the “ECM-receptor interaction” pathway is not present, but rather there is a larger focus on cell-cycle related pathways. Finally, when investigated upstream regulators, the two most significant regulators in PANC-1 cells were PCOLCE and PCOLCE2, which are upstream of several collagen subunits whereas the two most significant in PK-1 cells were E2F4 and RBL2, which are upstream of several cell cycle related genes.

5.2.2 Role of Tissue-specific ECM in Tumour Progression

Initial experiments aimed at investigating MMP9 using IHC techniques. MMP9 is a protease that is overexpressed during progression of many solid tumour type (364-369) including PDAC (370). In our comparative analysis, we found no noticeable change in expression of MMP9 in PANC-1 cells when cultured on liver or pancreas scaffolds but rather a very noticeable increase was observed in expression of MMP9 in PK-1 cells on liver scaffolds in comparison to pancreas.

Gene expression analysis of MMP9 between cells cultured on pancreas scaffolds, liver scaffolds and on 2D plastic were in agreement with the IHC results. PANC-1 MMP9 gene expression presented no significant change between the pancreas and liver scaffolds. However, this was not the case when comparing the 3D models with the 2D culture, as both 3D models presented a significant up-regulation of MMP9. Interestingly, PK-1 MMP9 gene expression was not significantly up-regulated between pancreas scaffolds and 2D cultures but was significantly up-regulated in the liver scaffolds when compared to pancreas scaffolds and 2D cultures. These results reflect those presented by Hag et al. which show that “2D plastic” *in vitro* PANC-1 cultures express modest amounts of MMP9, and mostly in latent form, whereas PANC-1 in murine *in vivo* models produced more MMP9, particularly in the active form. This

suggests that our *in vitro* 3D models more closely mimic *in vivo* PDAC behaviour in comparison to 2D cultures.

The MMP9 results presented here, alongside the histological discrepancies, bring along a key distinction between migration and invasion. It is very common to consider migration and invasion as synonyms. However, while “migration” occurs in almost every (healthy) biological process (371), “invasion”, and in particular “invasion of carcinomas”, describes the process/ability of a cell to migrate through the ECM of distant organs (372). Accordingly, PANC-1 cells were able to migrate rather than invade the pancreatic scaffolds that represents their natural ECM microenvironment; whereas, they were unable to populate the liver scaffolds because of a lack of invasive capability.

Studies that compare the migration capabilities of two or more PDAC cell lines are limited, but a good example of demonstrating differences between migration and invasion is the comparison between PANC-1 and BxPC-3 cells, an adenocarcinoma of the body of the pancreas (373). One study by Stahle et al., demonstrated that BxPC-3 were five times less motile than PANC-1 cells (374). However, when investigating invasiveness, several reports showed no differences between PANC-1 and BxPC-3 cells (375, 376). Additionally, Tang et al. overexpressed TPFR-2, an inhibitor of MMP9 activity, in PANC-1 cells and presented no reduction in migration but a 60% reduction in invasion (377).

TIMP1 is a protein that functions by establishing direct associations with several target MMPs, including MMP9, and irreversibly inhibits their function (378). However, the gene expression of TIMP1 of PANC-1 in pancreas scaffolds was significantly higher than in liver scaffolds. Additionally, both PANC-1 3D models had a significantly higher TIMP1 expression than in 2D plastic. Both these observations directly contradict the MMP9 results presented earlier. Similarly, PK-1 TIMP1 expressions did not directly correlate with MMP9 expressions. TIMP1 expression was not significantly changed in the pancreas scaffolds in comparison to liver scaffolds, but both the 3D models presented an up-regulated expression. This lack of correlation was addressed by Zhang et al. using IHC to investigate 256 patients with primary gastric carcinoma

(379). It was concluded with clear evidence that an imbalance of MMP9 and TIMP1 expression is presented in later stage carcinoma (380).

To best demonstrate the overall impact of tissue-specific ECM and to fully understand the genotype changes that occur in PANC-1 and PK-1 cells when cultured on pancreas or liver scaffolds, NGS RNAseq was performed. When investigating PANC-1 cells, it was found that 21 GO terms were significantly impacted that directly involved motility and migration. Further investigation into the GO term “cell motility” revealed that there were 115 significantly DE genes of which 87 genes had a LogFC of >0.5 in the liver scaffolds compared to the pancreas scaffolds. In contrast, 28 genes had a LogFC of >0.5 in the pancreas scaffolds compared to the liver scaffolds. Contradictory to our previous results, the only MMP that was significantly affected was MMP9, which was shown to have a LogFC of 0.91 ($p < 0.0001$) in the liver scaffolds in comparison to the pancreas.

Interestingly, two genes that are known to have an activating role to MMP9 were also up-regulated in PANC-1 cells cultured on the liver compared to pancreas scaffolds; namely CDH2 and LEF1. N-cadherin, the protein translated by its gene CDH2, is understood to stimulate collective cell migration. *In vitro* experiments showed that the inhibition of N-cadherin in epithelial cells decreases the ability of cells to migrate on fibronectin (381). Siret et al., presented similar findings when silencing N-cadherin expression in melanoma cells, which proved to disrupt their ability to invade collagen matrices (382). Lymphoid enhancer factor 1 (LEF1), which its expression is commonly altered in different human cancers, was once down-regulated, demonstrated to inhibit colon cancer viability and invasion *in vitro* and growth *in vivo* (383). Additionally, Wang et al., presented a direct link between LEF1 and MMP9, as the knockdown of LEF1 also down-regulated the expression of MMP9 (383). Overexpression of LEF1 was studied by Zhao et al., and showed that it was associated to an increased cancer stem cell-like phenotype (384). Further analysis of our cell motility linked genes showed that there were no known DE activators of MMP9 that were down-regulated or inhibitors that were up-regulated. Moreover, DPYSC3, a gene known to block the expression of MMP9 was down-regulated. Indeed, Yang et al., showed that the knockdown of DPYSC3 gene promoted metastasis in Lewis lung carcinoma cells both *in vitro* and *in vivo* (385).

When investigating PK-1 cells, it was found that 12 GO terms were significantly impacted that directly involved motility and migration. Analysis of the “cell motility” GO term showed that there were 147 significantly DE genes. Interestingly, and contrary to PANC-1 cells, there were more genes up-regulated in the pancreas scaffolds in comparison to the liver. It was found that 51 genes had a LogFC of >0.5 in the liver scaffolds compared to the pancreas scaffolds and 96 genes had a LogFC of >0.5 in the pancreas scaffolds compared to the liver scaffolds. Similar to the PANC-1 cells MMP-9 was up-regulated in the liver scaffolds, nonetheless, MMP1 was also DE expressed but rather up-regulated in the pancreas scaffolds. However, in the case of PK-1 cells, the only gene that was DE (up-regulated in liver scaffolds) that is known to have an activating role to MMP9 was LEF1.

Therefore, in attempt to understand this contradiction in MMP9 expression and its associated genes between PANC-1 and PK-1 cells, the change in expression between PANC-1 and PK-1 on liver scaffolds were directly investigated. Interestingly, it was found that MMP9 was 12.2-fold higher in the PK-1 cells in comparison to the PANC-1 cells. When investigating the difference of the MMP9 LogFCs between PK-1 (liver vs pancreas scaffolds, Figure 72; red arrow) vs PANC-1 (liver vs pancreas scaffolds, Figure 72; green arrow) cells, it was found that the increase in expression of MMP9 was 2.5-fold higher in PK-1 cell compared to PANC-1 cells.

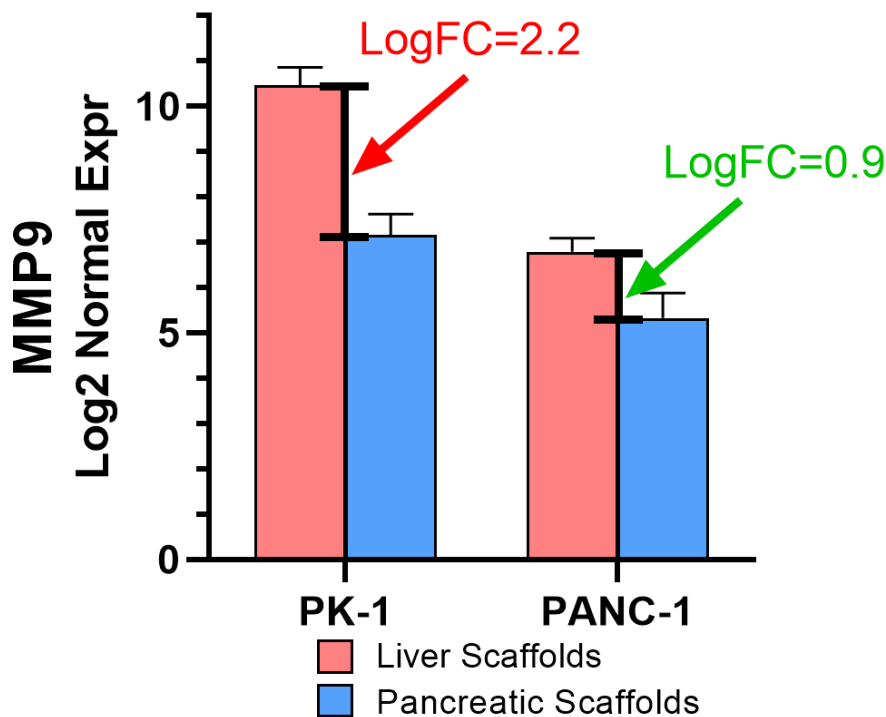


Figure 72. MMP9 gene expression of PK-1 and PANC-1 cells cultured on liver and pancreas scaffolds. Data presented as Log2 normalised expression. Red arrow represents the LogFC of MMP9 expression between PK-1 cells on liver vs pancreas scaffolds. Green arrow represents the LogFC of MMP9 expression between PANC-1 cells on liver vs pancreas scaffolds.

Future work on MMP9 in the PDAC models should include investigating whether MMP9 is in a latent or active form. As mentioned earlier, MMP-9 directly denatures ECM proteins, as well as stimulating cytokines and chemokines to regulate tissue remodelling (386). Latent MMP9 has been shown to bind cell surface receptors, and hence regulating their respective associated pathways, without the need to be activated itself. For example, Monferran et al., demonstrated the ability of latent MMP9 to bind to the Ku heterodimer and as a result regulate several downstream processes (387). Whereas, MMP9 is only able to directly degrade the ECM in an active form (388), therefore, it is important to conduct a zymography to determine the ratio of latent/active MMP9 within the different presented models. Finally, it was also interesting to find that MMP1, MMP10, MMP12, MMP14 and MMP28 were also

significantly up-regulated in PK-1 vs PANC-1 cells in liver scaffolds and therefore, further investigation into their role in invasion vs migration should be investigated.

In addition to cell motility, the GO term “tissue migration” was studied in further detail. Tissue migration is defined as “the process in which the population of cells that make up a tissue undergo directed movement” (316, 317). When investigating PANC-1 cell on pancreas vs liver scaffolds, there were 28 significantly DE genes and of these genes, 21 genes had a LogFC of >0.5 in the liver scaffolds compared to the pancreas. In contrast, 7 genes had a LogFC of >0.5 in the pancreas scaffolds compared to the liver scaffolds. Obviously, the majority of these genes are also involved in the GO of “cell motility”, but four DE genes that were not; namely ACTA1, ACTA2, ACTC1 and ACTG2, which were all up-regulated in the liver scaffolds.

All four genes, ACTA1, ACTA2, ACTC1 and ACTG2, are part of the actin gene family, which consists of seven isoforms (389). Interestingly, the actin cytoskeleton is highly involved in early metastasis and EMT of cancer cells. Peng et al., found that a convergent result of EMT-inducing intrinsic and extrinsic cues is the activation of actin cytoskeleton remodelling for cell morphological or functional change (390). Kakiuchi et al., performed a genome-wide analysis of organ-preferential metastasis and identified all four actin genes; ACTA1, ACTA2, ACTC1 and ACTG2, in addition to ACTB to be predominantly expressed in lung metastasis (391).

Analysis of the “tissue migration” GO term of PK-1 cells in pancreas vs liver scaffolds showed that there were 32 significantly DE genes. Of these genes, 10 genes had a LogFC of >0.5 in the liver scaffolds compared to the pancreas scaffolds. In contrast, 23 genes had a LogFC of >0.5 in the pancreas scaffolds compared to the liver scaffolds. Similar to the PANC-1 analysis, the majority of the DE genes are also involved in the GO of “cell motility” but one DE gene was not, namely GRHL2.

This finding is in agreement with our hypothesis that PK-1 cells on liver scaffolds represent a mature PDAC metastasis. Indeed, human metastases examined histologically appear epithelial in phenotype and resemble the primary tumour (392). In other words, the metastatic nodules are not mesenchymal. Several theories have been put forth to explain this issue. The most popular theory is the Mesenchymal-

Epithelial Transition (MET) (393). GRHL2 is an epithelial-specific transcription factor that regulates epithelial morphogenesis and differentiation (394). Xiang et al. reported that GRHL2 determines the epithelial phenotype of breast cancers and promotes tumour progression (395).

5.3 Tissue-specific PDAC models for the study of Chemoresistance

Resistance to chemotherapy treatment causes disease relapse, dissemination and morbid outcomes for patient OS. Chemoresistance arises when there are challenges in the local, cellular and/or molecular delivery of an anticancer agent to its target. The mechanisms promoting a resistance to treatment are related to both pre-existing and acquired phenotypes regulated by intrinsic genetic factors and the extrinsic tumour microenvironment.

Biological chemoresistance can be generally classified into two broad categories: innate/intrinsic, due to genetic factors, or acquired resistance where cancer cells develop resistance after showing initial sensitivity to treatment. Biological chemoresistance will often occur within weeks of initiating chemotherapy (252). Genetic factors that regulate signalling pathways, fundamental to cancer cell behaviour, such as growth, differentiation, apoptosis, angiogenesis, and motility will certainly influence sensitivity to treatment.

For treatment to provide therapeutic benefit, it first depends on the drug's ability to penetrate into the tumour area to access the cancer target. This can be challenging as stromal changes occur during malignancy to favour chemoresistance and a physical barrier of various cell types is created between the microvasculature and the cancer target (255). After access to the tumour environment has been established, a drug must then prove its metabolic availability and activity to be effective at a cellular and molecular level.

As mentioned, most pancreatic cancers are unresectable at the time of diagnosis and less than 20% of patients are able to undergo surgery as a main treatment option (201) – tumour resection being the only treatment strategy with curative potential (252). Survival for the majority of patients therefore largely depends on the available chemotherapeutic treatments. The current treatments available for pancreatic cancer, however, have not proven to be highly effective (201). Suboptimal effectiveness can be due to limitations in cellular uptake and metabolic activity of the drug. This conveys a clinical crisis for pancreatic cancer treatment. Pancreatic cancer has a 5-year OS rate of <10% worldwide (256), highlighting the unmet need to develop novel treatment strategies.

PDAC is considered one of the cancers most resistant to chemotherapeutic drugs. This, combined with the tendency of a delay in diagnosis, makes pancreatic cancer one of the most fatal cancers (252). The difficulty to treat signifies a poor outcome for patient prognosis and is illustrated by the fact that the majority of available treatments for PDAC are mostly palliative with a focus on improving the quality of life for the patient rather than being able to offer a curative outcome (198).

5.3.1 Increase in Chemoresistance of PDAC cells in Tissue-specific ECM models

The current first-line option for late-stage PDAC treatment is Gemcitabine in combination with other therapeutics. The results for survival outcome, OS and PFS, for the current available treatments are not overwhelming. A recent systematic review for different combinations of Gemcitabine with other agents reveals the lack of long-term effectiveness in chemotherapy treatment for pancreatic cancer. The median for OS is currently 8.1 months with a highest OS of 35.5 months (Gemcitabine and cisplatin), and PFS ranges from 2.4 to 11.0 months (201). Despite this, Gemcitabine has proven to be the most promising candidate for chemotherapy treatment since 1997 (257), most effective as a combined therapy.

Therefore, initial work has focused on proving that our models deliver a more realistic *in vivo* “human-like” chemotherapeutic response in comparison to 2D cultures. All cells, PANC-1, MIA PaCa-2 and PK-1 cells, presented a significantly higher resistance to both Gemcitabine and Doxorubicin in the 3D scaffolds (pancreas or liver) in comparison to 2D cultures. Focusing on Gemcitabine, treated PANC-1 cells had no significant change in cell survival between the pancreas and liver scaffolds and the difference in survival between the 3D models and 2D cultures was around 30%. When compared to published work, Wen et al. presented a spheroid-based 3D PDAC culture model, using the liquid overlay technique, which showed a ~6% difference in PANC-1 cell survival in comparison to 2D cultures at 0.5µm Gemcitabine concentration (396). Similarly, Longati et al. formed compact 3D PDAC spheroids, that also lacked an endogenous ECM. PANC-1 spheroids of that model showed a 20% increase in cell survival when treated with 1 µm Gemcitabine compared to 2D models (397). Several other groups reported an increase in Gemcitabine resistance of PANC-1 cells in their 3D models but lacked information for direct comparison with our models. For example, Yang et al. created PANC-1 spheroids in Matrigels and showed a ~1.5-fold increase in the IC₅₀ of PANC-1 cells when treated with Gemcitabine (398).

MIA PaCa-2 cells treated with 0.5µm Gemcitabine similarly had no significant change in cell survival between the pancreas and liver scaffolds. The difference in survival between the pancreas model and 2D cultures was around 37% and between the liver model and 2D cultures was around 45%. In comparison to published material, Wen et al. using the same spheroid-based 3D PDAC culture model mentioned above, found a ~10% difference in MIA PaCa-2 cell survival in comparison to 2D cultures at 0.5µm Gemcitabine concentration (396). Unlike work on PANC-1 cells, Wen et al. was the only article published that reported a direct comparison of MIA PaCa-2 cell viability after treatment with Gemcitabine between a 3D and 2D culture.

PK-1 cells treated with 0.5µm Gemcitabine were the only cell line that showed a significant change in cell survival between the pancreas and liver scaffolds, with a higher resistance in the pancreas scaffolds. The difference in survival between the pancreas model and 2D cultures was around 65% and between the liver model and 2D cultures was around 35%. Unfortunately, due to a lack of 3D *in vitro* metastatic models, there are no published articles that compare a 3D PK-1 model with a 2D culture, in terms of chemoresistance and particularly Gemcitabine.

As discussed above, the first line of chemoresistance is that of physiological nature, with the stromal compartment, particularly the ECM, blocking chemotherapeutics reaching the tumour cells. The second line of chemoresistance is biological, which involves (i) reduced drug uptake, (ii) mutations of nucleoside transporters, (iii) increased efflux and (iv) increased expression of anti-apoptotic proteins (399-402). Therefore, it was important to prove that the chemotherapy drugs were able to reach the cells through the scaffolds (physiological chemoresistance). Unfortunately, it is difficult to prove the uptake and localisation of Gemcitabine to the nucleus, as it is not fluorescent. However, the natural fluorescence of Doxorubicin can be utilised to prove that chemoresistance observed in the 3D cultures was not just a consequence of the chemotherapeutics' inability to penetrate the ECM due to a lack of a functional vasculature within the 3D models presented. Fluorescent microscopy of cryo-sectioned Doxorubicin treated PANC-1, MIA PaCa-2 and PK-1 cells cultured on pancreas scaffolds presented a positive signal for doxorubicin and interestingly this was localised to the nucleus.

5.3.2 Role of the ECM in Gemcitabine Resistance of PDAC cells

As mentioned earlier, unlike other tumours, PDAC is characterised by the presence of a hypovascularised, densely fibrous stroma. The total tumour volume is largely comprised of scar tissue, also known as desmoplasia, which encompasses the malignant epithelial cells (276). Dense stromal fibrosis is characteristic of PDAC and its main component, apart from the ECM, is pancreatic cancer-associated fibroblasts (CAFs). CAFs are the main fibrosis-producing cells and mainly originate from pancreatic stellate cells (PSCs) (277). Therefore, for an accurate understanding of PDAC chemoresistance, it is important to take into consideration all the factors that contribute to the overwhelming failure of tumour response to chemotherapeutics. However, to build a bottom-up approach, we eliminated many of the variables that contribute to the extensively dense fibrous stroma and focused only on the influence of the ECM.

To study the influence of the ECM on the biological chemoresistance of PDAC, NGS was deployed on Gemcitabine treated PANC-1 and PK-1 models on pancreas and liver scaffolds, respectively. When comparing between Gemcitabine treated and untreated (control) PANC-1 cells on pancreas scaffolds, 2879 DE genes were identified with a logFC >0.5. Of these, 2220 genes were up-regulated, and 659 genes were down-regulated in the Gemcitabine treated cells, when compared to those that were left untreated. These genes contributed to 42 significantly impacted pathways, 1308 GO terms and 278 upstream regulators. When comparing between Gemcitabine treated and untreated PK-1 cells on liver scaffolds, 1587 DE genes were identified with a logFC >0.5. Of these, 1242 genes were up-regulated, and 343 genes were down-regulated in the Gemcitabine treated PK-1 cells, when compared to those that were left untreated. These genes contributed to 57 significantly impacted pathways, 1692 GO terms and 418 upstream regulators.

5.3.2.1 Role of ECM on the Gemcitabine Metabolism Pathways of PDAC Cells

To reflect on the results presented by the NGS data, analysis of the chemoresistance entities associated with Gemcitabine metabolism pathways (Figure 73) were investigated. Gemcitabine (also known as dFdC) enters PDAC cells through nucleoside transporters, namely hENT1, hCNT1 and hCNT3. It has been demonstrated by several groups that patients with low tumour expression of nucleoside transporters show significantly worse survival compared to patients with high levels following Gemcitabine treatment (400, 403-405). In our models, the expression of both hENT1 and hCNT1 were found to be unchanged in both Gemcitabine treated PANC-1 cells on pancreas scaffolds and PK-1 on liver scaffolds. The expression of hCNT3 was unchanged in Gemcitabine treated PANC-1 cells on pancreas scaffolds, but was up-regulated in PK-1 cells on liver scaffolds. Hence, the ECM alone does not appear to be a sole contributor to Gemcitabine chemoresistance through the down-regulation of nucleoside transporters, hENT1, hCNT1 and hCNT3. Indeed, Hesler et al. found that CYR61 negatively regulates the nucleoside transporters hENT1 and hCNT3 and that the source of CYR61 protein was PSC cells (406). Additionally, Saiki et al. demonstrated that even though there was a rapid uptake of Gemcitabine into PK-1 cells, it did not result in any DNA damage (289).

(410). Similar to dCK, the expression of all the named genes were unaffected by Gemcitabine treatment in PANC-1 cells on pancreas scaffolds or PK-1 on liver scaffolds.

Other than the proteins involved in metabolising and activating Gemcitabine to reach and incorporate into the DNA, some proteins are involved in deactivating and eliminating Gemcitabine from the cell. Major inactivation of Gemcitabine (dFdC) occurs through cytidine deaminase (CDA)-induced deamination of Gemcitabine to a uracil Gemcitabine metabolite (dFdU) (411), which is in turn degraded and excreted out of the cells. High CDA expression has been shown to correlate with OS in pancreatic cancer patients, as well as preclinical responses to Gemcitabine (294, 412-414). In line with this, *in vitro* findings show that an up-regulation of CDA results in Gemcitabine resistance, while loss of CDA restores Gemcitabine sensitivity (294, 415, 416). Interestingly, the more resistant PANC-1 cells on our pancreas scaffolds were found to have a 3-fold higher expression of CDA in the Gemcitabine treated samples compared to untreated samples, whereas, the more sensitive (but still resistant) PK-1 cells on liver scaffolds had no change in the expression of CDA between Gemcitabine treated and untreated samples.

Additionally, Cellular 5' -nucleotidase (5'-NT), another Gemcitabine deactivator, opposes the activity of dCK via dephosphorylation of Gemcitabine monophosphate. This results in partial inactivation of Gemcitabine by preventing formation of Gemcitabine triphosphate (417). As such, 5'-NT levels may be one of the factors influencing the clinical outcome of Gemcitabine therapy. In our models, the expression of 5'-NT was unchanged in either Gemcitabine treated PANC-1 cells on pancreas scaffolds or PK-1 on liver scaffolds compared to their respective controls.

Further, Ribonucleotide reductase (RR); a rate-limiting enzyme of the DNA synthesis pathway, which consists of two subunits RRM1 and RRM2 have proved to be involved in Gemcitabine resistance. In pancreatic cancer patients treated with Gemcitabine, low RRM1 levels correlate with high OS whereas high RRM1 expression is linked to poor survival. This suggests an important role for RRM1 in intrinsic resistance to Gemcitabine (400, 408, 418). Moreover, inhibition of RR indirectly facilitates Gemcitabine triphosphate incorporation into DNA. Gemcitabine diphosphate-induced

inhibition of RR is thus a primary mechanism involved in the potentiation of Gemcitabine activity (419, 420). In our Gemcitabine treated PANC-1 cells on pancreas scaffolds and PK-1 on liver scaffolds models, the expression of both RRM1 and RRM2 were highly up-regulated compared to their respective control samples. Notably, Wang et al. found that in PANC-1 cells, overexpression of both RRM1 and RRM2 is necessary for the development of Gemcitabine resistance (421). However, in regards to PK-1 cells in 2D cultures, Nakano et al. found no change of RRM1 expression and a slight up-regulation of RRM2 after Gemcitabine treatment (404). These results may indicate an important role of the ECM towards Gemcitabine resistance through the up-regulation of RRM1 and RRM2 in pancreatic cancer.

5.3.2.2 Role of ECM on the anti-apoptotic pathways of PDAC Cells

As it became clear that the ECM plays a minor role on the Gemcitabine resistance pathways, we proceeded to investigate the anti-apoptotic pathways. It was evident that both PANC-1 and PK-1 cells in their respective tissue-specific ECM, increased all mechanisms involved in cell cycle progression and DNA repair, which (i) indicates that Gemcitabine reached and incorporated itself into the DNA strands and (ii) the cells responded by promoting cell cycle progression and proliferation.

The most significantly impacted pathway in PANC-1 cells on pancreas scaffolds treated with Gemcitabine was the “Cytokine-Cytokine Receptor” pathways. Out of all DE expressed cytokine receptors, 25 receptors except for CCR6, CX3CR1 and LEPR, were up-regulated in the Gemcitabine treated samples. Of these up-regulated cytokine receptors, nine are directly involved with the TNF family. Similarly, the fourth most significantly impacted pathway in PK-1 cells on liver scaffolds treated with Gemcitabine was the “Cytokine-Cytokine Receptor” pathways. Out of all DE expressed cytokine receptors, 13 receptors except for CSF3R and LEPR, were up-regulated in the Gemcitabine treated samples. Of these up-regulated cytokine receptors, five are directly involved with the TNF family. TNF represents one of the

most important activators of the NF- κ B “canonical pathway” (422). The NF- κ B signal transduction pathways is implicated in the resistance of numerous solid tumours against a variety of anticancer drugs (423).

Additionally, significantly impacted pathways in PANC-1 cells on pancreas scaffolds treated with Gemcitabine include “DNA replication” and “Cell cycle”. Differentially expressed genes involved in “DNA replication” were all up-regulated in the treated samples compared to the control. The most up-regulated gene was DNA2, which has previously been documented to be directly involved with PDAC cell survival and xenograft tumour growth (424). Moreover, 83% of DE genes involved in “Cell cycle” were up-regulated in the treated samples compared to the control. Significantly impacted pathways in PK-1 cells on liver scaffolds treated with Gemcitabine include “DNA replication”, “Cell cycle”, “Homologous recombination” and “Mismatch repair”. Interestingly, in all these pathways, every single DE gene was up-regulated in the Gemcitabine treated samples.

Finally, GO terms involved in “Cell adhesion”, “Cell Motility” and “Extracellular structure organisation” were further analysed. When investigating the GO “Cell adhesion” of PANC-1 cells on pancreas scaffolds treated with Gemcitabine, fourteen integrin’s were found to be >0.5 LogFC up-regulated in the treated samples. Whereas when investigating the GO “Cell adhesion” of PK-1 cells on liver scaffolds treated with Gemcitabine, only two integrin’s were found to be >0.5 LogFC up-regulated in the treated samples, ITGAL and ITGAX. These results are in correlation with Iseri et al., which studied stepwise selected resistant MCF-7 cells (breast cancer) and found that the most resistant cells up-regulated several integrin subunit genes (425).

The GO term “Cell Motility” revealed that both MMP1 and MMP9 were >0.5 LogFC up-regulated in the PANC-1 treated samples. Whereas in the PK-1 cells, MMP1 was up-regulated and MMP28 was down-regulated in the treated samples. Interestingly, there is no published work directly linking cell motility to chemoresistance, even though clinical data links an increase in metastasis in patients that resist chemotherapy (426,

427). Additionally, down-regulation of MMP28 in the metastatic model (PK-1 on liver scaffolds) could point towards a decrease in further metastasis in already metastasised tumours; Jian et al., demonstrated that MMP28 is a promoter of invasion and metastasis in gastric cancer (428).

Investigation of the GO term “Extracellular structure organisation” showed that in PANC-1 cell in pancreas scaffolds, eight collagen subtypes namely; COL2A1, COL3A1, COL4A2, COL6A3, COL7A1, COL8A2, COL9A3, COL11A2 were up-regulated in the treated samples and two subtypes, COL11A1 and COL5A2 were down-regulated. Whereas, PK-1 cell in liver scaffolds showed that one collagen subtype, COL16A1, was up-regulated in the treated samples and three subtypes, COL5A2, COL6A1 and COL9A2, were down-regulated. The ECM involvement in chemoresistance in primary vs metastatic PDAC, and other tumours, is not well understood but could be linked to cancer progression as discussed extensively earlier (Section 5.2.1).

To be able to gain a better understanding of the results obtained by the NGS data of Gemcitabine treated PDAC models, healthy pancreatic ductal cells should be cultured onto both pancreas and liver scaffolds to create a healthy *in vitro* model as a control to the existing PDAC models. H6C7 cells are an immortal epithelial cell line established after transduction of the HPV16-E6E7 genes into primary cultures of normal pancreatic duct epithelial cells (429). Single clones were isolated that demonstrated near normal genotype and phenotype (429). The cell line demonstrates many phenotypes of normal pancreatic duct epithelium, including mRNA expression of carbonic anhydrase II, MUC-1, and cytokeratin’s 7, 8, 18, and 19, as well as normal Ki-ras, p53, c-myc, and p16INK4A genotypes (429). Therefore, H6C7 models, both Gemcitabine treated and untreated, on pancreas and liver scaffolds should be sequenced using RNAseq and compared to the PDAC model dataset. This added comparison should provide insight into false positive PDAC gene expression.

6. CONCLUSION

In the presented thesis, decellularised human pancreata and livers were utilised as a scaffold for *in vitro* primary and metastatic PDAC models, respectively. Decellularised tissue from other organs have previously been utilised as *in vitro* 3D scaffolds for human tumour modelling, e.g. liver (1, 2), lung (3, 4), breast and adipose tissue (5, 6), and intestinal tissue (7, 8) but have not been described for PDAC.

When initiating this project, there were no published articles related to the decellularisation of human pancreata. Therefore, decellularisation protocols from other human organs had to be optimised to achieve scaffolds that eliminated cellular debris while preserving the ECM proteins and microarchitecture. After evaluating several strategies, we achieved successful decellularisation using a retrograde perfusion protocol. Characterisation of the decellularised pancreata showed no visible nuclear or cellular material, and DNA content was below 100ng/mg. Additionally, collagen I, III, IV, laminin and fibronectin as well as the microarchitecture were well preserved.

This technical achievement allowed the use of pancreatic scaffolds, along with liver scaffolds, as tissue-specific 3D cultures for PDAC cells. The cells chosen were PANC-1; a primary PDAC cell line with low metastatic potential, MIA PaCa-2; a primary PDAC cell line with a moderate metastatic potential and PK-1; a PDAC cell line isolated from the liver metastasis. Initially, histological analysis demonstrated that these cells exhibited different cellular behaviour depending on the tissue they were cultured on, i.e. pancreas or liver. Further, qPCR presented an altered expression of several ECM and EMT related genes between the 3D and 2D cultures.

Next generation sequencing of PANC-1 and PK-1 cells on pancreas and liver scaffolds presented exciting results that were exploited to identify important biological steps that progress PDAC from a primary tumour towards a mature metastatic tumour. These included understanding of the EMT process, initiated by primary cells in early metastasis and the MET process, initiated in mature metastasis. We further

established a differentiation between cell migration and invasion, which involved MMP9 and its associated genes/protein. Additionally, the contribution of PDAC cells towards ECM remodelling was also investigated; this included distinct differences in collagen and laminin subunits at the primary and metastatic site.

Finally, primary (PANC-1 on pancreas scaffolds) and metastatic (PK-1 on liver scaffolds) PDAC models were utilised to examine tissue-specific chemoresistance to Gemcitabine. Viability assays showed an increase of chemoresistance in the 3D models in comparison to 2D cultures, despite the drugs reaching the desired target within the PDAC cells. Similarly, NGS was performed on the 3D models to compare Gemcitabine treated and untreated (control) samples. It was found that the ECM did not particularly affect the Gemcitabine resistance pathway but rather prompted downstream regulators that allowed the PDAC cells to bypass apoptosis and progress through their cell cycle despite the DNA damage caused by Gemcitabine. Additionally, the expression of several cell adhesion molecules, as well as cell motility and ECM regulators were found to be altered in treated samples.

These results suggest that primary and metastatic PDAC cells manifest a conserved invasive behaviour depending on the 3D ECM structure of origin. Moreover, there is an evident alteration in cell response to cancer-therapies in the presence of a tissue-specific ECM niche. These observations provide a proof of concept for the development of an effective bio-engineered model for novel drug discovery, therapy screening and biomarker discovery.

REFERENCES

1. Li D, Xie K, Wolff R, Abbruzzese JL. Pancreatic cancer. *The Lancet*. 363(9414):1049-57.
2. Martinez-Hernandez A, Amenta PS. The hepatic extracellular-matrix. 1. Components and distribution in normal liver. *Virchows Archiv a-Pathological Anatomy and Histopathology*. 1993b;423(1):1-11.
3. Badylak SE, Gilbert TW. Immune response to biologic scaffold materials. *Seminars in Immunology*. 2008;20(2):109-16.
4. Badylak SF, Freytes DO, Gilbert TW. Extracellular matrix as a biological scaffold material: Structure and function. *Acta Biomater*. 2009;5(1):1-13.
5. Evangelatov A, Pankov R. The Evolution of Three-Dimensional Cell Cultures Towards Unimpeded Regenerative Medicine and Tissue Engineering. In: Andrades JA, editor. *Regenerative Medicine and Tissue Engineering*. Rijeka: InTech; 2013. p. Ch. 10.
6. Sheehy EJ, Cunniffe GM, O'Brien FJ. 5 - Collagen-based biomaterials for tissue regeneration and repair. In: Barbosa MA, Martins MCL, editors. *Peptides and Proteins as Biomaterials for Tissue Regeneration and Repair*: Woodhead Publishing; 2018. p. 127-50.
7. Saxena T, Karumbaiah L, Valmikinathan CM. Chapter 3 - Proteins and Poly(Amino Acids). In: Kumbar SG, Laurencin CT, Deng M, editors. *Natural and Synthetic Biomedical Polymers*. Oxford: Elsevier; 2014. p. 43-65.
8. Shoulders MD, Raines RT. Collagen structure and stability. *Annu Rev Biochem*. 2009;78:929-58.
9. Wang X, Ali MS, Lacerda CMR. A Three-Dimensional Collagen-Elastin Scaffold for Heart Valve Tissue Engineering. *Bioengineering (Basel)*. 2018;5(3).
10. Wang D-D, Liu W, Chang J-J, Cheng X, Zhang X-Z, Xu H, et al. Bioengineering three-dimensional culture model of human lung cancer cells: an improved tool for screening EGFR targeted inhibitors. *RSC Advances*. 2016;6(29):24083-90.
11. Puls TJ, Tan X, Whittington CF, Voytik-Harbin SL. 3D collagen fibrillar microstructure guides pancreatic cancer cell phenotype and serves as a critical design parameter for phenotypic models of EMT. *PLoS One*. 2017;12(11):e0188870.
12. Lee SJ, Wang HJ, Kim TH, Choi JS, Kulkarni G, Jackson JD, et al. In Situ Tissue Regeneration of Renal Tissue Induced by Collagen Hydrogel Injection. *Stem Cells Transl Med*. 2018;7(2):241-50.

13. Hussein K, Park K-M, Lee Y-S, Woo J-S, Kang B-J, Choi K-Y, et al. New insights into the pros and cons of cross-linking decellularized bioartificial organs. *The International journal of artificial organs*. 2017;40.
14. Li Y, Ju D. Chapter 12 - The Application, Neurotoxicity, and Related Mechanism of Cationic Polymers**Conflict of Interests: All the Figures and Table in “The application, neurotoxicity, and related mechanism of cationic polymers” are original, unpublished materials designed and prepared by Yubin Li and Dianwen Ju. The authors declared that there’s no conflict of interests. In: Jiang X, Gao H, editors. *Neurotoxicity of Nanomaterials and Nanomedicine*: Academic Press; 2017. p. 285-329.
15. Habibi Y, Lucia LA. *Polysaccharide Building Blocks: A Sustainable Approach to the Development of Renewable Biomaterials*: Wiley; 2012.
16. Harish Prashanth KV, Tharanathan RN. Crosslinked chitosan—preparation and characterization. *Carbohydrate Research*. 2006;341(1):169-73.
17. Han CM, Zhang LP, Sun JZ, Shi HF, Zhou J, Gao CY. Application of collagen-chitosan/fibrin glue asymmetric scaffolds in skin tissue engineering. *J Zhejiang Univ Sci B*. 2010;11(7):524-30.
18. Silva SS, Caridade SG, Mano JF, Reis RL. Effect of crosslinking in chitosan/aloe vera-based membranes for biomedical applications. *Carbohydrate Polymers*. 2013;98(1):581-8.
19. Boucard N, Viton C, Agay D, Mari E, Roger T, Chancerelle Y, et al. The use of physical hydrogels of chitosan for skin regeneration following third-degree burns. *Biomaterials*. 2007;28(24):3478-88.
20. Meng D, Dong L, Wen Y, Xie Q. Effects of adding resorbable chitosan microspheres to calcium phosphate cements for bone regeneration. *Mater Sci Eng C Mater Biol Appl*. 2015;47:266-72.
21. Ge S, Zhao N, Wang L, Yu M, Liu H, Song A, et al. Bone repair by periodontal ligament stem cellseeded nanohydroxyapatite-chitosan scaffold. *Int J Nanomedicine*. 2012;7:5405-14.
22. Alves da Silva ML, Crawford A, Mundy JM, Correlo VM, Sol P, Bhattacharya M, et al. Chitosan/polyester-based scaffolds for cartilage tissue engineering: assessment of extracellular matrix formation. *Acta Biomater*. 2010;6(3):1149-57.
23. Yan LP, Wang YJ, Ren L, Wu G, Caridade SG, Fan JB, et al. Genipin-cross-linked collagen/chitosan biomimetic scaffolds for articular cartilage tissue engineering applications. *J Biomed Mater Res A*. 2010;95(2):465-75.
24. Silva JM, Georgi N, Costa R, Sher P, Reis RL, Van Blitterswijk CA, et al. Nanostructured 3D constructs based on chitosan and chondroitin sulphate multilayers for cartilage tissue engineering. *PLoS One*. 2013;8(2):e55451.

25. Pusateri AE, McCarthy SJ, Gregory KW, Harris RA, Cardenas L, McManus AT, et al. Effect of a chitosan-based hemostatic dressing on blood loss and survival in a model of severe venous hemorrhage and hepatic injury in swine. *J Trauma*. 2003;54(1):177-82.
26. LeHoux JG, Grondin F. Some effects of chitosan on liver function in the rat. *Endocrinology*. 1993;132(3):1078-84.
27. H Borai I, Hanafi N, A M, I K Kandil M, Arafa, Kandil E. Role of Chitosan Nanoparticles in Reducing Pancreatitis in Rats Treated with L-arginine. 2017;7.
28. Cui W, Kim DH, Imamura M, Hyon SH, Inoue K. Tissue-engineered pancreatic islets: culturing rat islets in the chitosan sponge. *Cell Transplant*. 2001;10(4-5):499-502.
29. Yin R, He J, Bai M, Huang C, Wang K, Zhang H, et al. Engineering synthetic artificial pancreas using chitosan hydrogels integrated with glucose-responsive microspheres for insulin delivery. *Materials Science and Engineering: C*. 2019;96:374-82.
30. Nair LS, Laurencin CT. Biodegradable polymers as biomaterials. *Progress in Polymer Science*. 2007;32(8):762-98.
31. Ramakrishna S, Mayer J, Wintermantel E, Leong KW. Biomedical applications of polymer-composite materials: a review. *Composites Science and Technology*. 2001;61(9):1189-224.
32. Chatelet C, Damour O, Domard A. Influence of the degree of acetylation on some biological properties of chitosan films. *Biomaterials*. 2001;22(3):261-8.
33. Antonia Lizarbe M. Sustitutivos de tejidos: de los biomateriales a la ingeniería tisular. 2007;101.
34. Kiuchi H, Kai W, Inoue Y. Preparation and characterization of poly(ethylene glycol) crosslinked chitosan films. *Journal of Applied Polymer Science*. 2008;107(6):3823-30.
35. Adekogbe I, Ghanem A. Fabrication and characterization of DTBP-crosslinked chitosan scaffolds for skin tissue engineering. *Biomaterials*. 2005;26(35):7241-50.
36. Szymańska E, Winnicka K. Stability of chitosan-a challenge for pharmaceutical and biomedical applications. *Mar Drugs*. 2015;13(4):1819-46.
37. Fu J, Yang F, Guo Z. The chitosan hydrogels: from structure to function. *New Journal of Chemistry*. 2018;42(21):17162-80.
38. Bellich B, D'Agostino I, Semeraro S, Gamini A, Cesàro A. "The Good, the Bad and the Ugly" of Chitosans. *Mar Drugs*. 2016;14(5):99.
39. Croisier F, Jérôme C. Chitosan-based biomaterials for tissue engineering. *European Polymer Journal*. 2013;49(4):780-92.
40. Usov AI. Polysaccharides of the red algae. *Adv Carbohydr Chem Biochem*. 2011;65:115-217.

41. Bao X, Hayashi K, Li Y, Teramoto A, Abe K. Novel agarose and agar fibers: Fabrication and characterization. *Materials Letters*. 2010;64(22):2435-7.
42. Forget A, Arya N, Randriantsilefisoa R, Miessmer F, Buck M, Ahmadi V, et al. Nonwoven Carboxylated Agarose-Based Fiber Meshes with Antimicrobial Properties. *Biomacromolecules*. 2016;17(12):4021-6.
43. Lewitus DY, Landers J, Branch J, Smith KL, Callegari G, Kohn J, et al. Biohybrid Carbon Nanotube/Agarose Fibers for Neural Tissue Engineering. *Adv Funct Mater*. 2011;21(14):2624-32.
44. Cigan AD, Roach BL, Nims RJ, Tan AR, Albro MB, Stoker AM, et al. High seeding density of human chondrocytes in agarose produces tissue-engineered cartilage approaching native mechanical and biochemical properties. *Journal of Biomechanics*. 2016;49(9):1909-17.
45. Garcia-Martinez L, Campos F, Godoy-Guzman C, Del Carmen Sanchez-Quevedo M, Garzon I, Alaminos M, et al. Encapsulation of human elastic cartilage-derived chondrocytes in nanostructured fibrin-agarose hydrogels. *Histochem Cell Biol*. 2017;147(1):83-95.
46. Bloch K, Vanichkin A, Damshkaln LG, Lozinsky VI, Vardi P. Vascularization of wide pore agarose–gelatin cryogel scaffolds implanted subcutaneously in diabetic and non-diabetic mice. *Acta Biomaterialia*. 2010;6(3):1200-5.
47. Stokols S, Tuszynski MH. Freeze-dried agarose scaffolds with uniaxial channels stimulate and guide linear axonal growth following spinal cord injury. *Biomaterials*. 2006;27(3):443-51.
48. Iwata H, Takagi T, Amemiya H, Shimizu H, Yamashita K, Kobayashi K, et al. Agarose for a bioartificial pancreas. *J Biomed Mater Res*. 1992;26(7):967-77.
49. Tripathi A, Melo J. Preparation of sponge-like biocomposite agarose-chitosan scaffold with primary hepatocytes for establishing an in-vitro 3D liver tissue model. *RSC Adv*. 2015;5.
50. Zarrintaj P, Manouchehri S, Ahmadi Z, Saeb MR, Urbanska AM, Kaplan DL, et al. Agarose-based biomaterials for tissue engineering. *Carbohydrate Polymers*. 2018;187:66-84.
51. Mooney DJ, Mazzoni CL, Breuer C, McNamara K, Hern D, Vacanti JP, et al. Stabilized polyglycolic acid fibre-based tubes for tissue engineering. In: Williams DF, editor. *The Biomaterials: Silver Jubilee Compendium*. Oxford: Elsevier Science; 1996. p. 129-38.
52. Niaounakis M. 7 - Degradability on Demand. In: Niaounakis M, editor. *Biopolymers Reuse, Recycling, and Disposal*. Oxford: William Andrew Publishing; 2013. p. 193-241.
53. Rudnik E. Chapter 3 - Properties and applications. In: Rudnik E, editor. *Compostable Polymer Materials (Second Edition)*. Boston: Elsevier; 2019. p. 49-98.

54. Lin YM, Boccaccini AR, Polak JM, Bishop AE, Maquet V. Biocompatibility of poly-DL-lactic acid (PDLLA) for lung tissue engineering. *J Biomater Appl.* 2006;21(2):109-18.
55. Jeon S, Han J, Jeong W, Son J, Kim JB, Kang H-W. Flexibility Enhancement of Poly(lactide-co-glycolide) for Fused Deposition Modeling Technology. *International Journal of Precision Engineering and Manufacturing-Green Technology.* 2019;6(3):465-75.
56. Park JK, Utsumi T, Seo YE, Deng Y, Satoh A, Saltzman WM, et al. Cellular distribution of injected PLGA-nanoparticles in the liver. *Nanomedicine.* 2016;12(5):1365-74.
57. Sadeghi-Avalshahr A, Nokhasteh S, Molavi AM, Khorsand-Ghayeni M, Mahdavi-Shahri M. Synthesis and characterization of collagen/PLGA biodegradable skin scaffold fibers. *Regen Biomater.* 2017;4(5):309-14.
58. Gentile P, Chiono V, Carmagnola I, Hatton PV. An overview of poly(lactic-co-glycolic) acid (PLGA)-based biomaterials for bone tissue engineering. *International journal of molecular sciences.* 2014;15(3):3640-59.
59. Caminal M, Peris D, Fonseca C, Barrachina J, Codina D, Rabanal RM, et al. Cartilage resurfacing potential of PLGA scaffolds loaded with autologous cells from cartilage, fat, and bone marrow in an ovine model of osteochondral focal defect. *Cytotechnology.* 2016;68(4):907-19.
60. Kim M, Choi YS, Yang SH, Hong HN, Cho SW, Cha SM, et al. Muscle regeneration by adipose tissue-derived adult stem cells attached to injectable PLGA spheres. *Biochem Biophys Res Commun.* 2006;348(2):386-92.
61. Yu T, Zhao C, Li P, Liu G, Luo M. Poly(lactic-co-glycolic acid) conduit for repair of injured sciatic nerve: A mechanical analysis. *Neural Regen Res.* 2013;8(21):1966-73.
62. Woodard LN, Grunlan MA. Hydrolytic Degradation and Erosion of Polyester Biomaterials. *ACS Macro Lett.* 2018;7(8):976-82.
63. Korzhikov-Vlakh V, Krylova M, Sinitsyna E, Ivankova E, Averianov I, Tennikova TB. Hydrogel Layers on the Surface of Polyester-Based Materials for Improvement of Their Biointeractions and Controlled Release of Proteins. *Polymers (Basel).* 2016;8(12):418.
64. Bulbulla N, Kirkil C, Godekmerdan A, Aygen E, Ilhan YS. The Comparison of Inflammatory Responses and Clinical Results After Groin Hernia Repair Using Polypropylene or Polyester Meshes. *Indian J Surg.* 2015;77(Suppl 2):283-7.
65. Schneider F, O'Connor S, Becquemin JP. Efficacy of collagen silver-coated polyester and rifampin-soaked vascular grafts to resist infection from MRSA and Escherichia coli in a dog model. *Ann Vasc Surg.* 2008;22(6):815-21.

66. Edgar L, McNamara K, Wong T, Tamburrini R, Katari R, Orlando G. Heterogeneity of Scaffold Biomaterials in Tissue Engineering. *Materials* (Basel, Switzerland). 2016;9(5).
67. B Claase M, B Olde Riekerink M, de Bruijn J, W Grijpma D, Engbers G, Feijen J. Enhanced Bone Marrow Stromal Cell Adhesion and Growth on Segmented Poly(ether ester)s Based on Poly(ethylene oxide) and Poly(butylene terephthalate). *Biomacromolecules*. 2003;4:57-63.
68. Siltanen C, Diakatou M, Lowen J, Haque A, Rahimian A, Stybayeva G, et al. One step fabrication of hydrogel microcapsules with hollow core for assembly and cultivation of hepatocyte spheroids. *Acta Biomater*. 2017;50:428-36.
69. Skrzypek K, Groot Nibbelink M, van Lente J, Buitinga M, Engelse MA, de Koning EJP, et al. Pancreatic islet macroencapsulation using microwell porous membranes. *Scientific Reports*. 2017;7(1):9186.
70. Patlolla AK, Kumari SA, Tchounwou PB. A comparison of polyethylene-glycol-coated and uncoated gold nanoparticle-mediated hepatotoxicity and oxidative stress in Sprague Dawley rats. *Int J Nanomedicine*. 2019;14:639-47.
71. Macario DK, Entersz I, Bolikal D, Kohn J, Nackman GB. Iodine inhibits antiadhesive effect of PEG: Implications for tissue engineering. *Journal of Biomedical Materials Research Part B: Applied Biomaterials*. 2008;86B(1):237-44.
72. Williams DF. Challenges With the Development of Biomaterials for Sustainable Tissue Engineering. *Frontiers in Bioengineering and Biotechnology*. 2019;7(127).
73. Ayandele E, Sarkar B, Alexandridis P. Polyhedral Oligomeric Silsesquioxane (POSS)-Containing Polymer Nanocomposites. *Nanomaterials* (Basel). 2012;2(4):445-75.
74. Tan A, Farhatnia Y, Goh D, G N, de Mel A, Lim J, et al. Surface modification of a polyhedral oligomeric silsesquioxane poly(carbonate-urea) urethane (POSS-PCU) nanocomposite polymer as a stent coating for enhanced capture of endothelial progenitor cells. *Biointerphases*. 2013;8(1):23-.
75. Solouk A, G Cousins B, Mirahmadi F, Mirzadeh H, Reza Jalali Nadoushan M, Shokrgozar M, et al. Biomimetic modified clinical-grade POSS-PCU nanocomposite polymer for bypass graft applications: A preliminary assessment of endothelial cell adhesion and haemocompatibility. *Materials science & engineering C, Materials for biological applications*. 2015;46:400-8.
76. Chaloupka K, Motwani M, Seifalian AM. Development of a new lacrimal drainage conduit using POSS nanocomposite. *Biotechnology and applied biochemistry*. 2011;58(5):363-70.

77. Crowley C, Klanrit P, Butler CR, Varanou A, Platé M, Hynds RE, et al. Surface modification of a POSS-nanocomposite material to enhance cellular integration of a synthetic bioscaffold. *Biomaterials*. 2016;83:283-93.
78. Hawkes N. UCL laboratory that made artificial implants breached safety rules. *BMJ*. 2017;359:j4572.
79. Maughan EF, Butler CR, Crowley C, Teoh GZ, den Hondt M, Hamilton NJ, et al. A comparison of tracheal scaffold strategies for pediatric transplantation in a rabbit model. *Laryngoscope*. 2017;127(12):E449-e57.
80. Hess MW, Pfaller K, Ebner HL, Beer B, Hekl D, Seppi T. 3D versus 2D cell culture implications for electron microscopy. *Methods Cell Biol*. 2010;96:649-70.
81. Haycock J. *3D Cell Culture: Methods and protocols* 2011.
82. Naderi S, Khayat Zadeh J, Mahdavi Shahri N, Nejad Shahrokh Abady K, Cheravi M, Baharara J, et al. Three-dimensional scaffold from decellularized human gingiva for cell cultures: glycoconjugates and cell behavior. *Cell J*. 2013;15(2):166-75.
83. RAVI M, PAUL SF. *3D Cell Culture Systems - Advantages and Applications*. 2014.
84. DeQuach JA, Yuan SH, Goldstein LS, Christman KL. Decellularized porcine brain matrix for cell culture and tissue engineering scaffolds. *Tissue Eng Part A*. 2011;17(21-22):2583-92.
85. Edmondson R, Broglie JJ, Adcock AF, Yang L. *Three-Dimensional Cell Culture Systems and Their Applications in Drug Discovery and Cell-Based Biosensors*. *Assay and Drug Development Technologies*. 2014;12(4):207-18.
86. Baker BM, Chen CS. Deconstructing the third dimension: how 3D culture microenvironments alter cellular cues. *Journal of cell science*. 2012;125(Pt 13):3015-24.
87. Baker BM, Chen CS. Deconstructing the third dimension – how 3D culture microenvironments alter cellular cues. *Journal of cell science*. 2012;125(13):3015.
88. Hartung T. Thoughts on limitations of animal models. *Parkinsonism Relat Disord*. 2008;14 Suppl 2:S81-3.
89. McGonigle P, Ruggeri B. Animal models of human disease: challenges in enabling translation. *Biochem Pharmacol*. 2014;87(1):162-71.
90. Robinson V. Less is more: reducing the reliance on animal models for nausea and vomiting research. *Br J Pharmacol*. 2009;157(6):863-4.
91. Ketchedjian A, Jones AL, Krueger P, Robinson E, Crouch K, Wolfenbarger L, Jr., et al. Recellularization of decellularized allograft

- scaffolds in ovine great vessel reconstructions. *Ann Thorac Surg.* 2005;79(3):888-96; discussion 96.
92. Jucker M. The benefits and limitations of animal models for translational research in neurodegenerative diseases. *Nat Med.* 2010;16(11):1210-4.
93. Paul SM, Mytelka DS, Dunwiddie CT, Persinger CC, Munos BH, Lindborg SR, et al. How to improve R&D productivity: the pharmaceutical industry's grand challenge. *Nat Rev Drug Discov.* 2010;9(3):203-14.
94. Knight A. Systematic reviews of animal experiments demonstrate poor human clinical and toxicological utility. *Altern Lab Anim.* 2007;35(6):641-59.
95. Godoy P, Hewitt NJ, Albrecht U, Andersen ME, Ansari N, Bhattacharya S, et al. Recent advances in 2D and 3D in vitro systems using primary hepatocytes, alternative hepatocyte sources and non-parenchymal liver cells and their use in investigating mechanisms of hepatotoxicity, cell signaling and ADME. *Arch Toxicol.* 2013;87(8):1315-530.
96. Hosseinkhani H. 3D in vitro technology for drug discovery. *Curr Drug Saf.* 2012;7(1):37-43.
97. Soldatow VY, LeCluyse EL, Griffith LG, Rusyn I. In vitro models for liver toxicity testing. *Toxicology Research.* 2013;2(1):23-39.
98. Pampaloni F, Stelzer EH, Masotti A. Three-dimensional tissue models for drug discovery and toxicology. *Recent Pat Biotechnol.* 2009;3(2):103-17.
99. Gurski LA, Petrelli NJ, Jia X, Farach-Carson MC. 3D matrices for anti-cancer drug testing and development. *Oncology Issues.* 2010;25:20-5.
100. Efrat S, Russ HA. Making beta cells from adult tissues. *Trends Endocrinol Metab.* 2012;23(6):278-85.
101. Clegg PD, Strassburg S, Smith RK. Cell phenotypic variation in normal and damaged tendons. *International Journal of Experimental Pathology.* 2007;88(4):227-35.
102. Burk J, Erbe I, Berner D, Kacza J, Kasper C, Pfeiffer B, et al. Freeze-thaw cycles enhance decellularization of large tendons. *Tissue Eng Part C Methods.* 2014;20(4):276-84.
103. Bedossa P, Lemaigre G, Bacci J, Martin E. Quantitative Estimation of the Collagen Content in Normal and Pathologic Pancreas Tissue. *Digestion.* 1989;44(1):7-13.
104. Taskiran D, Taskiran E, Yercan H, Kutay F. Quantification of Total Collagen in Rabbit Tendon by the Sirius Red Method. *Turkish Journal of Medical Sciences.* 1999;29:7-9.

105. Pour PM, Konishi Y, Klöppel G, Longnecker DS. Microanatomy and Fine Structure of the Pancreas. In: Pour PM, Konishi Y, Klöppel G, Longnecker DS, editors. Atlas of Exocrine Pancreatic Tumors: Morphology, Biology, and Diagnosis with an International Guide for Tumor Classification. Tokyo: Springer Japan; 1994. p. 17-30.
106. Screen HRC, Berk DE, Kadler KE, Ramirez F, Young MF. Tendon functional extracellular matrix. *J Orthop Res.* 2015;33(6):793-9.
107. Flynn LE. The use of decellularized adipose tissue to provide an inductive microenvironment for the adipogenic differentiation of human adipose-derived stem cells. *Biomaterials.* 2010;31(17):4715-24.
108. Cortiella J, Niles J, Cantu A, Brettler A, Pham A, Vargas G, et al. Influence of acellular natural lung matrix on murine embryonic stem cell differentiation and tissue formation. *Tissue Eng Part A.* 2010;16(8):2565-80.
109. Cartmell JS, Dunn MG. Effect of chemical treatments on tendon cellularity and mechanical properties. *J Biomed Mater Res.* 2000;49(1):134-40.
110. Jackson DW, Grood ES, Arnoczky SP, Butler DL, Simon TM. Cruciate reconstruction using freeze dried anterior cruciate ligament allograft and a ligament augmentation device (LAD). An experimental study in a goat model. *Am J Sports Med.* 1987;15(6):528-38.
111. Szytkaruk M, Kemp SW, Wood MD, Gordon T, Borschel GH. Experimental and clinical evidence for use of decellularized nerve allografts in peripheral nerve gap reconstruction. *Tissue Eng Part B Rev.* 2013;19(1):83-96.
112. Prasertsung I, Kanokpanont S, Bunaprasert T, Thanakit V, Damrongsakkul S. Development of acellular dermis from porcine skin using periodic pressurized technique. *J Biomed Mater Res B Appl Biomater.* 2008;85(1):210-9.
113. Hopkinson A, Shanmuganathan VA, Gray T, Yeung AM, Lowe J, James DK, et al. Optimization of amniotic membrane (AM) denuding for tissue engineering. *Tissue Eng Part C Methods.* 2008;14(4):371-81.
114. Nonaka PN, Campillo N, Uriarte JJ, Garreta E, Melo E, de Oliveira LV, et al. Effects of freezing/thawing on the mechanical properties of decellularized lungs. *J Biomed Mater Res A.* 2014;102(2):413-9.
115. Fitzpatrick JC, Clark PM, Capaldi FM. Effect of Decellularization Protocol on the Mechanical Behavior of Porcine Descending Aorta. *International Journal of Biomaterials.* 2010;2010:11.
116. Oliveira AC, Garzon I, Ionescu AM, Carriel V, Cardona Jde L, Gonzalez-Andrades M, et al. Evaluation of small intestine grafts decellularization methods for corneal tissue engineering. *PLoS One.* 2013;8(6):e66538.

117. Sarig U, Au-Yeung GC, Wang Y, Bronshtein T, Dahan N, Boey FY, et al. Thick acellular heart extracellular matrix with inherent vasculature: a potential platform for myocardial tissue regeneration. *Tissue Eng Part A*. 2012;18(19-20):2125-37.
118. Takami Y. By treating separated dermis with a protease and a surfactant simultaneously, it is possible to decellularize dermis substantially completely without greatly denaturing intrinsic collagen structure of dermis while attenuating residual basement membrane components; use in burn treatment. Google Patents; 2005.
119. Hung SH, Su CH, Lee FP, Tseng H. Larynx decellularization: combining freeze-drying and sonication as an effective method. *J Voice*. 2013;27(3):289-94.
120. Azhim A, Syazwani N, Morimoto Y, Furukawa K, Ushida T. The use of sonication treatment to decellularize aortic tissues for preparation of bioscaffolds. *J Biomater Appl*. 2014;29(1):130-41.
121. Azhim A, Yamagami K, Muramatsu K, Morimoto Y, Tanaka M. The use of sonication treatment to completely decellularize blood arteries: a pilot study. *Conf Proc IEEE Eng Med Biol Soc*. 2011;2011:2468-71.
122. Brendel K, Duhamel RC. Body implants of extracellular matrix and means and methods of making and using such implants. Google Patents; 1989.
123. Bader A, Schilling T, Teebken OE, Brandes G, Herden T, Steinhoff G, et al. Tissue engineering of heart valves--human endothelial cell seeding of detergent acellularized porcine valves. *Eur J Cardiothorac Surg*. 1998;14(3):279-84.
124. Bishopric NH, Dousman L, Yao YM. Matrix substrate for a viable body tissue-derived prosthesis and method for making the same. Google Patents; 1999.
125. Dahl SL, Koh J, Prabhakar V, Niklason LE. Decellularized native and engineered arterial scaffolds for transplantation. *Cell Transplant*. 2003;12(6):659-66.
126. Elder BD, Eleswarapu SV, Athanasiou KA. Extraction techniques for the decellularization of tissue engineered articular cartilage constructs. *Biomaterials*. 2009;30(22):3749-56.
127. Schenke-Layland K, Vasilevski O, Opitz F, Konig K, Riemann I, Halhuber KJ, et al. Impact of decellularization of xenogeneic tissue on extracellular matrix integrity for tissue engineering of heart valves. *J Struct Biol*. 2003;143(3):201-8.
128. Steinhoff G, Stock U, Karim N, Mertsching H, Timke A, Meliss RR, et al. Tissue engineering of pulmonary heart valves on allogenic acellular matrix conduits: in vivo restoration of valve tissue. *Circulation*. 2000;102(19 Suppl 3):Ii50-5.

129. Gleason K. How to convert Centrifuge RPM to RCF or G-force: <http://clinfield.com>; 2012 [
130. Woods T, Gratzner PF. Effectiveness of three extraction techniques in the development of a decellularized bone-anterior cruciate ligament-bone graft. *Biomaterials*. 2005;26(35):7339-49.
131. Goissis G, Suzigan S, Parreira DR, Maniglia JV, Braile DM, Raymundo S. Preparation and characterization of collagen-elastin matrices from blood vessels intended as small diameter vascular grafts. *Artif Organs*. 2000;24(3):217-23.
132. De Filippo RE, Yoo JJ, Atala A. Urethral Replacement Using Cell Seeded Tubularized Collagen Matrices. *The Journal of Urology*. 2002;168(4, Supplement):1789-93.
133. Rosario DJ, Reilly GC, Ali Salah E, Glover M, Bullock AJ, Macneil S. Decellularization and sterilization of porcine urinary bladder matrix for tissue engineering in the lower urinary tract. *Regen Med*. 2008;3(2):145-56.
134. Christman KL, Young DA. Decellularized and delipidized extracellular matrix and methods of use. *Google Patents*; 2012.
135. Everaerts FJL, Torrianni MW, Everaerts FM, Trescony PV, den Hartog W. Process for producing decellularized biological tissues. *Google Patents*; 2013.
136. Hodde JP, Badylak SF, Brightman AO, Voytik-Harbin SL. Glycosaminoglycan content of small intestinal submucosa: a bioscaffold for tissue replacement. *Tissue Eng*. 1996;2(3):209-17.
137. Klebe RJ. Cell attachment to collagen: the requirement for energy. *J Cell Physiol*. 1975;86(2 Pt 1):231-6.
138. Seddon AM, Curnow P, Booth PJ. Membrane proteins, lipids and detergents: not just a soap opera. *Biochim Biophys Acta*. 2004;1666(1-2):105-17.
139. Grauss RW, Hazekamp MG, Oppenhuizen F, van Munsteren CJ, Gittenberger-de Groot AC, DeRuiter MC. Histological evaluation of decellularised porcine aortic valves: matrix changes due to different decellularisation methods. *European Journal of Cardio-Thoracic Surgery*. 2005;27(4):566-71.
140. Nari GA, Cid M, Comin R, Reyna L, Juri G, Taborda R, et al. Preparation of a three-dimensional extracellular matrix by decellularization of rabbit livers. *Rev Esp Enferm Dig*. 2013;105(3):138-43.
141. Rieder E, Kasimir MT, Silberhumer G, Seebacher G, Wolner E, Simon P, et al. Decellularization protocols of porcine heart valves differ importantly in efficiency of cell removal and susceptibility of the matrix to recellularization with human vascular cells. *J Thorac Cardiovasc Surg*. 2004;127(2):399-405.

142. Chen RN, Ho HO, Tsai YT, Sheu MT. Process development of an acellular dermal matrix (ADM) for biomedical applications. *Biomaterials*. 2004;25(13):2679-86.
143. Hudson TW, Liu SY, Schmidt CE. Engineering an improved acellular nerve graft via optimized chemical processing. *Tissue Eng*. 2004;10(9-10):1346-58.
144. Lin P, Chan WC, Badylak SF, Bhatia SN. Assessing porcine liver-derived biomatrix for hepatic tissue engineering. *Tissue Eng*. 2004;10(7-8):1046-53.
145. Hudson TW, Zawko S, Deister C, Lundy S, Hu CY, Lee K, et al. Optimized acellular nerve graft is immunologically tolerated and supports regeneration. *Tissue Eng*. 2004;10(11-12):1641-51.
146. Liao J, Joyce EM, Sacks MS. Effects of decellularization on the mechanical and structural properties of the porcine aortic valve leaflet. *Biomaterials*. 2008;29(8):1065-74.
147. Guyette J, Gilpin SE, Charest JM, Tapias LF. Perfusion decellularization of whole organs. *Nature Protocols*. 2014;9(6):1451-68.
148. Jensen T, Roszell B, Zang F, Girard E, Matson A, Thrall R, et al. A rapid lung de-cellularization protocol supports embryonic stem cell differentiation in vitro and following implantation. *Tissue Eng Part C Methods*. 2012;18(8):632-46.
149. Petersen TH, Calle EA, Colehour MB, Niklason LE. Matrix composition and mechanics of decellularized lung scaffolds. *Cells Tissues Organs*. 2012;195(3):222-31.
150. Gilbert TW, Sellaro TL, Badylak SF. Decellularization of tissues and organs. *Biomaterials*. 2006;27(19):3675-83.
151. Pierschbacher MD, Grzesiak JJ, Kirchofer D. Methods for modifying the binding activity of cell adhesion receptors. *Google Patents*; 1998.
152. Gamba PG, Conconi MT, Lo Piccolo R, Zara G, Spinazzi R, Parnigotto PP. Experimental abdominal wall defect repaired with acellular matrix. *Pediatr Surg Int*. 2002;18(5-6):327-31.
153. McFetridge PS, Daniel JW, Bodamyali T, Horrocks M, Chaudhuri JB. Preparation of porcine carotid arteries for vascular tissue engineering applications. *J Biomed Mater Res A*. 2004;70(2):224-34.
154. Crapo PM, Gilbert TW, Badylak SF. An overview of tissue and whole organ decellularization processes. *Biomaterials*. 2011;32(12):3233-43.
155. Yang B, Zhang Y, Zhou L, Sun Z, Zheng J, Chen Y, et al. Development of a porcine bladder acellular matrix with well-preserved extracellular bioactive factors for tissue engineering. *Tissue Eng Part C Methods*. 2010;16(5):1201-11.

156. Rubin P, Hansen JT. *TNM Staging Atlas with Oncoanatomy*: Wolters Kluwer Health; 2013.
157. Flint LM. *Trauma: Contemporary Principles and Therapy*: Wolters Kluwer Health/Lippincott Williams & Wilkins; 2008.
158. Chauhan A, Elsayes KM, Sagebiel T, Bhosale PR. The Pancreas. In: Elsayes KM, editor. *Cross-Sectional Imaging of the Abdomen and Pelvis: A Practical Algorithmic Approach*. New York, NY: Springer New York; 2015. p. 189-227.
159. Cruveilhier J, Pattison GS, Madden WH. *The Anatomy of the Human Body*: Harper & Brothers; 1844.
160. Dooley JS, Lok A, Burroughs AK, Heathcote J. *Sherlock's Diseases of the Liver and Biliary System*: Wiley; 2011.
161. Arias I, Wolkoff A, Boyer J, Shafritz D, Fausto N, Alter H, et al. *The Liver: Biology and Pathobiology*: Wiley; 2011.
162. Zambirinis CP, Allen PJ. Anatomy of the Pancreas and Biliary Tree. In: Bekaii-Saab T, El-Rayes B, editors. *Current and Emerging Therapies in Pancreatic Cancer*. Cham: Springer International Publishing; 2018. p. 23-47.
163. Cesmebasi A, Malefant J, Patel SD, Du Plessis M, Renna S, Tubbs RS, et al. The surgical anatomy of the lymphatic system of the pancreas. *Clin Anat*. 2015;28(4):527-37.
164. Pandol SJ. *The Exocrine Pancreas*: Morgan & Claypool; 2011.
165. Cruickshank AH, Benbow EW. *Pathology of the Pancreas*: Springer London; 2012.
166. Baert AL, Balthazar EJ, Megibow AJ, Mucelli RP. *Imaging of the Pancreas: Acute and Chronic Pancreatitis*: Springer Berlin Heidelberg; 2010.
167. Githens S. Pancreatic Duct Cell Cultures. *Annual Reviews of Physiology*. 1994;56(1):419-43.
168. Chen H, Martin B, Cai H, Fiori JL, Egan JM, Siddiqui S, et al. Pancreas++: Automated Quantification of Pancreatic Islet Cells in Microscopy Images. *Frontiers in Physiology*. 2012;3:482.
169. Campbell F, Verbeke CS. *Embryology, Anatomy, and Histology. Pathology of the Pancreas: A Practical Approach*. London: Springer London; 2013. p. 3-20.
170. Zhang S-x. Digestive System. In: Zhang S-x, editor. *An Atlas of Histology*. New York, NY: Springer New York; 1999. p. 187-251.
171. Juang JH, Kuo CH, Peng SJ, Tang SC. 3-D Imaging Reveals Participation of Donor Islet Schwann Cells and Pericytes in Islet Transplantation and Graft Neurovascular Regeneration. *EBioMedicine*. 2015;2(2):109-19.
172. Zhang SX. *An Atlas of Histology*: Springer New York; 2013.

173. Krstić RV. Endocrine System. Human Microscopic Anatomy: An Atlas for Students of Medicine and Biology. Berlin, Heidelberg: Springer Berlin Heidelberg; 1991. p. 257-93.
174. Wang X, Misawa R, Zielinski MC, Cowen P, Jo J, Periwal V, et al. Regional Differences in Islet Distribution in the Human Pancreas - Preferential Beta-Cell Loss in the Head Region in Patients with Type 2 Diabetes. PLoS ONE. 2013;8(6):e67454.
175. Feldmann G, Maitra A. Molecular Genetics of Pancreatic Ductal Adenocarcinomas and Recent Implications for Translational Efforts. The Journal of Molecular Diagnostics : JMD. 2008;10(2):111-22.
176. Pergolini I, Morales-Oyarvide V, Mino-Kenudson M, Honselmann KC, Rosenbaum MW, Nahar S, et al. Tumor engraftment in patient-derived xenografts of pancreatic ductal adenocarcinoma is associated with adverse clinicopathological features and poor survival. PLoS ONE. 2017;12(8):e0182855.
177. Rahib L, Smith BD, Aizenberg R, Rosenzweig AB, Fleshman JM, Matrisian LM. Projecting Cancer Incidence and Deaths to 2030: The Unexpected Burden of Thyroid, Liver, and Pancreas Cancers in the United States. Cancer Research. 2014;74(11):2913.
178. Lemke J, Schafer D, Sander S, Henne-Bruns D, Kornmann M. Survival and prognostic factors in pancreatic and ampullary cancer. Anticancer Res. 2014;34(6):3011-20.
179. Cid-Arregui A, Juarez V. Perspectives in the treatment of pancreatic adenocarcinoma. World Journal of Gastroenterology : WJG. 2015;21(31):9297-316.
180. Gleason MX, Mdzinarishvili T, Are C, Sasson A, Sherman A, Shats O, et al. Prognostic Estimator of Survival for Patients with Localized and Extended Pancreatic Ductal Adenocarcinoma. Cancer Informatics. 2013;12:103-14.
181. Fitzsimmons D, Kahl S, Butturini G, van Wyk M, Bornman P, Bassi C, et al. Symptoms and quality of life in chronic pancreatitis assessed by structured interview and the EORTC QLQ-C30 and QLQ-PAN26. Am J Gastroenterol. 2005;100(4):918-26.
182. Tong H-X, Zhang LEI, Rong Y-F, Wang D-S, Kuang TT, Xu X-F, et al. Long-term survival following total pancreatectomy and superior mesenteric-portal vein resection for pancreatic ductal adenocarcinoma: A case report. Oncology Letters. 2015;9(1):318-20.
183. Chun YS, Pawlik TM, Vauthey JN. 8th Edition of the AJCC Cancer Staging Manual: Pancreas and Hepatobiliary Cancers. Ann Surg Oncol. 2017.
184. Weledji EP, Enoworock G, Mokake M, Sinju M. How Grim is Pancreatic Cancer? Oncol Rev. 2016;10(1):294-.

185. Distler M, Aust D, Weitz J, Pilarsky C, Grutzmann R. Precursor lesions for sporadic pancreatic cancer: PanIN, IPMN, and MCN. *Biomed Res Int.* 2014;2014:474905.
186. Ying H, Dey P, Yao W, Kimmelman AC, Draetta GF, Maitra A, et al. Genetics and biology of pancreatic ductal adenocarcinoma. *Genes Dev.* 2016;30(4):355-85.
187. Hezel AF, Kimmelman AC, Stanger BZ, Bardeesy N, Depinho RA. Genetics and biology of pancreatic ductal adenocarcinoma. *Genes Dev.* 2006;20(10):1218-49.
188. Wormann SM, Song L, Ai J, Diakopoulos KN, Kurkowski MU, Gorgulu K, et al. Loss of P53 Function Activates JAK2-STAT3 Signaling to Promote Pancreatic Tumor Growth, Stroma Modification, and Gemcitabine Resistance in Mice and Is Associated With Patient Survival. *Gastroenterology.* 2016;151(1):180-93.e12.
189. Pusateri AJ, Krishna SG. Pancreatic Cystic Lesions: Pathogenesis and Malignant Potential. *Diseases.* 2018;6(2):50.
190. Ngamruengphong S, Lennon AM. Analysis of Pancreatic Cyst Fluid. *Surg Pathol Clin.* 2016;9(4):677-84.
191. Farrell JJ. Prevalence, Diagnosis and Management of Pancreatic Cystic Neoplasms: Current Status and Future Directions. *Gut Liver.* 2015;9(5):571-89.
192. Lewis R, Drebin JA, Callery MP, Fraker D, Kent TS, Gates J, et al. A contemporary analysis of survival for resected pancreatic ductal adenocarcinoma. *HPB : The Official Journal of the International Hepato Pancreato Biliary Association.* 2013;15(1):49-60.
193. Surveillance, Epidemiology, and End Results (SEER) Program (www.seer.cancer.gov) SEER*Stat Database: Mortality - All COD, Aggregated With State, Total U.S. (1969-2016) <Katrina/Rita Population Adjustment> [Internet]. National Cancer Institute. 2018 [cited August 2019].
194. Rawla P, Sunkara T, Gaduputi V. Epidemiology of Pancreatic Cancer: Global Trends, Etiology and Risk Factors. *World J Oncol.* 2019;10(1):10-27.
195. Cid-Arregui A, Juarez V. Perspectives in the treatment of pancreatic adenocarcinoma. *World journal of gastroenterology.* 2015;21(31):9297-316.
196. Pancreatic cancer in adults: diagnosis and management, NICE guideline [NG85] [Internet]. [cited July 2019].
197. Rossi ML, Rehman AA, Gondi CS. Therapeutic options for the management of pancreatic cancer. *World J Gastroenterol.* 2014;20(32):11142-59.

198. Adamska A, Domenichini A, Falasca M. Pancreatic Ductal Adenocarcinoma: Current and Evolving Therapies. *International Journal of Molecular Sciences*. 2017;18(7):1338.
199. Conroy T, Desseigne F, Ychou M, Ducreux M, Bouche O, Guimbaud R, et al. Randomized phase III trial comparing FOLFIRINOX (F: 5FU/leucovorin [LV], irinotecan [I], and oxaliplatin [O]) versus gemcitabine (G) as first-line treatment for metastatic pancreatic adenocarcinoma (MPA): Preplanned interim analysis results of the PRODIGE 4/ACCORD 11 trial. *Journal of Clinical Oncology*. 2010;28(15_suppl):4010-.
200. Vogl UM, Andalibi H, Klaus A, Vormittag L, Schima W, Heinrich B, et al. Nab-paclitaxel and gemcitabine or FOLFIRINOX as first-line treatment in patients with unresectable adenocarcinoma of the pancreas: does sequence matter? *BMC Cancer*. 2019;19(1):28.
201. Hajatdoost L, Sedaghat K, Walker EJ, Thomas J, Kosari S. Chemotherapy in Pancreatic Cancer: A Systematic Review. *Medicina (Kaunas)*. 2018;54(3).
202. Seufferlein T, Ettrich TJ. Treatment of pancreatic cancer-neoadjuvant treatment in resectable pancreatic cancer (PDAC). *Transl Gastroenterol Hepatol*. 2019;4:21-.
203. Gillen S, Schuster T, zum Bueschenfelde CM, Friess H, Kleeff J. Preoperative/Neoadjuvant Therapy in Pancreatic Cancer: A Systematic Review and Meta-analysis of Response and Resection Percentages. *Plos Medicine*. 2010;7(4).
204. Naidoo K, Jones R, Dmitrovic B, Wijesuriya N, Kocher H, Hart IR, et al. Proteome of formalin-fixed paraffin-embedded pancreatic ductal adenocarcinoma and lymph node metastases. *J Pathol*. 2012;226(5):756-63.
205. Garcia PL, Council LN, Christein JD, Arnoletti JP, Heslin MJ, Gamblin TL, et al. Development and Histopathological Characterization of Tumorgraft Models of Pancreatic Ductal Adenocarcinoma. *PLoS ONE*. 2013;8(10):e78183.
206. Andrén-Sandberg Å. Pancreatic cancer: Animal model and molecular biology. *North American Journal of Medical Sciences*. 2011;3(10):441-50.
207. Herreros-Villanueva M, Hijona E, Cosme A, Bujanda L. Mouse models of pancreatic cancer. *World Journal of Gastroenterology : WJG*. 2012;18(12):1286-94.
208. Murtaugh LC. Pathogenesis of pancreatic cancer: lessons from animal models. *Toxicol Pathol*. 2014;42(1):217-28.
209. Zator Z, Whitcomb DC. Insights into the genetic risk factors for the development of pancreatic disease. *Therapeutic Advances in Gastroenterology*. 2017;10(3):323-36.

210. Mohammed A, Janakiram NB, Pant S, Rao CV. Molecular Targeted Intervention for Pancreatic Cancer. *Cancers*. 2015;7(3):1499-542.
211. Eser S, Schnieke A, Schneider G, Saur D. Oncogenic KRAS signalling in pancreatic cancer. *British journal of cancer*. 2014;111(5):817-22.
212. Karandish F, Mallik S. Biomarkers and Targeted Therapy in Pancreatic Cancer. *Biomarkers in Cancer*. 2016;8(Suppl 1):27-35.
213. Jonckheere N, Vasseur R, Van Seuning I. The cornerstone K-RAS mutation in pancreatic adenocarcinoma: From cell signaling network, target genes, biological processes to therapeutic targeting. *Critical Reviews in Oncology / Hematology*. 111:7-19.
214. New M, Van Acker T, Long JS, Sakamaki JI, Ryan KM, Tooze SA. Molecular Pathways Controlling Autophagy in Pancreatic Cancer. *Front Oncol*. 2017;7:28.
215. Le Large TYS, Bijlsma MF, Kazemier G, van Laarhoven HWM, Giovannetti E, Jimenez CR. Key biological processes driving metastatic spread of pancreatic cancer as identified by multi-omics studies. *Seminars in Cancer Biology*. 2017;44(Supplement C):153-69.
216. Muerkoster S, Wegehenkel K, Arlt A, Witt M, Sipos B, Kruse ML, et al. Tumor stroma interactions induce chemoresistance in pancreatic ductal carcinoma cells involving increased secretion and paracrine effects of nitric oxide and interleukin-1beta. *Cancer Res*. 2004;64(4):1331-7.
217. Korc M. Pancreatic cancer associated stroma production. *American journal of surgery*. 2007;194(4 Supplement 1):s84-s6.
218. Bhowmick NA, Moses HL. Tumor-stroma interactions. *Curr Opin Genet Dev*. 2005;15(1):97-101.
219. Mahadevan D, Von Hoff DD. Tumor-stroma interactions in pancreatic ductal adenocarcinoma. *Mol Cancer Ther*. 2007;6(4):1186-97.
220. Miyamoto H, Murakami T, Tsuchida K, Sugino H, Miyake H, Tashiro S. Tumor-stroma interaction of human pancreatic cancer: acquired resistance to anticancer drugs and proliferation regulation is dependent on extracellular matrix proteins. *Pancreas*. 2004;28(1):38-44.
221. Beatty GL, Chiorean EG, Fishman MP, Saboury B, Teitelbaum UR, Sun W, et al. CD40 agonists alter tumor stroma and show efficacy against pancreatic carcinoma in mice and humans. *Science*. 2011;331(6024):1612-6.
222. Bremnes RM, Donnem T, Al-Saad S, Al-Shibli K, Andersen S, Sirera R, et al. The role of tumor stroma in cancer progression and prognosis: emphasis on carcinoma-associated fibroblasts and non-small cell lung cancer. *J Thorac Oncol*. 2011;6(1):209-17.

223. Schorn S, Demir IE, Haller B, Scheufele F, Reyes CM, Tieftrunk E, et al. The influence of neural invasion on survival and tumor recurrence in pancreatic ductal adenocarcinoma - A systematic review and meta-analysis. *Surg Oncol.* 2017;26(1):105-15.
224. Luzzi KJ, MacDonald IC, Schmidt EE, Kerkvliet N, Morris VL, Chambers AF, et al. Multistep Nature of Metastatic Inefficiency : Dormancy of Solitary Cells after Successful Extravasation and Limited Survival of Early Micrometastases. *Am J Pathol.* 1998;153(3):865-73.
225. Sousa CM, Biancur DE, Wang X, Halbrook CJ, Sherman MH, Zhang L, et al. Pancreatic stellate cells support tumour metabolism through autophagic alanine secretion. *Nature.* 2016;536(7617):479-83.
226. Apte M, Haber P, Darby S, Rodgers S, McCaughan G, Korsten M, et al. Pancreatic stellate cells are activated by proinflammatory cytokines: implications for pancreatic fibrogenesis. *Gut.* 1999;44(4):534-41.
227. Vonlaufen A, Phillips PA, Yang L, Xu Z, Fiala-Beer E, Zhang X, et al. Isolation of quiescent human pancreatic stellate cells: a promising in vitro tool for studies of human pancreatic stellate cell biology. *Pancreatology.* 2010;10(4):434-43.
228. Mews P, Phillips P, Fahmy R, Korsten M, Pirola R, Wilson J, et al. Pancreatic stellate cells respond to inflammatory cytokines: potential role in chronic pancreatitis. *Gut.* 2002;50(4):535-41.
229. Nielsen MFB, Mortensen MB, Detlefsen S. Key players in pancreatic cancer-stroma interaction: Cancer-associated fibroblasts, endothelial and inflammatory cells. *World Journal of Gastroenterology.* 2016;22(9):2678-700.
230. von Ahrens D, Bhagat TD, Nagrath D, Maitra A, Verma A. The role of stromal cancer-associated fibroblasts in pancreatic cancer. *J Hematol Oncol.* 2017;10(1):76-.
231. Van Cutsem E, de Velde HV, Karasek P, Oettle H, Vervenne WL, Szawlowski A, et al. Phase III trial of gemcitabine plus tipifarnib compared with gemcitabine plus placebo in advanced pancreatic cancer. *Journal of Clinical Oncology.* 2004;22(8):1430-8.
232. Ko AH, Cella D. Achieving the Best of Both Worlds. *Journal of Clinical Oncology.* 2013;31(1):3-4.
233. Javle MM, Shroff RT, Xiong H, Varadhachary GA, Fogelman D, Reddy SA, et al. Inhibition of the mammalian target of rapamycin (mTOR) in advanced pancreatic cancer: results of two phase II studies. *Bmc Cancer.* 2010;10.
234. O'Neil BH, Scott AJ, Ma WW, Cohen SJ, Aisner DL, Menter AR, et al. A phase II/III randomized study to compare the efficacy and safety of rigosertib plus gemcitabine versus gemcitabine alone in patients with

previously untreated metastatic pancreatic cancer(aEuro). *Annals of Oncology*. 2015;26(9):1923-9.

235. Moore MJ, Goldstein D, Hamm J, Figer A, Hecht JR, Gallinger S, et al. Erlotinib plus gemcitabine compared with gemcitabine alone in patients with advanced pancreatic cancer: A phase III trial of the National Cancer Institute of Canada clinical trials group. *Journal of Clinical Oncology*. 2007;25(15):1960-6.

236. Philip PA, Goldman B, Ramanathan RK, Lenz H-J, Lowy AM, Whitehead RP, et al. Dual Blockade of Epidermal Growth Factor Receptor and Insulin-Like Growth Factor Receptor-1 Signaling in Metastatic Pancreatic Cancer Phase Ib and Randomized Phase II Trial of Gemcitabine, Erlotinib, and Cixutumumab Versus Gemcitabine Plus Erlotinib (SWOG S0727). *Cancer*. 2014;120(19):2980-5.

237. Fountzilas G, Bobos M, Kalogera-Fountzila A, Xiros N, Murray S, Linardou H, et al. Gemcitabine combined with gefitinib in patients with inoperable or metastatic pancreatic cancer: A phase II study of the Hellenic Cooperative Oncology Group with biomarker evaluation. *Cancer investigation*. 2008;26(8):784-93.

238. Harder J, Ihorst G, Heinemann V, Hofheinz R, Moehler M, Buechler P, et al. Multicentre phase II trial of trastuzumab and capecitabine in patients with HER2 overexpressing metastatic pancreatic cancer. *British journal of cancer*. 2012;106(6):1033-8.

239. Safran H, Miner T, Bahary N, Whiting S, Lopez CD, Sun W, et al. Lapatinib and Gemcitabine for Metastatic Pancreatic Cancer A Phase II Study. *American Journal of Clinical Oncology-Cancer Clinical Trials*. 2011;34(1):50-2.

240. Fuchs CS, Azevedo S, Okusaka T, Van Laethem JL, Lipton LR, Riess H, et al. A phase 3 randomized, double-blind, placebo-controlled trial of ganitumab or placebo in combination with gemcitabine as first-line therapy for metastatic adenocarcinoma of the pancreas: the GAMMA trial. *Annals of Oncology*. 2015;26(5):921-7.

241. Kindler HL, Ioka T, Richel DJ, Bennouna J, Letourneau R, Okusaka T, et al. Axitinib plus gemcitabine versus placebo plus gemcitabine in patients with advanced pancreatic adenocarcinoma: a double-blind randomised phase 3 study. *Lancet Oncology*. 2011;12(3):256-62.

242. Van Cutsem E, Vervenne WL, Bennouna J, Humblet Y, Gill S, Van Laethem J-L, et al. Phase III Trial of Bevacizumab in Combination With Gemcitabine and Erlotinib in Patients With Metastatic Pancreatic Cancer. *Journal of Clinical Oncology*. 2009;27(13):2231-7.

243. Rougier P, Riess H, Manges R, Karasek P, Humblet Y, Barone C, et al. Randomised, placebo-controlled, double-blind, parallel-group phase III study evaluating aflibercept in patients receiving first-line

- treatment with gemcitabine for metastatic pancreatic cancer. *European Journal of Cancer*. 2013;49(12):2633-42.
244. Bramhall SR, Schulz J, Nemunaitis J, Brown PD, Baillet M, Buckels JAC. A double-blind placebo-controlled, randomised study comparing gemcitabine and marimastat with gemcitabine and placebo as first line therapy in patients with advanced pancreatic cancer. *British journal of cancer*. 2002;87(2):161-7.
245. Catenacci DVT, Junttila MR, Karrison T, Bahary N, Horiba MN, Nattam SR, et al. Randomized Phase Ib/II Study of Gemcitabine Plus Placebo or Vismodegib, a Hedgehog Pathway Inhibitor, in Patients With Metastatic Pancreatic Cancer. *Journal of Clinical Oncology*. 2015;33(36):4284-+.
246. Nakai Y, Isayama H, Ijichi H, Sasaki T, Takahara N, Ito Y, et al. A multicenter phase II trial of gemcitabine and candesartan combination therapy in patients with advanced pancreatic cancer: GECA2. *Investigational New Drugs*. 2013;31(5):1294-9.
247. Hingorani SR, Harris WP, Beck JT, Berdov BA, Wagner SA, Pshevlotsky EM, et al. Phase Ib Study of PEGylated Recombinant Human Hyaluronidase and Gemcitabine in Patients with Advanced Pancreatic Cancer. *Clinical Cancer Research*. 2016;22(12):2848-54.
248. Hingorani SR, Harris WP, Beck JT, Berdov BA, Wagner SA, Pshevlotsky EM, et al. Final results of a phase Ib study of gemcitabine plus PEGPH20 in patients with stage IV previously untreated pancreatic cancer. *Journal of Clinical Oncology*. 2015;33(3_suppl):359-.
249. Hurwitz HI, Uppal N, Wagner SA, Bendell JC, Beck JT, Wade SM, III, et al. Randomized, Double-Blind, Phase II Study of Ruxolitinib or Placebo in Combination With Capecitabine in Patients With Metastatic Pancreatic Cancer for Whom Therapy With Gemcitabine Has Failed. *Journal of Clinical Oncology*. 2015;33(34):4039-+.
250. Le DT, Lutz E, Uram JN, Sugar EA, Onners B, Solt S, et al. Evaluation of Ipilimumab in Combination With Allogeneic Pancreatic Tumor Cells Transfected With a GM-CSF Gene in Previously Treated Pancreatic Cancer. *Journal of Immunotherapy*. 2013;36(7):382-9.
251. Middleton G, Silcocks P, Cox T, Valle J, Wadsley J, Propper D, et al. Gemcitabine and capecitabine with or without telomerase peptide vaccine GV1001 in patients with locally advanced or metastatic pancreatic cancer (TeloVac): an open-label, randomised, phase 3 trial. *Lancet Oncology*. 2014;15(8):829-40.
252. Amrutkar M, Gladhaug IP. Pancreatic Cancer Chemoresistance to Gemcitabine. *Cancers (Basel)*. 2017;9(11).
253. Swayden M, Iovanna J, Soubeyran P. Pancreatic cancer chemoresistance is driven by tumor phenotype rather than tumor genotype. *Heliyon*. 2018;4(12):e01055.

254. Gnanamony M, Gondi CS. Chemoresistance in pancreatic cancer: Emerging concepts. *Oncol Lett.* 2017;13(4):2507-13.
255. Suarez-Carmona M, Lesage J, Cataldo D, Gilles C. EMT and inflammation: inseparable actors of cancer progression. *Mol Oncol.* 2017;11(7):805-23.
256. Bray F, Ferlay J, Soerjomataram I, Siegel RL, Torre LA, Jemal A. Global cancer statistics 2018: GLOBOCAN estimates of incidence and mortality worldwide for 36 cancers in 185 countries. *CA: A Cancer Journal for Clinicians.* 2018;68(6):394-424.
257. Conroy T, Bachet J-B, Ayav A, Huguet F, Lambert A, Caramella C, et al. Current standards and new innovative approaches for treatment of pancreatic cancer. *European Journal of Cancer.* 2016;57:10-22.
258. Nordh S, Ansari D, Andersson R. hENT1 expression is predictive of gemcitabine outcome in pancreatic cancer: a systematic review. *World J Gastroenterol.* 2014;20(26):8482-90.
259. Marechal R, Mackey JR, Lai R, Demetter P, Peeters M, Polus M, et al. Deoxycytidine kinase is associated with prolonged survival after adjuvant gemcitabine for resected pancreatic adenocarcinoma. *Cancer.* 2010;116(22):5200-6.
260. Grolmusz VK, Karászi K, Micsik T, Tóth EA, Mészáros K, Karvaly G, et al. Cell cycle dependent RRM2 may serve as proliferation marker and pharmaceutical target in adrenocortical cancer. *Am J Cancer Res.* 2016;6(9):2041-53.
261. Chen G, Luo Y, Warncke K, Sun Y, Yu DS, Fu H, et al. Acetylation regulates ribonucleotide reductase activity and cancer cell growth. *Nature Communications.* 2019;10(1):3213.
262. Gilbert JA, Salavaggione OE, Ji Y, Pelleymounter LL, Eckloff BW, Wieben ED, et al. Gemcitabine pharmacogenomics: cytidine deaminase and deoxycytidylate deaminase gene resequencing and functional genomics. *Clin Cancer Res.* 2006;12(6):1794-803.
263. Stern L, Giese N, Hackert T, Strobel O, Schirmacher P, Felix K, et al. Overcoming chemoresistance in pancreatic cancer cells: role of the bitter taste receptor T2R10. *J Cancer.* 2018;9(4):711-25.
264. Burris HA, 3rd, Moore MJ, Andersen J, Green MR, Rothenberg ML, Modiano MR, et al. Improvements in survival and clinical benefit with gemcitabine as first-line therapy for patients with advanced pancreas cancer: a randomized trial. *J Clin Oncol.* 1997;15(6):2403-13.
265. Berlin JD, Catalano P, Thomas JP, Kugler JW, Haller DG, Benson AB. Phase III study of gemcitabine in combination with fluorouracil versus gemcitabine alone in patients with advanced pancreatic carcinoma: Eastern Cooperative Oncology Group Trial E2297. *Journal of Clinical Oncology.* 2002;20(15):3270-5.

266. Conroy T, Desseigne F, Ychou M, Bouche O, Guimbaud R, Becouarn Y, et al. FOLFIRINOX versus gemcitabine for metastatic pancreatic cancer. *N Engl J Med*. 2011;364(19):1817-25.
267. Von Hoff DD, Ervin T, Arena FP, Chiorean EG, Infante J, Moore M, et al. Increased Survival in Pancreatic Cancer with nab-Paclitaxel plus Gemcitabine. *New England Journal of Medicine*. 2013;369(18):1691-703.
268. Heinemann V, Quietzsch D, Gieseler F, Gonnermann M, Schoenekaes H, Rost A, et al. Randomized phase III trial of gemcitabine plus cisplatin compared with gemcitabine alone in advanced pancreatic cancer. *Journal of Clinical Oncology*. 2006;24(24):3946-52.
269. Colucci G, Giuliani F, Gebbia V, Biglietto M, Rabitti P, Uomo G, et al. Gemcitabine alone or with cisplatin for the treatment of patients with locally advanced and/or metastatic pancreatic carcinoma - A prospective, randomized phase III study of the Gruppo Oncologico dell'Italia Meridionale. *Cancer*. 2002;94(4):902-10.
270. Reni M, Cordio S, Milandri C, Passoni P, Bonetto E, Oliani C, et al. Gemcitabine versus cisplatin, epirubicin, fluorouracil, and gemcitabine in advanced pancreatic cancer: a randomised controlled multicentre phase III trial. *Lancet Oncology*. 2005;6(6):369-76.
271. Louvet C, Labianca R, Hammel P, Lledo G, Zampino MG, Andre T, et al. Gemcitabine in combination with oxaliplatin compared with gemcitabine alone in locally advanced or metastatic pancreatic cancer: Results of a GERCOR and GISCAD phase III trial. *Journal of Clinical Oncology*. 2005;23(15):3509-16.
272. Herrmann R, Bodoky G, Ruhstaller T, Glimelius B, Bajetta E, Schueller J, et al. Gemcitabine plus capecitabine compared with gemcitabine alone in advanced pancreatic cancer: A randomized, multicenter, phase III trial of the Swiss Group for Clinical Cancer Research and the Central European Cooperative Oncology Group. *Journal of Clinical Oncology*. 2007;25(16):2212-7.
273. Cunningham D, Chau I, Stocken DD, Valle JW, Smith D, Steward W, et al. Phase III Randomized Comparison of Gemcitabine Versus Gemcitabine Plus Capecitabine in Patients With Advanced Pancreatic Cancer. *Journal of Clinical Oncology*. 2009;27(33):5513-8.
274. Li Y, Sun J, Jiang Z, Zhang L, Liu G. Gemcitabine and S-1 combination chemotherapy versus gemcitabine alone for locally advanced and metastatic pancreatic cancer: a meta-analysis of randomized controlled trials in Asia. *J Chemother*. 2015;27(4):227-34.
275. Lima CMR, Green MR, Rotche R, Miller WH, Jeffrey GM, Cisar LA, et al. Irinotecan plus gemcitabine results in no survival advantage compared with gemcitabine monotherapy in patients with locally

advanced or metastatic pancreatic cancer despite increased tumor response rate. *Journal of Clinical Oncology*. 2004;22(18):3776-83.

276. Whatcott CJ, Posner RG, Von Hoff DD, Han H. Desmoplasia and chemoresistance in pancreatic cancer. In: Grippo PJ, Munshi HG, editors. *Pancreatic Cancer and Tumor Microenvironment*. Trivandrum (India): Transworld Research Network

Transworld Research Network.; 2012.

277. Nielsen MF, Mortensen MB, Detlefsen S. Key players in pancreatic cancer-stroma interaction: Cancer-associated fibroblasts, endothelial and inflammatory cells. *World J Gastroenterol*. 2016;22(9):2678-700.

278. Walker C, Mojares E, Del Río Hernández A. Role of Extracellular Matrix in Development and Cancer Progression. *Int J Mol Sci*. 2018;19(10).

279. Yan Z, Ohuchida K, Fei S, Zheng B, Guan W, Feng H, et al. Inhibition of ERK1/2 in cancer-associated pancreatic stellate cells suppresses cancer–stromal interaction and metastasis. *Journal of Experimental & Clinical Cancer Research*. 2019;38(1):221.

280. Zhang H, Wu H, Guan J, Wang L, Ren X, Shi X, et al. Paracrine SDF-1alpha signaling mediates the effects of PSCs on GEM chemoresistance through an IL-6 autocrine loop in pancreatic cancer cells. *Oncotarget*. 2015;6(5):3085-97.

281. Vainer N, Dehlendorff C, Johansen JS. Systematic literature review of IL-6 as a biomarker or treatment target in patients with gastric, bile duct, pancreatic and colorectal cancer. *Oncotarget*. 2018;9(51):29820-41.

282. Sun Q, Zhang B, Hu Q, Qin Y, Xu W, Liu W, et al. The impact of cancer-associated fibroblasts on major hallmarks of pancreatic cancer. *Theranostics*. 2018;8(18):5072-87.

283. Zheng HC. The molecular mechanisms of chemoresistance in cancers. *Oncotarget*. 2017;8(35):59950-64.

284. Tsukasa K, Ding Q, Yoshimitsu M, Miyazaki Y, Matsubara S, Takao S. Slug contributes to gemcitabine resistance through epithelial-mesenchymal transition in CD133(+) pancreatic cancer cells. *Hum Cell*. 2015;28(4):167-74.

285. Morinaga S, Nakamura Y, Watanabe T, Mikayama H, Tamagawa H, Yamamoto N, et al. Immunohistochemical analysis of human equilibrative nucleoside transporter-1 (hENT1) predicts survival in resected pancreatic cancer patients treated with adjuvant gemcitabine monotherapy. *Ann Surg Oncol*. 2012;19 Suppl 3:S558-64.

286. Spratlin J, Sangha R, Glubrecht D, Dabbagh L, Young JD, Dumontet C, et al. The absence of human equilibrative nucleoside transporter 1 is associated with reduced survival in patients with

- gemcitabine-treated pancreas adenocarcinoma. *Clin Cancer Res.* 2004;10(20):6956-61.
287. Zhang YK, Wang YJ, Gupta P, Chen ZS. Multidrug Resistance Proteins (MRPs) and Cancer Therapy. *Aaps j.* 2015;17(4):802-12.
288. Horiguchi S, Shiraha H, Nagahara T, Kataoka J, Iwamuro M, Matsubara M, et al. Loss of runt-related transcription factor 3 induces gemcitabine resistance in pancreatic cancer. *Mol Oncol.* 2013;7(4):840-9.
289. Saiki Y, Yoshino Y, Fujimura H, Manabe T, Kudo Y, Shimada M, et al. DCK is frequently inactivated in acquired gemcitabine-resistant human cancer cells. *Biochem Biophys Res Commun.* 2012;421(1):98-104.
290. Kroep JR, Loves WJ, van der Wilt CL, Alvarez E, Talianidis I, Boven E, et al. Pretreatment deoxycytidine kinase levels predict in vivo gemcitabine sensitivity. *Mol Cancer Ther.* 2002;1(6):371-6.
291. Mackey JR, Mani RS, Selner M, Mowles D, Young JD, Belt JA, et al. Functional nucleoside transporters are required for gemcitabine influx and manifestation of toxicity in cancer cell lines. *Cancer Res.* 1998;58(19):4349-57.
292. Banerjee S, Nomura A, Sangwan V, Chugh R, Dudeja V, Vickers SM, et al. CD133+ tumor initiating cells in a syngenic murine model of pancreatic cancer respond to Minnelide. *Clin Cancer Res.* 2014;20(9):2388-99.
293. Aye Y, Li M, Long MJ, Weiss RS. Ribonucleotide reductase and cancer: biological mechanisms and targeted therapies. *Oncogene.* 2015;34(16):2011-21.
294. Weizman N, Krelin Y, Shabtay-Orbach A, Amit M, Binenbaum Y, Wong RJ, et al. Macrophages mediate gemcitabine resistance of pancreatic adenocarcinoma by upregulating cytidine deaminase. *Oncogene.* 2014;33(29):3812-9.
295. Wang M, Lu X, Dong X, Hao F, Liu Z, Ni G, et al. pERK1/2 silencing sensitizes pancreatic cancer BXPC-3 cell to gemcitabine-induced apoptosis via regulating Bax and Bcl-2 expression. *World Journal of Surgical Oncology.* 2015;13(1):66.
296. Mazza G, Al-Akkad W, Telese A, Longato L, Urbani L, Robinson B, et al. Rapid production of human liver scaffolds for functional tissue engineering by high shear stress oscillation-decellularization. 2017;7(1):5534.
297. Lieber M, Mazzetta J, Nelson-Rees W, Kaplan M, Todaro G. Establishment of a continuous tumor-cell line (panc-1) from a human carcinoma of the exocrine pancreas. *Int J Cancer.* 1975;15(5):741-7.

298. Yunis AA, Arimura GK, Russin DJ. Human pancreatic carcinoma (MIA PaCa-2) in continuous culture: sensitivity to asparaginase. *Int J Cancer*. 1977;19(1):128-35.
299. Kobari M, Hisano H, Matsuno S, Sato T, Kan M, Tachibana T. Establishment of six human pancreatic cancer cell lines and their sensitivities to anti-tumor drugs. *Tohoku J Exp Med*. 1986;150(3):231-48.
300. Livak KJ, Schmittgen TD. Analysis of relative gene expression data using real-time quantitative PCR and the $2^{-\Delta\Delta C(T)}$ Method. *Methods*. 2001;25(4):402-8.
301. Li H, Handsaker B, Wysoker A, Fennell T, Ruan J, Homer N, et al. The Sequence Alignment/Map format and SAMtools. *Bioinformatics*. 2009;25(16):2078-9.
302. Martin M. Cutadapt removes adapter sequences from high-throughput sequencing reads. 2011. 2011;17(1):3.
303. S A. FastQC: a quality control tool for high throughput sequence data. 2010.
304. Dobin A, Davis CA, Schlesinger F, Drenkow J, Zaleski C, Jha S, et al. STAR: ultrafast universal RNA-seq aligner. *Bioinformatics*. 2013;29(1):15-21.
305. Anders S, Pyl PT, Huber W. HTSeq--a Python framework to work with high-throughput sequencing data. *Bioinformatics*. 2015;31(2):166-9.
306. Love MI, Huber W, Anders S. Moderated estimation of fold change and dispersion for RNA-seq data with DESeq2. *Genome Biol*. 2014;15(12):550.
307. Draghici S, Khatri P, Tarca AL, Amin K, Done A, Voichita C, et al. A systems biology approach for pathway level analysis. *Genome Res*. 2007;17(10):1537-45.
308. Tarca AL, Draghici S, Khatri P, Hassan SS, Mittal P, Kim JS, et al. A novel signaling pathway impact analysis. *Bioinformatics*. 2009;25(1):75-82.
309. Khatri P, Draghici S, Tarca A, S. Hassan S, Romero R. A System Biology Approach for the Steady-State Analysis of Gene Signaling Networks 2007. 32-41 p.
310. Kanehisa M, Goto S. KEGG: kyoto encyclopedia of genes and genomes. *Nucleic Acids Res*. 2000;28(1):27-30.
311. Kanehisa M, Goto S, Furumichi M, Tanabe M, Hirakawa M. KEGG for representation and analysis of molecular networks involving diseases and drugs. *Nucleic Acids Res*. 2010;38(Database issue):D355-60.
312. Kanehisa M, Goto S, Sato Y, Furumichi M, Tanabe M. KEGG for integration and interpretation of large-scale molecular data sets. *Nucleic Acids Res*. 2012;40(Database issue):D109-14.

313. Kanehisa M, Goto S, Sato Y, Kawashima M, Furumichi M, Tanabe M. Data, information, knowledge and principle: back to metabolism in KEGG. *Nucleic Acids Res.* 2014;42(Database issue):D199-D205.
314. Draghici S, Khatri P, Martins RP, Ostermeier GC, Krawetz SA. Global functional profiling of gene expression. *Genomics.* 2003;81(2):98-104.
315. Drăghici S. *Statistics and data analysis for microarrays using R and Bioconductor.* 2nd ed. ed: Boca Raton (Fla.) : CRC Press; 2012.
316. Ashburner M, Ball CA, Blake JA, Botstein D, Butler H, Cherry JM, et al. Gene ontology: tool for the unification of biology. The Gene Ontology Consortium. *Nat Genet.* 2000;25(1):25-9.
317. Harris MA, Clark J, Ireland A, Lomax J, Ashburner M, Foulger R, et al. The Gene Ontology (GO) database and informatics resource. *Nucleic Acids Res.* 2004;32(Database issue):D258-61.
318. Alexa A, Rahnenfuhrer J, Lengauer T. Improved scoring of functional groups from gene expression data by decorrelating GO graph structure. *Bioinformatics.* 2006;22(13):1600-7.
319. Mazza G, Rombouts K, Rennie Hall A, Urbani L, Vinh Luong T, Al-Akkad W, et al. Decellularized human liver as a natural 3D-scaffold for liver bioengineering and transplantation. *Scientific Reports.* 2015;5:13079.
320. Miyauchi Y, Yasuchika K, Fukumitsu K, Ishii T, Ogiso S, Minami T, et al. A novel three-dimensional culture system maintaining the physiological extracellular matrix of fibrotic model livers accelerates progression of hepatocellular carcinoma cells. *Scientific Reports.* 2017;7:9827.
321. Hussein KH, Park KM, Ghim JH, Yang SR, Woo HM. Three dimensional culture of HepG2 liver cells on a rat decellularized liver matrix for pharmacological studies. *J Biomed Mater Res B Appl Biomater.* 2016;104(2):263-73.
322. Xiong G, Flynn TJ, Chen J, Trinkle C, Xu R. Development of an ex vivo breast cancer lung colonization model utilizing a decellularized lung matrix. *Integr Biol (Camb).* 2015;7(12):1518-25.
323. Mishra DK, Thrall MJ, Baird BN, Ott HC, Blackmon SH, Kurie JM, et al. Human Lung Cancer Cells Grown on Acellular Rat Lung Matrix Create Perfusible Tumor Nodules. *The Annals of thoracic surgery.* 2012;93(4):1075-81.
324. Dunne LW, Huang Z, Meng W, Fan X, Zhang N, Zhang Q, et al. Human decellularized adipose tissue scaffold as a model for breast cancer cell growth and drug treatments. *Biomaterials.* 2014;35(18):4940-9.
325. Rijal G, Li W. A versatile 3D tissue matrix scaffold system for tumor modeling and drug screening. *Science Advances.* 2017;3(9).

326. Pinto ML, Rios E, Silva AC, Neves SC, Caires HR, Pinto AT, et al. Decellularized human colorectal cancer matrices polarize macrophages towards an anti-inflammatory phenotype promoting cancer cell invasion via CCL18. *Biomaterials*. 2017;124:211-24.
327. Chen HJ, Wei Z, Sun J, Bhattacharya A, Savage DJ, Serda R, et al. A recellularized human colon model identifies cancer driver genes. *Nat Biotech*. 2016;34(8):845-51.
328. Shakesheff KM, Rose FRAJ. Tissue Engineering in the Development of Replacement Technologies. In: Balls M, Combes RD, Bhogal N, editors. *New Technologies for Toxicity Testing*. New York, NY: Springer US; 2012. p. 47-57.
329. Volk BW, Arquilla ER. *The Diabetic Pancreas*: Springer US; 2012.
330. Dolensek J, Rupnik MS, Stozer A. Structural similarities and differences between the human and the mouse pancreas. *Islets*. 2015;7(1):e1024405.
331. Nagata S, Hanayama R, Kawane K. Autoimmunity and the Clearance of Dead Cells. *Cell*. 2010;140(5):619-30.
332. Zheng MH, Chen J, Kirilak Y, Willers C, Xu J, Wood D. Porcine small intestine submucosa (SIS) is not an acellular collagenous matrix and contains porcine DNA: possible implications in human implantation. *J Biomed Mater Res B Appl Biomater*. 2005;73(1):61-7.
333. Zhang Q, Raoof M, Chen Y, Sumi Y, Sursal T, Junger W, et al. Circulating mitochondrial DAMPs cause inflammatory responses to injury. *Nature*. 2010;464(7285):104-7.
334. Peloso A, Urbani L, Cravedi P, Katari R, Maghsoudlou P, Fallas ME, et al. The Human Pancreas as a Source of Protolerogenic Extracellular Matrix Scaffold for a New-generation Bioartificial Endocrine Pancreas. *Annals of surgery*. 2016;264(1):169-79.
335. Sackett SD, Tremmel DM, Ma F, Feeney AK, Maguire RM, Brown ME, et al. Extracellular matrix scaffold and hydrogel derived from decellularized and delipidized human pancreas. 2018;8(1):10452.
336. Huang JS, Egger ME, Grizzle WE, McNally LR. MicroRNA-100 regulates IGF1-receptor expression in metastatic pancreatic cancer cells. *Biotechnic & histochemistry : official publication of the Biological Stain Commission*. 2013;88(7):397-402.
337. Gradiz R, Silva HC, Carvalho L, Botelho MF, Mota-Pinto A. MIA PaCa-2 and PANC-1 - pancreas ductal adenocarcinoma cell lines with neuroendocrine differentiation and somatostatin receptors. *Sci Rep*. 2016;6:21648.
338. Bhagwandin VJ, Bishop JM, Wright WE, Shay JW. The Metastatic Potential and Chemoresistance of Human Pancreatic Cancer Stem Cells. *PLOS ONE*. 2016;11(2):e0148807.

339. Suemizu H, Monnai M, Ohnishi Y, Ito M, Tamaoki N, Nakamura M. Identification of a key molecular regulator of liver metastasis in human pancreatic carcinoma using a novel quantitative model of metastasis in NOD/SCID/gammacnull (NOG) mice. *Int J Oncol.* 2007;31(4):741-51.
340. Lewis A, Du J, Liu J, Ritchie JM, Oberley LW, Cullen JJ. Metastatic progression of pancreatic cancer: changes in antioxidant enzymes and cell growth. *Clin Exp Metastasis.* 2005;22(7):523-32.
341. Meng Y, Lu Z, Yu S, Zhang Q, Ma Y, Chen J. Ezrin promotes invasion and metastasis of pancreatic cancer cells. *Journal of Translational Medicine.* 2010;8(1):61.
342. Okada T, Sawada T, Osawa T, Adachi M, Kubota K. MK615 inhibits pancreatic cancer cell growth by dual inhibition of Aurora A and B kinases. *World J Gastroenterol.* 2008;14(9):1378-82.
343. Watanabe K, Oochiai T, Kikuchi S, Kumano T, Matsui T, Morimoto K, et al. Dermokine expression in intraductal papillary-mucinous neoplasm and invasive pancreatic carcinoma. *Anticancer Res.* 2012;32(10):4405-12.
344. Liu N, Furukawa T, Kobari M, Tsao M-S. Comparative Phenotypic Studies of Duct Epithelial Cell Lines Derived from Normal Human Pancreas and Pancreatic Carcinoma. *Am J Pathol.* 153(1):263-9.
345. Daemen A, Peterson D, Sahu N, McCord R, Du X, Liu B, et al. Metabolite profiling stratifies pancreatic ductal adenocarcinomas into subtypes with distinct sensitivities to metabolic inhibitors. *Proceedings of the National Academy of Sciences.* 2015;112(32):E4410-E7.
346. Tomizawa M, Shinozaki F, Motoyoshi Y, Sugiyama T, Yamamoto S, Ishige N. SU11274 suppresses proliferation and motility of pancreatic cancer cells. *Oncol Lett.* 2015;10(3):1468-72.
347. Nakano Y, Tanno S, Koizumi K, Nishikawa T, Nakamura K, Minoguchi M, et al. Gemcitabine chemoresistance and molecular markers associated with gemcitabine transport and metabolism in human pancreatic cancer cells. *British journal of cancer.* 2007;96(3):457-63.
348. Ng SSW, Tsao M-S, Chow S, Hedley DW. Inhibition of Phosphatidylinositide 3-Kinase Enhances Gemcitabine-induced Apoptosis in Human Pancreatic Cancer Cells. *Cancer Research.* 2000;60(19):5451-5.
349. Hong J, Samudio I, Liu S, Abdelrahim M, Safe S. Peroxisome Proliferator-Activated Receptor γ -Dependent Activation of p21 in Panc-28 Pancreatic Cancer Cells Involves Sp1 and Sp4 Proteins. *Endocrinology.* 2004;145(12):5774-85.
350. Motomura W, Okumura T, Takahashi N, Obara T, Kohgo Y. Activation of peroxisome proliferator-activated receptor gamma by

troglitazone inhibits cell growth through the increase of p27KIP1 in human. Pancreatic carcinoma cells. *Cancer Res.* 2000;60(19):5558-64.

351. Motoi F, Sunamura M, Ding L, Duda DG, Yoshida Y, Zhang W, et al. Effective gene therapy for pancreatic cancer by cytokines mediated by restricted replication-competent adenovirus. *Hum Gene Ther.* 2000;11(2):223-35.

352. Amikura K, Kobari M, Matsuno S. The Mechanism of Liver Metastasis in Pancreatic Cancer

The Role of Basement Membrane Components in Attachment and Migration of Human Pancreatic Cancer Cells. *The Japanese Journal of Gastroenterological Surgery.* 1991;24(4):1112-6.

353. Matsuda Y, Yoshimura H, Ueda J, Naito Z, Korc M, Ishiwata T. Nestin Delineates Pancreatic Cancer Stem Cells in Metastatic Foci of NOD/Shi-scid IL2Rγ(null) (NOG) Mice. *Am J Pathol.* 2014;184(3):674-85.

354. Galli A, Ceni E, Crabb DW, Mello T, Salzano R, Grappone C, et al. Antidiabetic thiazolidinediones inhibit invasiveness of pancreatic cancer cells via PPARγ independent mechanisms. *Gut.* 2004;53(11):1688-97.

355. Justus CR, Leffler N, Ruiz-Echevarria M, Yang LV. In vitro cell migration and invasion assays. *J Vis Exp.* 2014(88):51046.

356. Zhang Y, Lukacova V, Reindl K, Balaz S. Quantitative characterization of binding of small molecules to extracellular matrix. *J Biochem Biophys Methods.* 2006;67(2-3):107-22.

357. Kibbey MC. Maintenance of the EHS sarcoma and Matrigel preparation. *Journal of tissue culture methods.* 1994;16(3):227-30.

358. Chia J, Kusuma N, Anderson R, Parker B, Bidwell B, Zamurs L, et al. Evidence for a role of tumor-derived laminin-511 in the metastatic progression of breast cancer. *Am J Pathol.* 2007;170(6):2135-48.

359. Ma F, Tremmel DM, Li Z, Lietz CB, Sackett SD, Odorico JS, et al. In Depth Quantification of Extracellular Matrix Proteins from Human Pancreas. 2019;18(8):3156-65.

360. Verstegen MMA, Willemsse J, Van Den Hoek S, Kremers G-J, Luidert TM, Van Huizen NA, et al. Decellularization of Whole Human Liver Grafts Using Controlled Perfusion for Transplantable Organ Bioscaffolds. *Stem Cells and Development.* 2017;26(18):1304-15.

361. Naba A, Clauser KR, Ding H, Whittaker CA, Carr SA, Hynes RO. The extracellular matrix: Tools and insights for the "omics" era. *Matrix biology : journal of the International Society for Matrix Biology.* 2016;49:10-24.

362. Martin TY, L. Sanders, A. J. Lane, J. and Jiang, W. G. *Cancer Invasion and Metastasis: Molecular and Cellular Perspective* Austin

(TX): Landes Bioscience2000-2013 [Available from:
<https://www.ncbi.nlm.nih.gov/books/NBK164700/>.

363. Hoyer AM, Erler JT. Structural ECM components in the premetastatic and metastatic niche. *American journal of physiology Cell physiology*. 2016;310(11):C955-67.
364. Mehner C, Hockla A, Miller E, Ran S, Radisky DC, Radisky ES. Tumor cell-produced matrix metalloproteinase 9 (MMP-9) drives malignant progression and metastasis of basal-like triple negative breast cancer. *Oncotarget*. 2014;5(9):2736-49.
365. Illemann M, Bird N, Majeed A, Sehested M, Laerum OD, Lund LR, et al. MMP-9 is differentially expressed in primary human colorectal adenocarcinomas and their metastases. *Molecular cancer research : MCR*. 2006;4(5):293-302.
366. Merchant N, Nagaraju GP, Rajitha B, Lammata S, Jella KK, Buchwald ZS, et al. Matrix metalloproteinases: their functional role in lung cancer. *Carcinogenesis*. 2017;38(8):766-80.
367. Kallakury BV, Karikhehalli S, Haholu A, Sheehan CE, Azumi N, Ross JS. Increased expression of matrix metalloproteinases 2 and 9 and tissue inhibitors of metalloproteinases 1 and 2 correlate with poor prognostic variables in renal cell carcinoma. *Clin Cancer Res*. 2001;7(10):3113-9.
368. Chen R, Cui J, Xu C, Xue T, Guo K, Gao D, et al. The significance of MMP-9 over MMP-2 in HCC invasiveness and recurrence of hepatocellular carcinoma after curative resection. *Ann Surg Oncol*. 2012;19 Suppl 3:S375-84.
369. Shan YQ, Ying RC, Zhou CH, Zhu AK, Ye J, Zhu W, et al. MMP-9 is increased in the pathogenesis of gastric cancer by the mediation of HER2. *Cancer Gene Ther*. 2015;22(3):101-7.
370. Jakubowska K, Pryczynicz A, Januszewska J, Sidorkiewicz I, Kemona A, Niewiński A, et al. Expressions of Matrix Metalloproteinases 2, 7, and 9 in Carcinogenesis of Pancreatic Ductal Adenocarcinoma. *Dis Markers*. 2016;2016:9895721-.
371. Kramer N, Walzl A, Unger C, Rosner M, Krupitza G, Hengstschläger M, et al. In vitro cell migration and invasion assays. *Mutation Research/Reviews in Mutation Research*. 2013;752(1):10-24.
372. Valastyan S, Weinberg RA. Tumor metastasis: molecular insights and evolving paradigms. *Cell*. 2011;147(2):275-92.
373. Tan MH, Nowak NJ, Loo R, Ochi H, Sandberg AA, Lopez C, et al. Characterization of a new primary human pancreatic tumor line. *Cancer investigation*. 1986;4(1):15-23.
374. Stahle M, Veit C, Bachfischer U, Schierling K, Skripczynski B, Hall A, et al. Mechanisms in LPA-induced tumor cell migration: critical role of phosphorylated ERK. *Journal of cell science*. 2003;116(Pt 18):3835-46.

375. Takada M, Nakamura Y, Koizumi T, Toyama H, Kamigaki T, Suzuki Y, et al. Suppression of human pancreatic carcinoma cell growth and invasion by epigallocatechin-3-gallate. *Pancreas*. 2002;25(1):45-8.
376. Greco E, Basso D, Fogar P, Mazza S, Navaglia F, Zambon CF, et al. Pancreatic cancer cells invasiveness is mainly affected by interleukin-1beta not by transforming growth factor-beta1. *The International journal of biological markers*. 2005;20(4):235-41.
377. Tang Z, Geng G, Huang Q, Xu G, Hu H, Chen J, et al. Prognostic significance of tissue factor pathway inhibitor-2 in pancreatic carcinoma and its effect on tumor invasion and metastasis. *Medical oncology (Northwood, London, England)*. 2010;27(3):867-75.
378. Pietruszewska W, Bojanowska-Pozniak K, Kobos J. Matrix metalloproteinases MMP1, MMP2, MMP9 and their tissue inhibitors TIMP1, TIMP2, TIMP3 in head and neck cancer: an immunohistochemical study. *Otolaryngol Pol*. 2016;70(3):32-43.
379. Zhang S, Li L, Lin JY, Lin H. Imbalance between expression of matrix metalloproteinase-9 and tissue inhibitor of metalloproteinase-1 in invasiveness and metastasis of human gastric carcinoma. *World J Gastroenterol*. 2003;9(5):899-904.
380. Lambert E, Dasse E, Haye B, Petitfrere E. TIMPs as multifacial proteins. *Critical reviews in oncology/hematology*. 2004;49(3):187-98.
381. Wasil LR, Shair KH. Epstein-Barr virus LMP1 induces focal adhesions and epithelial cell migration through effects on integrin-alpha5 and N-cadherin. *Oncogenesis*. 2015;4:e171.
382. Siret C, Terciolo C, Dobric A, Habib MC, Germain S, Bonnier R, et al. Interplay between cadherins and alpha2beta1 integrin differentially regulates melanoma cell invasion. *British journal of cancer*. 2015;113(10):1445-53.
383. Wang WJ, Yao Y, Jiang LL, Hu TH, Ma JQ, Liao ZJ, et al. Knockdown of lymphoid enhancer factor 1 inhibits colon cancer progression in vitro and in vivo. *PLoS One*. 2013;8(10):e76596.
384. Zhao Y, Zhu J, Shi B, Wang X, Lu Q, Li C, et al. The transcription factor LEF1 promotes tumorigenicity and activates the TGF- β signaling pathway in esophageal squamous cell carcinoma. *Journal of Experimental & Clinical Cancer Research*. 2019;38(1):304.
385. Yang Y, Jiang Y, Xie D, Liu M, Song N, Zhu J, et al. Inhibition of cell-adhesion protein DPYSL3 promotes metastasis of lung cancer. *Respir Res*. 2018;19(1):41-.
386. Yabluchanskiy A, Ma Y, Iyer RP, Hall ME, Lindsey ML. Matrix metalloproteinase-9: Many shades of function in cardiovascular disease. *Physiology (Bethesda)*. 2013;28(6):391-403.

387. Monferran S, Paupert J, Dauvillier S, Salles B, Muller C. The membrane form of the DNA repair protein Ku interacts at the cell surface with metalloproteinase 9. *EMBO J*. 2004;23(19):3758-68.
388. Ramos-DeSimone N, Hahn-Dantona E, Siple J, Nagase H, French DL, Quigley JP. Activation of matrix metalloproteinase-9 (MMP-9) via a converging plasmin/stromelysin-1 cascade enhances tumor cell invasion. *The Journal of biological chemistry*. 1999;274(19):13066-76.
389. Perrin BJ, Ervasti JM. The actin gene family: function follows isoform. *Cytoskeleton (Hoboken)*. 2010;67(10):630-4.
390. Peng JM, Bera R, Chiou CY, Yu MC. Actin cytoskeleton remodeling drives epithelial-mesenchymal transition for hepatoma invasion and metastasis in mice. 2018;67(6):2226-43.
391. Kakiuchi S, Daigo Y, Tsunoda T, Yano S, Sone S, Nakamura Y. Genome-wide analysis of organ-preferential metastasis of human small cell lung cancer in mice. *Molecular cancer research : MCR*. 2003;1(7):485-99.
392. Chui MH. Insights into cancer metastasis from a clinicopathologic perspective: Epithelial-Mesenchymal Transition is not a necessary step. *Int J Cancer*. 2013;132(7):1487-95.
393. Thiery JP. Epithelial-mesenchymal transitions in tumour progression. *Nature reviews Cancer*. 2002;2(6):442-54.
394. Chen W, Kang KL, Alshaikh A, Varma S, Lin Y-L, Shin K-H, et al. Grainyhead-like 2 (GRHL2) knockout abolishes oral cancer development through reciprocal regulation of the MAP kinase and TGF- β signaling pathways. *Oncogenesis*. 2018;7(5):38.
395. Xiang X, Deng Z, Zhuang X, Ju S, Mu J, Jiang H, et al. Grhl2 determines the epithelial phenotype of breast cancers and promotes tumor progression. *PLoS One*. 2012;7(12):e50781.
396. Wen Z, Liao Q, Hu Y, You L, Zhou L, Zhao Y. A spheroid-based 3-D culture model for pancreatic cancer drug testing, using the acid phosphatase assay. *Braz J Med Biol Res*. 2013;46(7):634-42.
397. Longati P, Jia X, Eimer J, Wagman A, Witt MR, Rehnmark S, et al. 3D pancreatic carcinoma spheroids induce a matrix-rich, chemoresistant phenotype offering a better model for drug testing. *BMC Cancer*. 2013;13:95.
398. Mohammad J, Dhillon H, Chikara S, Mamidi S, Sreedasyam A, Chittem K, et al. Piperlongumine potentiates the effects of gemcitabine in in vitro and in vivo human pancreatic cancer models. *Oncotarget*. 2018;9(12):10457-69.
399. Longo-Sorbello GS, Bertino JR. Current understanding of methotrexate pharmacology and efficacy in acute leukemias. Use of newer antifolates in clinical trials. *Haematologica*. 2001;86(2):121-7.

400. Giovannetti E, Del Tacca M, Mey V, Funel N, Nannizzi S, Ricci S, et al. Transcription analysis of human equilibrative nucleoside transporter-1 predicts survival in pancreas cancer patients treated with gemcitabine. *Cancer Res.* 2006;66(7):3928-35.
401. Borst P, Evers R, Kool M, Wijnholds J. The multidrug resistance protein family. *Biochim Biophys Acta.* 1999;1461(2):347-57.
402. Hamacher R, Schmid RM, Saur D, Schneider G. Apoptotic pathways in pancreatic ductal adenocarcinoma. *Mol Cancer.* 2008;7:64.
403. Marechal R, Mackey JR, Lai R, Demetter P, Peeters M, Polus M, et al. Human equilibrative nucleoside transporter 1 and human concentrative nucleoside transporter 3 predict survival after adjuvant gemcitabine therapy in resected pancreatic adenocarcinoma. *Clin Cancer Res.* 2009;15(8):2913-9.
404. Nakano Y, Tanno S, Koizumi K, Nishikawa T, Nakamura K, Minoguchi M, et al. Gemcitabine chemoresistance and molecular markers associated with gemcitabine transport and metabolism in human pancreatic cancer cells. *British journal of cancer.* 2007;96(3):457-63.
405. Ciccolini J, Mercier C, Dahan L, Andre N. Integrating pharmacogenetics into gemcitabine dosing--time for a change? *Nat Rev Clin Oncol.* 2011;8(7):439-44.
406. Hesler RA, Huang JJ, Starr MD, Treboschi VM, Bernanke AG, Nixon AB, et al. TGF- β -induced stromal CYR61 promotes resistance to gemcitabine in pancreatic ductal adenocarcinoma through downregulation of the nucleoside transporters hENT1 and hCNT3. *Carcinogenesis.* 2016;37(11):1041-51.
407. Kocabas NA, Aksoy P, Pellemounter LL, Moon I, Ryu J-S, Gilbert JA, et al. Gemcitabine pharmacogenomics: deoxycytidine kinase and cytidylate kinase gene resequencing and functional genomics. *Drug Metab Dispos.* 2008;36(9):1951-9.
408. Nakano Y, Tanno S, Koizumi K, Nishikawa T, Nakamura K, Minoguchi M, et al. Gemcitabine chemoresistance and molecular markers associated with gemcitabine transport and metabolism in human pancreatic cancer cells. *British journal of cancer.* 2007;96(3):457-63.
409. Ohhashi S, Ohuchida K, Mizumoto K, Fujita H, Egami T, Yu J, et al. Down-regulation of deoxycytidine kinase enhances acquired resistance to gemcitabine in pancreatic cancer. *Anticancer Res.* 2008;28(4b):2205-12.
410. Alvarellos ML, Lamba J, Sangkuhl K, Thorn CF, Wang L, Klein DJ, et al. PharmGKB summary: gemcitabine pathway. *Pharmacogenet Genomics.* 2014;24(11):564-74.

411. Shipley LA, Brown TJ, Cornpropst JD, Hamilton M, Daniels WD, Culp HW. Metabolism and disposition of gemcitabine, and oncolytic deoxycytidine analog, in mice, rats, and dogs. *Drug Metab Dispos.* 1992;20(6):849-55.
412. Frese KK, Neesse A, Cook N, Bapiro TE, Lolkema MP, Jodrell DI, et al. nab-Paclitaxel potentiates gemcitabine activity by reducing cytidine deaminase levels in a mouse model of pancreatic cancer. *Cancer Discov.* 2012;2(3):260-9.
413. Marechal R, Bachet JB, Mackey JR, Dalban C, Demetter P, Graham K, et al. Levels of gemcitabine transport and metabolism proteins predict survival times of patients treated with gemcitabine for pancreatic adenocarcinoma. *Gastroenterology.* 2012;143(3):664-74.e6.
414. Greenhalf W, Ghaneh P, Neoptolemos JP, Palmer DH, Cox TF, Lamb RF, et al. Pancreatic cancer hENT1 expression and survival from gemcitabine in patients from the ESPAC-3 trial. *J Natl Cancer Inst.* 2014;106(1):djt347.
415. Funamizu N, Okamoto A, Kamata Y, Misawa T, Uwagawa T, Gocho T, et al. Is the resistance of gemcitabine for pancreatic cancer settled only by overexpression of deoxycytidine kinase? *Oncol Rep.* 2010;23(2):471-5.
416. Eda H, Ura M, K FO, Tanaka Y, Miwa M, Ishitsuka H. The antiproliferative activity of DMDC is modulated by inhibition of cytidine deaminase. *Cancer Res.* 1998;58(6):1165-9.
417. Galmarini CM, Mackey JR, Dumontet C. Nucleoside analogues: mechanisms of drug resistance and reversal strategies. *Leukemia.* 2001;15(6):875-90.
418. Nakahira S, Nakamori S, Tsujie M, Takahashi Y, Okami J, Yoshioka S, et al. Involvement of ribonucleotide reductase M1 subunit overexpression in gemcitabine resistance of human pancreatic cancer. *Int J Cancer.* 2007;120(6):1355-63.
419. Heinemann V, Xu YZ, Chubb S, Sen A, Hertel LW, Grindey GB, et al. Cellular elimination of 2',2'-difluorodeoxycytidine 5'-triphosphate: a mechanism of self-potential. *Cancer Res.* 1992;52(3):533-9.
420. Heinemann V, Xu YZ, Chubb S, Sen A, Hertel LW, Grindey GB, et al. Inhibition of ribonucleotide reduction in CCRF-CEM cells by 2',2'-difluorodeoxycytidine. *Mol Pharmacol.* 1990;38(4):567-72.
421. Wang C, Zhang W, Fu M, Yang A, Huang H, Xie J. Establishment of human pancreatic cancer gemcitabine-resistant cell line with ribonucleotide reductase overexpression. *Oncol Rep.* 2015;33(1):383-90.
422. Bazzichetto C, Conciatori F, Falcone I, Cognetti F, Milella M, Ciuffreda L. Advances in Tumor-Stroma Interactions: Emerging Role of

- Cytokine Network in Colorectal and Pancreatic Cancer. *J Oncol.* 2019;2019:5373580.
423. Arlt A, Gehrz A, Muerkoster S, Vorndamm J, Kruse ML, Folsch UR, et al. Role of NF-kappaB and Akt/PI3K in the resistance of pancreatic carcinoma cell lines against gemcitabine-induced cell death. *Oncogene.* 2003;22(21):3243-51.
424. Kumar S, Peng X, Daley J, Yang L, Shen J, Nguyen N, et al. Inhibition of DNA2 nuclease as a therapeutic strategy targeting replication stress in cancer cells. *Oncogenesis.* 2017;6(4):e319.
425. Iseri OD, Kars MD, Arpaci F, Gunduz U. Gene expression analysis of drug-resistant MCF-7 cells: implications for relation to extracellular matrix proteins. *Cancer Chemother Pharmacol.* 2010;65(3):447-55.
426. Chabner BA. Does Chemotherapy Induce Metastases? *Oncologist.* 2018;23(3):273-4.
427. Fischer R, Breidert M, Keck T, Makowiec F, Lohrmann C, Harder J. Early recurrence of pancreatic cancer after resection and during adjuvant chemotherapy. *Saudi Journal of Gastroenterology.* 2012;18(2):118-21.
428. Jian P, Yanfang T, Zhuan Z, Jian W, Xueming Z, Jian N. MMP28 (epilysin) as a novel promoter of invasion and metastasis in gastric cancer. *BMC Cancer.* 2011;11:200.
429. Ouyang H, Mou L, Luk C, Liu N, Karaskova J, Squire J, et al. Immortal human pancreatic duct epithelial cell lines with near normal genotype and phenotype. *Am J Pathol.* 2000;157(5):1623-31.

SUPPLEMENTARY TABLES

Gene Name	LogFC	Gene Name	LogFC	Gene Name	LogFC
CDH11	-1.09717	FOXA1	0.649087	ITGB3	0.870214
TNFSF9	-1.08745	RAC2	0.662903	SDK1	0.890718
MIR221	-1.06334	C1QTNF1	0.663512	WNT4	0.891827
GPNMB	-0.97466	TNIP1	0.667743	PCDHA4	0.936849
NLGN3	-0.89107	ROBO1	0.667961	DSP	1.002466
THY1	-0.87067	PIK3R1	0.676702	CCL5	1.017486
TENM4	-0.81353	PCDHGB1	0.686238	ROBO2	1.021972
CDH17	-0.81151	ICAM5	0.695881	PCDH9	1.037069
PKP2	-0.80703	CDH6	0.698081	ITGB2	1.079931
SMAGP	-0.74251	CDH3	0.699109	CX3CL1	1.090956
CRTAM	-0.72489	ZMIZ1	0.702237	PCDHGB2	1.109778
CAMSAP3	-0.72063	KRT18	0.704785	SHH	1.145736
LAT	-0.67417	WNT7B	0.706835	PCDHGB7	1.155573
NINJ2	-0.66469	CADM2	0.711529	CTNND1	1.180016
CD55	-0.64321	SOCS1	0.713378	BMP2	1.187065
CD24	-0.64219	FLNA	0.713689	PVRL3	1.190024
HLA-DPA1	-0.64171	ITGAV	0.721223	FLRT3	1.196151
CLDN6	-0.63726	PCDHA12	0.722486	PCDHGC3	1.213508
CEACAM5	-0.63657	IRF1	0.733443	CDH2	1.228326
HLA-DMB	-0.63418	ICAM1	0.733484	COL13A1	1.254912
LAG3	-0.60568	CCM2L	0.735048	LEF1	1.277809
COL8A2	0.593315	DSCAML1	0.735879	CD74	1.292739
PCDHA13	0.593387	PRKG1	0.740828	BMP5	1.30098
JUP	0.598673	TNFRSF18	0.752489	CADM1	1.391066
PCDHB2	0.606411	LAMB1	0.78848	PCDHAC2	1.43133
ZNF703	0.633358	EBI3	0.810893	IGF2	1.538668
PLXNB2	0.637171	ICOSLG	0.814256	PCDH7	1.564951
FBLIM1	0.641858	CCL2	0.815711	RET	1.585267
CYFIP2	0.6426	PCDH20	0.835269	PODXL	1.631807
MYH9	0.648624	IL7	0.860877	NTN1	1.746243

Supplementary Table 1. Significantly ($p < 0.05$) DE genes of the GO term “cell-cell adhesion” between PANC-1 cells cultured on pancreas vs liver scaffolds. Negative numbers represent genes up-regulated in the pancreas scaffolds. Positive numbers represent genes up-regulated in the liver scaffolds.

Gene Name	LogFC	Gene Name	LogFC
DLC1	-1.30357	COL16A1	0.766148
STRC	-0.96018	ITGA10	0.817882
THY1	-0.87067	SORBS1	0.835476
HPSE	-0.8297	ITGB3	0.870214
CAMSAP3	-0.72063	WNT4	0.891827
COL5A3	0.590987	LAMA5	0.927203
DDR1	0.618298	CSF1	1.039953
PIK3R1	0.676702	ITGB2	1.079931
ROCK2	0.695743	THBS1	1.138045
ITGAV	0.721223	ITGB4	1.197617
VEGFC	0.72198	COL13A1	1.254912
ITGA3	0.738333	L1CAM	1.541987
BCAM	0.756725		

Supplementary Table 2. Significantly ($p < 0.05$) DE genes of the GO term “cell-matrix adhesion” between PANC-1 cells cultured on pancreas vs liver scaffolds. Negative numbers represent genes up-regulated in the pancreas scaffolds. Positive numbers represent genes up-regulated in the liver scaffolds.

Gene Name	LogFC	Gene Name	LogFC	Gene Name	LogFC	Gene Name	LogFC
PRSS3	-1.88773	PARP9	0.59427859	ICAM1	0.73348414	FMNL3	1.01378196
DPYSL3	-1.74955	DNAH5	0.59696503	ITGA3	0.73833289	CCL5	1.01748616
DLC1	-1.30357	JUP	0.5986735	SCARB1	0.73944136	PLXNA2	1.01886295
MIR221	-1.06334	EPHB4	0.60390361	PRKG1	0.74082813	CSF1	1.03995271
SPOCK1	-0.99437	CRB2	0.61410118	TNFRSF18	0.75248896	NAV3	1.04602678
GPNMB	-0.97466	DDR1	0.61829759	SBK2	0.76431686	SEMA3A	1.05963753
C5AR1	-0.97028	PDGFB	0.61867572	PLXND1	0.7674035	DOCK4	1.06089396
NDRG4	-0.90487	PLXNA1	0.63210075	MDGA1	0.77241622	ITGB2	1.07993132
THY1	-0.87067	ZNF703	0.6333578	AUTS2	0.78094698	CX3CL1	1.09095585
FGF18	-0.85068	PLXNB2	0.63717058	CDKL5	0.78621951	MYO18A	1.10546433
SGK1	-0.84783	SEMA3C	0.64168935	LAMB1	0.78848033	THBS1	1.13804519
VANGL2	-0.83983	S100P	0.64272231	DDIT4	0.78853279	SHH	1.14573574
LRRC16A	-0.80972	PLTP	0.64343767	SPOCK3	0.79081754	BMP2	1.18706485
PKP2	-0.80703	MYH9	0.64862416	UNC5C	0.80460999	FLRT3	1.19615081
CCL20	-0.80383	FLRT2	0.64881195	TNS3	0.80591556	ITGB4	1.1976168
FOXP1	-0.77546	KITLG	0.65077104	LAMA3	0.8090398	PTPRG	1.20350471
ABCC8	-0.72161	EPPK1	0.6530685	CCL2	0.81571097	CDH2	1.22832601
CAMSAP3	-0.72063	DOCK10	0.65928695	SLC8A1	0.82181233	LEF1	1.27780889
FZD3	-0.72052	RAC2	0.66290343	CSPG4	0.83478013	CD74	1.29273942
DNER	-0.71285	SOD2	0.66645235	ITGB3	0.87021359	BMP5	1.30097982
VHLL	-0.66527	ROBO1	0.66796101	CYGB	0.87474497	NBL1	1.46925771
SEPT12	-0.65851	ROR2	0.67239078	RFFL	0.87484392	LAMC2	1.52369378
CD24	-0.64219	PIK3R1	0.6767019	SDC2	0.87802464	L1CAM	1.54198664
ADRA2A	-0.64123	MEGF8	0.6944928	WNT4	0.89182656	RET	1.58526693
CEACAM5	-0.63657	ROCK2	0.69574304	MMP9	0.9056683	PODXL	1.6318068
SPEF1	-0.62516	COL5A1	0.70432086	LAMA5	0.92720277	NTN1	1.74624333
FCER1G	-0.62153	FLNA	0.71368891	AMOTL1	0.93747238	NTRK2	2.00220569
EPHB1	-0.58546	ITGAV	0.72122277	PTPRF	0.95204145	GPC6	2.1780994
KRT16	0.589739	VEGFC	0.72197966	IL16	0.99985363		

Supplementary Table 3. Significantly ($p < 0.05$) DE genes of the GO term “cell motility” between PANC-1 cells cultured on pancreas vs liver scaffolds. Negative numbers represent genes up-regulated in the pancreas scaffolds. Positive numbers represent genes up-regulated in the liver scaffolds.

Gene Name	LogFC	Gene Name	LogFC
PRSS3	-1.88773	ACTA2	0.665242
MIR221	-1.06334	ROBO1	0.667961
FGF18	-0.85068	ROCK2	0.695743
FOXP1	-0.77546	VEGFC	0.72198
ACTC1	-0.77057	ITGA3	0.738333
VHLL	-0.66527	SCARB1	0.739441
ACTA1	-0.64587	PLXND1	0.767404
KRT16	0.589739	ITGB3	0.870214
EPHB4	0.603904	MMP9	0.905668
PDGFB	0.618676	AMOTL1	0.937472
ACTG2	0.621538	SEMA3A	1.059638
S100P	0.642722	ITGB2	1.079931
MYH9	0.648624	THBS1	1.138045
EPPK1	0.653069	PTPRG	1.203505

Supplementary Table 4. Significantly ($p < 0.05$) DE genes of the GO term “tissue migration” between PANC-1 cells cultured on pancreas vs liver scaffolds. Negative numbers represent genes up-regulated in the pancreas scaffolds. Positive numbers represent genes up-regulated in the liver scaffolds.

Gene Name	LogFC	Gene Name	LogFC
CCDC80	-2.04744	COL11A1	0.784841
ADAMTS14	-1.12897	LAMB1	0.78848
TEX14	-1.04221	TGFBI	0.806245
CTSK	-0.73936	LAMA3	0.80904
VHLL	-0.66527	ERO1LB	0.815605
LOX	-0.64258	ITGA10	0.817882
HAPLN2	-0.59383	VWA1	0.82576
COL6A2	0.588726	ITGB3	0.870214
COL5A3	0.590987	A2M	0.894397
COL8A2	0.593315	MMP9	0.905668
CTSS	0.60158	LAMA5	0.927203
DDR1	0.618298	AGRN	0.92811
PDGFB	0.618676	ELF3	1.048
FLRT2	0.648812	ITGB2	1.079931
ANTXR1	0.672406	ITGB8	1.106503
ICAM5	0.695881	THBS1	1.138045
COL5A1	0.704321	COL12A1	1.172796
COL27A1	0.70495	ITGB4	1.197617
MMP16	0.718714	COL9A3	1.229652
ITGAV	0.721223	COL13A1	1.254912
ICAM1	0.733484	TNC	1.387895
ITGA3	0.738333	HSPG2	1.485561
COL16A1	0.766148	LAMC2	1.523694
BGN	0.784012	SCUBE3	2.239323

Supplementary Table 5. Significantly ($p < 0.05$) DE genes of the GO term “extracellular structure organisation” between PANC-1 cells cultured on pancreas vs liver scaffolds. Negative numbers represent genes up-regulated in the pancreas scaffolds. Positive numbers represent genes up-regulated in the liver scaffolds.

Gene Name	LogFC	Gene Name	LogFC
MIR221	-1.06334	ITGAV	0.721223
GPNMB	-0.97466	VEGFC	0.72198
C5AR1	-0.97028	ARHGAP22	0.737798
THY1	-0.87067	GTF2I	0.764782
FGF18	-0.85068	PLXND1	0.767404
HPSE	-0.8297	TGFBI	0.806245
ABCC8	-0.72161	CCL2	0.815711
GATA6	-0.67181	CSPG4	0.83478
VHLL	-0.66527	TYMP	0.851484
KLF5	-0.60257	ITGB3	0.870214
EPHB1	-0.58546	RAMP1	0.918115
COL8A2	0.593315	LAMA5	0.927203
EPHB4	0.603904	LRG1	0.940068
MFGE8	0.633248	FMNL3	1.013782
MYH9	0.648624	ITGB2	1.079931
FAM129B	0.651676	CX3CL1	1.090956
ERAP1	0.654138	THBS1	1.138045
THSD7A	0.658985	TNFAIP2	1.144435
ROBO1	0.667961	SHH	1.145736
PLCD3	0.683223	LEF1	1.277809
ROCK2	0.695743	ANPEP	1.317698
RNF213	0.718118	HSPG2	1.485561

Supplementary Table 6. Significantly ($p < 0.05$) DE genes of the GO term “angiogenesis” between PANC-1 cells cultured on pancreas vs liver scaffolds. Negative numbers represent genes up-regulated in the pancreas scaffolds. Positive numbers represent genes up-regulated in the liver scaffolds.

Gene Name	LogFC	Gene Name	LogFC	Gene Name	LogFC
CD177	-1.59416	MYB	-0.7728262	BAIAP2L1	-0.5939922
IFNL1	-1.49126	EFNA5	-0.7717854	PRKCQ	0.58501766
GPNMB	-1.41644	TRPV4	-0.7704627	PODXL	0.58566403
CCL5	-1.3776	ITGB2	-0.7686239	GPAM	0.59628937
DCHS2	-1.25011	FANCA	-0.7653011	JAK2	0.60389439
BMP7	-1.24251	PAK1	-0.7512202	CDC42EP1	0.61433451
CEACAM5	-1.21914	IL1RN	-0.7403331	TGFB2	0.61655389
TNFSF9	-1.21409	EPHB3	-0.7243096	PCDHB12	0.6289464
CDH26	-1.19456	ASS1	-0.7167215	PAWR	0.63323317
SPINK5	-1.19018	IGFBP2	-0.7132156	ADA	0.64654119
SOX2	-1.18763	CSTA	-0.6992796	CDH22	0.64795211
NOV	-1.17719	IFNL2	-0.6977815	PCDHGB2	0.66861749
IL7R	-1.15336	LCK	-0.6851232	CLDN9	0.68736016
SERPINE2	-1.08514	MPZL2	-0.6744002	FAT4	0.71017894
TNFRSF13C	-1.06854	MPZ	-0.6739507	AJUBA	0.72350908
ICAM1	-1.06008	PCDH20	-0.6686795	KIRREL3	0.77398744
RGCC	-1.05848	PCDHGA12	-0.660833	PODXL2	0.78123857
ITGAM	-0.99233	FANCD2	-0.6553723	FSTL3	0.78594447
PRKCA	-0.924	NFKBID	-0.644206	PCDHB10	0.81556901
GPR98	-0.92114	GNRH1	-0.6420947	RASGRP1	0.83300882
NPNT	-0.89297	ITGAX	-0.6297261	DOCK8	0.85771488
CD24	-0.88034	BCL6	-0.6274874	B4GALNT2	0.87356239
MAP3K8	-0.87309	SOX13	-0.6251331	AMIGO1	0.89951507
ARG2	-0.87159	CCDC88B	-0.6247316	COL13A1	1.02024721
CNN3	-0.82718	CLDN8	-0.6202797	LOXL3	1.02444343
PCDHGC5	-0.82656	NR4A3	-0.616361	C1QTNF1	1.03567785
ITGB7	-0.82162	PKD1L1	-0.6115387	MYL9	1.03780381
PCDHA7	-0.81777	PCDH9	-0.6101485	AMIGO2	1.20154702
SOCS1	-0.81661	FOXA2	-0.6050894	FYN	1.25771811
LEF1	-0.8033	SERPINB8	-0.6050601	KIT	1.55547648
MIR221	-0.79124	CRTAM	-0.6022062	FAT3	1.85424553
TNFRSF14	-0.789768974	KLF4	-0.5979297		

Supplementary Table 7. Significantly ($p < 0.05$) DE genes of the GO term “cell-cell adhesion” between PK-1 cells cultured on pancreas vs liver scaffolds. Negative numbers represent genes up-regulated in the pancreas scaffolds. Positive numbers represent genes up-regulated in the liver scaffolds.

Gene Name	LogFC
MIR29C	-0.94152
APOD	-0.9322
BCL6	-0.62749
SERPINE1	0.766135
THBS1	1.036319
DLC1	1.281306

Supplementary Table 8. Significantly ($p < 0.05$) DE genes of the GO term “negative regulation cell-matrix adhesion” between PK-1 cells cultured on pancreas vs liver scaffolds. Negative numbers represent genes up-regulated in the pancreas scaffolds. Positive numbers represent genes up-regulated in the liver scaffolds.

Gene Name	LogFC	Gene Name	LogFC	Gene Name	LogFC	Gene Name	LogFC
CCL20	-2.22859	ARC	1.00258589	DNAH2	0.67507928	SLC16A1	0.704683
NKX2-1	-2.12194	ITGAM	-0.99233	GRB7	-0.66801	SLC7A7	0.711692
CEMIP	-2.06016	VAV3	-0.99203	BST1	-0.65802	AJUBA	0.723509
CXCL8	-1.80715	GLIPR2	-0.9649	PLAU	-0.65586	SIX4	0.724812
EMR2	-1.66369	TREM1	-0.95856	ERBB4	-0.64931	NR2F2	0.735048
CD177	-1.59416	MIR29C	-0.94152	ZC3H12A	-0.64652	MATN2	0.740288
CDK1	-1.58736	APOD	-0.9322	C9orf117	-0.64509	PDGFD	0.75054
GTSE1	-1.48147	PRKCA	-0.924	SLC16A3	-0.64467	ABHD6	0.759141
CACNA1I	-1.47492	EGR3	-0.92195	GNRH1	-0.64209	SERPINE1	0.766135
KIF14	-1.45562	PRSS3	-0.91032	PROS1	-0.64104	ATP1A4	0.769361
GPNMB	-1.41644	CD24	-0.88034	ITGAX	-0.62973	SEMA5A	0.771361
CCL5	-1.3776	CXCL10	-0.87867	VANGL2	-0.62084	KIRREL3	0.773987
FAM83D	-1.37643	ASPM	-0.86052	IDH2	-0.61443	PRR5L	0.774888
ARID5B	-1.36085	STRIP2	-0.8519	EPHA2	-0.61339	PODXL2	0.781239
ANLN	-1.35245	MIR200A	-0.84245	HMCN2	-0.60992	SLC9B2	0.794788
CXCL2	-1.33402	ARTN	-0.84052	CXCL14	-0.6059	LY6K	0.800187
DEPDC1B	-1.24855	INPP5D	-0.82199	CCL17	-0.59824	DDIT4	0.816695
ANGPT4	-1.24596	ITGB7	-0.82162	KLF4	-0.59793	LRP12	0.830377
BMP7	-1.24251	RASGEF1A	-0.8042	HDAC5	-0.59499	PTRF	0.83086
CEACAM5	-1.21914	LEF1	-0.8033	KIAA1462	-0.59171	LAMA1	0.851213
DLL4	-1.21427	MIR221	-0.79124	RAB13	-0.58904	DOCK8	0.857715
PAX6	-1.18865	TNFRSF14	-0.78977	PLEKHG5	-0.58866	NEURL1	0.960364
NOV	-1.17719	BDKRB1	-0.78771	PRKCQ	0.585018	TPM1	0.981029
CXCL3	-1.16718	MIR29B2	-0.7858	PODXL	0.585664	ATOX8	1.018598
HDAC9	-1.14882	STYK1	-0.78311	SIX1	0.593403	THBS1	1.036319
MMP1	-1.14358	TRPV4	-0.77046	SYDE1	0.597586	ACKR3	1.061859
NR4A2	-1.14208	ITGB2	-0.76862	JAK2	0.603894	SPOCK2	1.134625
TP53INP1	-1.13428	PTK6	-0.76567	NDRG4	0.612485	SIRPA	1.198485
MCTP1	-1.12219	PAK1	-0.75122	SLC7A5	0.613291	FYN	1.257718
ECM1	-1.10871	CEACAM6	-0.74658	TGFB2	0.616554	DLC1	1.281306
NR4A1	-1.10778	KIAA0319	-0.74011	L1CAM	0.616703	APOE	1.412475
SERPINE2	-1.08514	SPNS2	-0.73363	PREX1	0.618441	BMPER	1.540242
ICAM1	-1.06008	EPHB3	-0.72431	SATB2	0.630327	KIT	1.555476
RGCC	-1.05848	TEKT2	-0.72417	FZD3	0.633093	FN1	2.046472
KALRN	-1.05371	ARHGEF16	-0.69505	SOX8	0.635886	SPOCK1	2.192858
HMGB2	-1.03332	LCK	-0.68512	ADA	0.646541	MMP9	2.204733
DCLK1	-1.01208	DAB2	-0.68345	EDN2	0.658175		

Supplementary Table 9. Significantly ($p < 0.05$) DE genes of the GO term “cell motility” between PK-1 cells cultured on pancreas vs liver scaffolds. Negative numbers represent genes up-regulated in the pancreas scaffolds. Positive numbers represent genes up-regulated in the liver scaffolds.

Gene Name	LogFC	Gene Name	LogFC
ANLN	-1.35245	EPHA2	-0.61339
ANGPT4	-1.24596	KLF4	-0.59793
DLL4	-1.21427	HDAC5	-0.59499
NOV	-1.17719	KIAA1462	-0.59171
HDAC9	-1.14882	RAB13	-0.58904
NR4A1	-1.10778	PLEKHG5	-0.58866
RGCC	-1.05848	GRHL2	0.59931
GLIPR2	-0.9649	TGFB2	0.616554
MIR29C	-0.94152	NR2F2	0.735048
PRKCA	-0.924	SEMA5A	0.771361
EGR3	-0.92195	ATOH8	1.018598
PRSS3	-0.91032	THBS1	1.036319
MIR200A	-0.84245	APOE	1.412475
MIR221	-0.79124	BMPER	1.540242
ITGB2	-0.76862	KIT	1.555476
ZC3H12A	-0.64652	MMP9	2.204733

Supplementary Table 10. Significantly ($p < 0.05$) DE genes of the GO term “tissue migration” between PK-1 cells cultured on pancreas vs liver scaffolds. Negative numbers represent genes up-regulated in the pancreas scaffolds. Positive numbers represent genes up-regulated in the liver scaffolds.

Gene Name	LogFC	Gene Name	LogFC	Gene Name	LogFC
MMP7	-1.42086	ITGB7	-0.821624	TGFBI	0.71853838
CAPNS2	-1.39645	MIR29B2	-0.785798	SERPINE1	0.76613466
COL9A3	-1.31233	ITGB2	-0.7686239	ANTXR1	0.76837895
VCAN	-1.26171	ERO1L	-0.7410872	MATN3	0.82482303
SPINK5	-1.19018	LOX	-0.7154613	LAMA1	0.8512128
MMP1	-1.14358	NOXO1	-0.6812074	TNC	0.89176507
FBN2	-1.06219	SH3PXD2A	-0.6525485	COL13A1	1.02024721
ICAM1	-1.06008	SERPINB5	-0.6336487	LOXL3	1.02444343
RGCC	-1.05848	ITGAX	-0.6297261	MMP2	1.02947984
CCDC80	-1.04392	SCUBE3	-0.6168654	THBS1	1.03631894
EFEMP2	-1.02682	TIMP2	0.61195335	SULF2	1.0903728
ITGAM	-0.99233	TGFB2	0.61655389	SPOCK2	1.13462544
CTSK	-0.96583	COL4A1	0.62586167	FN1	2.04647206
TEX14	-0.9104	COL4A2	0.64946681	MMP9	2.20473261
NPNT	-0.89297	COL27A1	0.66777346		
ADAMTSL2	-0.873880773	COL12A1	0.68934855		

Supplementary Table 11. Significantly ($p < 0.05$) DE genes of the GO term “extracellular structure organisation” between PK-1 cells cultured on pancreas vs liver scaffolds. Negative numbers represent genes up-regulated in the pancreas scaffolds. Positive numbers represent genes up-regulated in the liver scaffolds.

Gene Name	LogFC	Gene Name	LogFC
APOE	1.412475	MIR29C	-0.94152
EGR3	-0.92195	GRHL2	0.59931
EPHA2	-0.61339	ZC3H12A	-0.64652
NR4A1	-1.10778	ANGPT4	-1.24596
KIT	1.555476	GLIPR2	-0.9649
MMP9	2.204733	ANLN	-1.35245
BMPER	1.540242	DLL4	-1.21427
PRKCA	-0.924	PLEKHG5	-0.58866
PRSS3	-0.91032	KIAA1462	-0.59171
RAB13	-0.58904	NOV	-1.17719
NR2F2	0.735048	TGFB2	0.616554
THBS1	1.036319	MIR200A	-0.84245
SEMA5A	0.771361	ATOH8	1.018598
KLF4	-0.59793	RGCC	-1.05848
HDAC9	-1.14882	MIR221	-0.79124
HDAC5	-0.59499	ITGB2	-0.76862

Supplementary Table 12. Significantly ($p < 0.05$) DE genes of the GO term “angiogenesis” between PK-1 cells cultured on pancreas vs liver scaffolds. Negative numbers represent genes up-regulated in the pancreas scaffolds. Positive numbers represent genes up-regulated in the liver scaffolds.

Gene Name	LogFC	Gene Name	LogFC	Gene Name	LogFC	Gene Name	LogFC
ALOX15	-2.79267	PTAFR	-1.0971985	PTPN22	-0.7250258	MIR31	0.72244265
RAC2	-2.68247	FANCA	-1.0931663	SELPLG	-0.7247937	PDE5A	0.73947778
CEACAM1	-2.50509	VNN1	-1.0813877	SPN	-0.7145446	PCDHB13	0.74058844
ITGAX	-2.31944	CCM2L	-1.0624625	MYB	-0.7098654	MYO10	0.74586184
SERPINE2	-2.28802	CLDN6	-1.0405689	DUSP10	-0.6999774	FER	0.7630263
TRPV4	-2.28153	LRRC32	-1.0287088	CCL5	-0.697645	ZMIZ1	0.7801022
IL12RB1	-2.17693	TYRO3	-1.0094526	FOXA1	-0.689113	PCDHB12	0.78148174
HLA-DPA1	-2.03373	GPR98	-0.9929397	CLDN10	-0.6835216	ICOSLG	0.78468126
GPNMB	-2.022	CDH23	-0.9858096	APOA1	-0.6718077	PCDH7	0.80344718
MPZL2	-1.89508	LEF1	-0.9840931	ROPN1B	-0.6703483	IGSF9B	0.83648011
CD74	-1.88116	SDK2	-0.9832996	GAS6	-0.668116	SELE	0.83689907
ICAM2	-1.85394	CRTAM	-0.9675702	EPHB3	-0.6659787	PCDHGA6	0.83827385
PKP1	-1.8302	CD177	-0.9549379	DTX1	-0.6626265	PCDHGB3	0.85434312
HLA-DQB1	-1.79758	CD247	-0.9463966	ITGB7	-0.662419	TENM4	0.87173738
TBX21	-1.71061	COL8A2	-0.944453073	C1QTNF1	-0.6423321	CCL2	0.8731857
FANCD2	-1.6043	DMTN	-0.9441763	IL23A	-0.6397268	PCDHB4	0.87352062
FBLIM1	-1.60056	ELANE	-0.9257732	HLA-DPB1	-0.6385546	MIR21	0.89709519
HLA-DMB	-1.54712	ITGAM	-0.9227877	ARG2	-0.6359145	NFATC2	0.89811958
NRXN2	-1.52932	LCK	-0.912555	TARM1	-0.6338255	PCDH20	0.90772335
THY1	-1.5153	CD226	-0.9091498	CCDC88B	-0.6311445	PCDHB15	0.92224169
CDHR4	-1.50875	ITGAD	-0.9039707	PTPRU	-0.6276491	PCDHGA1	0.92904724
ITGB2	-1.49961	CDH16	-0.903424	DCHS1	-0.6252175	CEACAM5	0.93671055
EFNB2	-1.4686	PKD1L1	-0.9034096	BCL6	-0.6179238	PCDHGA7	0.94021459
CSTA	-1.41897	LILRB1	-0.9010952	CADM4	-0.6067712	PCDHB2	1.01291344
ESAM	-1.39775	IGF2	-0.8861973	FAT1	0.59228208	PCDHGA4	1.0198819
LAG3	-1.38792	CD4	-0.8762032	CTNND1	0.61851502	PCDHB14	1.02010976
VAV1	-1.34746	MEGF11	-0.8664541	MBP	0.63485876	PCDH18	1.10688279
SNAI2	-1.33468	PLA2G2D	-0.8341679	PCDHB16	0.63537461	PCDHGB1	1.11911008
TTYH1	-1.27162	ITGB3	-0.8238936	SERPINB8	0.64142883	CDH11	1.12375343
EBI3	-1.27012	CDH17	-0.8171344	EFNA5	0.64219659	PCDHA12	1.12927213
VTCN1	-1.26369	SOCS1	-0.8110787	PCDHB3	0.6434593	IL1RAPL1	1.13551975
CDH24	-1.26045	ITGA2B	-0.8094079	ANXA2	0.64372409	PCDHB11	1.14424166
CARD11	-1.22958	PTPN6	-0.7953639	PCDHB7	0.64448964	CDH1	1.14901757
WNT4	-1.16496	KIRREL2	-0.7934829	HFE	0.65035737	PCDHGA11	1.24476313
ITGA7	-1.13824	CLDN3	-0.7919096	GPAM	0.65145593	PCDHGB7	1.29644383
RET	-1.13682	MADCAM1	-0.7828372	KIRREL	0.66287448	PCDHGA5	1.36404646
CDHR2	-1.11219	NPHS1	-0.7824023	FADD	0.67523645	PCDHGB2	1.3998689
CLDN4	-1.10397	TNFSF9	-0.7762859	CTNNA2	0.67601078	PCDHA4	1.44772093
NFASC	-1.10327	CLC	-0.7687026	PCDHB8	0.70405226	PCDHGA10	2.01907699
IL1B	-1.10257	PAG1	-0.7401949	CD24	0.71918121		

Supplementary Table 13. Significantly ($p < 0.05$) DE genes of the GO term “cell-cell adhesion” between Gemcitabine treated and untreated (control) PANC-1 cells cultured on pancreas scaffolds. Negative numbers represent genes up-regulated in the treated samples. Positive numbers represent genes up-regulated in the control samples.

Gene Name	LogFC	Gene Name	LogFC	Gene Name	LogFC
ITGA1	-2.02461	CD36	-1.04752	ITGB4	-0.6859
VWA2	-1.66488	DMTN	-0.94418	PLAU	-0.66318
LYPD5	-1.56569	GPM6B	-0.89356	ITGB7	-0.66242
THY1	-1.5153	BST1	-0.86266	EMILIN1	-0.66099
ITGB2	-1.49961	GREM1	-0.85751	ACTN2	-0.65967
COL17A1	-1.49347	ACVRL1	-0.83248	BCL6	-0.61792
FBLN5	-1.48431	ITGB3	-0.82389	EFNA5	0.642197
SLC9A1	-1.35779	NID1	-0.8135	SGCE	0.643114
HPSE	-1.28137	ITGA2B	-0.80941	CDK6	0.735129
WNT4	-1.16496	MADCAM1	-0.78284	MIR29C	0.809795
ITGA7	-1.13824	MSLN	-0.7211	CSF1	0.829861
APOD	-1.12345	TESK2	-0.71115	FERMT1	0.864069
KDR	-1.11192	ACTN3	-0.70079	COL3A1	0.967188
ITGA11	-1.07083	ACER2	-0.69543		

Supplementary Table 14. Significantly ($p < 0.05$) DE genes of the GO term “cell-matrix adhesion” between Gemcitabine treated and untreated (control) PANC-1 cells cultured on pancreas scaffolds. Negative numbers represent genes up-regulated in the treated samples. Positive numbers represent genes up-regulated in the control samples.

Gene Name	LogFC						
DLL4	-3.25736	FBLN1	-1.15039	ITGB3	-0.82389	DCHS1	-0.62522
ATP1B2	-2.85905	GPBR1	-1.14808	WNT11	-0.81786	DNAI1	-0.62445
CSF1R	-2.82004	RET	-1.13682	LDC	-0.81688	PRDM14	-0.62272
RAC2	-2.68247	APOD	-1.12345	ITGA2B	-0.80941	PROCR	-0.6193
AGT	-2.6239	KDR	-1.11192	OVOL2	-0.80167	PLTP	-0.6145
SLC7A8	-2.51275	IL1B	-1.10257	TMSB15B	-0.80048	ASAP3	-0.61301
CEACAM1	-2.50509	PTAFR	-1.0972	PTPN6	-0.79536	GTSE1	-0.60931
LRRC15	-2.32741	SNAI1	-1.09327	BLK	-0.79487	INSL3	-0.60783
ITGAX	-2.31944	SLC7A7	-1.09042	CNR2	-0.78624	IGFBP3	-0.60542
SERPINE2	-2.28802	EMR2	-1.08711	MADCAM1	-0.78284	DAB2	-0.59899
TRPV4	-2.28153	PROC	-1.08067	SERPINF1	-0.76982	SP100	-0.59889
ITGA1	-2.02461	ITGA11	-1.07083	TSPAN1	-0.76023	FAT1	0.592282
GPNMB	-2.022	DAPK2	-1.07083	EDNRB	-0.75611	TRIM32	0.604928
MDGA1	-1.89531	CXCR2	-1.05565	SCRT1	-0.74603	SLC9B2	0.605593
S100P	-1.89356	CHRD	-1.04319	ROBO4	-0.74454	RAP2C	0.631687
NR2E1	-1.89031	SLC9A3R1	-1.031	MYPN	-0.74377	CXCL3	0.633921
CD74	-1.88116	BCL11B	-1.0294	GPX1	-0.74212	NRAS	0.642055
ARHGDI1	-1.87448	TYRO3	-1.00945	HBEGF	-0.73149	SPARC	0.652447
CCK	-1.76763	TNK1	-1.00856	HN1	-0.73107	ARID2	0.655723
STRIP2	-1.75616	NR4A1	-1.00824	ROPN1L	-0.72516	POMK	0.664162
ARC	-1.73265	EGR3	-1.0057	SELPLG	-0.72479	CPNE3	0.664251
TIE1	-1.72014	CSF3R	-1.0025	DNAH2	-0.71866	HDAC4	0.674268
TBX21	-1.71061	GLIPR2	-0.99938	SPN	-0.71454	FADD	0.675236
MATN2	-1.67192	LEF1	-0.98409	DRD2	-0.71392	CTNNA2	0.676011
MMP1	-1.63336	MIXL1	-0.97522	KIAA0319	-0.70829	THBD	0.694827
CSPG4	-1.5855	KRT16	-0.97299	UTS2	-0.70189	RAPGEF2	0.703202
CYGB	-1.54416	LY6K	-0.96423	DUSP10	-0.69998	CD24	0.719181
NEURL1	-1.525	KIF20B	-0.96164	CCL5	-0.69764	RASGEF1A	0.719873
THY1	-1.5153	PAK6	-0.95996	ARHGEF16	-0.69614	CXCL2	0.722951
ITGB2	-1.49961	CD177	-0.95494	TNS1	-0.69284	PAX6	0.724154
ERBB3	-1.47227	ADORA1	-0.95241	LAMA1	-0.69133	CCDC39	0.729944
LGR6	-1.47155	FOXE1	-0.94719	ITGB4	-0.6859	CDK6	0.735129
EFNB2	-1.4686	DMTN	-0.94418	KITLG	-0.68115	NTRK2	0.751005
CATSPER1	-1.43612	MCAM	-0.94027	TUBB2B	-0.67877	DOCK7	0.755921
ECM1	-1.42157	S100A14	-0.93473	ADRA2A	-0.67757	FER	0.763026
ESAM	-1.39775	ELANE	-0.92577	HMCN2	-0.67245	C5orf30	0.76766
HCK	-1.36979	ITGAM	-0.92279	APOA1	-0.67181	TOP2B	0.768583
CXCR4	-1.36633	TRPM2	-0.92165	SH3BP1	-0.67168	MAGI2	0.808392
SLC9A1	-1.35779	ANLN	-0.91884	IDH2	-0.6706	MIR29C	0.809795
VAV1	-1.34746	CALCA	-0.91445	MMP9	-0.67045	DNAH7	0.816976
SNAI2	-1.33468	LCK	-0.91256	ROPN1B	-0.67035	CSF1	0.829861
SIX2	-1.32827	SPOCK3	-0.9075	GAS6	-0.66812	SELE	0.836899
FLT4	-1.32248	CXCL14	-0.87954	CKLF	-0.66697	CCBE1	0.843021
TAC1	-1.30766	LAMC2	-0.86914	EPHB3	-0.66598	FERMT1	0.864069
GRB7	-1.30565	WAS	-0.86845	FMNL3	-0.66516	MIR24-1	0.864752
P2RY6	-1.29315	BTC	-0.86531	PLAU	-0.66318	CCL2	0.873186
F10	-1.27371	BST1	-0.86266	ITGB7	-0.66242	CXCL1	0.885114
BST2	-1.27035	GREM1	-0.85751	TEKT2	-0.66195	MIR21	0.897095
PGF	-1.25286	CACNA1I	-0.85411	ZMYND8	-0.66162	NFATC2	0.89812
SAA1	-1.24488	SLC7A10	-0.85353	CCL22	-0.66147	CX3CR1	0.928086
TERT	-1.22986	S100A2	-0.84815	EMILIN1	-0.66099	CEACAM5	0.936711
CDK1	-1.20932	NLRP12	-0.84039	PPARD	-0.65897	HMOX1	0.958588
TNFRSF10D	-1.20875	RLTPR	-0.84013	IL23A	-0.63973	TNS3	0.96558
PDGFRB	-1.19244	SPOCK2	-0.83355	GATA2	-0.63818	COL3A1	0.967188
GFRA3	-1.18903	ACVRL1	-0.83248	BAMBI	-0.63294	GPC6	1.044765
PSTPIP2	-1.18415	MESP1	-0.83174	PTPRU	-0.62765	EPHB1	1.122
WNT4	-1.16496	PRSS3	-0.8243	GPSM3	-0.62725	CCR6	1.271623

Supplementary Table 15. Significantly ($p < 0.05$) DE genes of the GO term “cell motility” between Gemcitabine treated and untreated (control) PANC-1 cells cultured on pancreas scaffolds. Negative numbers represent genes up-regulated in the treated samples. Positive numbers represent genes up-regulated in the control samples.

Gene Name	LogFC	Gene Name	LogFC	Gene Name	LogFC
ATP1B2	-2.85905	EMR2	-1.0871087	KITLG	-0.681148
RAC2	-2.68247	DAPK2	-1.0708257	MMP9	-0.6704517
SLC7A8	-2.51275	CXCR2	-1.0556524	GAS6	-0.668116
CEACAM1	-2.50509	CSF3R	-1.0024984	CKLF	-0.6669657
ITGAX	-2.31944	CD177	-0.9549379	ITGB7	-0.662419
TRPV4	-2.28153	ADORA1	-0.9524083	CCL22	-0.6614677
ITGA1	-2.02461	S100A14	-0.9347292	IL23A	-0.6397268
CD74	-1.88116	ELANE	-0.9257732	GPSM3	-0.627249
TBX21	-1.71061	ITGAM	-0.9227877	PROCR	-0.6193048
MMP1	-1.63336	TRPM2	-0.9216481	FCER1G	-0.5941762
THY1	-1.5153	CALCA	-0.9144464	CXCL3	0.63392072
ITGB2	-1.49961	LCK	-0.912555	NRAS	0.64205533
ECM1	-1.42157	CXCL14	-0.8795374	FADD	0.67523645
ESAM	-1.39775	BST1	-0.8626646	THBD	0.69482725
HCK	-1.36979	GREM1	-0.8575133	CXCL2	0.72295138
CXCR4	-1.36633	SLC7A10	-0.8535274	FER	0.7630263
VAV1	-1.34746	NLRP12	-0.8403856	CSF1	0.82986103
GRB7	-1.30565	ITGB3	-0.8238936	SELE	0.83689907
PGF	-1.25286	ITGA2B	-0.8094079	MIR24-1	0.86475194
SAA1	-1.24488	PTPN6	-0.7953639	CCL2	0.8731857
TNFRSF10D	-1.20875	CNR2	-0.7862414	CXCL1	0.88511391
RET	-1.13682	MADCAM1	-0.7828372	CX3CR1	0.92808573
APOD	-1.12345	EDNRB	-0.7561128	CEACAM5	0.93671055
IL1B	-1.10257	SELPLG	-0.7247937	HMOX1	0.95858789
PTAFR	-1.0972	SPN	-0.71454462	CCR6	1.27162312
SLC7A7	-1.090416504	CCL5	-0.697645	PROC	-1.080666192

Supplementary Table 16. Significantly ($p < 0.05$) DE genes of the GO term “leukocyte migration” between Gemcitabine treated and untreated (control) PANC-1 cells cultured on pancreas scaffolds. Negative numbers represent genes up-regulated in the treated samples. Positive numbers represent genes up-regulated in the control samples.

Gene Name	LogFC	Gene Name	LogFC	Gene Name	LogFC
AGT	-2.6239	ADAM12	-0.96748	VWF	-0.7242
ITGAX	-2.31944	CCDC80	-0.962180259	TLL2	-0.71586
ITGA1	-2.02461	COL8A2	-0.94445	TNXB	-0.69708
ADAMTS14	-1.93213	ELANE	-0.92577	LAMA1	-0.69133
NR2E1	-1.89031	RAMP2	-0.92451	ITGB4	-0.6859
ICAM2	-1.85394	ITGAM	-0.92279	ADAMTS3	-0.6809
MMP1	-1.63336	HTRA1	-0.91779	MMP9	-0.67045
FBLN2	-1.61509	ACAN	-0.91647	GAS6	-0.66812
TEX14	-1.552	ITGAD	-0.90397	MFI2	-0.66528
ITGB2	-1.49961	LAMB3	-0.90074	ITGB7	-0.66242
CTSS	-1.498	GPM6B	-0.89356	MATN4	-0.65351
FBLN5	-1.48431	MMP19	-0.88162	BMP1	-0.64796
CRISPLD2	-1.4723	LAMC2	-0.86914	COMP	-0.62382
CTSV	-1.45444	GREM1	-0.85751	CHADL	-0.60988
SCUBE1	-1.32712	CREB3L1	-0.85097	MPZL3	-0.60612
COL6A3	-1.31434	FBN1	-0.84903	LEPREL4	0.624657
MFAP4	-1.30773	ADAMTS2	-0.84275	ANXA2	0.643724
A2M	-1.28521	RLTPR	-0.84013	SPARC	0.652447
PXDN	-1.26132	COL11A2	-0.83827	COL5A2	0.684266
FBLN1	-1.15039	SPOCK2	-0.83355	MMP16	0.723208
ITGA7	-1.13824	ITGB3	-0.82389	ITGB8	0.744841
KDR	-1.11192	TIMP2	-0.82176	FERMT1	0.864069
SPINT1	-1.0976	NID1	-0.8135	COL11A1	0.873176
COL9A3	-1.08005	COL4A2	-0.81343	VIT	0.886095
ITGA11	-1.07083	ITGA2B	-0.80941	THSD4	0.905311
ELF3	-1.03765	MADCAM1	-0.78284	VWA1	0.908778
COL7A1	-1.00379	NPHS1	-0.7824	COL3A1	0.967188
COL2A1	-0.99031	VCAN	-0.75717	CDH1	1.149018
NCAN	-0.97508	HN1	-0.73107		

Supplementary Table 17. Significantly ($p < 0.05$) DE genes of the GO term “extracellular structure organisation” between Gemcitabine treated and untreated (control) PANC-1 cells cultured on pancreas scaffolds. Negative numbers represent genes up-regulated in the treated samples. Positive numbers represent genes up-regulated in the control samples.

Gene Name	LogFC	Gene Name	LogFC
DLL4	-3.25736	NGFR	-1.00195
CEACAM1	-2.50509	LEF1	-0.98409
NR2E1	-1.89031	PPP1R16B	-0.93415
E2F8	-1.64375	RAMP2	-0.92451
EFNB2	-1.4686	GREM1	-0.85751
FLT4	-1.32248	ACVRL1	-0.83248
PGF	-1.25286	DLL1	-0.79882
KDR	-1.11192	HN1	-0.73107
NR4A1	-1.00824	MIR29C	0.809795
EGR3	-1.0057	CCBE1	0.843021

Supplementary Table 18. Significantly ($p < 0.05$) DE genes of the GO term “sprouting angiogenesis” between Gemcitabine treated and untreated (control) PANC-1 cells cultured on pancreas scaffolds. Negative numbers represent genes up-regulated in the treated samples. Positive numbers represent genes up-regulated in the control samples.

Gene Name	LogFC	Gene Name	LogFC	Gene Name	LogFC
TNFSF18	-2.66403	TNF	-0.972367674	HES1	-0.63144
FANCD2	-1.77561	PDCD1LG2	-0.93236	MALT1	-0.61193
GPNMB	-1.60476	SOCS1	-0.90582	BCL10	-0.60303
NR4A3	-1.58174	CDHR4	-0.89059	ETS1	-0.59924
IL7R	-1.53267	NPHS1	-0.85872	CLDN1	-0.59707
FANCA	-1.51618	BMP2	-0.85804	IL1RN	-0.59637
IFNL1	-1.32636	CD274	-0.85759	PTAFR	-0.58924
SERPINE2	-1.2945	PRDM1	-0.84612	SDK1	0.59708
TNFRSF13C	-1.28545	PKD1L1	-0.83554	CLDN11	0.613844
LCK	-1.27266	TENM4	-0.79777	FAT3	0.631346
PCDHGC4	-1.26119	IL36B	-0.79078	MIR141	0.641859
IL23A	-1.21732	CDH24	-0.78588	MIR21	0.645077
ITGAL	-1.1711	CYP1B1	-0.77977	SCARF2	0.646276
IL6	-1.15117	SPINK5	-0.77617	PCDH19	0.674031
TNFSF9	-1.14378	RGCC	-0.7714	JAM2	0.712281
ICAM1	-1.12583	ITGAX	-0.76768	PYCARD	0.725938
NOV	-1.11165	PCDHGC5	-0.76415	PCDHB9	0.782668
IL20RB	-1.10036	EPHB3	-0.76376	NRXN2	0.786256
DUSP10	-1.09277	VCAM1	-0.76019	CDH15	0.786768
CD83	-1.09263	CNN3	-0.7357	LIMS2	0.790784
DSG3	-1.08643	LAX1	-0.71848	ZEB1	0.875901
PCDH12	-1.07764	LEF1	-0.71447	PCDHGA11	0.878732
ARG2	-1.07296	TGFB2	-0.69422	AMIGO1	0.879916
ALOX15	-1.03632	LGALS7B	-0.68016	PPARA	0.951832
ZP3	-1.00233	S100A9	-0.67765	CDH26	0.984471
CCL5	-0.99358	IRF1	-0.67207		
PCDH9	-0.9813	IFNL2	-0.66255		

Supplementary Table 19. Significantly ($p < 0.05$) DE genes of the GO term “cell-cell adhesion” between Gemcitabine treated and untreated (control) PK-1 cells cultured on liver scaffolds. Negative numbers represent genes up-regulated in the treated samples. Positive numbers represent genes up-regulated in the control samples.

Gene Name	LogFC	Gene Name	LogFC	Gene Name	LogFC
TNFSF18	-2.66403	DUSP10	-1.09277	S100A9	-0.67765
FANCD2	-1.77561	CD83	-1.09263	IRF1	-0.67207
GPNMB	-1.60476	ARG2	-1.07296	IFNL2	-0.66255
NR4A3	-1.58174	ZP3	-1.00233	HES1	-0.63144
IL7R	-1.53267	CCL5	-0.99358	MALT1	-0.61193
FANCA	-1.51618	TNF	-0.97237	BCL10	-0.60303
IFNL1	-1.32636	PDCD1LG2	-0.93236	ETS1	-0.59924
TNFRSF13C	-1.28545	SOCS1	-0.90582	PTAFR	-0.58924
LCK	-1.27266	NPHS1	-0.85872	MIR141	0.641859
IL23A	-1.21732	CD274	-0.85759	MIR21	0.645077
ITGAL	-1.1711	PRDM1	-0.84612	PYCARD	0.725938
IL6	-1.15117	IL36B	-0.79078	ZEB1	0.875901
TNFSF9	-1.14378	SPINK5	-0.77617	PPARA	0.951832
ICAM1	-1.12583	VCAM1	-0.76019		
IL20RB	-1.10036	LAX1	-0.71848		

Supplementary Table 20. Significantly ($p < 0.05$) DE genes of the GO term “leukocyte cell-cell adhesion” between Gemcitabine treated and untreated (control) PK-1 cells cultured on liver scaffolds. Negative numbers represent genes up-regulated in the treated samples. Positive numbers represent genes up-regulated in the control samples.

Gene Name	LogFC	Gene Name	LogFC	Gene Name	LogFC	Gene Name	LogFC
CDK1	-3.0105	LCK	1.27266450	PAX6	0.85129902	ABL2	0.62871516
FAM83D	-2.98748	OLR1	-1.2599	MERTK	-0.84164	IL1A	-0.62858
KIF14	-2.90442	IL23A	-1.21732	CXCL14	-0.8279	MMP1	-0.62628
GTSE1	-2.77547	MKKS	-1.19565	ACVRL1	-0.80948	LY6K	-0.60416
CCL20	-2.67725	TNFAIP6	-1.17864	GRB7	-0.79805	ARHGEF2	-0.59994
TNFSF18	-2.66403	NRP1	-1.17458	MCAM	-0.79622	ETS1	-0.59924
ANLN	-2.65604	ARID5B	-1.17267	CYP1B1	-0.77977	HMCN2	-0.59899
ARC	-2.55045	ITGAL	-1.1711	PKN3	-0.77348	LAMA2	-0.59777
ASPM	-2.4919	IL6	-1.15117	RGCC	-0.7714	ATP1B3	-0.59444
CXCL8	-2.29068	ICAM1	-1.12583	STYK1	-0.77031	TNS1	-0.59373
NOS3	-2.25568	STRIP2	-1.11715	ITGAX	-0.76768	NDE1	-0.59224
CXCL3	-2.24984	NOV	-1.11165	GPSM3	-0.76766	MYPN	-0.59042
DEPDC1B	-2.22452	ARHGEF39	-1.10361	EPHB3	-0.76376	PTAFR	-0.58924
HMGB2	-2.15558	ATP1B2	-1.10301	SLC9A1	-0.76062	SLC7A8	-0.58657
CXCL2	-2.12538	DAB2	-1.09416	VCAM1	-0.76019	MMP28	0.637767
RELN	-2.11535	DUSP10	-1.09277	PADI2	-0.75761	ANG	0.639169
SNAI1	-2.07568	EREG	-1.09252	BAMBI	-0.74992	MIR21	0.645077
KIF20B	-1.69393	JUN	-1.05962	LAMA1	-0.72926	PIK3C2B	0.69434
CEMIP	-1.6185	PTGS2	-1.03614	FOLR1	-0.71975	JAM2	0.712281
DLL4	-1.60988	C5	-1.01235	LEF1	-0.71447	WNT11	0.722929
GPNMB	-1.60476	ISL1	-1.0068	NLRP12	-0.70894	PYCARD	0.725938
NEURL1	-1.56931	ZP3	-1.00233	SLC3A2	-0.70711	SOX8	0.73072
EGR3	-1.50583	CCL5	-0.99358	INPP5D	-0.70609	CD81	0.736986
FGFR1	-1.48662	TNF	-0.97237	DNAH2	-0.69699	WNT5B	0.803199
TREM1	-1.48219	MCTP1	-0.94718	TGFB2	-0.69422	DDR2	0.820811
DCLK1	-1.48005	KIAA0319	-0.93631	S100A9	-0.67765	MIR29C	0.822662
APOD	-1.44935	BTG1	-0.92813	BTC	-0.67455	CSF3R	0.839227
MYLK	-1.37205	KALRN	-0.92466	NTRK2	-0.67157	TGFBR3	0.862547
CSF1R	-1.36107	CCL26	-0.91972	FES	-0.66146	MIR29B2	0.86853
HDAC9	-1.3518	FBLN1	-0.89212	KRT16	-0.65908	IGSF10	0.994217
HBEGF	-1.3509	EDN1	-0.86354	DOCK4	-0.64832	AZU1	1.038518
NR4A1	-1.31395	BMP2	-0.85804	MDGA1	-0.6405	ACE	1.094919
SERPINE2	-1.2945	CD274	-0.85759	HES1	-0.63144		

Supplementary Table 21. Significantly ($p < 0.05$) DE genes of the GO term “cell motility” between Gemcitabine treated and untreated (control) PK-1 cells cultured on liver scaffolds. Negative numbers represent genes up-regulated in the treated samples. Positive numbers represent genes up-regulated in the control samples.

Gene Name	LogFC	Gene Name	LogFC	Gene Name	LogFC
CCL20	-2.67725	C5	-1.012348513	INPP5D	-0.70609
TNFSF18	-2.66403	ZP3	-1.00233	TGFB2	-0.69422
CXCL8	-2.29068	CCL5	-0.99358	S100A9	-0.67765
CXCL3	-2.24984	TNF	-0.97237	IL1A	-0.62858
CXCL2	-2.12538	CCL26	-0.91972	MMP1	-0.62628
TREM1	-1.48219	EDN1	-0.86354	ATP1B3	-0.59444
APOD	-1.44935	MERTK	-0.84164	PTAFR	-0.58924
LCK	-1.27266	CXCL14	-0.8279	SLC7A8	-0.58657
OLR1	-1.2599	GRB7	-0.79805	MMP28	0.637767
IL23A	-1.21732	ITGAX	-0.76768	JAM2	0.712281
ITGAL	-1.1711	GPSM3	-0.76766	PYCARD	0.725938
IL6	-1.15117	VCAM1	-0.76019	CSF3R	0.839227
ICAM1	-1.12583	PADI2	-0.75761	AZU1	1.038518
NOV	-1.11165	NLRP12	-0.70894		
ATP1B2	-1.10301	SLC3A2	-0.70711		

Supplementary Table 22. Significantly ($p < 0.05$) DE genes of the GO term “leukocyte migration” between Gemcitabine treated and untreated (control) PK-1 cells cultured on liver scaffolds. Negative numbers represent genes up-regulated in the treated samples. Positive numbers represent genes up-regulated in the control samples.

Gene Name	LogFC	Gene Name	LogFC	Gene Name	LogFC
PRSS1	-1.76548	RGCC	-0.771400821	CAPNS2	-0.60821
TEX14	-1.44793	ITGAX	-0.76768	ETS1	-0.59924
VCAN	-1.38968	ADAMTS14	-0.76547	LAMA2	-0.59777
FBN2	-1.22595	VCAM1	-0.76019	COL9A2	0.618552
ITGAL	-1.1711	SCUBE1	-0.75597	TNXB	0.625285
ICAM1	-1.12583	NID2	-0.74386	JAM2	0.712281
TNF	-0.97237	LAMA1	-0.72926	ABI3BP	0.715965
CTSV	-0.93116	MMP16	-0.71691	COL5A2	0.808739
VWF	-0.92983	TGFB2	-0.69422	DDR2	0.820811
FBLN1	-0.89212	TNC	-0.68956	EFEMP2	0.854315
NPHS1	-0.85872	ECM2	-0.67739	KLK7	0.855494
COL16A1	-0.80378	ADAM12	-0.67679	COL6A1	0.861779
NFKB2	-0.78529	MMP7	-0.65749	MIR29B2	0.86853
CYP1B1	-0.77977	FBLN5	-0.63346	LAMB2	0.941772
SPINK5	-0.77617	MMP1	-0.62628		

Supplementary Table 23. Significantly ($p < 0.05$) DE genes of the GO term “extracellular structure organisation” between Gemcitabine treated and untreated (control) PK-1 cells cultured on liver scaffolds. Negative numbers represent genes up-regulated in the treated samples. Positive numbers represent genes up-regulated in the control samples.

Gene Name	LogFC	Gene Name	LogFC
E2F8	-2.62048	NRP1	-1.17458
E2F7	-2.40175	PTGS2	-1.03614
DLL4	-1.60988	ACVRL1	-0.80948
EGR3	-1.50583	LEF1	-0.71447
NGFR	-1.48152	ESM1	-0.70353
HDAC9	-1.3518	MIR29C	0.822662
NR4A1	-1.31395		

Supplementary Table 24. Significantly ($p < 0.05$) DE genes of the GO term “sprouting angiogenesis” between Gemcitabine treated and untreated (control) PK-1 cells cultured on liver scaffolds. Negative numbers represent genes up-regulated in the treated samples. Positive numbers represent genes up-regulated in the control samples.